

THE PALEOPROTEROZOIC METAPLUTONIC SUITE
OF VOISEY'S BAY, LABRADOR:
A GEOCHEMICAL, TECTONIC AND
METALLOGENIC INVESTIGATION

CENTRE FOR NEWFOUNDLAND STUDIES

**TOTAL OF 10 PAGES ONLY
MAY BE XEROXED**

(Without Author's Permission)

ALANA MAXINE RAWLINGS

INFORMATION TO USERS

This manuscript has been reproduced from the microfilm master. UMI films the text directly from the original or copy submitted. Thus, some thesis and dissertation copies are in typewriter face, while others may be from any type of computer printer.

The quality of this reproduction is dependent upon the quality of the copy submitted. Broken or indistinct print, colored or poor quality illustrations and photographs, print bleedthrough, substandard margins, and improper alignment can adversely affect reproduction.

In the unlikely event that the author did not send UMI a complete manuscript and there are missing pages, these will be noted. Also, if unauthorized copyright material had to be removed, a note will indicate the deletion.

Oversize materials (e.g., maps, drawings, charts) are reproduced by sectioning the original, beginning at the upper left-hand corner and continuing from left to right in equal sections with small overlaps.

**ProQuest Information and Learning
300 North Zeeb Road, Ann Arbor, MI 48106-1346 USA
800-521-0600**

UMI[®]



**National Library
of Canada**

**Acquisitions and
Bibliographic Services**

**395 Wellington Street
Ottawa ON K1A 0N4
Canada**

**Bibliothèque nationale
du Canada**

**Acquisitions et
services bibliographiques**

**395, rue Wellington
Ottawa ON K1A 0N4
Canada**

Your file / Votre référence

Our file / Notre référence

The author has granted a non-exclusive licence allowing the National Library of Canada to reproduce, loan, distribute or sell copies of this thesis in microform, paper or electronic formats.

The author retains ownership of the copyright in this thesis. Neither the thesis nor substantial extracts from it may be printed or otherwise reproduced without the author's permission.

L'auteur a accordé une licence non exclusive permettant à la Bibliothèque nationale du Canada de reproduire, prêter, distribuer ou vendre des copies de cette thèse sous la forme de microfiche/film, de reproduction sur papier ou sur format électronique.

L'auteur conserve la propriété du droit d'auteur qui protège cette thèse. Ni la thèse ni des extraits substantiels de celle-ci ne doivent être imprimés ou autrement reproduits sans son autorisation.

0-612-73631-8

Canada



Memorial

University of Newfoundland

This is to authorize the Dean of Graduate Studies to deposit two copies of my thesis/report entitled

The Paleoproterozoic Metaplutonic Suite of Kelsey's Bay Labrador:
A Geochemical, Tectonic and Metagenetic Investigation.

in the University Library, on the following conditions. I understand that I may choose only ONE of the Options here listed, and may not afterwards apply for any additional restriction. I further understand that the University will not grant any restriction on the publication of thesis/report abstracts.

(After reading the explanatory notes at the foot of this form, delete TWO of (a), (b) and (c), whichever are inapplicable.)

The conditions of deposit are:

(a) that two copies are to be made available to users at the discretion of their custodians,

OR

(b) that access to, and quotation from, this thesis/report is to be granted only with my written permission for a period of one year from the date on which the thesis/report, after the approval of the award of a degree, is entrusted to the care of the University, namely, _____ 19 ____, after which time the two copies are to be made available to users at the discretion of their custodians,

OR

(c) that access to, and quotation from, this thesis/report is to be granted only with my written permission for a period of _____ years from the date on which the thesis/report, after approval for the award of a degree, is entrusted to the care of the University; namely, _____ 19 ____, after which time two copies are to be made available to users at the discretion of their custodians.

Date Aug 14 2001
[Signature]
 Dean of Graduate Studies

Signed [Signature]
 Witnessed by Maureen Moore

NOTES

1. Restriction (b) will be granted on application, without reason given.

However, applications for restriction (c) must be accompanied with a detailed explanation, indicating why the restriction is thought to be necessary, and justifying the length of time requested. Restrictions required on the grounds that the thesis is being prepared for publication, or that patents are awaited, will not be permitted to exceed three years.

Restriction (c) can be permitted only by a Committee entrusted by the University with the task of examining such applications, and will be granted only in exceptional circumstances.

2. Thesis writers are reminded that, if they have been engaged in contractual research, they may have already agreed to restrict access to their thesis until the terms of the contract have been fulfilled.

**The Paleoproterozoic Metaplutonic Suite of Voisey's
Bay, Labrador: A Geochemical, Tectonic and
Metallogenic Investigation**

By

© Alana Maxine Rawlings, B.Sc. (Hons.)

A thesis submitted to the School of
Graduate Studies in partial fulfillment of
the requirements for the degree of
Master of Science

Department of Earth Sciences
Memorial University of Newfoundland
St. John's Newfoundland

August 2001

Abstract

The Paleoproterozoic Torngat Orogen of northern Labrador welds the Nain and Rae Archean cratons. A suite of calc-alkaline metaplutonic rocks has been identified in the Voisey's Bay area and these rocks are believed to represent a southern extension of similar metaplutonic rocks identified along the some 500 km length of the orogen. In addition the ore-bearing troctolites of the recently discovered Voisey's Bay Ni-Cu-Co deposit are located within the metaplutonic suite.

This study involves detailed geology, geochemistry, isotopic composition and geochronology of the Paleoproterozoic metaplutonic suite in the Voisey's Bay area. To determine: (1) the petrogenesis of the metaplutonic rocks and constrain the Paleoproterozoic tectonic setting of the region; and (2) the role of the metaplutonic rocks in crustal contamination of the Voisey's Bay troctolitic intrusion and the genesis of the Ni-Cu-Co deposit.

The Paleoproterozoic metaplutonic rocks are a relatively undifferentiated, mafic to intermediate calc-alkaline batholith. The rocks have been metamorphosed to upper amphibolite or granulite facies and interleaved with newly discovered sulfide-rich paragneisses, amphibolite and meta-anorthosite. Recent mapping of this thesis shows that the metaplutonic suite covers a sizeable geographic area encompassing most parts of the Voisey's Bay Ni-Cu-Co ore system. Two samples give ages of 1893 \pm 1 Ma and 1890 \pm 2 Ma by U-Pb zircon TIMS geochronology. Based on LAM-ICP-MS, one of these samples contained inherited zircon cores, some 50-100 Ma older than the igneous population, but no Archean cores were found in this sample of the two others. Meta-tonalite rocks of this suite probably form during a slightly younger magmatic event dated at 1883 \pm 5 Ma. All the compositions are enriched in relative amounts of Ba, Sr, Rb, Zr and Hf; and have negative Nb-Ta anomalies. This trace element chemistry of the rocks is distinctive and markedly similar to the Voisey's Bay deposit, specifically in possessing Th-U and Nb-Ta depletions and exhibits elevated La/Sm ratios (2.92 to 11.02) with a range of Th/Nb ratios (0.004 to 1.065). The sulfur content of the metaplutonic suite reaches levels of 0.1 weight percent. Their REE patterns exhibit fractionation of LREE relative to HREE, with the extent of fractionation increasing with silica content. The $\epsilon\text{Nd}_{(1890 \text{ Ma})}$ values for the samples range from +0.13 to -5.3. The Pb isotopic ratios were 15.160-15.834 for $^{206}\text{Pb}/^{204}\text{Pb}$ and 15.000 to 15.145 for $^{207}\text{Pb}/^{204}\text{Pb}$ and suggest that the contaminant formed in the lower crust. When calculated to the age of the Voisey's Bay troctolite intrusion, the Paleoproterozoic metaplutonic rocks define two distinct isotopic groups: an enriched group with $\epsilon\text{Nd}_{(1320 \text{ Ma})}$ of -11.1 and -11.2, $^{87}\text{Sr}/^{86}\text{Sr}_{(1320 \text{ Ma})}$ ratios between 0.7032 and 0.7050 and μ^* values of 7.66 to 7.77; and a more depleted group which exhibits $\epsilon\text{Nd}_{(1320 \text{ Ma})}$ values between -2.8 to -6.8, $^{87}\text{Sr}/^{86}\text{Sr}_{(1320 \text{ Ma})}$ ratios between 0.7038 and 0.7041 and μ^* values 7.75 to 7.98.

Meta-gabbro to meta-quartz diorite compositions of this suite defines a magmatic series that probably evolved through fractional crystallization. The meta-tonalites formed during a slightly younger magmatic event and the increasing fractionation of LREE to HREE suggests the meta-tonalites had more residual garnet in their source regions than did other members of the suite. The range in $\epsilon\text{Nd}_{(1890 \text{ Ma})}$ suggests interaction between the

primary magmas and continental crust. The Pb isotopic values suggest that the contaminant formed in the lower crust. A model for the metaplutonic suite is presented in which the meta-gabbro to meta-quartz diorite series formed by partial melting of the mantle wedge and interacted with crustal contaminant either in the source or lower crust. The meta-tonalites were derived by partial melting of subducting oceanic crust. Crustal genesis by both slab melting and wedge melting in the Paleoproterozoic may mark the transition from Archean to post-Archean processes.

In terms of the role of the metaplutonic suite in the crustal contamination and genesis of the Voisey's Bay Ni-Cu-Co deposit. The trace element and isotopic data of the Voisey's Bay troctolitic intrusion and mineralized conduit rocks can be most readily explained by 5-10 percent contamination of a picritic basalt magma with the enriched group of the metaplutonic rocks. Contamination by the Tasiuyak paragneiss produced more subtle effects on the compositions of the intrusion. This new evidence indicates that the Paleoproterozoic metaplutonic rocks played a key role in the crustal contamination of the Voisey's Bay intrusion, which may have led to sulfur saturation and precipitation of sulfides. Metaplutonic contamination may be an essential element in the formation of similar deposits in the region and elsewhere.

Acknowledgements

Many people contributed to production and completion of this thesis. Firstly I would like to thank my supervisors Paul Sylvester and John Myers. I extend my sincere thanks to Paul for presenting the opportunity to do this project. Paul provided endless academic support and guidance. He worked tirelessly throughout this thesis and especially in the more arduous final stages. John is thanked for his expertise and guidance with the geology of northern Labrador. Both of you are dearly thanked for providing a great learning experience.

In addition, Greg Dunning actively became involved in the geochronology aspects of this thesis. His willingness to share his expertise in this area has been very beneficial to my learning experience. Jan Kosler is thanked for his assistance in the laser dating and especially in the preparation of the GAC-MAC talk. Toby Rivers and Mark Wilson are thanked for their contributions in technical advice and eagerness to discuss geological ideas.

Many technical staff at Memorial University contributed to this thesis, in particular Pam King, Lakmali Hewa, Robbi Hicks, Pat Horan, Mike Turbrett and Rick Soper. Their assistance in many aspects of sample analysis or preparation is greatly appreciated.

This study was made possible through the generous financial and technical support of the Voisey's Bay Nickel Company Inc. Numerous people provided endless support in the field and back in Newfoundland. The exploration team was always willing to share their expertise and were always interested in my project. All of the employees in Anaktalak Camp made me feel welcome from the first day of my field seasons to the last. Many people assisted me both with my project and in finding things to do in my off hours. They provided excellent food and countless helicopter hours. All of the VBNC employees are thanked, though too numerous to list here. Dan Lee and Dawn Evans-Lamswood are especially thanked.

My field assistant Lucy-Ann Bradley is thanked for good-natured companionship, and providing comical relief during those excruciatingly hot days. She was excessively patient even though I dragged her all over "fly infested" northern Labrador and faced numerous bears.

Fellow graduate students provided insight and willingness to discuss academic ideas, as well as providing a social haven. I would like to thank numerous friends including Christina and Richard Cox. Christina provided an often-needed break from geology, while Richard provided extensive knowledge of geology and numerous other subjects as well as some fabulous meals. Jason Krauss is thanked for his support and occasionally "putting his hand down". Trevor MacHattie is thanked for his enthusiasm and for providing endless entertainment. Many of my friends are thanked for their support

of my move to Newfoundland, and their continuous efforts to keep me in touch with the “mainland”, including Amy Wood, Jen Kosmenko, Jeff Lalonde, Sarah Tait, Karyne Pinette, Shweta Kumar, Vashti Singh and Reuben Dinsmore.

My family is thanked for their continuous encouragement and support through the years. They gave me the faith and courage in myself that allowed me to leave the Yukon and pursue post-secondary education. So to my mother, my father, Lisa and Blair, thank you for your love. Finally I would like to thank my fiancé John Hinchey, whose love has changed my life. He has provided endless support, encouragement, inspiration and guidance. He has made Newfoundland home for me and showed me a world that I never knew existed. Thank you.

Table of Contents

Title Page	i
Abstract	ii
Acknowledgments	iv
Table of Contents	vi
List of Figures	xi
List of Maps	xvi
List of Tables	xvii
List of Plates	xviii

Chapter One - Introduction

1.1	Introduction	Page 1-1
1.2	Regional Geology	Page 1-2
1.2.1.	Geological Framework of Labrador	Page 1-2
1.2.2.	Tectonic and Magmatic Evolution	Page 1-5
1.2.2.1	Tectonic and Magmatic Evolution of the Nain Province (pre-Torngat Orogen)	Page 1-5
1.2.2.2	Tectonic and Magmatic Evolution of the Eastern Churchill Province and Torngat Orogen	Page 1-8
1.2.2.3	The Nain Plutonic Suite – Magmatic Evolution and Genesis	Page 1-13
1.3	Presentation of Study Area- Voisey’s Bay Labrador	Page 1-16
1.3.1	Introduction	Page 1-16
1.3.2	Previous Work and Outstanding Problems	Page 1-16
1.3.3	Brief Outline of Local Geology	Page 1-17
1.3.4	Thesis Goals	Page 1-19
1.3.5	Field Component of the Project	Page 1-20

1.4	Methodology	Page 1-20
1.4.1	Introduction	Page 1-20
1.4.2	Major and Trace Element Geochemistry	Page 1-21
1.4.2.1	Introduction	Page 1-21
1.4.2.2	Discrimination Diagrams	Page 1-21
1.4.2.3	Bivariant Diagrams	Page 1-22
1.4.2.4	Normalized Rare-earth-element and Multi-element Plots	Page 1-23
1.4.2.5	Effects of Metamorphism on the Geochemistry	Page 1-25
1.4.3	Radiogenic Isotopes	
1.4.3.1	Introduction	Page 1-26
1.4.3.2	Sr Isotopes	Page 1-27
1.4.3.3	Nd Isotopes	Page 1-29
1.4.3.4	Pb Isotopes	Page 1-32
1.4.4	U-Pb Geochronology	Page 1-33
1.5	Structure of the Thesis	Page 1-35
1.5.1	Introduction	Page 1-35
1.5.2	Chapter 2 – “Southern Extension of the Torngat Orogen: Remnants of a Calc-alkaline Batholith in the Voisey’s Bay Area, Labrador.”	Page 1-35
1.5.3	Chapter 3 – “A New Perspective on the Role of the Paleoproterozoic Metaplutonic Rocks in the Voisey’s Bay Ni-Cu-Co mineralization, Labrador, Canada.”	Page 1-36
	Figures	Page 1-37

2.8.2.3.2 With Modern Arc Magmas	Page 2-39
2.9 Conclusion	Page 2-40
Figures	Page 2-42
Tables	Page 2-81
Plates	Page 2-97

**Chapter Three - A New Perspective on the Role of the Paleoproterozoic
Metaplutonic Suite in the Voisey's Bay Ni-Cu-Co mineralization,
Labrador, Canada**

3.1 Abstract	Page 3-1
3.2 Introduction	Page 3-3
3.3 Regional Geology	Page 3-4
3.4 Previous Geochemical Studies	Page 3-6
3.5 Geographic Distribution of the Paleoproterozoic Metaplutonic Suite	Page 3-10
3.6 Sulfur Content of the Paleoproterozoic Metaplutonic Suite	Page 3-11
3.7 Trace Element Geochemistry	Page 3-12
3.8 Nd-Sr-Pb Isotopic Data	Page 3-14
3.9 Discussion and Conclusion	Page 3-21
Figures	Page 3-25

Chapter Four – Summary and Conclusion

4.1 Introduction	Page 4-1
4.2 Summary	Page 4-1
4.2.1 Southern Extension of the Torngat Orogen: Remnant of a Calc-alkaline Batholith in the Voisey's Bay Area, Labrador.	Page 4-2
4.2.2 A New Perspective on the Role of the Paleoproterozoic Metaplutonic Suite in the Voisey's Bay Ni-Cu-Co mineralization, Labrador, Canada	Page 4-4
4.3 Directions for Further Study	Page 4-6

References	Page R-1
-------------------	----------

Appendix A – Analytical Methods	Page A-1
A.1 Major and Trace element Analyses	Page A-1
A.1.1 X-Ray Fluorescence (XRF)	Page A-1
A.1.2 Inductively Coupled Plasma Mass Spectrometry	Page A-3
A.2 Radiogenic Isotopes	Page A-6
A.2.1 Sm-Nd and Rb-Sr Isotopes	Page A-6
A.2.2 Pb-Pb Isotopes	Page A-9
A.3 U-Pb Zircon Thermal Ionization Mass Spectrometry (TIMS) Analyses	Page A-9
A.4 U-Pb Zircon Laser Ablation Microprobe-Inductively Coupled Plasma-Mass Spectrometry (LAM-ICP-MS)	Page A-11
Figures	Page A-14
Tables	Page A-16
Appendix B – Sample List and Locations	Page B-1

List of Figures

1.1	Structural Provinces and major tectonic features of Labrador	Page 1-37
1.2	Simplified geological map of Labrador	Page 1-38
1.3	Generalized map of the Torngat Orogen, Churchill and Nain Provinces	Page 1-39
2.1	Generalized map of the Torngat Orogen, Churchill and Nain Provinces	Page 2-42
2.2	Detailed geologic map of Anaktalak to Voisey's Bay, Labrador	Page 2-43
2.3	Quartz-alkali feldspar-plagioclase classification diagram (Le Maitre, 1989)	Page 2-44
2.4	Anorthite-albite-orthoclase classification diagram (Barker, 1979)	Page 2-44
2.5	Classification diagrams: (A) Irvine and Barager's (1971) AFM plot; (B) Jensen's cation plot	Page 2-45
2.6	Pearce et al.'s (1984) tectonic discrimination diagram	Page 2-46
2.7	SiO ₂ versus major element diagrams	Page 2-47
2.8	SiO ₂ versus trace element or trace element Ratio Diagrams	Page 2-49
2.9	Chondrite normalized REE spider-diagrams	Page 2-52
2.10	Primitive mantle normalized multi-element spider-diagram	Page 2-53
2.11	Mid-ocean ridge basalt (MORB) normalized multi-element spider-diagram	Page 2-54
2.12	U-Pb locations on a simplified geological map of Voisey's Bay	Page 2-55
2.13	U-Pb concordia plot of the meta-quartz diorite sample VB-99-108	Page 2-56

2.14	U-Pb concordia plot of the meta-hornblende gabbro sample VB-99-106	Page 2-57
2.15	U-Pb concordia plot of the meta-tonalite sample DDH-496-549	Page 2-58
2.16	Rb-Sr isotopic data for the metaplutonic suite	Page 2-59
2.17	Sm-Nd isotopic data for the metaplutonic suite	Page 2-60
2.18	Sm-Nd isotopic data of this study compared to other studies of the metaplutonic suite and Archean Nain gneisses	Page 2-61
2.19	Sr versus ϵNd for the metaplutonic suite	Page 2-62
2.20	Pb-Pb isotopic data for the metaplutonic suite	Page 2-63
2.21	ϵNd versus μ^* and κ^* of the metaplutonic suite	Page 2-64
2.22	U-Pb versus Pb-Pb plot for the LAM-ICP-MS zircon analyses from the metaplutonic suite	Page 2-65
2.23	Rb (ppm) versus K_2O (wt. %) for the metaplutonic suite	Page 2-66
2.24	U (ppm) versus Th (ppm) for the metaplutonic suite	Page 2-67
2.25	Time versus ϵNd for the metaplutonic suite compared to Rae Province gneiss, Nain Province gneiss and Tasiuyak paragneiss	Page 2-68
2.26	ϵNd versus (A) SiO_2 and (B) MgO for the metaplutonic suite	Page 2-69
2.27	SiO_2 versus selected major element diagrams for the metaplutonic suite compared to Paleoproterozoic supracrustal units in the region	Page 2-70
2.28	SiO_2 versus selected major element diagrams for the metaplutonic suite compared to Nain and Rae Province gneisses	Page 2-71

2.29	ϵ_{Nd} versus fraction factor for the metaplutonic suite compared to Paleoproterozoic supracrustal units in the region	Page 2-72
2.30	ϵ_{Nd} versus fraction factor for the metaplutonic suite compared to Nain and Rae Province gneisses	Page 2-73
2.31	μ^* versus ϵ_{Nd} for the metaplutonic suite compared with lower and upper crust mixing lines. Nain and Rae Province gneisses.	Page 2-74
2.32	SiO_2 versus selected major element diagrams for the metaplutonic suite compared to Burwell Domain metaplutonic rocks	Page 2-75
2.33	SiO_2 versus selected major element diagrams for the metaplutonic suite compared to North River-Nutak (southern Torngat Orogen) area metaplutonic rocks	Page 2-76
2.34	Chondrite normalized REE spider diagrams of the metaplutonic suite compared to Burwell Domain metaplutonic rocks	Page 2-77
2.35	Chondrite normalized REE spider diagrams of the metaplutonic suite compared to North River-Nutak (southern Torngat Orogen) area metaplutonic rocks	Page 2-78
2.36	ϵ_{Nd} versus fraction factor for the metaplutonic suite compared to Paleoproterozoic metaplutonic rocks from the Burwell Domain and North River-Nutak (southern Torngat Orogen) area	Page 2-79
2.37	$Yb_{(N)}$ versus $La_{(N)}$, $Yb_{(N)}$ diagram for the Paleoproterozoic metaplutonic rocks from Voisey's Bay, the Burwell Domain and the North River-Nutak (southern Torngat Orogen)	Page 2-80

3.1	Simplified geologic map of Labrador	Page 3-25
3.2	Simplified geologic map of Voisey's-Anaktalak Bay area	Page 3-26
3.3	Simplified geologic map of the Voisey' Bay deposit	Page 3-27
3.4	SiO ₂ versus sulfur for the metaplutonic suite	Page 3-28
3.5	γ_{Os} versus $\delta^{34}S$ for the metaplutonic suite, the Voisey's Bay conduit rocks and the Tasiuyak paragneiss	Page 3-28
3.6	Primitive mantle normalized spider diagram of the average metaplutonic rock, Archean Nain Province orthogneiss, Tasiuyak Paragneiss, Voisey's Bay troctolite and conduit.	Page 3-29
3.7	Th/Nb versus La/Sm for the metaplutonic rock, Archean Nain Province orthogneiss, Tasiuyak Paragneiss, Voisey's Bay troctolite and conduit.	Page 3-30
3.8	Sr versus ϵNd for the Voisey's Bay intrusion and potential crustal contaminants	Page 3-31
3.9	μ^* versus ϵNd for the Voisey's Bay intrusion and potential crustal contaminants	Page 3-32
3.10	κ^* versus ϵNd for the Voisey's Bay intrusion and potential crustal contaminants	Page 3-33
3.11	Mixing model between a basaltic parental magma end-member and potential contaminants in comparison with Sr versus ϵNd of the Voisey's Bay intrusion	Page 3-34

3.12	Mixing model between a basaltic parental magma end-member and potential contaminants in comparison with μ^* versus ϵNd of the Voisey's Bay intrusion	Page 3-35
3.13	Mixing model between a picritic parental magma end-member and potential contaminants in comparison with Sr versus ϵNd of the Voisey's Bay intrusion	Page 3-36
3.14	Mixing model between a picritic parental magma end-member and potential contaminants in comparison with μ^* versus ϵNd of the Voisey's Bay intrusion	Page 3-37
A.1	Primitive mantle normalized multi-element spider diagrams comparing samples prepared by HF-nitric or Na_2O_2 sinter method for ICP-MS analysis	Page A-14
A.2	Comparison of certain trace elements concentration analysed by ICP-MS versus XRF.	Page A-15

List of Maps

(located in pocket, inside back cover)

1. Detailed geologic map of the Anaktalak to Voisey's Bay are, northern Labrador.

List of Tables

2.1	Major element analyses of the Paleoproterozoic metaplutonic suite	Page 2-81
2.2	Trace element analyses of the Paleoproterozoic metaplutonic suite	Page 2-85
2.3	U-Pb TIMS data metaplutonic samples	Page 2-92
2.4	Rb-Sr and Sm-Nd TIMS data for the metaplutonic rocks	Page 2-93
2.5	Pb isotopic MC-ICP-MS data for metaplutonic rocks	Page 2-94
2.6	LAM-ICP-MS U-Pb data for the igneous zircons from the metaplutonic suite	Page 2-95
2.7	LAM-ICP-MS U-Pb data for the inherited zircons cores of the metaplutonic suite	Page 2-96
A.1	Precision and Accuracy for XRF trace and semi-quantitative determinations from replicate analyses of standard DNC-1	Page A-16
A.2	Precision and Accuracy for ICP-MS trace and REE determinations from replicate analyses of standard MRG-1	Page A-17

List of Plates

- | | | |
|------|--|------------|
| 2.1 | Paleoproterozoic metaplutonic suite (A) pristine meta-quartz diorite, and (B) highly foliated meta-tonalite | Page 2-97 |
| 2.2 | Paleoproterozoic metaplutonic suite (A) undeformed meta-gabbro in drill core, and (B) undeformed meta-gabbro in outcrop | Page 2-98 |
| 2.3 | Paleoproterozoic metaplutonic suite in outcrop (A) meta-gabbro, and (B) weathered meta-tonalite | Page 2-99 |
| 2.4 | Paleoproterozoic metaplutonic suite in outcrop (A) meta-tonalite cross-cut by a pegmatite, and (B) syn-deformational dyke in meta-tonalite | Page 2-100 |
| 2.5 | Metasedimentary unit (A) metapelite, and (B) Tightly folded quartz-rich metasediments | Page 2-101 |
| 2.6 | Meta-anorthosite unit (A) Foliated in contact with meta-gabbro, and (B) tightly folded | Page 2-102 |
| 2.7 | Contact relationships between the meta-sedimentary and metaplutonic units (A) meta-gabbro in contact with quartzite, and (B) meta-tonalite in contact with metapelites | Page 2-103 |
| 2.8 | Contact relationships between the Nain Province gneisses and metaplutonic suite (A) drill core contact, and (B) outcrop contact | Page 2-104 |
| 2.9 | Contact relationships between the Tasuiyak paragneiss and meta-tonalite of the metaplutonic suite | Page 2-105 |
| 2.10 | Photomicrographs of a meta-tonalite from the metaplutonic suite | Page 2-106 |

2.11	Photomicrographs of a meta-hornblende gabbro from the metaplutonic suite	Page 2-107
2.12	U-Pb sample VB-99-108 (meta-quartz diorite) (A) field appearance, (B) photomicrograph	Page 2-108
2.13	Zircons from VB-99-108 (meta-quartz diorite) (A) selected morphology, (B) general population	Page 2-109
2.14	U-Pb sample VB-99-106c (meta-hornblende gabbro) (A) field appearance, (B) photomicrograph	Page 2-110
2.15	Zircons from VB-99-106c (meta-hornblende gabbro) (A) selected morphology, (B) general population	Page 2-111
2.16	U-Pb sample DDH-496-549 (meta-tonalite) (A) field appearance, (B) photomicrograph	Page 2-112
2.17	Zircons from DDH-496-549 (meta-tonalite) (A) selected morphology, (B) general population	Page 2-113
2.18	Back-scattered electron images of potential inherited cores in zircons from sample VB-99-106c	Page 2-114

Chapter 1

Introduction and Background

1.1 INTRODUCTION

The discovery of the troctolite-hosted, Voisey's Bay Ni-Cu-Co sulfide deposit in 1994 unleashed a new interest, and influx of activity into the area of Northern Labrador. At the time of discovery, there was limited research on this type of deposit and as a result its genesis was poorly understood (Ryan, 1995; Naldrett et al., 1996). Subsequent work led to a genetic model in which crustal contamination of the mafic magma plays a key role in sulfide saturation and precipitation (i.e. Naldrett et al., 1996; Amelin et al., 2000; Li et al., 2000). Current interest is in defining the detailed processes and components involved in the crustal contamination and, more broadly, understanding the tectonic, and magmatic history of Northern Labrador.

The present study focuses on the geology, geochemistry, isotopic composition and geochronology of the Paleoproterozoic metaplutonic rocks that host the ore-bearing troctolites of the Voisey's Bay area. The aim of this study is two-fold: (1) to understand the petrogenesis of the metaplutonic rocks in hopes of constraining the Paleoproterozoic tectonic setting of this region; and (2) determining the role of the metaplutonic rocks in crustal contamination of the Voisey's Bay troctolitic intrusion and genesis of the Ni-Cu-Co deposit.

This chapter is the background and framework for the remainder of the thesis. The regional geology of the area is introduced, followed by a presentation of the outstanding

problems and previous studies in the area. Next, the goals of the thesis are presented, and a brief description of the field and laboratory methodology is reviewed. This is followed by a brief summary of the main chapters.

1.2 REGIONAL GEOLOGY

The regional geology of Labrador is of particular importance because of its long geologic history, spanning over 3.5 Ga, and the variety of magmatism and tectonism that formed there. This section is a brief overview of the geological framework of Labrador, with descriptions focussing on the tectonic and magmatic development of the area.

1.2.1 Geologic Framework of Labrador

The geology of Labrador encompasses 5 major structural provinces and covers an area greater than 250,000 km² preserving rock units that span from ca. 3.8 to 0.6 Ga (Figure 1.1 and 1.2; Wardle, 1995). This section will focus on the major components that make up Labrador and a subsequent section will deal in detail with the geology of the Voisey's Bay area.

The Superior and Nain provinces preserve the oldest known rock units, which are bounded by the Paleoproterozoic mobile belts of the Makkovik and Churchill province (Wardle, 1995). The Superior province accounts only for a small amount of western Labrador, comprising mostly metasedimentary gneisses, orthogneisses, mafic and granitoid plutons (James, 1993; 1995).

Lying to the south of Nain province is the triangular-shaped Makkovik Province. The northern part of the Makkovik province consists of reworked equivalents of the Nain

Province, while the southern part comprises accreted, juvenile volcanic and plutonic rocks intruded by syn-and post-orogenic granites (Wardle, 1995).

The Grenville province is a significant portion of southern Labrador, and truncates the Churchill, Superior and Makkovik province, leaving a residual mobile belt referred to as the Labrador orogen (Rivers et al., 1989; Wardle, 1995). This province is dominated by high-grade metasedimentary gneisses, sedimentary rocks (siliciclastic and carbonaceous), metamorphosed tonalites-granitoids and their gneissic equivalents, felsic volcanics, granitoids plutons, anorthosite-mangerite-charnockite-granite suites and mafic dyke swarms (Kamo et al., 1989; Rivers et al., 1989; Gower et al., 1995; Rivers, 1997). The orogenic suites and juvenile Labradorian crust that form the Grenville province was subsequently thrust over the basement rocks ca. 1000 Ma (Gower et al., 1995; Rivers, 1997).

The Nain province comprises a large portion of central-northern Labrador and is divided into 2 main blocks: 1) the Saglek block to the north (>3.85-3.1 Ga); and 2) the Hopedale block to the south (ca. 3.2-2.8). These blocks are interpreted to represent separate Archean cratons, which appear to have different geological and metallogenic histories. The Saglek and Hopedale blocks were not thought to have been juxtaposed until the Late Archean (Connelly and Ryan, 1996). Evidence of the suture between them has been obscured by the Mesoproterozoic intrusion of the Nain Plutonic Suite. The Saglek block is dominantly a terrain of upper-amphibolite to granulite facies quartzo-feldspathic gneisses. The Hopedale block is dominantly greenschist to amphibolite facies quartzo-feldspathic gneisses containing extensive metavolcanic supracrustal rocks. This terrain

contains two distinct northeast trending greenstone belts, the Florence Lake and Hunt River (Wardle and Wilton, 1995).

The southeastern Churchill Province is situated between the Nain and Superior Provinces and includes a core of remnant Archean rocks originally termed the Rae Province (Hoffman, 1988), though now is referred to as the "core zone". The core zone is bounded to the west by the New Quebec Orogen and to the east by the Torngat Orogen (Taylor, 1979; Hoffman, 1990; Wardle and Wilton, 1995; James et al., 1996a). The New Quebec Orogen welds the Churchill province to the Superior Province and is composed predominately of low-grade metavolcanic and metasedimentary rocks (Hoffman, 1988; Wardle et al., 1995). The Rae Province contains reworked Archean gneisses, Paleoproterozoic supracrustal rocks and deformed granitic plutons (1.83-1.81 Ga, Wardle et al., 1995). The Torngat Orogen dominantly consists of Paleoproterozoic supracrustal rocks, reworked Archean granitoid gneisses, and variably deformed granitoid gneisses (Wardle et al., 1995; van Kranendonk and Wardle, 1996). The collision began at ~1880 Ma and post-collisional tectonism and metamorphism lasted until ~1740 Ma (Bertrand et al., 1993; van Kranendonk and Wardle, 1996). The Abloviak shear zone marks the last collisional movement of the two cratons between 1845-1820 Ma (van Kranendonk, 1996).

The Mesoproterozoic was marked by extensional tectonism and the intrusion of anorthositic-mangerite-charnokite-rapakivi granite complexes (AMCG) into the Nain, Churchill and Grenville Provinces of Northern and central Labrador (Ryan et al., 1995; Emslie et al., 1994; Wardle, 1995).

1.2.2 Tectonic and Magmatic Evolution

The tectonic evolution of Labrador, particularly the northern segments, is significant for this thesis in terms of constraining the processes that formed the Paleoproterozoic metaplutonic rocks. In addition, the genesis of mineralization (i.e. Ni-Cu-Co deposits) is undoubtedly linked to magmatism and tectonism in the area. For these reasons a brief overview of the tectonic and magmatic evolution of the Nain Province (with emphasis on the northern segments), the eastern Churchill Province, the Torngat Orogen and the Nain plutonic suite is given below.

1.2.2.1 Tectonic and Magmatic Evolution of the Nain Province (pre-Torngat Orogen)

The Nain Province (cf. Taylor, 1971) contains some of the oldest continental crust on Earth (ca. 3.9-3.7 Ga; Collerson, 1991). Consequently the geology of this area is better documented than much of Labrador. It has been proposed that the Nain Province represents a heterogeneous collage of Archean terrains, each recording a different magmatic, sedimentary, tectonic and metamorphic history prior to assembly at 2.7-2.8 Ga (Schjøtte et al., 1990). This section will focus on the evolution of the Nain province prior to the ca. 1880 development of the Torngat Orogen (Bertrand et al., 1993).

There are two main blocks that constitute the Nain Province, the Saglek and Hopedale (Figure 1.3). The Saglek block is older, and thus has a longer geologic history (>3.2-2.5 Ga), including the preservation of very old zircon cores in Nanok gneisses (>3.9 Ga, Schjøtte et al., 1989a; Collerson, 1991; Connelly and Ryan, 1992, 1994). The Saglek block preserves metamorphic conditions at the level of upper amphibolite to granulite

facies. Besides the Nanok gneisses, another very old unit is the ca. 3.8 Ga Nulliak supracrustal sequence. The Nulliak are intruded by and likely related to the 3732 \pm 6 Ma Uivak I gneisses (Schiøtte et al., 1989; Nutman et al., 1989; Nutman and Collerson, 1991). Following metamorphism and migmatization of the Uivak I gneisses, the igneous precursor of the Uivak II gneiss formed at ca. 3620 Ma (Schiøtte et al., 1989a, b, 1990). All of these units (Nanok, Nulliak, Uivak I and II) were subjected to ca. 2.8-2.7 Ga regional scale granulite facies metamorphism (Schiøtte et al., 1989a, b, 1990).

The Hopedale block is generally younger (ca. 3.3-3.2) than the Saglek Block and preserves metamorphism at grades of amphibolite rather than granulite facies (Wardle and Wilton, 1995). The oldest components are the 3105 \pm 2 Ma Hunt River Group, the 3258 - - 24 Weekes Amphibolite and the ca. 3105 Ma Maggo gneisses (Ryan, 1984; Ermanovics 1993; James et al., 1996b, 1997; James, 1997). The Weekes amphibolite forms small enclaves in the Saglek block, they also occur in the Hopedale Block but in lesser amounts (Wardle and Wilton, 1995). The Hunt River group comprises a 'greenstone' belt, dominated by metagabbroic and metavolcanic rocks. Sheets of amphibolite, thought to represent dykes, intruded into the Maggo gneisses and are called the Hopedale Dykes (Ermanovics, 1993). The block experienced a regional, metamorphic, migmatitic and deformational event ca. 3.1-3.0 Ga, which is considered to be part of the Hopedalian structural event (Finn, 1989; Ermanovics, 1993). Subsequent to this tectonism, the Florence Lake greenstone belt formed between 3002 \pm 2 and 2979 Ma (Ermanovics, 1993). It consists dominantly of mafic flows, pillow lavas and mafic subvolcanic intrusives (Brace and Wilton, 1991; Wardle and Wilton, 1995). Both the Florence Lake and Hunt River belts were intruded by the Kanairiktok Intrusive suite of

tonalite-trondjemite-granodiorite rocks from 2858 \pm 4 Ma to 2383 Ma (Ermanovics and Raudsepp, 1979; Loveridge et al., 1987; Ermanovics, 1993). The region was then subjected to large-scale deformation and metamorphism in the Fiordian event from 2825 \pm 20 Ma to ca. 2550 Ma (Finn, 1989; Ermanovics, 1993; Wardle and Wilton, 1995).

Though they are distinct blocks, there is evidence to suggest a possible genetic link between the Saglek and Hopedale prior to amalgamation. The volumetrically minor 3200-3260 Ma Lister gneisses of the Saglek block (Schjøtte et al., 1991) could represent the same magmatic event as the ca. 3260-3100 Ma Maggo gneisses of the Hopedale block (Loveridge et al., 1987; Schjøtte et al., 1991). Crustal processes in the Archean are not as well defined as those in the Phanerozoic, and it is thus difficult to determine how closely the amalgamation of these terrains resembled present day crust-forming events. It is clear, however, that prior to amalgamation the Hopedale and Saglek blocks had largely different histories.

Following collision of the Saglek and Hopedale block between 2578 \pm 3 Ma and 2549 \pm 3 Ma, the two blocks shared the same history, which included widespread deformation and metamorphism, and emplacement of mafic dykes and mylonization (Connelly and Ryan, 1994). There was also a period of dyke swarm activity, which included the emplacement of ca. 2450-2200 Ma Napaktok and Domes dykes into the Saglek block, and the ca. 2235 \pm 2 Ma Kikkertertevak dyke swarm into the Hopedale block (Ermanovics et al., 1989; Ermanovics and van Kranendonk, 1990; Ryan, 1990a; Cadman, et al., 1993; Ryan et al., 1995). The Saglek block was then intruded by less abundant, fluorite-bearing granites between ca. 2.1 to 2.0 Ga (Emslie and Loveridge,

1992). Subsequently, the block was intruded by anorthosites, granites and basic dykes from 2135-2045 Ma (Ryan et al. 1997, 1998; Hamilton, 1997; Hamilton et al., 1998)

Following this magmatic activity ca. 2.0 Ga, there was a period of erosion and then deposition of supracrustal rocks. The northern Nain craton (Saglek block) was buried beneath the sedimentary and volcanic rocks of Ramah, Mugford and Snyder Groups (Smyth and Knight, 1978; Wardle and Wilton, 1995; Hamilton, 1994). On the southern Nain craton (Hopedale block), deposition of sedimentary and mafic volcanic rocks of the Moran Lake, Ingrid and Lower Aillik Group occurred (Gower et al., 1982; Ryan, 1984; Ermanovics, 1993; Wardle and Wilton, 1995).

1.2.2.2 Tectonic and Magmatic Evolution of the Eastern Churchill Province and Torngat Orogen

The southeastern Churchill Province and the Torngat Orogen are of regional importance for several reasons, namely (a) they shed light on the tectonic evolution of the area, (b) they may have played a role in the formation of the Nain Plutonic suite, and (c) Paleoproterozoic structures of the Churchill Province and Torngat Orogen may have controlled the location of the Voisey's Bay deposit during the Mesoproterozoic (Evans-Lamswood, 1999, Evans-Lamswood et al., 2000).

The southeastern Churchill Province formed during the oblique collision of Nain and Superior cratons during the Paleoproterozoic. It is considered a composite terrane of strongly reworked Archean and Proterozoic rocks, with three main divisions: (1) a central terrane of reworked Archean gneisses termed the core zone; (2) the New Quebec Orogeny

which welds the Rae Province to the Superior craton and (3) the Torngat Orogen, which welds the Rae province to the Nain craton (Wardle et al., 1995).

The Torngat Orogen represents a north-south trending, deeply exhumed root of the transpressional collision between the Nain and Churchill (Rae) Provinces (Korstgaard et al., 1987; Mengel, 1988; Wardle et al., 1990; van Kranendonk et al., 1994; van Kranendonk and Wardle 1997). The orogen comprises four major domains which are from west to east: the Lac Lomier complex, the Burwell Domain, a reworked part of the Nain Province that forms some of the Torngat foreland, and the Tasiuyak gneiss complex (Figure 1.3, Wardle et al., 1995).

The Lac Lomier complex is dominantly composed of Archean granitoid gneisses interlayered or mixed with Paleoproterozoic supracrustal rocks (Lake Harbour Group). It was intruded by now-deformed and metamorphosed orthopyroxene-bearing tonalite to granodiorite plutons. Similar metaplutonic rocks are present in the Tasiuyak gneiss complex (van Kranendonk and Ermanovics, 1990; Ermanovics and van Kranendonk, 1990; van Kranendonk et al., 1992).

The northern segment of the Torngat Orogen is structurally complex due to the presence of the wedge-shaped Burwell Domain. This domain is composed dominantly of Paleoproterozoic (meta) plutonic rocks of calc-alkaline composition that intrude pelitic gneisses similar to the Tasiuyak Paragneiss. The rocks vary from east to west across the domain. In the western section of the Burwell domain, the metaplutonic rocks are an extensive package of orthopyroxene-bearing tonalite to granodiorite (referred to as charnockitic), which formed between 1885-1869 Ma with peak magmatism occurring at 1895-1885 Ma (Scott, 1995b; Scott and Machado, 1995). They are preserved as tectonic

slices, or intrusive sheets, although contacts are often obscured (Campbell, 1997), and they are retrogressed from granulite to amphibolite facies. The eastern metaplutonic rocks were intruded into the eastern Burwell domain between 1910-1864 Ma (Scott and Machado, 1995). They are mildly deformed, homogenous bodies, ranging in composition from dioritic to granodioritic with a few granitic rocks. Surviving orthopyroxene is commonly rimmed by amphibole (Campbell, 1997; Scott, 1998).

The third domain is the western Nain Province within the Torngat Orogen, which is composed dominantly of Archean migmatitic, granulite facies tonalitic orthogneisses. The gneisses are intruded along their western margin by the Paleoproterozoic Hutton anorthosite body and by metaplutonic rocks similar to the Burwell Domain (van Kranendonk et al., 1992; Wardle et al., 1994; Wardle et al., 1995). These gneisses, along with interleaved Hutton anorthosite and the Paleoproterozoic metaplutonic rocks present on the western margin of the Nain Province, were deformed in the Kormaktorvik shear zone, which represents intense deformation ca. 1791-1710 Ma, primarily between 1798-1740 Ma (van Kranendonk and Scott, 1992; Bertrand et al., 1993; Scott and Machado, 1995). This shear zone is interpreted as either a tectonic boundary between the western margin of the Nain province and the Burwell domain (Hoffman, 1988, 1990), or as a long-lived crustal weakness within the Nain Province that was reactivated during the Torngat Orogeny (Scott 1995b, van Kranendonk and Wardle, 1996).

The Tasiuyak gneiss complex is dominated by an extensive package garnet-sillimanite-biotite-graphite bearing metasedimentary (pelitic) paragneisses, which are locally sulphide-rich (Wardle, 1983). This unit extends the length of the Torngat Orogen and was deposited after 1940 Ma and prior to 1895 Ma; it has been interpreted as a lateral

equivalent of the Lake Harbour Group (van Kranendonk et al., 1992; Scott and Gauthier, 1996). It has also been suggested that the protolith of the Tasiuyak paragneiss was derived from a sequence of turbidites, with a source of mixed Archean and Proterozoic age; this source was different than either of the sources for the Lake Harbour Group or the Ramah Group (van Kranendonk and Wardle, 1996). Evidence from the southern part of the orogen suggests deposition of the Tasiuyak precursors on the eastern margin of the Rae craton (Wardle 1984; Feininger and Ermanovics, 1994), while in the north it has been suggested that the Tasiuyak represents off shore trench deposits along the Nain craton (Scott and Machado, 1994). Based on Nd isotope and age dating, it has been suggested that the Tasiuyak gneiss represents an accretionary prism that may have formed on both the Rae and Nain cratonic margins, and were subsequently juxtaposed (Scott and Machado, 1994; Theriault et al., 1994; Theriault and Ermanovics, 1997; van Kranendonk and Wardle, 1996, 1997). South of the Burwell Domain, the Tasiuyak paragneiss is intruded by now-deformed, Paleoproterozoic (c. 1880 Ma), calc-alkaline orthopyroxene-bearing metaplutonic rocks, ranging in composition from tonalite to granodiorite. The metaplutonic suite has been referred to as the enderbite suite (van Kranendonk and Ermanovics, 1990; Bertrand et al. 1992, Theriault and Ermanovics, 1997), interpreted to represent the deep roots of a magmatic arc that extended northward, including similar calc-alkaline rocks in the Burwell Domain (Wardle et al., 1992; Campbell, 1997). The Tasiuyak gneiss is coincident with the Abloviak shear zone over most of its length. The Abloviak is a major, granulite facies, sinistral shear zone that formed ca. 1845-1822 (Bertrand et al., 1993). It is interpreted as the focal point of collisional deformation and within the shear zone forms a homogenous unit of mylonized rock (Wardle et al., 1995).

The Torngat Orogen developed over a period of 130 million years. The early stages of the Torngat Orogen began with the onset of calc-alkaline magmatism at 1910-1840 Ma, which is interpreted to be arc related (Bertrand et al., 1993; Scott, 1995a, Scott and Machado, 1995; Campbell, 1997). This was followed by crustal thickening and nappe tectonism as a result of continental collision of the Nain and Churchill provinces at 1870-1853 Ma (Bertrand et al., 1993; Scott and Machado, 1995; Scott 1995a, b). During continued oblique collision, resulted in the onset of granulite facies, sinistrial, transpressional tectonism, which developed two major shear zones. The Abloviak shear zone is a sinistrial, transcurrent shear zone, which formed ca. 1845-1820 Ma and is believed to mark the present day location of the Nain-Churchill boundary (Bertrand et al., 1993). The less extensive, Kormaktorvik shear zone is an oblique-sinistrial shear zone that was mainly active from 1798 to 1740 Ma (Bertrand et al., 1993, Scott, 1995a). The reworked Archean Nain gneisses in the Abloviak shear zone boundary were intruded by ca. 1806 granitoid stocks (Bertrand et al., 1993). During crustal thickening there was the development of east-verging fold and thrust belts within the Ramah Group and Nain Province basement (Calon and Jamison, 1992, 1994). A thin mylonitic zone formed during re-activation of the Nain-Tasiuyak gneiss boundary zone (primarily in the central and southern areas) ca. 1794-1786 Ma (van Kranendonk and Wardle, 1996). This boundary zone was subjected to large scale uplift and thrust faulting, particularly, sub-vertical, west-side up, crustal faults during the latter stages and subsequent cooling of the orogen (Mengel et al., 1991; Bertrand et al., 1993; van Kranendonk and Wardle, 1996).

1.2.2.3 The Nain Plutonic Suite – Magmatic Evolution and Genesis

The Nain Plutonic Suite (NPS) forms a volumetrically significant (~19,000 km²) igneous province in Labrador. The association of the Voisey's Bay Ni-Cu-Co deposit with troctolitic components of the NPS warrants an overview of its characteristics and origin.

Ryan and Morse (1985) introduced the name NPS for the composite suite of dominantly anorthosite and granite with subordinate troctolite and diorite intrusions that were spatially and temporally related (1350-1290 Ma) in Labrador. Pioneering, early work on the NPS was carried out by E.P. Wheeler II and forms the basis of the present understanding of the geologic units (Wheeler, 1942, 1960). This work was extended by S.E. Morse during the Nain Anorthosite Project, which focussed on the Nain area from 1971-1981, and with his contributors (J. Berg, R.A. Weibe, R.F. Emslie) produced a considerable amount of knowledge. More recently the work of B. Ryan has provided a synthesis and more detailed subdivision of the NPS, while M. A. Hamilton has provided much needed geochronological information. Since the discovery of the Voisey's Bay deposit, there has been a substantial amount of new information generated by government surveys and exploration companies active in the area.

Much of this work has resulted in the definition of four major components of the NPS and in detail, numerous specific intrusion or intrusive complexes. The four main subdivisions are: 1) anorthositic rocks; 2) granitic rocks; 3) ferrodioritic rocks; and 4) troctolitic rocks (Ryan, 1990b, 1995).

The anorthositic rocks are volumetrically significant and form over several hundred plutons in the NPS. These rocks are predominately plagioclase cumulates with

intercumulus orthopyroxene, and range in composition from anorthosite to leuconorite with minor local leucogabbro and leucotroctolite (Ryan, 1995). These plutons reflect an array of emplacement styles from solid state diapirs with foliated margins, to magmas that crystallized in situ with preserved sub-ophitic textures (Emslie, 1975; Ryan et al., 1995; Ryan, 1995). Examples from this group are: the Mount Lister Intrusion, Kikkertavak Island pluton, Pearly Gate Intrusion, and Bird Lake Massif.

The granitic rocks are comparable in volume to the anorthositic units. They are similar to rapikivi granites of Finland (Emslie and Stirling, 1993), which likely formed from high temperature, water-poor magmas. Older intrusions are generally fayalite- and orthopyroxene-bearing quartz monzonite, while younger intrusions are hornblende-biotite granite (Emslie et al., 1994; Ryan et al., 1995). Examples of these intrusions include the Makhavinekh Lake pluton, Dog Island granites and Umiakovik Batholith.

The ferrodioritic rocks are dominantly small plutons and dykes, and are interpreted to represent the residual liquids from the anorthosite crystallization (Wiebe, 1990; Emslie et al., 1994; Hamilton, 1997). These rocks exhibit a range of textures from well-layered, cumulate to massive plutons, while others form pillows, interpreted as near-liquid compositions in granitic rocks (Wiebe, 1980; Weibe, 1990; Emslie et al., 1994). Examples of these intrusions include the Ukpaume intrusion, the Cabot Lake intrusion and the Tigalak intrusion.

The troctolitic group is dominated by layered plutons of troctolite with minor olivine gabbro (Ryan, 1995; Ryan et al., 1995). The Kiglapait is the best known example (Morse, 1969). It is a funnel-shaped intrusion that contains recognisable floor cumulates and downward-crystallized roof sequences (Morse, 1969; Ryan, 1995; Ryan et al., 1995).

Other examples are the Hettasch intrusion, the Barth Island intrusion and the Voisey's Bay troctolite intrusion.

The NPS intruded in a series of temporally distinct pulses (Ryan et al., 1991; Hamilton, 1997). Magmatism began in the west and migrated eastward (Berg et al., 1994) lasting from ca. 1350-1290 Ma (Ryan and Emslie, 1994). The currently accepted model was proposed by Emslie et al. (1994) to explain the formation of the NPS and most AMCG suites in general, based on field, geochemical and isotopic data. The model contends that formation of the NPS occurred in an anorogenic, upper mantle-lower crustal area associated with basaltic mantle plumes or 'hot spots'. The granitoid rocks are believed to be the oldest members of the suite. As they formed by partial melting, their separation from lower crustal source region as magmas left a hot lower crustal pyroxene-plagioclase rich residue depleted in SiO₂, K, Rb, Ba, Zr, Pb, U and REE and enriched in Ca, Al, Sr, Eu and Ti (Emslie and Hegner, 1993; Emslie and Stirling, 1993; Emslie et al., 1994). Subsequent mantle-derived basalt magmas became contaminated by this residue, which was easily melted due to its already high temperature (Emslie et al., 1994). The result was the production of plagioclase-rich anorthositic magmas, which would have been very buoyant and readily rose to high crustal levels. Fractionation of the anorthositic magma resulted in production of Fe-rich residual liquids that were denser than the anorthosites, and thus easily separated from them (Emslie et al., 1994). These Fe-rich liquids would intrude as bodies of ferrodiorite and troctolite.

1.3 PRESENTATION OF STUDY AREA – VOISEY’S BAY, LABRADOR

1.3.1 Introduction

The Voisey’s Bay area of Labrador is characterized by the tectonic contact between the Nain-Churchill Provinces and the intrusion of the Nain Plutonic Suite, which hosts the Voisey’s Bay Ni-Cu-Co deposit. This section presents a brief introduction to the localized geology of the study area, addresses previous work and outlines outstanding problems.

1.3.2 Previous Work and Outstanding Problems

Prior to the discovery of the Voisey’s Bay deposit, little was known about the geology of the Voisey’s Bay area. Ryan and Lee (1985) had regionally mapped the area and, in combination with data from Wheeler (1942, 1960) and Morse (1969), Ryan (1990), created a regional map. Since the discovery of the deposit, much research has focused on the deposit and the derivation of a genetic model for formation of this type of ore. This research on the troctolitic intrusion and the associated deposit is described in detail by numerous authors (including, Ryan, 1996; Naldrett et al. 1996; Evans-Lamswood, 1999; Li and Naldrett, 1999; Evans-Lamswood et al. 2000). Most of the previous petrological, geochemical and mineralogical studies on the deposit and host rocks are addressed in the third chapter of this thesis. Particularly noteworthy are studies by Lambert et al. (1999), Ripley et al. (1999), Amelin et al. (2000), Ripley et al. (2000), Scoates and Mitchell (2000), Li et al. (2000), Brennan and Li (2000), Naldrett et al. (2000a, b) and Lambert et al. (2000).

Though much insight has been gained with regard to the deposit and troctolitic bodies in the area, little was known of the surrounding rocks, particularly the gneissic units. This left many questions surrounding the tectonic development of the area prior to emplacement of the Nain Plutonic Suite. In addition, since the discovery of the Voisey's Bay deposit, there have been no subsequent discoveries of any economically viable sulfide deposit, which implies that though an general understanding of the genesis of these deposit types has been attained, there are still many unanswered questions.

1.3.3 Brief Outline of the Local Geology

In the Voisey's Bay area, three main gneissic units are recognised (Map 1, back pocket). To the east, are granulite facies, heterogeneous, quartzo-feldspathic gneisses alternating with amphibolitic and gabbroic gneisses, which are interpreted as Archean orthogneisses belonging to the Nain Province. They have been cross cut by at least two sets of mafic dykes, subjected to several deformational events, and contain numerous tectonic fabrics. To the west, lies the Tasiuyak gneiss complex comprising of interbanded garnet-sillimanite and sulphide-, graphite-bearing paragneiss that is part of the Churchill Province. Between these two gneissic units, lies a belt of homogenous, metagabbroic through to metadioritic and metatonalitic, upper amphibolite to granulite facies, orthogneisses that are referred to in this thesis as Paleoproterozoic metaplutonic rocks. This group includes the less extensive group of gneisses that have previously been referred to as the enderbitic gneiss by Ryan (2000) and others: an explanation of the terminology is addressed in more detail in the subsequent chapters. These metaplutonic gneisses are interleaved and deformed with belts of anorthosite, amphibolite and various

metasedimentary units (dominantly quartzite and metapelite). The metasedimentary units are also particularly abundant along the margin of the eastern contact of the metaplutonic rocks with the Archean Nain orthogneisses.

Following collision of the Nain and Churchill provinces, the gneisses of this area were intruded by the Nain Plutonic Suite. Based on intrusive contacts and published geochronological data, the following timing of intrusion is assumed. The volumetrically minor, Voisey's Bay troctolitic intrusion with minor amount of gabbro was emplaced at 1332 ± 1 Ma (Amelin et al., 1999). This was followed by the extensive Makhavinekh granite, to the west of the study area, at 1322 ± 1 Ma (Ryan, 1991, Ryan et al., 1991). The Makhavinekh granite was subsequently intruded by the Ikadlivik anorthosite complex, though the timing of this event relative to other intrusions is not known. Intrusion of the Mushuau troctolite followed: it comprises a layered body of alternating leucotroctolite and melatroctolite with minor amounts norite, olivine norite and troctolite. The southern and central intrusive bodies straddle the contact between the Paleoproterozoic metaplutonic rocks and the adjacent metasedimentary gneisses. A leucotroctolite of this intrusion has been dated at 1317 Ma, while a melatroctolite layer was dated at 1313 Ma (Amelin et al., 2000). At the same time or afterwards, the western margin of the study area was intruded by extensive Kangeklualuk Anorthosite. At 1305 ± 0.8 Ma, the Voisey's Bay troctolite intrusion and the Kangeklualuk Anorthosite were intruded by subhorizontal, sheet-like bodies of granite and syenite, referred to as the Voisey granitic suite (Amelin et al. 1999). The detailed geometry of the Voisey's Bay troctolite and the associated deposit is addressed in chapter three.

1.3.4 Thesis Goals

This thesis presents a geological mapping, geochemical, isotopic and geochronological study of Paleoproterozoic metaplutonic rocks of the Voisey's Bay area of Labrador, Canada (Map 1). The overall goals of this study are to define and characterize this belt of rocks in order to (1) identify their igneous origin and the tectonic processes involved in their formation; and (2) discern the role they may have played in crustal contamination of the parental magmas of Voisey's Bay Ni-Cu-Co deposit. The thesis has been broken down into several components, which include:

- a) A field and petrographic description of the lithological elements of the metaplutonic rocks, including a detailed field map of the area, in order to adequately describe the nature and distribution of the constituent units.
- b) Extensive geochemical (major and trace element), isotopic (Sm-Nd, Rb-Sr, Pb-Pb) analyses of the compositions of the metaplutonic suite to define variations within and between units and geochemical constraints on formation of these rocks
- c) Geochronological data to provide information on the age of plutonic activity, the timing of tectonic activity in the area, and the age of potential contaminants or source rocks (through inherited zircon cores).
- d) Geological synthesis, combining all of these observations to construct a large-scale tectonic evolution model of the Paleoproterozoic of northern Labrador.

1.3.5 Field Component of the Project

The aim of the field component was to provide a detailed (1:10 000) map of the Voisey's Bay area, with particular attention to defining the distribution of gneisses in the area. The field work was carried out in August, 1999 and from June to mid-August, 2000, with the logistical support of Voisey's Bay Nickel Company. In addition to detailed geologic mapping, four drill core holes from Voisey's Bay Nickel Company were logged, in order to assess variations with depth in units of the metaplutonic suite. Samples were collected for geochemical, isotopic and geochronological analysis in order to characterise the lithological units in the area, with particular emphasis on the Paleoproterozoic metaplutonic rocks.

1.4 METHODOLOGY

1.4.1 Introduction

The main goal of this study is to understand the origin of the Paleoproterozoic metaplutonic rocks, and to define their implications for Paleoproterozoic tectonism. In combination with geological mapping, several laboratory methods were applied to achieve this end.

Major and trace element geochemistry in combination with geochronology and radiogenic isotope studies (Sm-Nd, Rb-Sr, and Pb-Pb), provide a valuable means to address these problems. This study employs these studies. The following is a brief discussion of the use and applicability of each of these methods.

1.4.2 Major and Trace Element Geochemistry

1.4.2.1 Introduction

Major and trace element geochemistry and provide insight into the petrological and petrogenetic magmatic history of plutonic rocks. The chemical composition and mineralogy of the parental source regions exert considerable control over the chemistry of magmatic rocks (Rollinson, 1993). This is also true of crustal contaminants in a magma.

This study evaluated the major element, trace element and rare-earth-element (REE) geochemistry of the Paleoproterozoic metaplutonic suite. In order to (1) identify petrogenetic controls on the source region of igneous precursor of these rocks including any likely crustal contaminants; and (2) decipher the role the Paleoproterozoic metaplutonic suite may have played in contamination of the parental magma of the Voisey's Bay deposit.

The geochemical analyses were carried out at Memorial University of Newfoundland. The major and trace element chemistry was completed by analysis of pressed-powder pellet by X-ray Fluorescence (XRF) using the method of Longrich (1995). The trace element and REE element analyses were done by inductively-coupled-plasma mass spectrometry (ICP-MS) using the HF-HNO₃ preparation method of Jenner et al. (1990). Analytical details (sampling protocol, elements analysed, analytical method and precision and accuracy) are given in Appendix A.

1.4.2.2 Discrimination Diagrams

Firstly, to interpret the geochemistry of these rocks, the major and trace elements were plotted on discrimination diagrams to identify particular geochemical affinities.

There exists a myriad of discrimination plots that are useful for the classification of igneous rocks. Plots used in this thesis include: the QAP plot of LeMaitre (1989), the Anorthite-Albite-Orthoclase plot of Baker (1979), the AFM plot of Irvine and Barager (1971), Jensen's (1976) cation plot, and Pearce et al.'s (1984) Rb-Y-Nb plot. Most of these plots were developed for basaltic rocks; however, they can be applied to igneous rocks for a relative understanding of the chemical behaviour. It is important to note, however, that not all the trends on discrimination diagrams are geologically meaningful (Rollinson, 1993).

The QAP and Anorthosite-Albite-orthoclase diagrams are utilised to identify and characterise compositional variations within the metaplutonic suite. The AFM diagram and the cation plot are utilised to identify calc-alkaline versus tholeiitic trends in igneous rocks. The mobilisation of elements due to alteration is poorly represented on the AFM diagram, which is a concern for metamorphic rocks. The Rb-Y-Nb diagram separates syn-collisional and volcanic arc granites based on the relative amounts of these elements. As Rb is relatively mobile, this diagram is also susceptible to variations caused by alteration.

1.4.2.3 Bivariant Diagrams

Variations diagrams of SiO_2 versus the major elements (Harker diagrams), trace elements and trace element ratios were utilised to visualise fractionation trends and magmatic relationships of the Paleoproterozoic metaplutonic rocks.

In this thesis, major element Harker diagrams were utilised, which included the following elements: Al_2O_3 , Na_2O , Fe_2O_3 , K_2O , CaO , MgO , MnO , TiO_2 and P_2O_5 .

Selected trace elements and trace element ratios were also plotted against SiO_2 , including: Ba, La, Rb, Sr, Nb, Eu, Y, Th, Ni, V, Sc and the ratios: Rb/Sr, La/Yb, La/Y, $\text{K}_2\text{O/Rb}$. These diagrams served to identify fractionation trends within the metaplutonic suite and significant chemical differences between the compositional units.

As SiO_2 is the most abundant element, the Harker diagrams can be subjected to false trends based on silica. These include (1) negative trends that reflect an increase in silica relative to other minerals and are not a real fractionation trend; (2) deceptive correlations; and (3) reduced scatter as SiO_2 increases. These limitations are outweighed by the ability of these diagrams to clearly identify chemical trends between compositional varying units.

1.4.2.4 Normalized Rare-earth element and Multi-element Plots

Trace elements are more capable of discrimination between petrogenetic processes than major elements, and thus are useful indicators of the history of a magmatic suite. This is because distribution of trace elements in the crust can be mathematically modelled and ultimately utilised to identify geological processes (Rollinson, 1993).

This study used a combination of chondrite, primitive mantle and MORB normalized REE diagrams and multi-element diagrams, to identify trace element signatures within the Paleoproterozoic metaplutonic unit. Primitive mantle and chondrite normalized diagrams were utilised for interpreting trace-element signatures and the relationship to other metaplutonic suites in the region, while MORB-normalized values were used for comparison with other similarly formed igneous rocks and tectonic environments.

The REE elements can be particularly useful due to their similar chemical behaviour and low mobility with alteration. The REE elements can also be expressed as the degree of fractionation, being the concentration of light REE ratioed to heavy REE $(La/Yb)_N$, in addition to normalized diagrams. The REE element pattern of an igneous rock is fundamentally controlled by the REE chemistry of its source and by the crystal-melt equilibria, through its magmatic evolution (Rollinson, 1993). Thus it is possible to identify the roles of individual minerals on the REE pattern of a magmatic rock (i.e. extreme depletion in heavy REE is likely indicates the presence of garnet in the source region).

Multi-element diagrams are based on the grouping of elements that are incompatible with respect to typical mantle mineralogy. Specific element depletions or enrichments can characterise a specific tectonic environment. For example, a Nb-Ta depletion is characteristic of a subduction-zone component in the source region (Rollinson, 1993), and the lower continental crust is characterized by Th-U depletion, though this may reflect the loss of these elements during granulite facies metamorphism.

Multi-element diagrams allow for discrimination between tectonic environments and comparison with modern analogues. The possibility for enhanced spikes allows for greater contrast in element behaviour than a simpler REE diagram. The similarities and differences between modern arcs and Paleoproterozoic arc magmas are important in this study for understanding the tectonic processes at work during the evolution of the region. Modern arc compositions are characterized by a pattern of increasing concentration with increasing element incompatibility. These diagrams are key to identifying characteristic of a source region or crustal contaminant.

1.4.2.5 Effects of Metamorphism on the Geochemistry

The effects of metamorphism on the geochemical signature of a suite of rocks are of particular importance in this thesis, as the Paleoproterozoic rocks have undergone amphibolite to granulite facies metamorphism. Thus, it is likely that the chemical composition of the metaplutonic rocks is not identical to the protolith composition.

It is possible to interpret the effects of metamorphism by comparing the chemical composition of metamorphosed rocks to their assumed igneous protolith. Granulite facies metamorphism typically results in extreme large-ion-lithophile-element depletion (LILE; Heir, 1965, 1973). Thus multi-element plots that compare metamorphic rocks with equivalent igneous rocks can provide insight into the degree and effects of metamorphism.

Another way of determining the extent of the LILE depletion is to compare the Rb/K ratio of granulite facies rocks. This is a good indicator because Rb responds more sensitively to granulite facies metamorphism than K (Rudnick et al., 1985; Taylor and McLennan). Low potassium rocks (<1 wt. %), in which biotite is the dominant Rb- and also K-bearing phase, show this association most readily because biotite easily breaks down during high grade metamorphism, resulting in a preferential depletion of Rb. Rocks that have higher potassium levels, in which K-feldspar is the dominant Rb- and K-bearing phase, are less sensitive to the Rb loss because K-feldspar is more resistant to breakdown during high grade metamorphism. As a result low-K rocks show a preferential depletion in Rb/K ratios due to granulite facies metamorphism, than do high-K, K-feldspar bearing rocks.

Thus, one can interpret, measure and evaluate the effects of high-grade metamorphism on the chemical composition of the igneous precursors. These tests allow some degree of assurance when interpreting the geochemistry of metamorphic rocks.

1.4.3 Radiogenic Isotopes

1.4.3.1 Introduction

Radiogenic isotopes are capable of providing valuable insights into the petrogenetic history of magmatic rocks. Isotopic data can also constrain the tectonic development of a region by highlighting the relationship between crust-mantle processes, crustal contamination and basement influences (DePaolo, 1988).

One of the main foci of this study was determine what role the Paleoproterozoic metaplutonic rocks may have played in contaminating the Voisey's Bay troctolite, and thus inducing the precipitation of sulfide mineralization. Radiogenic isotopes can be utilised to determine 1) the origin and extent of crustal contamination; and 2) assess the role of crustal contamination in mineralization.

The other main objective of this study was to characterise these Paleoproterozoic metaplutonic rocks in order to determine their igneous origin. Radiogenic isotopes can help highlight sources of magmas; determine whether they result from mantle melting in a subduction zone or anatexis of Archean basement gneisses due to high-grade metamorphism. Isotopic data can also shed light on the overall geologic history of a terrane by dating the sequence of magmatic events.

The Sm-Nd and Rb-Sr analyses were carried out on the thermal-ionization mass spectrometer (TIMS) at Memorial University of Newfoundland and the Pb-Pb analysis were carried out on a multi-collector mass-spectrometer (MC-ICP) at Université de Québec à Montréal, Québec. The analytical details (i.e. sample preparation, analytical method) are given in Appendix A.

1.4.3.2 Sr Isotopes

The Rb-Sr system was developed as a method of determining the age of rocks and minerals but is also used as a tracer for petrogenetic processes (Rollinson, 1993). The Rb-Sr system is based on the decay of ^{87}Rb to ^{87}Sr over time, measured relative to the unradiogenic ^{86}Sr isotope (Faure, 1986).

The $^{87}\text{Sr}/^{86}\text{Sr}$ ratio of mantle source regions changes with time, thus knowledge of the initial $^{87}\text{Sr}/^{86}\text{Sr}$ ratio at the start of the earth is critical to modelling the evolution of this isotopic system. It is generally believed that the crust-mantle evolved from a uniform reservoir (UR) with the Sr isotopic composition of basaltic achondrite meteorites (Rollinson, 1993). This Sr isotopic UR is referred to as BABI (Basaltic Achondrite Best Initial) and is defined as a $^{87}\text{Sr}/^{86}\text{Sr}$ ratio of 0.69897 ± 0.000003 , whereas estimates for the bulk Earth today vary between 0.7045 and 0.7052 (Rollinson, 1993).

The evolution of this system during Earth history is dictated by the fractionation of Rb and Sr during the crust-mantle formation, and by the isotopic ratios of the starting reservoir (Faure, 1986). Thus the time of the appearance of continental crust and depleted mantle plays a critical role in the isotopic modelling of Rb-Sr. The age of ca. 3.7 Ga for

the appearances of both continental crust and depleted mantle has been adopted by several authors to simplify the modelling (Faure, 1986; Rollinson, 1993).

The Rb-Sr system differs from the Sm-Nd system in that the parent-daughter elements are chemically different from each other and fractionate more strongly from each other during melting (Rollinson, 1993). Both Sr and Rb are lithophile, incompatible elements: however Rb is a group I (-1 valence) alkali metal whereas Sr is a group IIA (-2 valence) alkaline earth element (Faure, 1986; Dickin, 1995). This results in large fractionations of Rb and Sr, and thereby large variations in terrestrial Rb/Sr whole rock ratios. The crustal reservoir has higher Rb/Sr ratios than the mantle because Rb is more incompatible than Sr and hence enriched in the crust. Over time the crust has evolved towards higher $^{87}\text{Sr}/^{86}\text{Sr}$ ratios relative to bulk Earth. Conversely the depleted mantle has lower Rb/Sr and $^{87}\text{Sr}/^{86}\text{Sr}$ ratios compared to bulk Earth (Faure, 1986). Due to the large fractionation between these elements and the irreversible loss of Rb from the mantle during formation of the continental crust, the evolution of the Sr isotopes in mantle-crust is system curvilinear (Rollinson, 1993).

Though complex, the Rb-Sr system potentially provides a very distinctive signature for particular sources and igneous processes (particularly crustal contamination) especially in conjunction with Nd-Sm system. Unfortunately, however, the system is limited by the extremely mobile behaviour of Rb during post-magmatic hydrothermal alteration and metamorphism. Though Sr is more robust, radiogenic ^{87}Sr can be mobilised as well, even during low-grade metamorphism (Faure, 1986; Rollinson, 1993). The open system behaviour of the Rb-Sr system is particularly problematic for older rocks that have

experienced high-grade metamorphism, like those in this study. Thus care must be taken when interpreting Rb-Sr isotopic data.

1.4.3.3 Nd Isotopes

The Sm-Nd isotopic system is a useful petrogenetic tool for identifying the sources from which magmas formed and as a method of identifying crustal contaminants (DePaolo, 1988). This method can also be used for geochronological dating. The premise of this system is similar to that of the Rb-Sr, in that a parent isotope (^{147}Sm) decays to a daughter isotope (^{143}Nd); however, the Sm-Nd system is much more robust because Sm-Nd are more resistant to mobilization due to secondary processes such as metamorphism and alteration (DePaolo, 1988; Rollinson, 1993). There is some evidence, however, for fractionation of Sm-Nd during high-grade (granulite facies) metamorphism (Collerson, 1989). This is relevant for the metaplutonic suite of Voisey's Bay, as this has been metamorphosed to a high-grade.

Bulk Earth values for the Sm-Nd system are believed to be represented by chondritic meteorites, which are referred to as the "chondrite uniform reservoir", or CHUR (DePaolo and Wasserburg, 1976; DePaolo, 1988). The Sm-Nd ratios of crust and mantle reservoirs were subsequently fractionated during presumed widespread partial melting of the bulk earth (primitive mantle) to form the crust and depleted mantle (DM, DePaolo, 1988). The Nd isotopic composition of each reservoir evolves as a function of their Sm/Nd ratios due to the radioactive decay of ^{147}Sm to ^{143}Nd (Rollinson, 1993; DePaolo, 1988).

Sm and Nd are both light rare earth elements and almost identical in a chemical behaviour, with the exception that Nd has a larger ionic radius. This difference results in the preferential partitioning of Nd into the melt phase during partial melting of the upper mantle (DePaolo, 1988). This preferential partitioning produces a residual (depleted) mantle with higher Sm/Nd ratios than the continental crust, which formed from the resulting melt. Thus over time, the crustal reservoir is enriched in LREE and has a low Sm/Nd ratio relative to CHUR; while DM reservoir is depleted in LREE and has a Sm/Nd ratio higher than CHUR (DePaolo, 1988). Although, the geochemical dynamics of crust and mantle reservoirs are undoubtedly more complex, this model does provide a method for describing and interpreting the Nd isotopic variations of the crust-mantle evolution (DePaolo, 1988).

The range of $^{147}\text{Sm}/^{144}\text{Nd}$ for terrestrial rocks is rather small from 0.1 to 0.3 (DePaolo, 1988). In combination with the long half-life of ^{147}Sm (10^9 Ga), this results in a relatively narrow range of $^{143}\text{Nd}/^{144}\text{Nd}$ values in rocks. It has therefore become a common practice to describe the $^{143}\text{Nd}/^{144}\text{Nd}$ ratios using epsilon values given by ϵNd (DePaolo, 1988), using the equation:

$$\epsilon\text{Nd}_{(t)} = \left\{ \left[\frac{^{143}\text{Nd}/^{144}\text{Nd}_{\text{rock}, t}}{^{143}\text{Nd}/^{144}\text{Nd}_{\text{CHUR}, t}} \right] - 1 \right\} * 10^4$$

where $^{143}\text{Nd}/^{144}\text{Nd}_{\text{rock}, t}$ is the isotopic ratio of the rock at time t , and $^{143}\text{Nd}/^{144}\text{Nd}_{\text{CHUR}, t}$ is the isotopic ratio of CHUR at time t . The use of this notation allows for the methodical presentation and comparison of Nd isotopes relative to CHUR. Thus the ϵNd values are dependent on the CHUR model and the age of the rock needs to be known.

Based on this convention, ϵ_{Nd} values for CHUR are always 0, independent of age (DePaolo, 1988). In general, rocks derived from a LREE-depleted source (i.e. DM or another mantle reservoir) will have $\epsilon_{Nd} > 0$; while rocks derived from a LREE-enriched source (continental crust or enriched mantle) or rocks affected by crustal contamination will have $\epsilon_{Nd} < 0$. Rocks with ϵ_{Nd} close to 0 could have been derived from a CHUR-like source (primitive mantle) or magmas that represent a mixture of depleted and enriched sources.

Another method of denoting the Sm-Nd isotopic system, used in this thesis, is the fractionation factor (DePaolo, 1988), which is given by the equation:

$$f^{Sm,Nd} = [(^{147}Sm/^{144}Nd_{rock}) / (^{147}Sm/^{144}Nd_{CHUR})] - 1$$

where $^{147}Sm/^{144}Nd_{rock}$ and $^{147}Sm/^{144}Nd_{CHUR}$ are the isotopic values of the rock and CHUR, respectively. The fractionation factor represents the extent of fractionation of the samples relative to CHUR, ultimately providing an estimate of the Sm/Nd ratio of the reservoir rock. By convention the $f^{Sm,Nd}$ of CHUR will always be 0. typical depleted sources (i.e. depleted mantle or another mantle source) have $f^{Sm,Nd}$ values greater than CHUR and typical continental crust or rocks affected by crustal contamination will have values $f^{Sm,Nd} < 0$ (DePaolo, 1988).

As this method of notation is not time integrated it can be strongly influenced by partial melting and fractional crystallization processes (DePaolo, 1988). Thus remelting of a common source region without recycling of Sm and Nd, results in a strong fractionation in Sm/Nd with time, consequently the $f^{Sm,Nd}$ values of that region and rocks derived from it can increase over time.

Distinguishing depleted and enriched sources for the metaplutonic rocks of Voisey's Bay using Nd isotopes is particularly appropriate. The Nd isotopic composition of the two likely end-member sources of the metaplutonic suite, Archean crust and depleted mantle had quite distinct values (approximately -6 to -18 , and $+5$, respectively, Campbell, 1997; and DePaolo, 1988) in the Paleoproterozoic. Thus, this isotope system can potentially provide critical insight into the igneous history of these rocks.

1.4.3.4 Pb Isotopes

The lead isotopic system is a more complex, and potentially more powerful, tracing method than either the Rb-Sr, or Sm-Nd systems. It combines two different decay schemes for U (^{238}U to ^{206}Pb and ^{235}U to ^{207}Pb), which eliminates the need to measure U and is also ultimately insensitive to the loss of U during secondary processes (Faure, 1986). A third decay scheme for Th (^{232}Th to ^{208}Pb) provides a further constraint on lead isotope behaviour. This is important because in general both U and Pb are mobile during secondary processes, particularly in magmatic/hydrothermal situations (Rollinson, 1993). Thus use of the U-Pb isotope system is limited as a direct geochronometer for whole rocks or as a method to constrain initial isotopic composition. Regardless, the Pb-Pb isotopic system may still be a useful indicator for tracing crust-mantle evolution through time.

Variations observed in Pb isotopes on earth are a reflection of the geochemical behaviour of U, Th and Pb during terrestrial differentiation processes over time (DePaolo, 1988). Several isotopic reservoirs have been identified based on lead isotopes. For instance, during early evolution of the Earth, ^{235}U decayed faster than ^{238}U , which

resulted in rapid production of ^{207}Pb . Thus, the abundance of ^{207}Pb is a sensitive indicator of old crust and mantle sources (Rollinson, 1993). In addition, during partial melting of the mantle, Th is slightly more incompatible than U, and Pb is also incompatible but less so than either U or Th, resulting in the U/Pb and Th/Pb values for magmas that are higher than those of their mantle sources (Faure, 1986). Fractionation of U/Pb and Th/Pb ratios also occurs during intracrustal melting. Thus the crust has a different isotopic composition than the mantle, and the lower and upper crust have different isotopic compositions. There is commonly mixing between different crust and mantle reservoirs, which can result in heterogeneous isotopic compositions for magmatic rocks (Gariépe and Dupré, 1991).

The Pb-Pb isotopic system can be particularly useful for determining crustal contamination in magmatic rocks because the concentration of Pb isotopes in the crust is much greater than those in mantle-derived melts. This results in displacement of the isotopic composition of the melt towards crustal values. This occurs to a greater degree in the Pb-Pb system than in the Sm-Nd isotopic systems (Gariépe and Dupré, 1991).

It is common for high-grade metamorphic terrains (i.e. the lower crust) to experience large depletions in Th and U (i.e. Bridgwater et al., 1989; Gariépe and Dupré, 1991). Several theories have been developed to explain this phenomenon, including the removal of U and Th by fluid or melt phase during granulite facies metamorphism (i.e. Touret, 1996). As a result of the lower crustal Th-U depletion over time, old (Archean) granulite facies terranes often possess unradiogenic Pb. Subsequent orogenies may add radiogenic Pb to the lower crust from the upper-crust and mantle-derived sources (Rudnick and Goldstein, 1990).

1.4.4 U-Pb Zircon Geochronology

The U-Pb zircon geochronology was carried out at Memorial University of Newfoundland. Determination of the age igneous crystallization of the metaplutonic suite was done by thermal-ionization mass-spectrometry (TIMS) after the method of Krogh (1973,1982). Determination of the ages of inherited zircon cores was done by laser-ablation-microprobe inductively-couples-plasma mass-spectrometry. Analytical details for both methods are given in Appendix A.

U-Pb geochronology relies on decay of U to Pb in a closed system and is based on the following equations:

$$\frac{{}^{206}\text{Pb}^*}{{}^{238}\text{U}} = (e^{\lambda_{238}t} - 1) \text{ and } \frac{{}^{207}\text{Pb}^*}{{}^{235}\text{U}} = (e^{\lambda_{235}t} - 1).$$

where Pb* represents radiogenic lead only. Minerals that remain a closed system for U and Pb (e.g. zircon) should give concordant values of t when their isotopic concentrations are inserted into the above equations (Dickin, 1995). A locus of concordant ages for both ${}^{238}\text{U}$ and ${}^{235}\text{U}$ decay, will define a curve, termed concordia curve. Zircon is particularly useful mineral for U-Pb geochronology because it is U-rich and widely distributed in intermediate to acidic rocks.

Any initial or 'common' Pb in the zircon is corrected for by measuring ${}^{204}\text{Pb}$ contents in the mineral and then using the ${}^{206}\text{Pb}/{}^{204}\text{Pb}$ and the ${}^{207}\text{Pb}/{}^{204}\text{Pb}$ whole rock ratios to estimate initial ${}^{206}\text{Pb}$ and ${}^{207}\text{Pb}$ (Dickin, 1995). Due to the low levels of common Pb in zircon, it is adequate to estimate the amount of common lead from a general terrestrial Pb evolution model (i.e. Stacey and Kramers, 1975).

Samples with discordance between the $^{206}\text{Pb}/^{238}\text{U}$ and the $^{207}\text{Pb}/^{235}\text{U}$ ratios, are interpreted to have suffered lead loss, which leads to the definition of linear arrays (Dickin, 1995). These arrays have an upper and lower intercept on the concordia diagram, which are interpreted as having a petrologic significance (i.e. igneous crystallization and metamorphism or inheritance). Thus the U-Pb geochronological method provides valuable insight into the petrogenetic history of the rocks. Age relationships are often critical to any model of crustal tectonic evolution of an area, and this is true of the metaplutonic rocks of Voisey's Bay, Labrador.

1.5 STRUCTURE OF THE THESIS

1.5.1 Introduction

This thesis is divided into four chapters, of which chapter 2 and 3 are intended to be publishable papers that focus on particular aspects of this study. Chapter 1 is the introductory chapter that defines the general geologic background of the study, the scope and goals of the research, and briefly outlines the various methodologies used. As chapters 2 and 3 are stand-alone manuscripts, there is a certain amount of unavoidable repetition (i.e. regional setting, geology of the area, references). Chapter 4 is a brief conclusion, which links the work together. The following is a brief outline of chapters 2 and 3.

1.5.2 Chapter 2 - “Southern Extension of the Torngat Orogen: Remnants of a Calc-alkaline Batholith in the Voisey’s Bay area, Labrador” (A.M. Rawlings, P.J. Sylvester, J.S. Myers, G.R. Dunning and J. Kosler)

This paper addresses the field geology, geochemistry, isotopic composition and geochronology of the Paleoproterozoic metaplutonic rocks that occur from Voisey’s Bay to Anaktalak Bay. The paper characterises and defines this package of rocks, provides a general petrological model for their formation, and compares them to similar metaplutonic rocks of the Northern Torngat Orogen. Also addressed are the effects of granulite facies metamorphism on trace element and isotope geochemistry. The data are used to formulate a model for the formation of these rocks and for the tectonic evolution of the region during the Paleoproterozoic.

1.5.3 Chapter 3 – “A New Perspective on the Role of the Paleoproterozoic Metaplutonic Rocks in the Voisey’s Bay Ni-Cu-Co mineralization, Labrador, Canada.” (A.M. Rawlings, P.J. Sylvester and J.S. Myers)

This paper addresses the role that the Paleoproterozoic metaplutonic rocks may have had in triggering sulfide precipitation from the parent troctolite magma of the Voisey’s Bay Ni-Cu-Co deposit. This is accomplished by considering the geographic extent of the metaplutonic suite and comparing their geochemical and isotopic signatures to those of the deposit. The role of these metaplutonic rocks in crustal contamination is of particular interest in understanding magmatic Ni-Cu-Co ore genesis in Labrador.

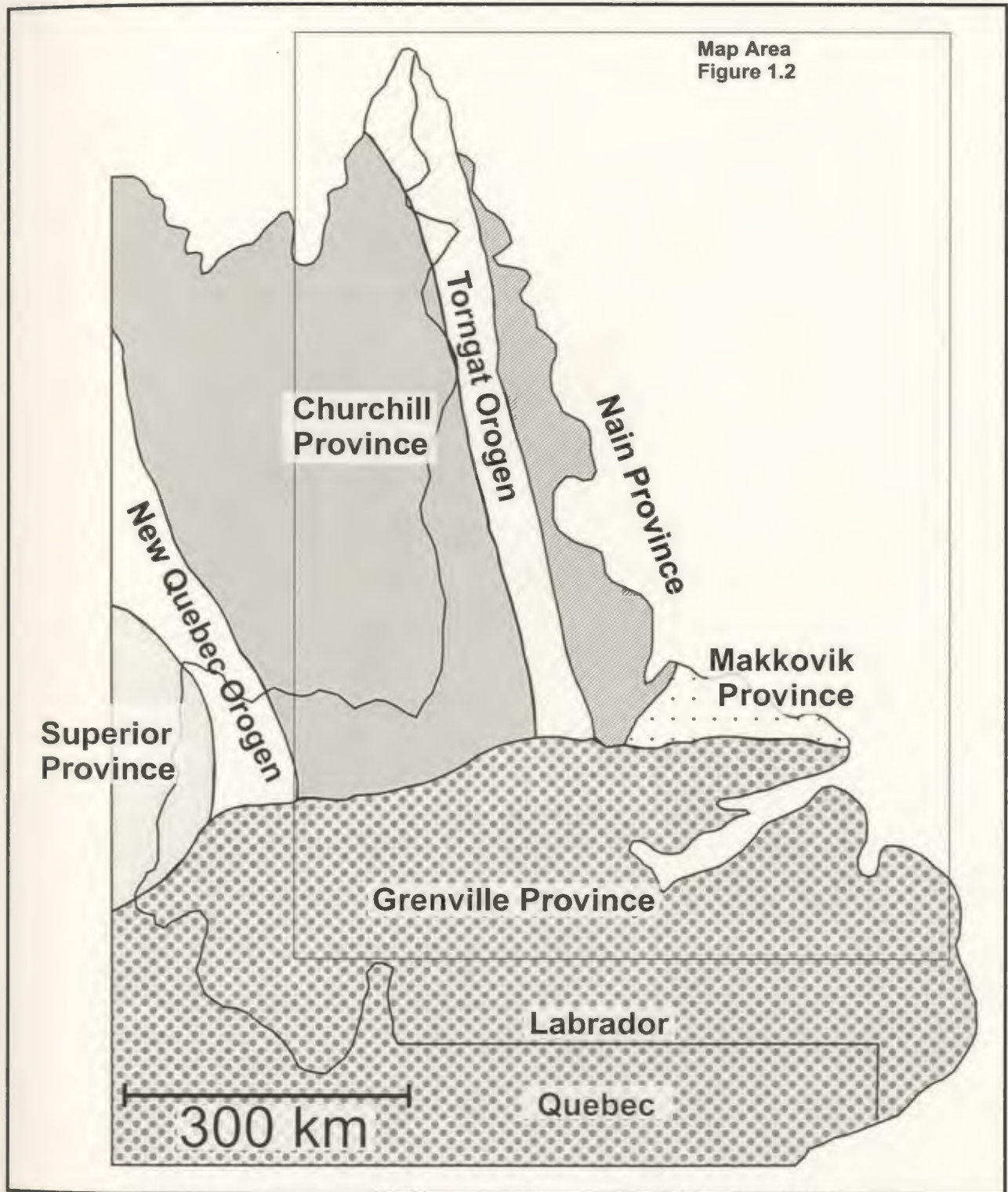


Figure 1.1. Structural Provinces and major tectonic features of Labrador (simplified after Wardle et al., 1997).



Figure 1.2. Simplified geologic map of Labrador, showing the main tectonic provinces, lithotectonic elements and geographic locations mentioned in the text. (Modified after van Kranendonk and Wardle, 1996, and Wardle et al., 1997).

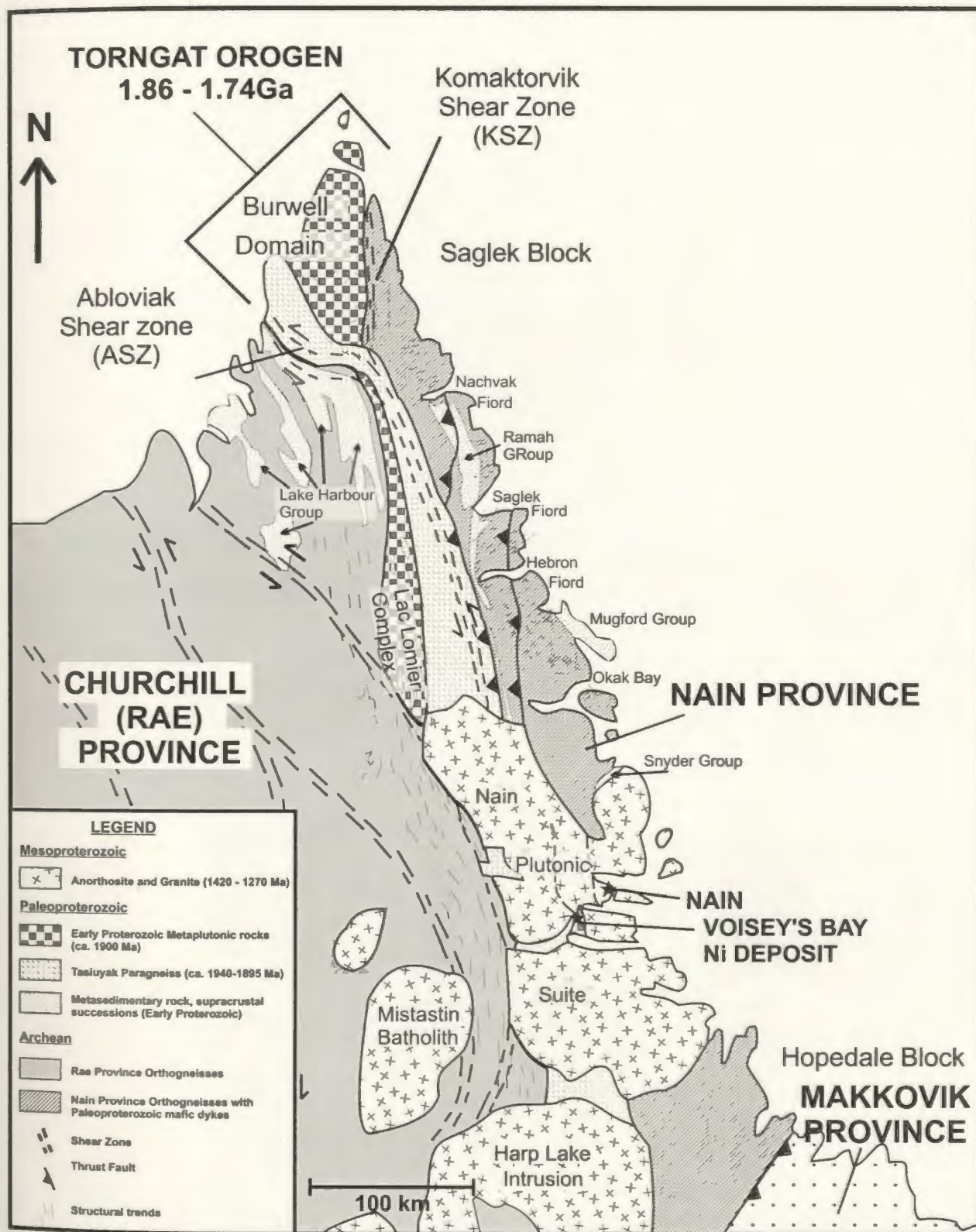


Figure 1.3. Generalized map of the Torngat Orogen, Churchill and Nain Provinces (simplified after van Kranendonk, 1990).

Chapter 2

Southern Extension of the Torngat Orogen: Remnants of a Calc-alkaline Batholith in the Voisey's Bay area, Labrador

2.1 ABSTRACT

The Paleoproterozoic Torngat Orogen of northern Labrador welds the Nain and Rae Archean cratons. A suite of calc-alkaline metaplutonic rocks has been identified in the Voisey's Bay area and these rocks are believed to represent a southern extension of similar metaplutonic rocks identified along the 500 km length of the orogen.

This suite defines a relatively undifferentiated, mafic to intermediate calc-alkaline batholith. The rocks have been metamorphosed to upper amphibolite or granulite facies. Meta-gabbro to meta-quartz diorite compositions of this suite define a magmatic series that probably evolved through fractional crystallization. U-Pb zircon TIMS geochronology yield ages of 1893 ± 1 Ma and 1890 ± 2 Ma for samples of meta-quartz diorite and of meta-hornblende gabbro yield. Based on LAM-ICP-MS analyses, one of these samples contained inherited zircon cores, some 50-100 Ma older than the igneous population, but no Archean cores were found. Meta-tonalite rocks of this suite probably formed during a slightly younger magmatic event dated at 1883 ± 5 Ma. All the compositions are enriched in Ba, Sr, Rb, Zr and Hf; and have negative Nb-Ta anomalies, which are thought to be related to subduction processes. Their REE patterns exhibit fractionation of LREE relative to HREE, with the extent of fractionation increasing with

silica content. This suggests the meta-tonalites had more residual garnet in their source regions than did other members of the suite. The $\epsilon\text{Nd}_{(1.890\text{ Ma})}$ values for the samples range from -0.13 to -5.3 suggesting interaction between the primary magmas and continental crust. The Pb isotopic ratios were 15.160 - 15.834 for $^{206}\text{Pb}/^{204}\text{Pb}$ and 15.000 to 15.145 for $^{207}\text{Pb}/^{204}\text{Pb}$ and suggest that the contaminant formed in the lower crust.

A model for the metaplutonic suite is presented in which the meta-gabbro to meta-quartz diorite series form by partial melting of mantle wedge and interaction with a crustal contaminant either in the source region or lower crust. The meta-tonalites were derived by partial melting of subducting oceanic crust. Thus, crustal genesis by both slab melting and wedge melting in the Paleoproterozoic may mark the transition from Archean to post-Archean processes.

2.2 INTRODUCTION

The north-south trending, Paleoproterozoic Torngat Orogen is the deeply exhumed root of a transpressional collision zone between two Archean crustal blocks, the Nain province to the east and the Churchill (Rae) Province to the west (Figure 2.1; Korstgaard et al., 1987; Mengel, 1988; Wardle et al., 1990; van Kranendonk et al., 1994; van Kranendonk and Wardle, 1997). This granulite to amphibolite facies orogen is one of a number of belts juxtaposing Archean components of Laurentia. These Paleoproterozoic belts provide insight into the mechanics of plate tectonics at that time and allow for comparison to Phanerozoic analogues. Of particular interest is whether Phanerozoic mechanisms for generation of new continental crust along convergent plate margins, i.e. as a result of partial melting of a mantle wedge at a subduction zone, were important during the early Proterozoic. The Torngat Orogen, particularly its northern parts, has been well documented both on structural and geochronologic grounds and thus provides valuable insight into these questions.

The Torngat Orogen is divided into northern (Burwell domain, north of 59°15'N) and southern components (south of 59°15'N to 57°30'N, Figure 2.2). Paleoproterozoic metaplutonic rocks are present sporadically throughout the entire Torngat Orogen and have been interpreted as continental arc magmatism. South of Okak Bay (Figure 2.1), the Torngat Orogen is almost entirely obliterated by the Mid-Proterozoic anorogenic Nain Plutonic Suite. However, a sliver of the orogen dominated by Paleoproterozoic metaplutonic rocks is preserved between Anaktalak Bay and Voisey's Bay. This most southerly exposure provides new insights into (1) processes of crust formation in the early

Proterozoic; and (2) tectonic evolution of the Torngat Orogen, particularly the extent of associated calc-alkaline magmatism.

2.3 REGIONAL GEOLOGY OF THE TORNGAT OROGEN

The Torngat Orogen has been the focus of several large-scale mapping projects. The northern segments of the orogen were first investigated by the Geological Survey of Canada (GSC), especially the team led by Fred Taylor from 1967-1971 (Taylor, 1979), which carried out reconnaissance geology. Subsequent work in the 1990's was carried out by the GSC and the Newfoundland Department of Mines and Energy (NDME). Taylor (1979) recognised that north-eastern Quebec and northern Labrador contained two Archean cratons, the Nain province and Superior province, separated by a region of Paleoproterozoic rocks termed the Churchill Province, which were later named the Southeast Rae Province by Hoffman (1988). Both terms (Churchill and Rae) continue to be used, however, the general consensus is that the term Rae refers to the Archean core craton of the Churchill Province, which also includes Proterozoic rocks formed during the Torngat and New Quebec orogenies. Paleoproterozoic deformation increases in intensity eastward across the Churchill (Rae) Province, including mylonitization of an extensive package of metasediments named the Tasiuyak paragneiss by Wardle (1983). The precursor sediments of the Tasiuyak paragneiss were deposited between 1940 and 1895 Ma and are believed to have formed in an accretionary prism (Scott and Machado, 1994; Scott and Gauthier, 1996).

The southern and central segments of the Torngat Orogen received extensive study during the 1980's. Mapping projects by the NDME were initiated in the areas of Saglek, Hebron and Nachvak Fiords (Ryan et al., 1983,1984; Wardle, 1983,1984; Mengel, 1984, 1985). The GSC was active in the Okak area (Ermanovics and van Kranendonk, 1990; Ermanovics et al., 1989). These projects resulted in several studies aimed at interpreting the structural and metamorphic history of the Torngat Orogen (e.g. Mengel, 1988; Mengel and Rivers, 1990; van Kranendonk and Ermanovics, 1990; Mengel et al., 1991; van Kranendonk & Wardle, 1994; Theriault and Ermanovics, 1997). Based on these studies and additional work on the geochronological and geochemical components of the orogen, several conclusions regarding the main structures, lithotectonic elements and evolution of the southern Torngat Orogen have been reached. As summarised by van Kranendonk and Wardle (1996), the Rae province margin was subjected to arc magmatism ca. 1880 Ma from Nachvak Fiord to Nain (Figure 2.1) and following this, the Torngat Orogen evolved in three tectono-metamorphic events: 1) Oblique collision of the Nain and Rae provinces (ca 1860 Ma); 2) formation of the Abloviak shear zone ca 1845-1822 Ma (Bertrand et al., 1993) along the margin of the Rae (Churchill) province; and 3) formation of a mylonite zone within the orogen during its reactivation ca. 1794-1786 Ma. This was followed by cooling and uplift from 1780-1740 Ma.

The northern Torngat Orogen is recognised as being more structurally complex than the southern due to the presence of the wedge-shaped, Burwell domain. The name Burwell domain was proposed by Korstgaard et al. (1987) for the segment of crust bounded between the sinistral Abloviak Shear Zone (ASZ), which is interpreted as the

focal point of collisional deformation, and the Komaktorvik shear zone (KSZ). The KSZ marks intense deformation ca. 1791 to 1710 Ma (Scott and Machado, 1995) within the Nain Province gneisses and Paleoproterozoic metaplutonic rocks along the western margin of the Nain Province. In the northern segment, the ASZ and the Tasiuyak gneiss trend off to the west around the Burwell terrain while the KSZ extends northward (Figure 2.1). The Burwell terrain contains tectonically juxtaposed para- and orthogneisses that may represent an autochthonous, Archean terrain, though some of the paragneisses may also be Paleoproterozoic. This idea is based on chemical (elemental and isotopic) similarities with the Nain gneisses, the presence of Paleoproterozoic mafic dykes, and the intrusion of a 1.92-1.86 Ga granitoid suite. The deflection of the Tasiuyak paragneiss to the west of the Burwell domain, is consistent with the domain marking the western-most margin of the collisional boundary of the Rae and Nain craton (van Kranendonk and Wardle, 1996; Campbell, 1997; Scott, 1998).

Characteristics of the metaplutonic rocks in the northern Torngat Orogen vary from east to west and define two broad categories. In the western part of the Burwell domain, the metaplutonic rocks have ages ranging from 1985-1869 Ma with peak magmatism at 1895-1885 Ma (Scott, 1995; Scott and Machado, 1995). The rocks are orthopyroxene-bearing and tonalitic to granodioritic in composition (referred to as charnockitic). They are preserved as tectonic slices, or intrusive sheets though contacts are often obscured (Campbell, 1997), and are retrogressed from granulite to amphibolite facies. Metaplutonic rocks in the eastern Burwell domain and east of the KSZ were intruded from 1910-1864 Ma (Scott and Machado, 1995). The rocks are mildly deformed, homogenous bodies, ranging in composition from dioritic to granodioritic and rarely

granitic rocks. The boundary between the western and eastern metaplutonic suites corresponds to the metamorphic retrograde reaction of orthopyroxene to hornblende: thus these two suites may reflect a single, eroded magmatic suite (van Kranendonk et al., 1994; Campbell, 1997; Scott, 1998).

2.4 GEOLOGICAL SETTING OF THIS STUDY

This study focuses on a transect between Anaktalak Bay (south east of Nain) and Voisey's Bay (Figure 2.2). The regional geology of this area, the Nain area and Nain Plutonic Suite (NPS) has been described by Ryan (1990, 1996, and 2000), Berg et al. (1994), Emslie et al. (1994), and Ryan et al. (1995). The troctolitic bodies in the area have also received much attention due to the serendipitous discovery of the Voisey's Bay Ni-Cu-Co deposit in 1994. The Voisey's Bay troctolite-gabbro intrusion and associated deposit have been described by Ryan et al. (1995), Naldrett et al. (1996), Ryan (1996), Li and Naldrett (1999), Lightfoot and Naldrett (1999), and Evans-Lamswood et al. (2000). Aspects of geochemistry, petrology and mineralogy of the deposit and surrounding host rocks have been described by Lambert et al. (1999), Ripley et al. (1999), Amelin et al. (2000), Ripley et al. (2000), Scoates and Mitchell (2000), Li et al. (2000), Brenan and Li (2000), Naldrett et al. (2000) and Lambert et al. (2000).

In the Voisey's area, three major gneissic units are present (Figure 2.2). To the east, there are heterogeneous, quartzo-feldspathic gneisses alternating with amphibolitic and gabbroic gneisses. This unit is interpreted as Archean orthogneiss belonging to the Nain Province. They have been cross cut by at least two sets of mafic dykes, subjected to several deformational events and contain numerous tectonic fabrics. The gneisses to the

west comprise the Churchill Paleoproterozoic Tasiuyak gneiss complex, which consists of interbanded garnet-sillimanite and sulphide-, graphite-bearing paragneiss. Between these two gneissic units lies a belt of metaplutonic gneisses. These rocks have previously been referred to as "enderbitic orthogneisses" (Li and Naldrett, 1999; Ryan, 2000). This name is somewhat ambiguous in that enderbites may be igneous or metamorphic rocks. Hence the term Paleoproterozoic metaplutonic rocks or simply metaplutonic rocks is preferred. This unit is a relatively homogenous belt of massive to foliated, orthopyroxene-bearing, meta-gabbroic to meta-tonalitic gneisses. Metasedimentary units comprising dominantly quartzite, metapelitic gneisses (possibly Tasiuyak paragneisses), amphibolitic gneiss and minor meta-semipelitic gneisses are present within the metaplutonic rocks, particularly along their contact with the Nain orthogneisses. The metaplutonic rocks are associated with minor anorthositic gneisses that are interpreted to be of similar age as the metaplutonic rocks, but little is known of the origin or tectonic history of the anorthositic gneisses. All of the gneissic units have experienced upper amphibolite to granulite facies metamorphism with some areas exhibiting retrogression to amphibolite facies.

The 1.35-1.29 Ga (Berg et al., 1994; Emslie et al., 1994) NPS was intruded the area and conceals portions of the contacts between the gneisses. The NPS is an expansive, anorogenic AMCG (anorthosite-mangerite-charnokite-granite) igneous complex that is dominated by four major compositional divisions: granitic and anorthositic, which are dominant, and dioritic and troctolitic, which are minor (Emslie et al., 1994; Ryan et al., 1995). The southern segments of the Mushuau troctolitic suite hide the contact between the metaplutonic rocks and/or the metasedimentary gneisses with the Nain Archean

Province. Western parts of the contact between the metaplutonic rocks and the Tasiuyak paragneiss are concealed by the expansive Makhavinekh Lake granitic suite.

The location of the Nain-Churchill Province boundary is of particular interest due to the proximity of the Voisey's Bay Ni-Cu-Co deposit. The deposit is hosted in one of the oldest (1332.7 ± 1 Ma, Amelin et al., 1999) known troctolitic-gabbroic intrusions of the Nain Plutonic Suite. It has been suggested that the deposit straddles the tectonic contact (Ryan et al., 1995), although the mapping of this thesis (Figure 2.2) does not support this view. The deposit and host troctolitic body were, in fact, emplaced into the Paleoproterozoic metaplutonic rocks. The intrusion consists of two sulphide-poor magma chambers termed the Eastern Deeps and Western Deeps. The mineralization is dominantly located in two sulphide-rich conduit dikes, the Ovoid conduit and the Eastern Deeps feeder. Evans-Lamswood et al. (2000) noted that the deposit appears to be structurally controlled in that the mineralized conduit dikes exploited the structure of the previously emplaced Voisey's Bay chambers.

2.5 SCOPE OF THIS STUDY

The importance of defining and characterising the metaplutonic rocks of the Anaktalak - Voisey's Bay area is threefold. First, the metaplutonic rocks in the Voisey's Area are substantially more expansive than previous mapping indicated. They constitute an important component of Torngat Orogen; particularly with respect to understanding the regional geology along the most southerly contact between the Nain-Rae cratons where much of the exposure is obliterated by the NPS. Second, petrogenetic studies of the rocks would enable an evaluation of early Proterozoic subduction zone processes.

Finally, the association of the Voisey's Bay Ni-Cu-Co deposit with the metaplutonic suite may not be simply fortuitous; the metaplutonic suite may play a key role in the formation of this type of ore deposit.

Several tasks were employed in order to define and characterise this unit of rocks. A detailed map (1:10000, Figure 2.2) was created for the area, which defined the lateral extent and heterogeneity (both compositional and metamorphic) of the metaplutonic suite and its contacts with adjacent units. Over 50 samples were chemically analysed for variations in whole rock, major and trace element concentrations. Three samples were selected, for precise Thermal Ionization Mass Spectrometry (TIMS) U-Pb zircon dating based on their location and composition. The same samples plus one additional were analysed for Sm-Nd, Rb-Sr and Pb-Pb isotope ratios. Laser ablation microprobe-inductively coupled plasma-mass spectrometry (LAM-ICP-MS) was employed to search for inherited cores in zircons of the samples that were dated by TIMS.

These chemical, isotopic and chronological measurements characterized these metaplutonic rocks, and allowed development of a tectonic interpretation for their formation and more broadly, the Torngat Orogen.

2.6 DESCRIPTION OF SAMPLES

2.6.1 Field Description

Samples of the metaplutonic rocks were examined in both surface outcrops and drill core throughout the area. In the field, the rocks show variable levels of deformation from massive or slightly foliated to highly strained (Plate 2.1). This degree of deformation intensifies from west to east across the field. The rocks appear to have been

subjected to only one major deformational event and relict igneous textures are widespread, though these textures are more commonly observed in drill core (Plate 2.2). The rocks have experienced metamorphism at the upper-amphibolite to granulite facies condition. This is reflected in the mineral assemblages of either 1) dominantly hornblende and plagioclase or 2) orthopyroxene, clinopyroxene and plagioclase.

Compositional variations between the metaplutonic samples are continuous from gabbro through tonalite (Plate 2.3). In the field it is possible to distinguish more mafic metaplutonics (meta-gabbro and meta-diorite) from more felsic metaplutonics (meta-quartz diorite and meta-tonalite). The latter are more voluminous, comprising some 65% of the metaplutonic suite. The more mafic metaplutonics occur mostly as two north-south-trending belts within the felsic metaplutonic rocks. The unit also contains a network of pegmatite veins and minor amphibolite dykes (Plate 2.4).

Inter-layered within the metaplutonic suite are metasedimentary gneisses, composed dominantly of quartzite and metapelite (Plate 2.5) and minor anorthosite (Plate 2.6). Intrusive contacts between metaplutonics and adjacent gneisses are rarely seen in the field due to the intensity of metamorphism and deformation. Contacts with the metasedimentary units interlayered within and to the east of the metaplutonic rocks are highly deformed, tectonized and hard to find (Plate 2.7). As a result, the nature of these contacts is difficult to assess. This is also true of the contact between the metaplutonics and heterogeneous Archean Nain orthogneisses, in the east and northeast of the field area (Plate 2.8). The sinusoidal nature of the western contact of the metaplutonic rocks with the Tasiuyak paragneiss (Figure 2.2) seems to indicate an intrusive rather than tectonic boundary, as most of the tectonic contacts in this region are north-south trending.

However, this western contact is only preserved in outcrop in the Discovery Hill area within the field area and, thin veinlets of meta-plutonic rocks are seen in the paragneiss suggesting an intrusive relationship (Plate 2.9). Though the precise relationship between the metaplutonic rocks and adjacent gneisses is not entirely discernible.

2.6.2 Petrography

The majority of metaplutonic rocks were partially or completely recrystallized during granulite facies metamorphism. Although some samples preserve relict igneous textures, most show a thorough granoblastic recrystallization, which hides the previous texture. Both mafic and felsic samples generally show slight foliation.

In felsic samples (Plate 2.10), which range in composition from meta-tonalite to meta-quartz diorite, plagioclase is the dominant phase ranging from 40 to 60 %. The abundance of quartz is 5 to 25%. Clinopyroxene accounts for 5 to 15 % and is often rimmed by retrograde hornblende (1-10%). Orthopyroxene occurs at the <10% level and appears to be retrograded to biotite (10 to 20 %). Also present are minor K-feldspar (0-5%) and Fe-Ti oxides (2-5%), dominantly magnetite and ilmenite, which formed by the retrograde breakdown of orthopyroxene. In the more strongly retrogressed samples minor chlorite replaces biotite, and actinolite-tremolite replace hornblende.

The mafic samples (Plate 2.11), which range in composition from meta-gabbro to meta-hornblende gabbro and meta-diorite, contain plagioclase at 40-53 %. Clinopyroxene (10-35%) and orthopyroxene (5-15%) are the dominant mafic minerals. Retrograde hornblende (1-25%) and biotite (5-15%) are also abundant. Quartz is present as an accessory phase (<5 %). Fe-Ti oxides (commonly magnetite with lesser ilmenite) range

from 2% to 10%; these phases most likely formed during the retrograde reaction of pyroxene with hydrous fluid. Minor garnet and carbonate are present in some samples. Zircon and apatite form accessory phases.

The felsic compositions of the metaplutonic suite are more dominant in the field than the mafic compositions, with approximate ratios of 65% felsic to 35% mafic. The estimated relative proportions of each rock type are: 25% meta-tonalite, 35% meta-quartz diorite, 5% meta-diorite, 10% meta-gabbro and 25% meta-hornblende gabbro.

In general, quartz is quite strongly strained, exhibits undulatory extinction and in some samples appears to have been recrystallized. Plagioclase shows deformation in the form of pinched lamella twins or by the absence of twinning. Samples that have experienced more intense deformation contain pods of fine-grained mafic minerals, defining an incipient mafic mineral fabric. Reactions of clinopyroxene to hornblende and of orthopyroxene to biotite, magnetite and ilmenite; are suggested by the petrography of many samples. These reactions indicate widespread retrogression from granulite to amphibolite facies conditions. Relict igneous textures are apparent in the coarsest-grained, least deformed samples.

2.7 PRESENTATION OF DATA

2.7.1 Geochemistry of the metaplutonic rocks

Major element (recalculated to an anhydrous total of 100%) and trace element compositions of 57 samples from the metaplutonic suite of the Voisey's Bay area are presented in Tables 2.1 and 2.2. The data are grouped by rock type as determined by

petrographic classification. The felsic group of rocks is divided into two major protolith rock types: tonalite and quartz-diorite. The mafic group is divided into three groups based on the same criteria: gabbro, hornblende gabbro and diorite. Samples from drill core are labelled with DDH (Diamond Drill Hole) followed by their drill hole number. Analytical methods for all data are presented in Appendix A.

2.7.1.1 Major and Trace Element Geochemistry

On the basis of their normative mineralogy, the protoliths of the metaplutonic rocks range in composition from gabbro through diorite to tonalite (Figures 2.3 and 2.4). These rocks display a broad calc-alkaline trend on an AFM diagram (Figure 2.5a). The probable mobilisation of alkalis due to metamorphism is poorly represented on this diagram. The Jensen diagram (Figure 2.5b) accounts for alteration resulting in the mobilisation of alkalis. Although this diagram is intended for volcanic rocks, the metaplutonic rocks define a calc-alkaline trend here as well. The metaplutonic suite displays a volcanic-arc granite (VAG; Pearce et al., 1984) tectonic affinity based on relative abundances of Rb, Y and Nb (Figure 2.6).

SiO₂ contents of the calc-alkaline metaplutonic rocks range from 46 to 64 wt. %. Al₂O₃ ranges from 13 to 20.5 %. At SiO₂ levels below about 55 wt.%, the samples define a trend of increasing Al₂O₃ and Na₂O and of decreasing with Fe₂O₃, CaO, MgO, MnO, and TiO₂ with increasing SiO₂ (Figure 2.7). Above 55 wt.% SiO₂, these trends are interrupted, with little change in the concentrations of these other oxides with further increase of SiO₂. K₂O, P₂O₅ and Na₂O/K₂O are more scattered throughout the entire range of SiO₂ values, presumably reflecting mobility during metamorphism and/or alteration.

The trace element compositions of these rocks exhibit large ranges for certain elements such as Ba (200-2600 ppm), Sr (280-1800 ppm), Zr (30-550 ppm) and Hf (0.4-5 ppm). Trace element variations are largely consistent with the major element trends, showing a progressive and predictable increase in strongly incompatible elements (i.e. Ba, La) and some moderately incompatible elements (Sr) with increasing SiO₂ up to about 55 wt.%, and thereafter little systematic change. Certain trace element ratios (Rb/Sr) show the same pattern. The inverse relationship is seen with compatible elements (Ni, Sc, V), which decrease with increasing SiO₂ to about 55 wt.% (Figure 2.8). However, above 55 wt.% SiO₂, there is little change in the concentrations of compatible elements. La/Yb and La/Y ratios tend to increase with increasing SiO₂ over the entire SiO₂ range. Other elements (Rb, Nb, Y, Eu, Th) and ratios (K/Rb) show more scattered patterns. The break in element trends at 55 wt.% SiO₂ values suggests that the most silicic metaplutonic rocks did not form by simple fractional crystallization of the same parental magma that formed the more mafic metaplutonic rocks. Fractional crystallization of expected liquid phases in a mafic-intermediate system, olivine + pyroxene + plagioclase hornblende, could explain the observed trends below 55 wt.% SiO₂. However, above SiO₂, where there is little change in the concentrations of both compatible and incompatible elements with increasing silica content, crustal contamination is a more plausible model than fractional crystallization. Alternatively, the more felsic samples may have been derived by partial melting of different source rocks than the more mafic samples.

The chondrite-normalized rare earth element (REE) patterns of the metaplutonic rocks are strongly fractionated with La_(N)/Yb_(N) between 3 and 59 times chondrite with the more mafic compositions showing less fractionation than the more felsic ones (Figure

2.9). The samples have little or no Eu anomaly. LREE concentrations range between 50 and 200x chondrite values, whereas HREE range between 4 and 9x chondrite values (Figure 2.9).

On an extended trace element primitive-mantle normalized spider diagram, the rocks exhibit large enrichments in Ba, LREEs, Sr, Zr and Hf relative to primitive mantle (Figure 2.10). Ti and Y are slightly depleted. There are also pronounced negative Th-U and Nb-Ta anomalies. The negative Th-U anomaly may reflect loss of these elements during granulite facies metamorphism. The negative Nb-Ta anomaly probably is a signature of subduction-zone processes, which will be discussed later.

On a MORB-normalized spider diagram (Figure 2.11), like the primitive-mantle normalized diagram, the trace elements in the metaplutonic rocks generally decrease in abundance with increased compatibility (from left to right). Concentrations of elements plotted on Figure 2.11 are greater in the metaplutonic rocks than in MORB with the exception of Ti, Y, and Yb. Average values of continental arc tholeiitic basalt (Ewart, 1982) and calc-alkaline island arc basalt (Sun, 1980) are also plotted on Figure 2.11, using normalized values from McCulloch and Gamble (1991). The modern arc compositions show the same elemental pattern of increasing concentration with increasing incompatibility as seen in the metaplutonic suite. There are some subtle differences, however: in particular the high Ba/Rb and Nb/Zr ratios and low U/Th ratios in the metaplutonics compared to the modern arc magmas. The low U/Th ratios of the metaplutonic rocks may represent preferential loss of uranium during high-grade metamorphism. The high Ba/Rb and Nb/Zr ratios may reflect the trace element signature of potential crustal sources involved in the petrogenesis of the metaplutonic suite.

2.7.2 U-Pb TIMS Geochronology

Samples of the meta-tonalite, meta-quartz diorite and meta-hornblende gabbro of the Voisey's Bay metaplutonic suite were dated (Figure 2.12) by Thermal Ionization Mass Spectrometry (TIMS). Samples were dated by the U-Pb zircon method in order to determine the timing of igneous crystallisation. The meta-tonalite sample (DDH-496-549) was from drill core while the other two samples were from surface outcrop. An overview of the analytical technique is provided in Appendix A and the results of the analysis are presented in Table 2.3.

2.7.2.1 U-Pb Samples

Meta-quartz diorite (VB-99-108).

This sample is a strongly foliated meta-quartz diorite that is located to the east of the Voisey's Bay deposit (Figure 2.12). The sample is composed of annealed grains of plagioclase, orthopyroxene and clinopyroxene, which have retrograded in part to biotite, magnetite and hornblende respectively (Plate 2.12). This sample yielded a relatively large volume of zircons, ranging in morphology from small sub-rounded to prismatic needles, although dominated by long, needle-like zircons (Plate 2.13). Three fractions of clear zircons were selected from the NM (non-magnetic) 0° Franz split and abraded. All three analyses were concordant (Figure 2.13) and give an age of 1893 \pm 1 Ma (Table 2.3).

Meta-hornblende gabbro (VB-99-106c).

The second surface sample is a strongly foliated meta-hornblende gabbro and is located just to the east of sample VB-99-108 (Figure 2.12). The sample displays a granoblastic texture; the mafic minerals (hornblende and biotite are dominant) define a strong foliation (Plate 2.14). Hornblende and biotite have replaced a large percentage of the pyroxene. The sample yielded a large volume of sub-rounded prismatic zircons. Of these, three fractions of high-quality, clear zircons were selected for analysis (Plate 2.15). Two fractions (Z2 and Z4) lie slightly off concordia, with 0.64% and 1% discordia and $^{207}\text{Pb}/^{206}\text{Pb}$ ages of 1885 Ma and 1880 Ma respectively. A third fraction (Z3) appears to have suffered more extensive Pb-loss and is 7% discordant. A tight discordia line can be drawn through the three points with a 29.3 % probability of fit and an upper intercept age of 1890 ± 2 Ma (Figure 2.14, Table 2.3).

Meta-tonalite (DDH-99-496).

This sample is a meta-tonalite from drill core (DDH-99-496) that had an approximate depth of 260 meters below surface. Figure 2.12 shows the location the drill hole on surface. The drill hole is dominated by meta-tonalite with thin sheets of VB granite intruding. This sample is the most felsic component dated and preserves relict igneous textures. The sample is composed primarily of plagioclase and quartz with variable amounts of orthopyroxene, biotite, clinopyroxene and hornblende (Plate 2.16). The sample yielded abundant prismatic zircons. Four fractions of clear, prismatic zircons were abraded and analysed (Plate 2.17). One fraction (Z2) is concordant with an age of 1883 ± 5 Ma. The other three fractions (Z1, Z3 and Z4) suffered Pb-loss and were

discordant at 3 %, 4% and 5% giving $^{207}\text{Pb}/^{206}\text{Pb}$ ages of 1741 Ma, 1778 Ma and 1751 Ma respectively. The fractions define a discordia line with a probability of fit of 24% with an upper intercept of igneous crystallization at 1883 +/- 5 Ma and a lower intercept of 1344 - - 80 Ma, which is interpreted to be the result of a disturbance during the emplacement of the Nain Plutonic Suite (Figure 2.15, Table 2.3). The data suggest that the meta-tonalite is slightly younger than the meta-quartz diorite and meta-hornblende gabbro.

2.7.3 Isotope Geochemistry

Neodymium-samarium, rubidium-strontium, and lead isotopic data for the metaplutonic suite are summarised in tables 2.4 and 2.5. Analytical details are given in Appendix A. Four whole-rock samples were analysed, three that were analysed for U-Pb geochronology (VB-99-106f – the fine grained component of VB-99-106, VB-99-108 and DDH-496-549), plus a meta-hornblende gabbro sample (AR-00-02) from west of the deposit. The results are compared to those of Amelin et al. (2000), who reported isotopic data for whole rocks and mineral separates from six orthogneisses at Voisey's Bay. Amelin et al. (2000) described two of the orthogneisses as Paleoproterozoic "enderbitic gneisses", and the other four samples as Archean "Nain gneisses". U-Pb zircon ages have not been reported for any of the samples but it is likely, based on their drill core locations, that at least five of the six samples are members of the Paleoproterozoic metaplutonic suite as mapped in Figure 2.2. These five samples are located around the Voisey's Bay ore deposit, near Discovery Hill and the Eastern Deeps troctolite chamber, just south and west of the three samples dated in this study. The sixth orthogneiss sample of Amelin et al. (2000) is from near the Mushuau intrusion, but the precise location is not given.

2.7.3.1 Strontium Isotopic Geochemistry

The four samples of this study were analysed for Sr isotopes by TIMS. They have measured $^{87}\text{Sr}/^{86}\text{Sr}$ ratios between 0.704929 to 0.708536 and measured $^{87}\text{Rb}/^{86}\text{Sr}$ ratios between 0.04605 to 0.25811 (Table 2.4). These samples have a relatively unradiogenic nature with respect to their $^{87}\text{Sr}/^{86}\text{Sr}$. The initial $^{87}\text{Sr}/^{86}\text{Sr}$ ratios (calculated for 1890 Ma based on U-Pb geochronology) have values between 0.70104 and 0.70426 (Figure 2.16a). These data are similar to $^{87}\text{Sr}/^{86}\text{Sr}_{(1890\text{ Ma})}$ values of 0.70356 to 0.70387 for plagioclase and apatite from the “enderbite” and values of 0.70375 to 0.70827 for whole rock, plagioclase and potassium feldspar from the “Nain gneisses” as defined by Amelin et al. (2000). The initial $^{87}\text{Sr}/^{86}\text{Sr}$ ratios reported by Amelin et al. (2000) for the “Nain gneisses” overlap with those reported here for the metaplutonic suite with the exception of one sample, suggesting a common origin. In comparison, Archean Nain gneisses from the Saglek area are much more radiogenic with $^{87}\text{Sr}/^{86}\text{Sr}_{(1890\text{ Ma})}$ values between 0.71061 and 0.78348 (Collerson et al., 1989).

The use of Rb-Sr systematics to interpret source characteristic of igneous precursors can be difficult in high-grade metamorphic rocks. Rubidium may become highly mobile in response to metasomatism and metamorphism. Radiogenic ^{87}Sr may readily diffuse in and out of minerals and whole rocks during even low-grade metamorphism. As the metaplutonic rocks have experienced granulite-facies metamorphism and amphibolite facies retrogression, care must be taken in interpreting the Sr isotope data. In this regard, it is noteworthy that the data do not all fall along a 1.89 Ga isochron in $^{87}\text{Sr}/^{86}\text{Sr}$ versus $^{87}\text{Rb}/^{86}\text{Sr}$ space (Figure 2.16b), assuming an initial $^{87}\text{Sr}/^{86}\text{Sr}$ ratio of 0.704, as a value around which much of the data cluster. In particular,

the two samples of this study that have the highest Rb/Sr ratios fall significantly below the 1.89 Ga reference isochron, and closer to a 1.32 Ga reference isochron. The Sr isotopic system of these two samples seems to have been significantly disturbed by metamorphism or metasomatism. This issue will be addressed further in the discussion section.

2.7.3.2 Neodymium Isotopic Geochemistry

The four samples of this study were analysed for Nd isotopes by TIMS. $\epsilon\text{Nd}_{(\text{CHUR})}$ values were calculated for 1890 Ma. These samples have measured $^{143}\text{Nd}/^{144}\text{Nd}$ ratios of 0.511141 to 0.511470 with $^{147}\text{Sm}/^{144}\text{Nd}$ measured ratios of 0.08964–0.11765 and $\epsilon\text{Nd}_{(1890 \text{ Ma})}$ values from –0.13 to –5.3 (Figure 2.17, Table 2.4). These values are more evolved than those reported by Amelin et al (2000) for plagioclase and apatite from the “enderbite”, which have $\epsilon\text{Nd}_{(1890 \text{ Ma})}$ values –3.2 and +4.7, measured $^{143}\text{Nd}/^{144}\text{Nd}$ ratios of 0.511125 to 0.511786 and $^{147}\text{Sm}/^{144}\text{Nd}$ measured ratios of 0.05587 to 0.11518 (Figure 2.17). Again, the Nd data reported by Amelin et al. (2000) for the “Nain gneisses” are more similar to the metaplutonic suite rather than those of true Nain province gneisses. They have measured $^{143}\text{Nd}/^{144}\text{Nd}$ ratios of 0.510495 to 0.511180 with $^{147}\text{Sm}/^{144}\text{Nd}$ measured ratios of 0.04155 to 0.10829 and $\epsilon\text{Nd}_{(1890 \text{ Ma})}$ values between –0.4 to –11.8 (Figure 2.17). The most enriched sample (–11.8) is from the gneiss of ambiguous affinity near the Mushuau intrusion. In comparison, the Early Archean Nain gneisses of Collerson et al. (1989) have $\epsilon\text{Nd}_{(1890 \text{ Ma})}$ values of –29.2 to –40.8, $^{143}\text{Nd}/^{144}\text{Nd}$ versus $^{147}\text{Sm}/^{144}\text{Nd}$, the samples of the metaplutonic suite from this study and Amelin et al. (2000) fall along a

1.89 Ga reference isochron, whereas the Nain gneisses of Collerson et al. (1989) fall along a 2.79 Ga reference isochron (Figure 2.18).

Based on the combined data, there appears to be two separate groups: (1) an enriched group with $\epsilon\text{Nd}_{(1890)}$ values between -3.3 and -1.8 and $^{87}\text{Sr}/^{86}\text{Sr}_{(1890)}$ ratios between 0.70104 and 0.70827 ; (2) a depleted group with $\epsilon\text{Nd}_{(1890)}$ values between -0.8 and 4.7 with $^{87}\text{Sr}/^{86}\text{Sr}_{(1890)}$ ratios between 0.703586 and 0.700482 (Figure 2.19). Only the enriched samples were dated by U-Pb geochronology (i.e. VB-99-108, VB-99-106c and DDH-496-549); but based on field relationships, it seems likely that the depleted group is of similar age.

2.7.3.3 Lead Isotopic Geochemistry

The same four samples were analysed for lead isotopes by MC (multi-collector)-ICP-MS. The samples have measured $^{206}\text{Pb}/^{204}\text{Pb}$ ratios between 15.160 and 15.834 , measured $^{207}\text{Pb}/^{204}\text{Pb}$ ratios between 15.000 and 15.145 and $^{208}\text{Pb}/^{204}\text{Pb}$ ratios between 35.507 and 37.277 (Table 2.5, Figure 2.20). The samples of Amelin et al. (2000) that are presumed to be from the metaplutonic suite have similar Pb isotope compositions: 14.226 - 15.443 for $^{206}\text{Pb}/^{204}\text{Pb}$, 14.573 - 15.157 for $^{207}\text{Pb}/^{204}\text{Pb}$ and 33.996 - 35.455 for $^{208}\text{Pb}/^{204}\text{Pb}$. The sample of Amelin et al. (2000) with the anomalous low Pb isotopic ratio is the orthogneiss of ambiguous affinity near the Mushuau intrusion. The combined data from this study and Amelin et al. (2000) fall along a 1.89 Ga reference isochron in lead isotope space (Figure 2.20). There is some scatter that could represent disturbance of the

lead isotopic system during metamorphism and/or heterogeneity in the source region of the metaplutonic suite.

The lead data are presented in Figure 2.21 in terms of μ^* , which is the time-integrated $^{238}\text{U}/^{204}\text{Pb}$ of the mantle and crustal sources of each sample and in terms of κ^* values, which is the time integrated $^{232}\text{Th}/^{238}\text{U}$ of the mantle and crustal sources of each sample. The data from this study have a range in μ^* values from 7.66 to 7.94 and κ^* values from 3.84 to 5.81. These values overlap with those reported by Amelin et al. (2000). The combined data sets suggest that there is no clear difference in μ^* and κ^* between the depleted and enriched Nd isotope (Figure 2.21).

2.7.4 U-Pb Zircon Dating by LAM-ICP-MS

The recent development of in situ U-Pb zircon dating by laser ablation microprobe-inductively coupled plasma-mass spectrometry (LAM-ICP-MS) at Memorial University has been utilized in this study. The goal was to apply this technique to distinguish igneous from inherited U-Pb ages in zircon grains in order to identify and date potential crustal contributions to the mantle-derived parent magmas of the metaplutonic suite. This technique provides in situ spot or raster analysis of zircon grains. Thus it is possible to analyse a large number of zircons relatively quickly. An overview of the analytical technique is presented in Appendix A. The zircons from samples VB-99-108, VB-99-106 and DDH-496-549 were used for the analysis, (i.e. zircons were selected from the NM (non-magnetic) 0° Franz split that were used for the U-Pb zircon TIMS analysis). This technique is capable of age determinations with errors of less than 0.5% (~10 Ma for

a 2 Ga zircon); however typically this technique achieves errors of 1.0% (or ~20 Ma for a 2 Ga zircon; Horn et al., 2000). Errors of this size overlap the range of igneous ages determined by the U-Pb TIMS analysis for the samples. Therefore, LAM analyses from all three samples were combined into one data set.

Zircons from each rock type were selected based on clarity, and varied morphology in an attempt to maximise the likelihood of analyzing a relict core. The zircons were mounted in an epoxy resin for analysis. Back-scattered electron (BSE) microscopy was utilised to image the zircons in order to identify potential cores within individual grains (Plate 2.18).

The LAM-ICP-MS results for the igneous zircons agree with the igneous crystallization ages determined by TIMS (Table 2.6). Seventeen spots in the three samples have a mean $^{207}\text{Pb}/^{206}\text{Pb}$ age of 1908 ± 15.4 Ma. Several inherited cores were identified in sample VB-99-106c (Table 2.7). This distinct group of zircons is determined to be 50 to 100 Ma years older than the igneous population (Figure 2.22). No inherited cores were identified in the other samples. Of particular note, no Archean zircon cores were identified even in sample VB-99-106c.

2.8 DISCUSSION

2.8.1 Geochemical Effects of Granulite Facies Metamorphism

In order to sensibly interpret the geochemical and isotopic characteristics of the Paleoproterozoic metaplutonic rocks it is essential to recognise the effects of metamorphism on their compositions. The metaplutonic rocks have all experienced peak-

metamorphism at the upper-amphibolite to granulite facies and many have subsequently been retrogressed to amphibolite facies. These events presumably occurred during the Nain-Rae collision at ca. 1860 Ma, and the subsequent shearing and uplift, which was completed by 1740 Ma. It has long been recognised that intense metamorphic conditions can result in mobilisation of certain elements on the scale of hand samples, particularly alkali elements (Heir, 1965, 1973; Rudnick et al., 1985). As a result, the effects of this metamorphism on the geochemistry of these rocks need to be addressed.

The Paleoproterozoic metaplutonic rocks are enriched in large ion lithophile elements (LILE) such as Rb, Ba, Pb and K relative to the MORB values but not relative to island arc calc-alkaline basalt (Figure 2.11). They do not exhibit the large depletion in LILE that is commonly observed in granulite facies terrains (Heir, 1965, 1973:). A good indication of the extent of granulite facies metamorphism on whole rock chemical composition is the Rb/K ratio, as K is far more resistant to depletion than Rb (Rudnick et al., 1985). On a plot of Rb versus K_2O (Figure 2.23), the metaplutonic rocks show a slight depletion relative to the main trend of continental igneous rocks (Shaw, 1968). However, the depletion is not as extreme as the "granulite trend" observed by Rudnick et al. (1985) that is typical of most granulite facies rocks. The slight LILE depletion is particularly apparent for some of the more felsic samples, which fall slightly outside the field of Shaw (1968).

On a primitive-mantle normalized spider-diagram (Figure 2.10), the rocks also exhibit a Th-U depletion that is commonly observed in granulite facies metamorphism. On a plot of U versus Th (Figure 2.24), the metaplutonic rocks show only a slight depletion. Some of the metaplutonic rocks appear to have suffered more depletion than

the rest of suite. The average ratio of the metaplutonic suite is 8.3, while extreme depletion is a ratio above 10 (Rudnick et al., 1985), though many samples fall on or below the average igneous rock ratio of 3.5–4.0 (Rogers and Adams, 1978). The degree of Th-U depletion in granulites depends on the protolith composition, the ability of mixed volatile fluids to interact with rocks, and the stability of accessory phases during metamorphism (Rudnick et al., 1985). Overall, the whole rock compositions of the metaplutonic rocks appear to have been only mildly modified by granulite metamorphism.

There is also evidence that the rock compositions have been modified by post granulite facies events. As noted in Figure 2.16, the Sr isotope compositions of some samples fall off a 1.89 Ga reference isochron and more closely along a 1.32 Ga reference isochron. This suggests the possibility of disturbance of the Rb-Sr system of the metaplutonic rocks during the Mesoproterozoic emplacement of the proximal large volume Nain Plutonic Suite.

Because there is some evidence that these rocks may not represent the chemical compositions of their protoliths, care must be taken in interpreting their igneous history especially in terms of the LILE, which appear to have been most mobile during metamorphism. However, based on the broad systematic major and trace element trends of the metaplutonic rocks (Figure 2.7 and 2.8) and their chemical similarities to modern arc magmas (Figure 2.11), it is likely the effects of metamorphism were relatively minor and did not significantly alter the chemical composition of the igneous protolith material.

2.8.2 Origin of the Metaplutonic Suite

2.8.2.1 Major Characteristics of the Metaplutonic Suite

The Paleoproterozoic metaplutonic rocks of the Voisey's Bay area form a north-south belt between Archean Nain gneisses to the east and Archean Rae and Proterozoic Churchill gneisses to the west. The rocks vary in composition from meta-gabbro through meta-tonalite, and are dominated by meta-quartz diorite. The suite represents a fairly undifferentiated, mafic-intermediate calc-alkaline batholith. The metamorphic grade is high, ranging from upper-amphibolite to granulite facies.

The metaplutonic suite shows broad compositional variations in their major and trace element concentrations. The more mafic samples (meta-gabbro to quartz diorite) are characterised by systematically increasing Al_2O_3 and Na_2O and decreasing Fe_2O_3 , CaO , MgO , MnO and TiO_2 with increasing SiO_2 (Figure 2.7). This systematic behaviour is also mirrored in most trace elements, which display a positive correlation between silica and strongly and moderately incompatible trace elements (Ba, La and Sr) and some trace elements ratios (Rb/Sr; Figure 2.8). The inverse relationship is seen with compatible elements. These characteristics suggest that the mafic compositions (meta-gabbro to quartz-diorite) are magmatically related, likely by fractional crystallization of a common parent magma. The fractionation assemblage probably was dominated by mafic silicates such as pyroxene and olivine, and Fe-Ti oxides in order to explain the observed chemical variations. However, as metamorphism has obliterated the primary, igneous mineralogy of the rocks, the details of the fractional crystallization history are difficult to determine.

The break in the continuous, systematic relationship of the major and trace elements at about 55 wt.% SiO_2 (Figure 2.7 and 2.8) suggests that the meta-tonalites

followed a different magmatic evolution and are not simply related to the more mafic rocks by fractional crystallization. In principle, it is possible that the break in chemical variation at 55 wt.% SiO₂ represents a change in the fractionating mineral assemblage. For instance the appearance of plagioclase on the liquidus might explain the lack of further increases in Al₂O₃ and Na₂O with increasing SiO₂ over 55 wt.%. In detail, however, it is difficult to achieve a rather constant concentration of most elements with increasing SiO₂ observed for the meta-tonalites without a rather delicate balance of mafic and felsic phases in the fractionation assemblage.

All of the metaplutonic rocks are characterised by strongly fractionated and crossing REE patterns (Figure 2.9). The heavy REE depletion is consistent with residual garnet in the source region of the metaplutonic rocks (Taylor and McLennan, 1985). Negative Th-U anomalies are also characteristic of the metaplutonic suite. This may result from loss of these elements during high-grade metamorphism. Alternatively they may reflect input of a lower crustal source or contaminant that is also characterized by this depletion (Rollinson, 1993). The negative Nb-Ta anomalies present in the metaplutonic suite probably represent a metasomatized subduction-related (ocean slab or mantle wedge) source region of their igneous precursors (Rollinson, 1993). The systematic decrease in trace element concentrations with increasing compatibility on a MORB normalized diagram (Figure 2.11) further suggests enrichment in the LILE are controlled by metasomatism in the mantle source by subduction zone fluids and/or partial melts. This is consistent with the idea that the metaplutonic suite formed from arc magmas.

Precise U-Pb zircon TIMS ages for the metaplutonic suite are 1893 \pm 3 Ma for the meta-quartz diorite, 1890 \pm 2 Ma for a meta-hornblende gabbro, and 1883 \pm 5 Ma for a meta-tonalite. The slightly younger age of the meta-tonalite is consistent with a somewhat different magmatic history than the more mafic rocks.

Measured $^{147}\text{Sm}/^{144}\text{Nd}_{(M)}$ versus $^{143}\text{Nd}/^{144}\text{Nd}_{(M)}$ for the metaplutonic suite largely fall along a reference isochron of 1.89 Ga (Figure 2.18). This suggests that there has been only minor disturbance of the Sm-Nd isotopic system during metamorphism and secondary alteration events. In contrast, the Rb-Sr isotopic system for the metaplutonic suite appears to have been more significantly disturbed. Some samples fall along a 1.32 Ga reference isochron suggesting a possible isotopic disturbance as a result of emplacement of the Nain Plutonic Suite (Figure 2.16). Isotopic resetting of the Rb-Sr system also possibly occurred during granulite facies metamorphism and amphibolite facies retrogression. The Pb isotope geochemistry of the metaplutonic suite was not been strongly disturbed by secondary processes. Most samples fall along a 1.89 Ga reference isochron in the Pb-isotope space (Figure 2.20).

The observed ϵNd values of the metaplutonic suite (from $\sim +5$ to -7 , excluding the gneiss of ambiguous origin near the Mushuau intrusion) extend from those expected for depleted mantle in the Paleoproterozoic to highly enriched (Figure 2.25). The depleted Nd isotope group may be near direct melts of the depleted mantle; however the enriched Nd group either formed by melting of older crust or crustal contamination of a mantle-derived magma. Except for the meta-tonalites, the metaplutonic suite is probably too mafic to have been derived from direct melting of crustal rocks. The most plausible

explanation is that the mafic metaplutonic rocks formed by interaction of depleted mantle melts with a continental crust component. The meta-tonalites could have formed from direct melts of a mafic crustal source, or crustal contaminated mantle-derived melts.

The U-Pb zircon analyses by LAM-ICP-MS are important in assessing the role of crustal contamination in the genesis of the metaplutonic suite. A small group of inherited cores that were 50-100 Ma older than the igneous crystallization age were identified in one sample of meta-hornblende gabbro (Figure 2.22). The inherited cores were not found in samples of meta-quartz diorite and meta-tonalite. These data imply that the parent magmas of the metaplutonic suite had only limited interaction with pre-existing, particularly pre-existing Archean crust.

Another more general problem of crustal contamination models for the metaplutonic suite is the lack of correlation between the ϵ_{Nd} and chemical indices of contamination. Bulk crustal assimilation of a more mantle-derived mafic magma would be expected to produce trends of decreasing ϵ_{Nd} with increasing SiO_2 and decreasing MgO . This is not observed in the metaplutonic suite (Figure 2.26).

2.8.2.2 Interpretations of the Origin of the Metaplutonic Suite

2.8.2.2.1 Meta-gabbro to Meta-quartz diorite

The meta-gabbro, -hornblende gabbro, -diorite and -quartz diorite appear to define a common magmatic series based on systematic variations in trace and major elements. Their overall mafic composition implies formulation from a relatively primitive, mantle-derived magma or from a magma possibly derived from the mantle wedge above a

subduction zone. The rocks are calc-alkaline with compositional characteristics of arc magmas such as negative Nb-Ta anomalies. Evolution of this magmatic series to form the more felsic compositions (quartz diorite) was probably the result of fractional crystallization of mafic silicates and Fe-Ti oxides. However, crustal contamination of the mantle-derived magma also probably occurred because (1) there is a range of depleted to enriched Nd isotope compositions and (2) inherited zircon grains are present in a sample of meta-hornblende gabbro.

If these rocks formed by interaction of the mantle melts with a crustal component, there are two likely contaminants based on field mapping: 1) the Tasiuyak paragneiss, belonging to the Churchill Province, to the west or 2) the Archean orthogneisses, belonging to the Nain Province, to the east. However, along the length of the Torngat Orogen several more potential contaminants are present. These include the Paleoproterozoic supracrustal sequences of the: Ramah Group, Mugford Group and Lac Lomier-Lake Harbour Group. The Lac Lomier sediments are thought to be the metamorphosed equivalent of the Lake Harbour Group (Theriault and Ermanovics, 1997). Mafic and felsic orthogneisses of the Rae craton and from parts of the Nain craton north of the field area are also potential contaminants.

Each of the potential contaminants can first be evaluated in terms of their major element trends and those of the meta-gabbro to meta-quartz diorite compositions. None of the Paleoproterozoic supracrustal sequences (Ramah, Tasiuyak, Mugford or Lac Lomier-Lake Harbour Group) can adequately explain the trends observed in the major elements (Al_2O_3 , Fe_2O_3 , CaO and Na_2O) of the meta-gabbro to meta-quartz diorite compositions of

the metaplutonic suite (Figure 2.27). The high concentrations of CaO and Na₂O in the metaplutonic rocks are particularly problematic.

The Rae and Nain orthogneisses have similar compositions, and they do not exhibit the elemental concentrations required to be the crustal contaminant necessary to explain the major element trends observed in the meta-gabbro to meta-quartz diorite series (Figure 2.28). In particular the elevated trends of the Al₂O₃ and Na₂O observed in the metaplutonic suite are not consistent with crustal contamination of Nain and Rae orthogneisses.

In terms of the Sm-Nd isotopic composition of the meta-gabbro to meta-quartz diorite rocks of the metaplutonic suite, the Paleoproterozoic supracrustals also are not a viable contaminant. The $\epsilon\text{Nd}_{(1.890 \text{ Ma})}$ of these metaplutonic rocks overlap almost completely with the supracrustal rocks and thus would require huge amounts of contamination (Figure 2.29). In contrast, the Rae and Nain Province gneisses have sufficiently evolved $\epsilon\text{Nd}_{(1.890)}$ to explain the range in $\epsilon\text{Nd}_{(1.890)}$ values of the metaplutonic suite with small amounts of crustal contamination (Figure 2.30).

Evaluating potential contaminants in terms of Pb isotopes is somewhat difficult as only a few Pb isotope studies have been published for the Paleoproterozoic supracrustals and Archean gneisses. However recent data for the Tasiuyak paragneisses, the Rae orthogneisses and the Nain orthogneisses allow for consideration of these units. Figure 2.31 is an $\epsilon\text{Nd}_{(1.890)}$ versus μ^* diagram for the metaplutonic suite and possible crustal contaminants in the region. Also shown are mixing lines between a hypothetical mantle magma with $\epsilon\text{Nd}_{(1.890)}$ of -5 and μ^* of 8, and Archean upper crustal ($\epsilon\text{Nd}_{(1.890)} = -12$, μ^*

= 9.7) and lower crustal ($\epsilon Nd_{1890} = -12$, $\mu^* = 7$) sources. The end-member compositions are those used by Arndt and Todt (1994) for the 1.9 Ga Trans-Hudson Batholith. On this plot, the metaplutonic suite is more closely associated with the lower crustal contamination trajectory. None of the observed potential contaminants in the area, however, have the same characteristics as the hypothetical lower crustal contaminant. The Tasiuyak paragneiss and the Rae orthogneisses clearly have μ^* values that are too high (8.10 to 8.24 for the Tasiuyak paragneiss and 7.8 to 8.19 for the Rae Province) to explain the μ^* values of the metaplutonic suite. Contamination of the mafic magma by some part of the Nain orthogneiss suite could explain the range in μ^* observed in the metaplutonic suite (Figure 2.31). However, based on the above stated major element variations, the Nain orthogneisses can not explain the trends defined by the meta-gabbro to meta-quartz diorite members of the metaplutonic suite.

The lack of inherited Archean zircon cores in the metaplutonic suite, suggests that the mafic parent magma did not interact with Archean crustal contaminants. Instead the identified inherited zircons range in age from 50 to 100 Ma older than the igneous crystallization age. This would be consistent with contamination by the Tasiuyak paragneiss, whose detrital zircon ages overlap with these ages (Scott and Gauthier, 1996). However, contamination by the Tasiuyak paragneiss cannot explain the geochemical or isotopic characteristics of the metaplutonic suite.

As none of the obvious potential contaminants in Northern Labrador (i.e. Tasiuyak paragneiss, Ramah group, Mugford group, Lac Lomier-Lake Harbour group, Rae felsic and mafic orthogneisses or the Nain mafic and felsic orthogneisses), can

readily explain the fractionation trend of the meta-gabbro to meta-quartz diorite and the isotopic characteristics, it seems unlikely that these rocks were a major contaminant of the primitive magma of the metaplutonic suite. In terms of μ^* versus $\epsilon\text{Nd}_{(1890\text{ Ma})}$ relationships, the source rocks of the metaplutonic suite most likely contain a lower crustal component that is not preserved (or known) in present day surface geology, as opposed to an upper crustal source. The scatter of the metaplutonics along the lower crust mixing line, in figure 2.31, indicates that the hypothetical lower crustal contaminant may have been isotopically heterogeneous.

There are two ways in which the hypothetical lower crustal contaminant may have interacted with the mantle-derived parent magmas of the metaplutonic suite. The first is through bulk assimilation of lower crustal rocks by the mafic parent magmas during their upward passage through the continental crust. The second is by subduction of the lower crustal rocks, or by their sedimentary detritus, on a down-going lithospheric slab and contamination of the mantle wedge source region of the parent magmas of the metaplutonic suite prior to partial melting. In modern subduction zones, contamination of the mantle wedge by subducting crustal material is assumed to occur largely by metasomatism. The data of this study do not indicate which of these two models is correct. However, the metasomatic source model is more compatible with the paucity of inherited zircons in the metaplutonic suite. It also is consistent with the lack of correlation between the ϵNd and chemical indices of contamination (increasing SiO_2 , decreasing MgO , ect).

2.8.2.2.2 *Meta-tonalite*

The significant difference between the meta-tonalite and the other compositions of the metaplutonic suite is that the major and trace element ratios appear to have evolved along a different fractionation trend (Figure 2.7 and 2.8). In essence the meta-tonalite trend extends from about 55 wt.% SiO₂, where it overlaps the composition of the meta-quartz diorite, toward a silica content of almost 60 wt.%. The distinctive characteristic of the meta-tonalite trend is that the concentrations in a number of elements with various affinities remain largely unchanged with increasing silica. There are three possible interpretations of the chemical variations of the meta-tonalites. The first is that the parent magmas of the meta-tonalite are related to those of the meta-quartz diorite by fractional crystallization. In this model, the break in chemical variations of the metaplutonic suite at 55 wt.% SiO₂ represents a change in the fractionation phase assemblage. In particular, the appearance of plagioclase on the liquidus could explain the variations in Al₂O₃, CaO and Na₂O with silica. There are several problems with this model, however: (1) Trace elements that are normally incompatible (La) and compatible (Ni) during fractional crystallization both tend to be relatively constant with increasing silica in the meta-tonalites; (2) The heavy REE patterns of the meta-tonalites tend to be more strongly fractionated than the meta-quartz diorite (Figure 2.9), which probably indicates different sources containing variable amounts of residual garnet; and (3) U-Pb zircon TIMS geochronology suggest the meta-tonalites are slightly younger, just outside analytical uncertainty, than the meta-quartz diorite.

A second possible interpretation of the meta-tonalites is that they formed by crustal contamination to the parent magmas of the meta-quartz diorites. The chemical

variations of the meta-tonalites are inconsistent with any of the observed Paleoproterozoic supracrustal rocks in the region being the contaminant (Figure 2.27), but the quartzofeldspathic gneisses from the Nain and Rae cratons can explain the trend (Figure 2.28). In this model, the concentrations of normally incompatible and compatible trace elements and the degree of heavy REE fractionation are controlled by the composition of the Archean contaminant. Again, however, if the meta-tonalite is younger than the meta-quartz diorite, their parent magmas cannot be related directly.

A third model for the meta-tonalites is that they formed from a parent magma that had a different source than the rest of the metaplutonic suite. Tonalite magmas cannot be derived from melting of the mantle but instead require a less mafic source. In the context of the proposed mantle wedge origin for the majority of the metaplutonic suite, the meta-tonalites could have been derived from partial melts of the subducting ocean crust. The isotopic characteristics of the meta-tonalites would be inherited from their ocean crust sources. Slab melting is thought to have been more common in the Archean than post-Archean, as is discussed in next section of this paper.

2.8.2.3 Comparisons of the Metaplutonic Suite

2.8.2.3.1. With Calc-alkaline Metaplutonic Rocks of the Torngat Orogen

Calc-alkaline metaplutonic rocks have been identified along the length of the Torngat Orogen from both northern (Burwell Domain) and southern (Nutak-North River) segments. Similarities or differences with the metaplutonic suite of the Voisey's Bay area could provide insight into the tectonic relationships along the length of the orogen.

In terms of major element compositions, the Voisey's Bay metaplutonic rocks are very similar to the Groups 1 and 2 of metaplutonic rocks from the Burwell Domain (Campbell, 1997) and to the eastern and western groups of the Southern orogen (Theriault and Ermanovics, 1997). Major element compositions of these calc-alkaline suites overlap to some degree with one another, being dominated by intermediate compositions (Figure 2.32 and 2.33). In contrast, Group 3 ($\epsilon\text{Nd}_{1895 \text{ Ma}} < -5$) from the Burwell domain is far more felsic. There are some notable differences in the trends and composition ranges of the various metaplutonic suites. The Eastern metaplutonic suite of the southern orogen mirrors the major element trends versus silica seen in the Voisey's Bay metaplutonic suite, including the break in the trend at 55 wt.% SiO_2 . However, Fe_2O_3 values are much more elevated than in the Voisey's Bay metaplutonic suite. Major element trends of the Group 1 ($\epsilon\text{Nd}_{1895 \text{ Ma}} > 0$) and 2 ($\epsilon\text{Nd}_{1895 \text{ Ma}} -5$ to 0) of the Burwell Domain and the Western metaplutonic suite are more felsic than the Voisey's Bay metaplutonic suite with most samples greater than 52 wt.% SiO_2 (Figure 2.32 and 2.33). Major element trends for these three units are similar to the meta-tonalites, with the exception of Fe_2O_3 in the western metaplutonic suite that is elevated and displays no clear trend. Group 3 ($\epsilon\text{Nd}_{1895 \text{ Ma}} < -5$) is more felsic than all of the other suites with 65-71.6 wt.% SiO_2 , however, its major elements lie along the same trend as the Voisey's Bay meta-tonalites and also the Group 1 rocks.

The chondrite-normalized REE plots of the Group 1 and 2 of meta-plutonic rocks, in the Burwell domain, display the same fractionation of LREE from HREE that is seen in the Voisey's Bay metaplutonic rocks (Figure 2.34). The exception is Group 2 of the

Burwell Domain, which is extremely depleted in HREE, suggesting usually large amounts of residual garnet in their source regions. This fractionation of LREE/HREE elements is also seen in the Eastern and Western suites in the southern orogen (Figure 2.35). Again, however, some compositions, particularly the Eastern metaplutonic suite, are more depleted in HREE. In terms of Nd isotopes, the Voisey's Bay metaplutonic suite fall within the range of the other metaplutonic rocks of the Torngat Orogen (Figure 2.36). (The apparent difference between the low $f_{Sm,Nd}$ of the Amelin et al. (2000) samples and of the other compositions is the result of the former including mineral separates).

U-Pb zircon TIMS ages for the Voisey's Bay calc-alkaline metaplutonic rocks are 1893 ± 3 Ma, 1890 ± 2 Ma and 1883 ± 5 Ma. These ages correspond with the ages of calc-alkaline intrusive activity in the Northern segments (Burwell Domain) of the Torngat Orogen, which lasted between 1.91 to 1.86 Ga (Scott and Machado, 1994; Scott, 1995) and with the 1.88 Ga age of calc-alkaline activity in the southern segments (Nutak-North River map area) of the orogen (Bertrand et al., 1993). It is clear that mafic to intermediate-dominated, calc-alkaline magmatic activity occurred along the length of the Torngat Orogen from 1.91 to 1.86 Ga and, with the results of this study, can now be extended as far south as the Voisey's Bay area, a distance of some 500 km. This suggestion is that the calc-alkaline rocks of the Torngat Orogen formed along a convergent plate margin of substantial length.

There has been some debate about the polarity of subduction during the calc-alkaline magmatism in the Torngat Orogen in the Paleoproterozoic. Some authors (Bertrand et al., 1993; Theriault and Ermanovics, 1997) have suggested west-dipping

subduction beneath the Rae craton; others have proposed east dipping subduction beneath the Nain craton (Scott, 1995; Rivers et al., 1996). More complex models of dual subduction with opposing polarity and flipping of subducted polarity from east to west ca. 1885 Ma (van Kranendonk and Wardle, 1996; 1997) have also been suggested. The results from this study add little to this debate as the contact relationships of the metaplutonic suite in the Voisey's Bay area are deformed and tectonized. Thus, it is not possible to determine whether the metaplutonic suite intruded the Nain orthogneisses to the east or the Tasiuyak paragneisses to the west. Moreover the evidence for crustal contamination in the metaplutonic suite does not point to any observed Archean or Proterozoic units in the area being a contaminant.

2.8.2.3.2. With Modern Arc Magmas

The calc-alkaline metaplutonic rocks of the Voisey's Bay area provide insight into the formation of subduction-related magmatism during the Paleoproterozoic. This time period is transitional between the Archean, when subduction-related magmatism was dominated by tonalite-trondhjemite-granodiorite (TTG) derived by melting of the subducting slab, and the late Proterozoic and Phanerozoic when arc melts were produced mainly from the mantle wedge. The difference is thought to be related to higher heat flow in the Archean mantle than thereafter. Martin (1994) suggested that distinctions between Archean "slab" melts and post-Archean "wedge" melts could be made on the basis of the REE patterns of juvenile granitoids of subduction-related suites. Figure 2.37 compares the granitoids of the Torngat Orogen, including the meta-quartz diorite and meta-tonalites of the Voisey's Bay metaplutonic suite, to Archean and post-Archean granitoids in terms of

La/Yb versus Yb. The Torngat samples tend to have high La/Yb and low Yb, more like the Archean granitoids. This suggests that slab melting was an important processes in the formation of arc magmatism in the Torngat Orogen. As described earlier in this paper, however, slab melting did not dominate in the Voisey's Bay metaplutonic suite, as voluminous magmatic products from the mantle wedge formed as well (meta-gabbro to meta-quartz diorite series). Thus, at least in the Torngat Orogen of northern Labrador, Paleoproterozoic subduction processes were transitional between those of the Archean and those of today.

2.9 CONCLUSION

The Voisey's Bay Paleoproterozoic metaplutonic rocks were defined and characterized based on the field mapping, petrography, geochemistry, isotopic data and geochronology. This has led to several major conclusions, which include the following:

- 1) The metaplutonic suite is a relatively undifferentiated, mafic to intermediate calc-alkaline batholith (composition from meta-gabbro to meta-tonalite) that was generated above a Paleoproterozoic subduction zone. Meta-quartz diorite is the dominant lithology.
- 2) The ca. 1890 meta-gabbro to meta-quartz diorite rocks of this suite appear to have evolved along an igneous fractionation trend. Primitive parent magmas of the suite were probably derived by partial melting of the mantle wedge but interacted with crustal material, either in the source region or lower crust.

- 3) The meta-tonalites are slightly younger (1883 \pm 5 Ma), and have a different magmatic evolution based on major and trace element variations, than the other components of the suite. They may have been derived by partial melting of subducting oceanic crust in the Paleoproterozoic subduction zone.
- 4) The Voisey's Bay metaplutonic suite is similar in composition and age to calc-alkaline magmatic rocks that occur along the length of the Torngat Orogen. The calc-alkaline magmatism may have formed along a single convergent plate margin, some 500 km in length.
- 5) As both slab and wedge melting were important in producing calc-alkaline magmatism in the Paleoproterozoic Torngat Orogen, transition from slab-dominated Archean magmatism to wedge-dominated post-Archean magmatism may have occurred progressively through the Paleoproterozoic.

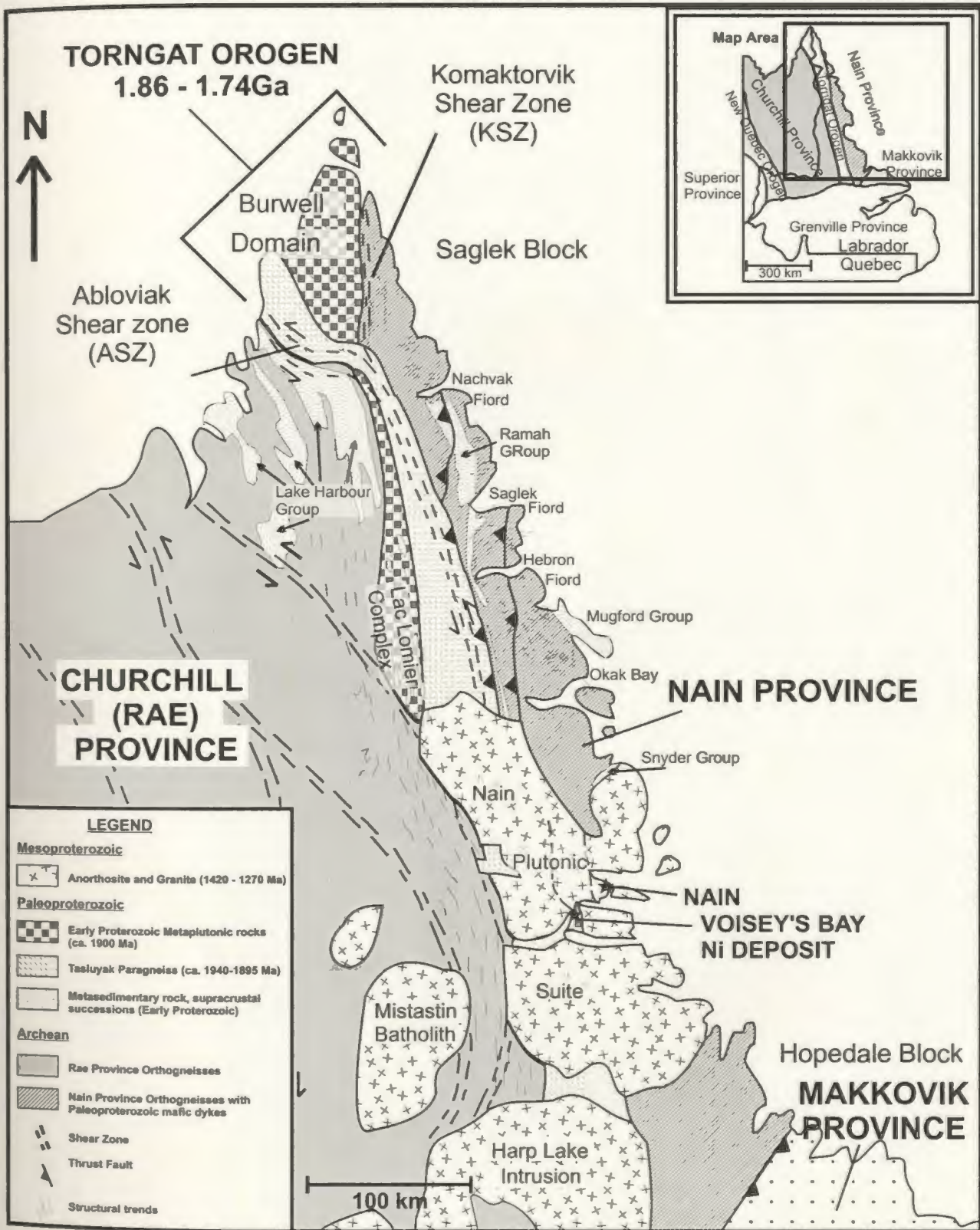


Figure 2.1 Generalized map of the Torngat Orogen, Churchill and Nain Provinces. Showing the major geological units of the area (simplified after van Kranendonk, 1990).

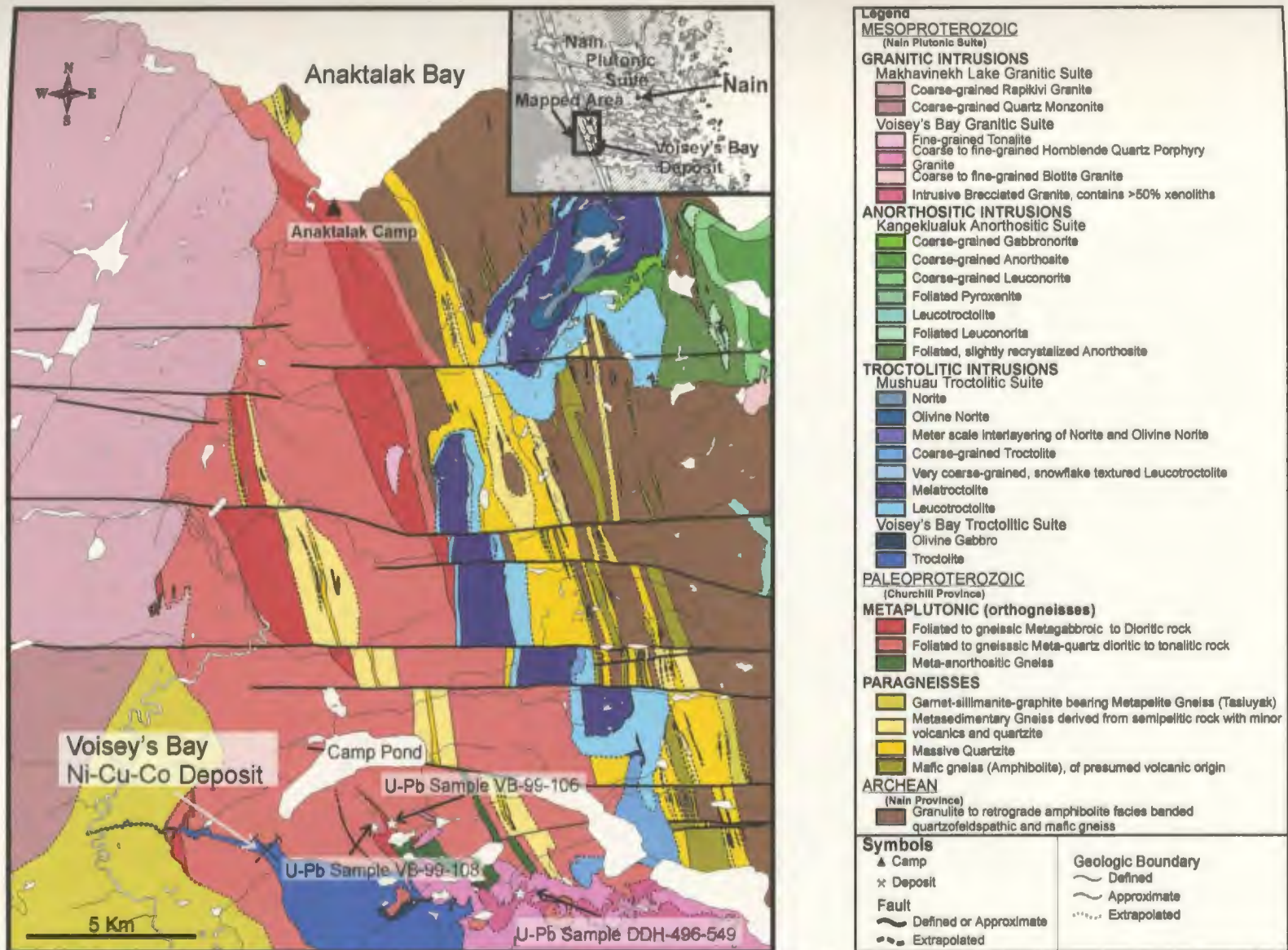


Figure 2.2 Detailed geologic map of Anaktalak to Voisey's Bay area, Labrador. Major units and U-Pb samples are labeled. Mapping by A. M. Rawlings at 1:10,000 scale. Maps by Ryan and Lee (1985) at 1:50,000 and Voisey's Bay Nickel Company (1997) at 1:25,000 were used as guides.

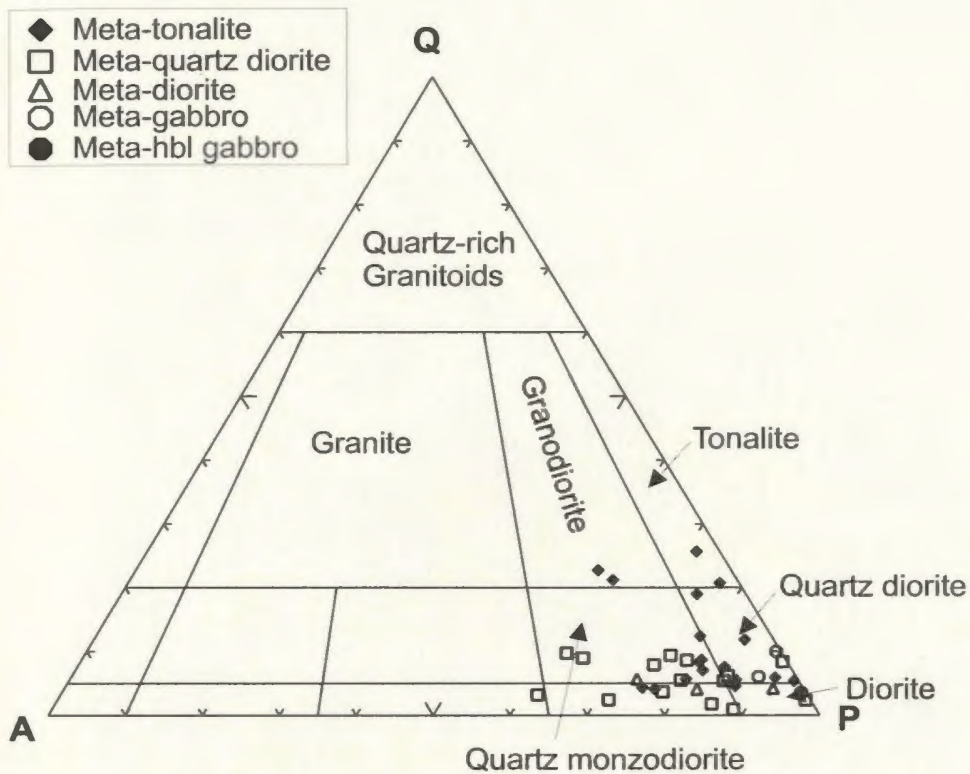


Figure 2.3. Quartz-Alkali-feldspar-Plagioclase (QAP) classification diagram of Paleoproterozoic metaplutonic rocks from Voisey's Bay, Labrador. QAP diagram from Le Maitre (1989).

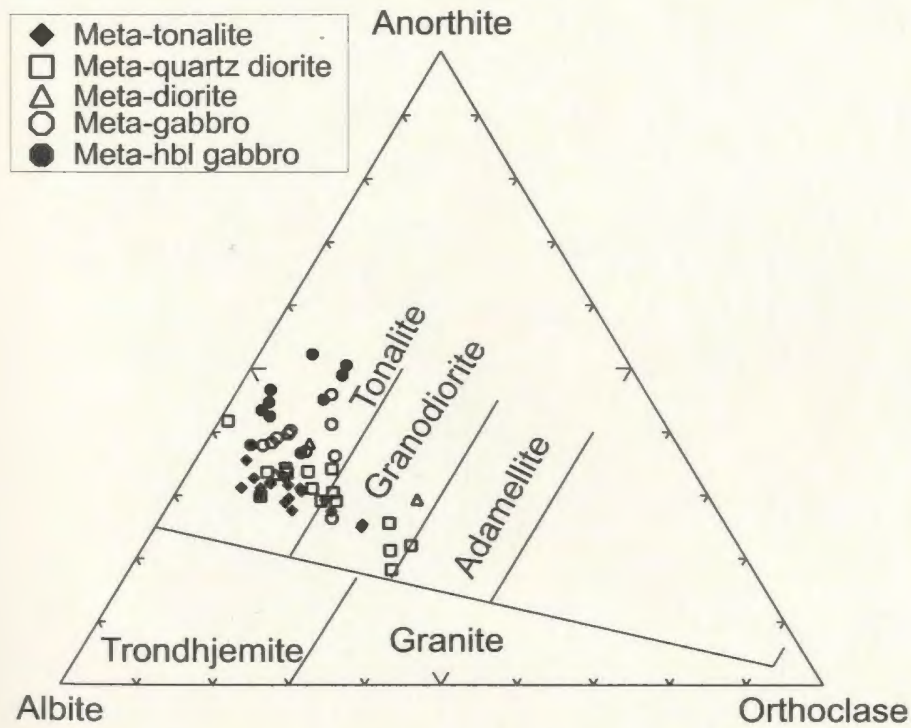


Figure 2.4. Anorthite-Albite-Orthoclase classification diagram of Paleoproterozoic metaplutonic rocks from Voisey's Bay, Labrador. Classification fields from Barker (1979).

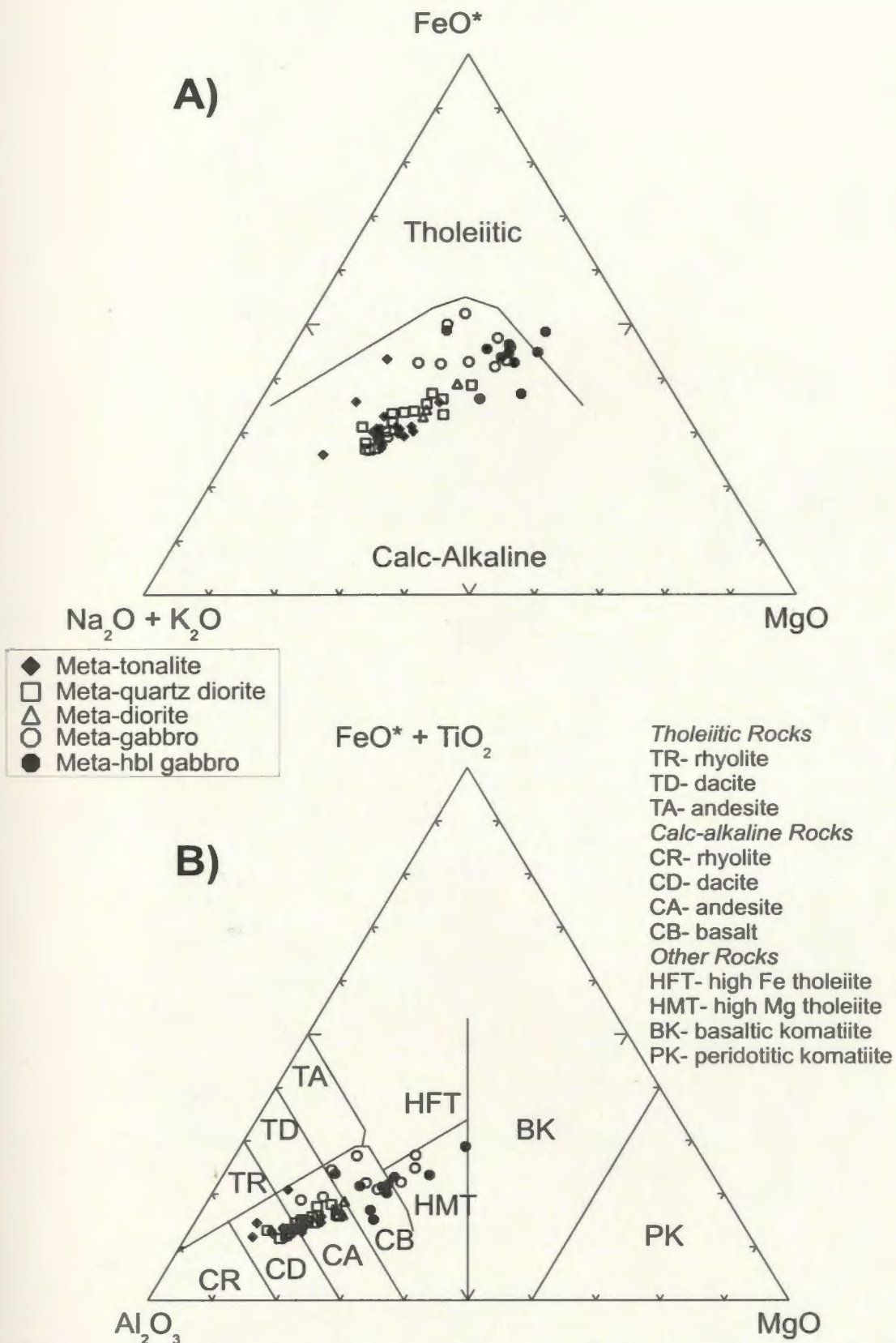


Figure 2.5. Classification diagram of Paleoproterozoic metaplutonic rocks from Voisey's Bay, Labrador. A) AFM diagram (Irvine and Baragar, 1971). B) Cation plot (Jensen, 1976). FeO* was recalculated from total Fe using the method by Le Maitre (1976).

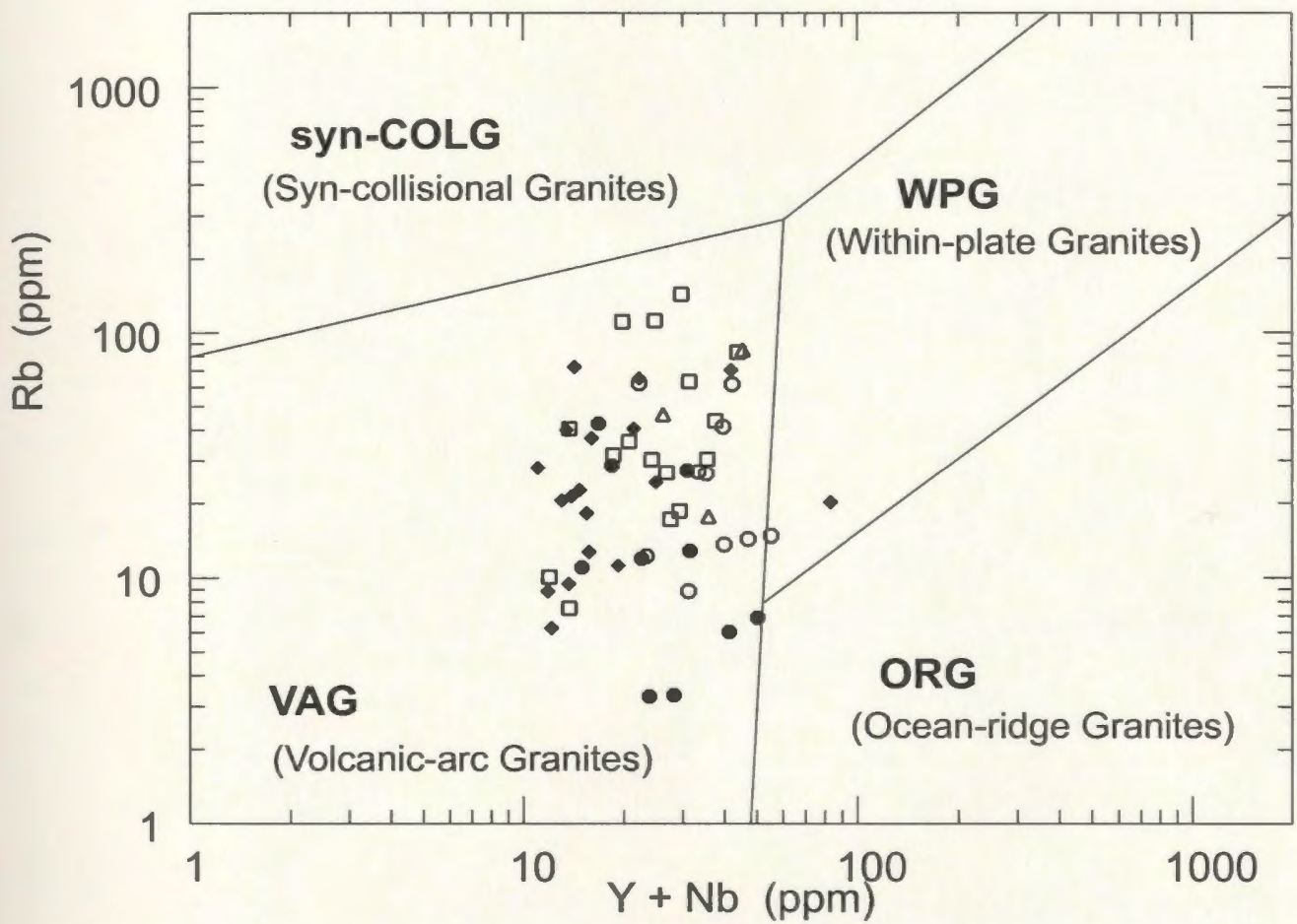
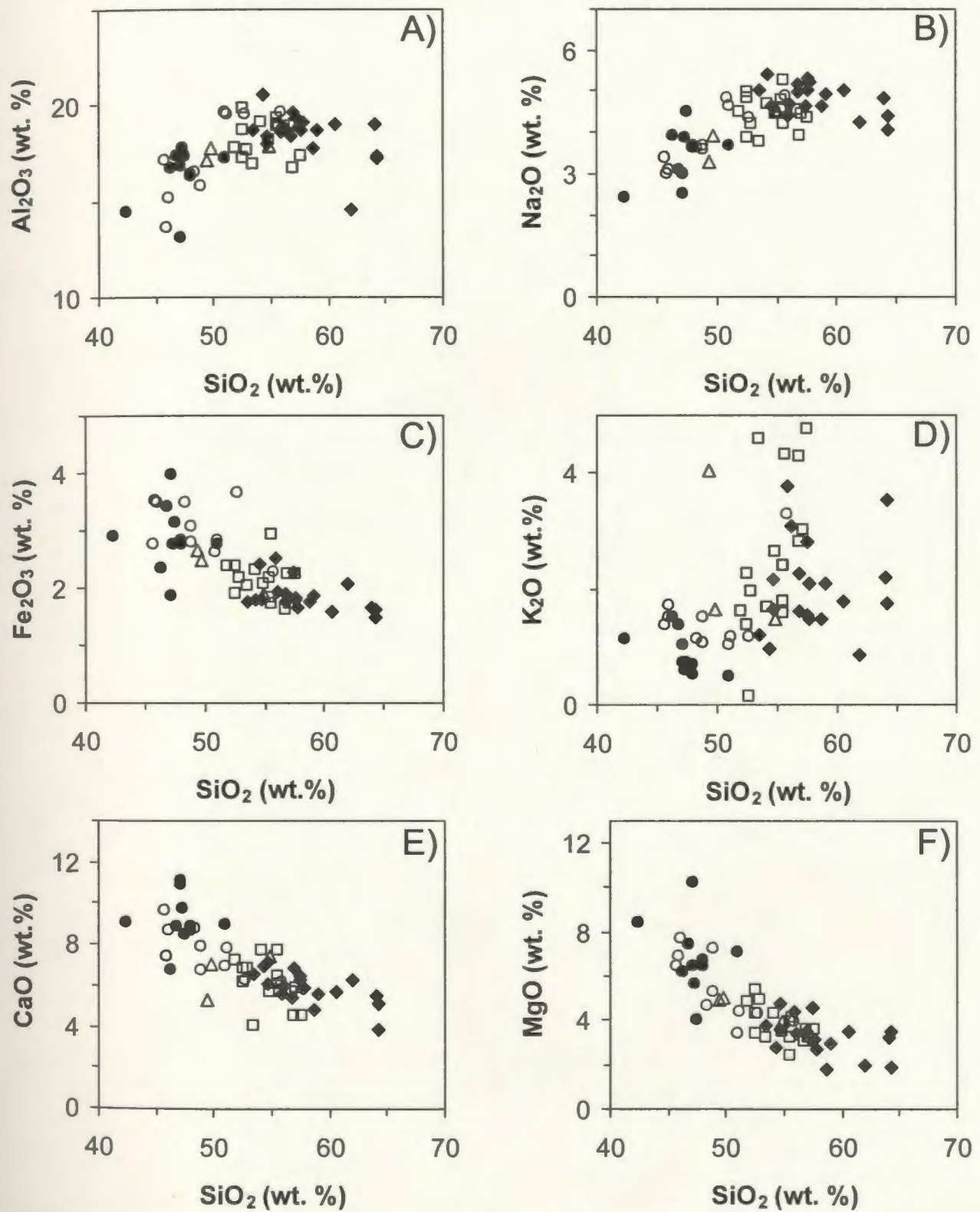
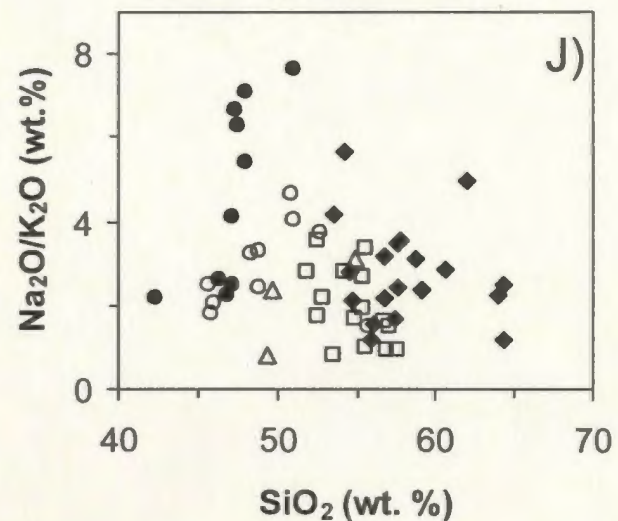
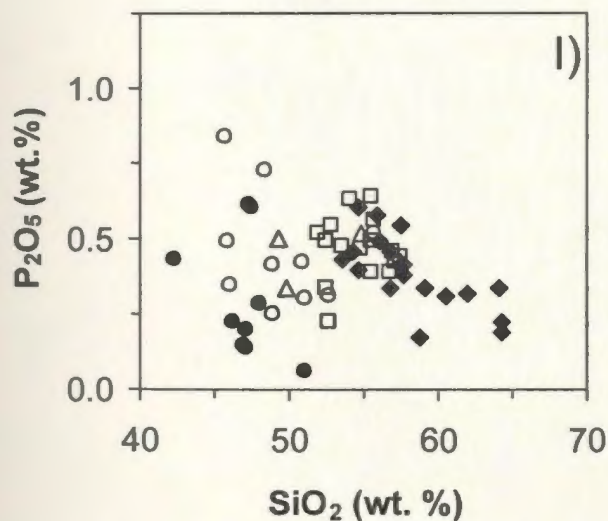
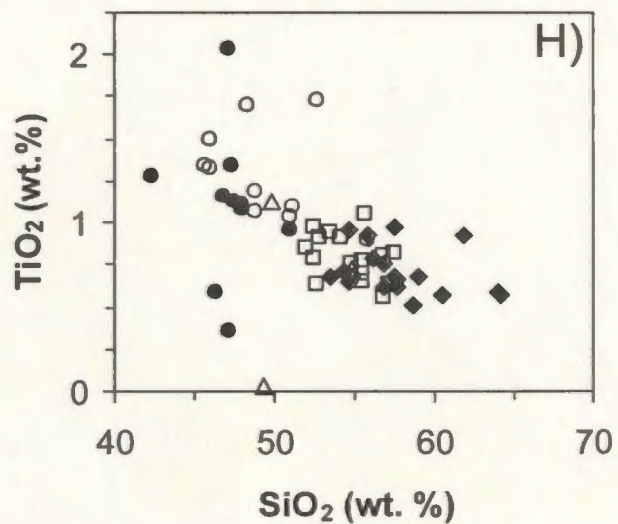
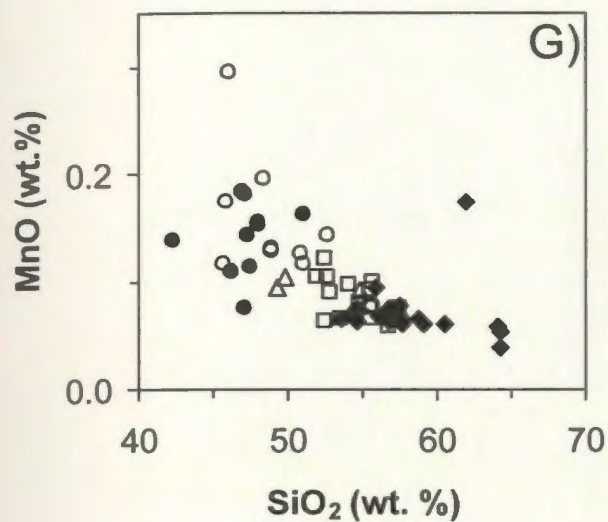


Figure 2.6. Tectonic discrimination diagram of Paleoproterozoic metaplutonic rocks from Voisey's Bay, Labrador. Diagram from Pearce et al. (1984). Symbols as in Figure 2.5 for samples.



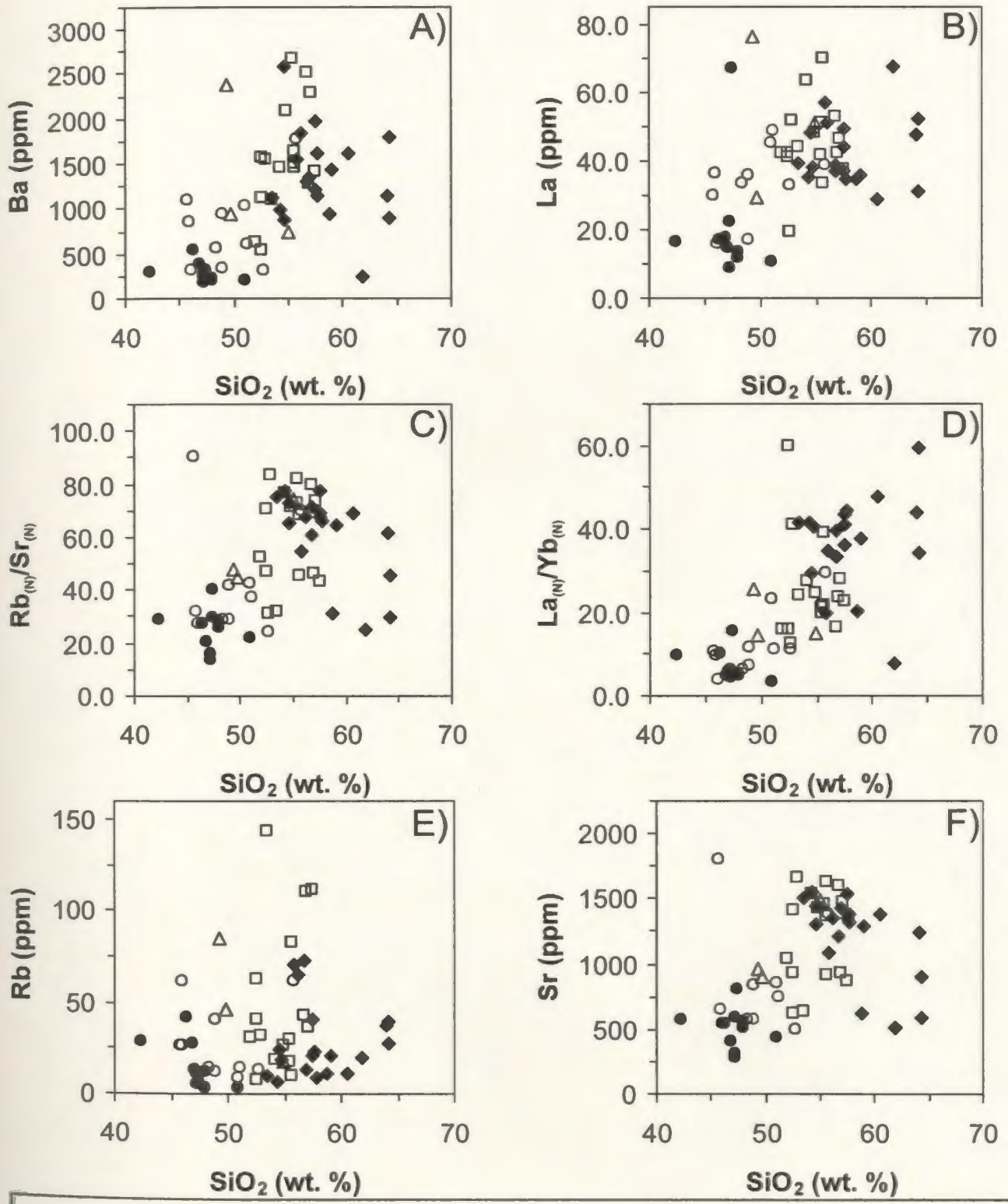
◆ Meta-tonalite □ Meta-quartz diorite ▲ Meta-diorite ○ Meta-gabbro ● Meta-hbl gabbro

Figure 2.7. SiO₂ versus major element (Harker) diagrams of Paleoproterozoic metaplutonic rocks from Voisey's Bay, Labrador, including (A) Al₂O₃, (B) Na₂O, (C) Fe₂O₃, (D) K₂O, (E) CaO, (F) MgO, (G) MnO, (H) TiO₂, (I) P₂O₄, (J) Na₂O/K₂O ratio.



◆ Meta-tonalite □ Meta-quartz diorite △ Meta-diorite ○ Meta-gabbro ● Meta-hbl gabbro

Figure 2.7. (Continued).



◆ Meta-tonalite □ Meta-quartz diorite △ Meta-diorite ○ Meta-gabbro ● Meta-hbl gabbro

Figure 2.8. SiO₂ versus selected trace elements or ratios versus for Paleoproterozoic metaplutonic rocks from Voisey's Bay, Labrador, including (A) Ba, (B) La, (C) Rb_(N)/Sr_(N), (D) La_(N)/Yb_(N), (E) Rb, (F) Sr, (G) K₂O/Rb, (H) La_(N)/Y_(N), (I) Nb, (J) Y, (K) Eu, (L) Th, (M) Ni, (N) V, and (O) Sc. Data for Ni and Sc that are below detection are not plotted. Normalized values _(N) are primitive mantle from Sun and McDonough (1989).

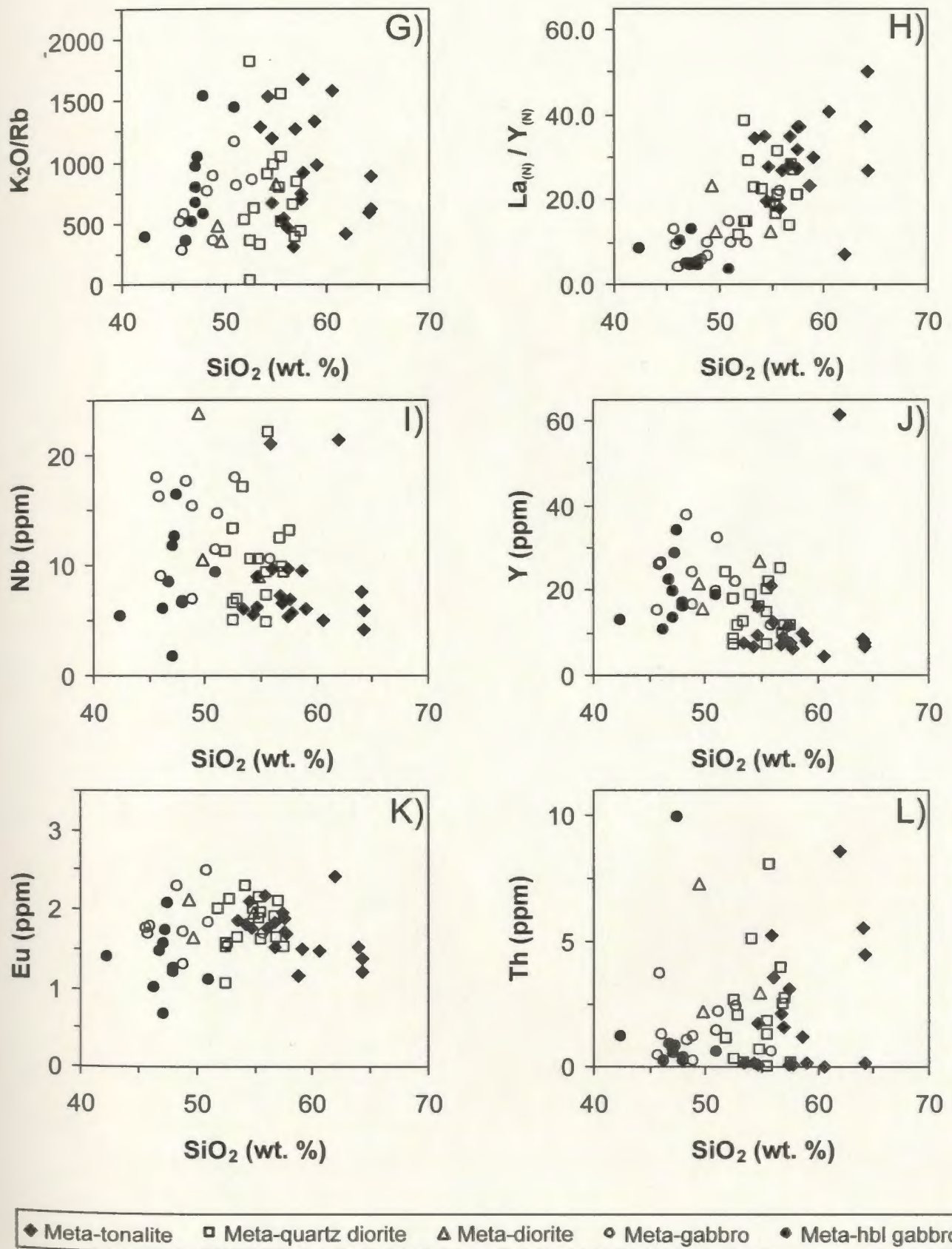
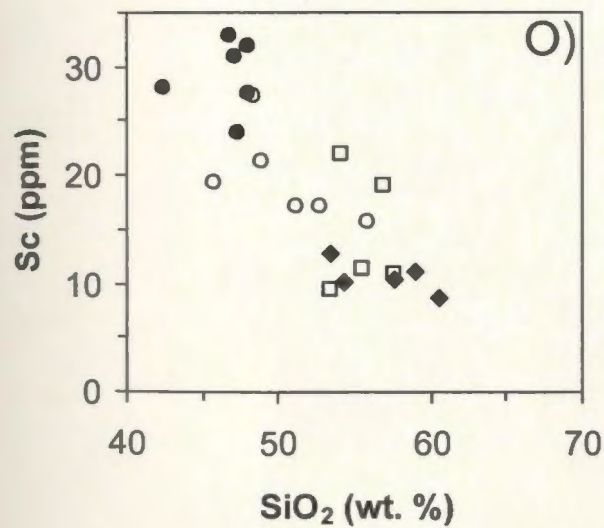
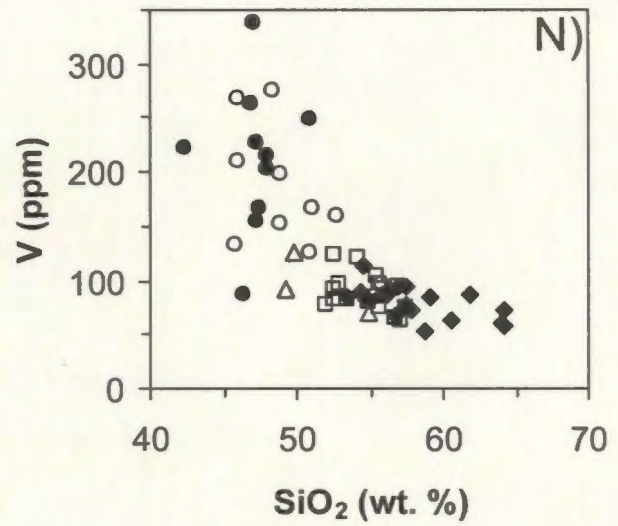
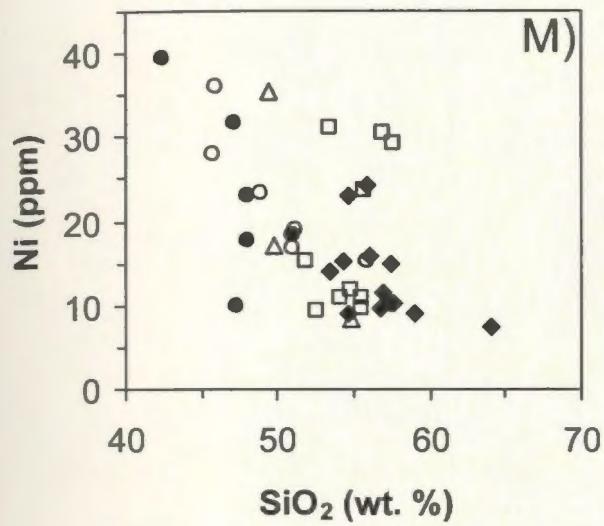


Figure 2.8. (Continued).



◆ Meta-tonalite □ Meta-quartz diorite △ Meta-diorite ○ Meta-gabbro ● Meta-hbl gabbro

Figure 2.8. (Continued).

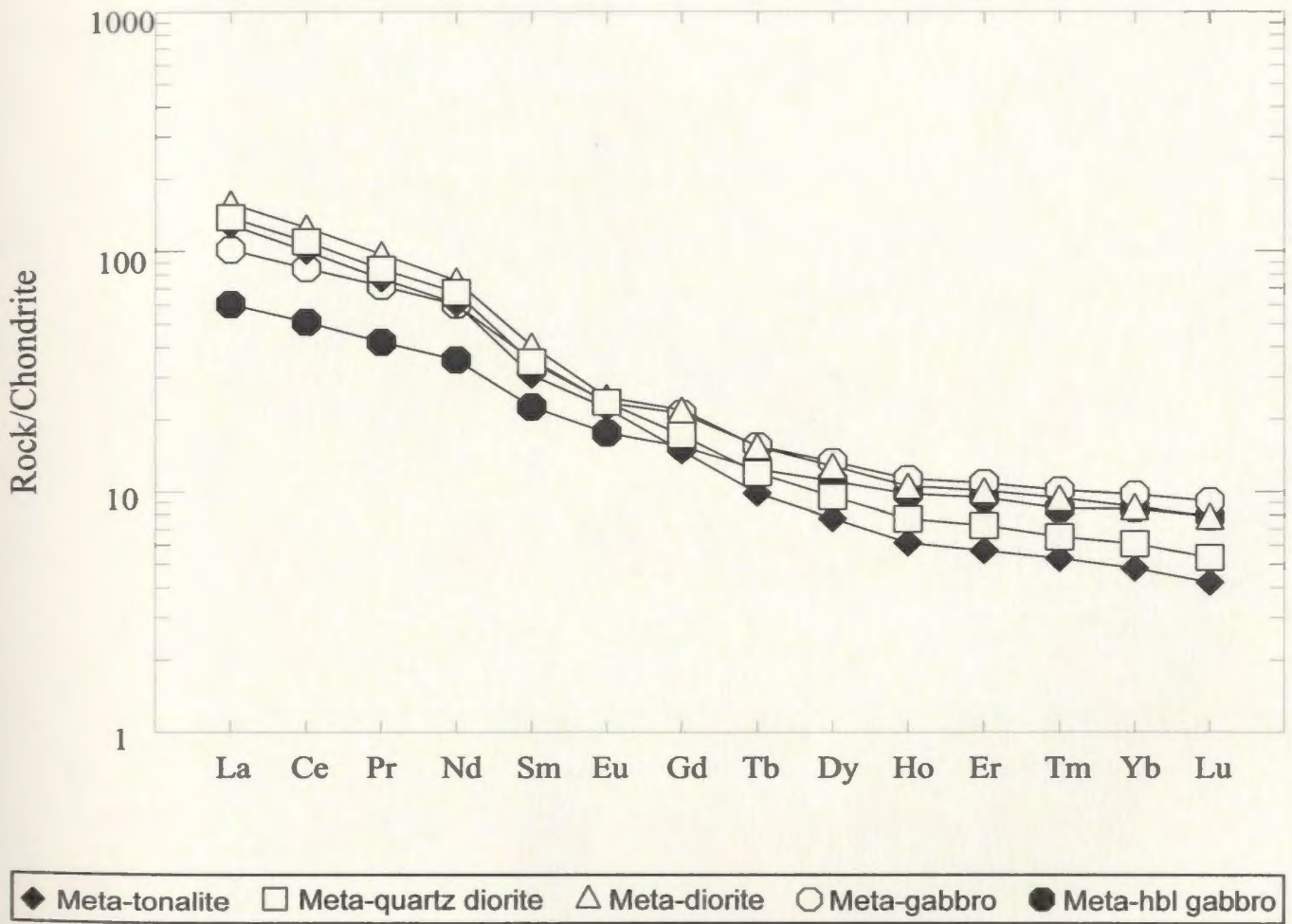


Figure 2.9. Chondrite normalized REE diagrams for the average of each the group of the Paleoproterozoic metaplutonic rocks from Voisey's Bay, Labrador. Normalizing values from Sun (1980).

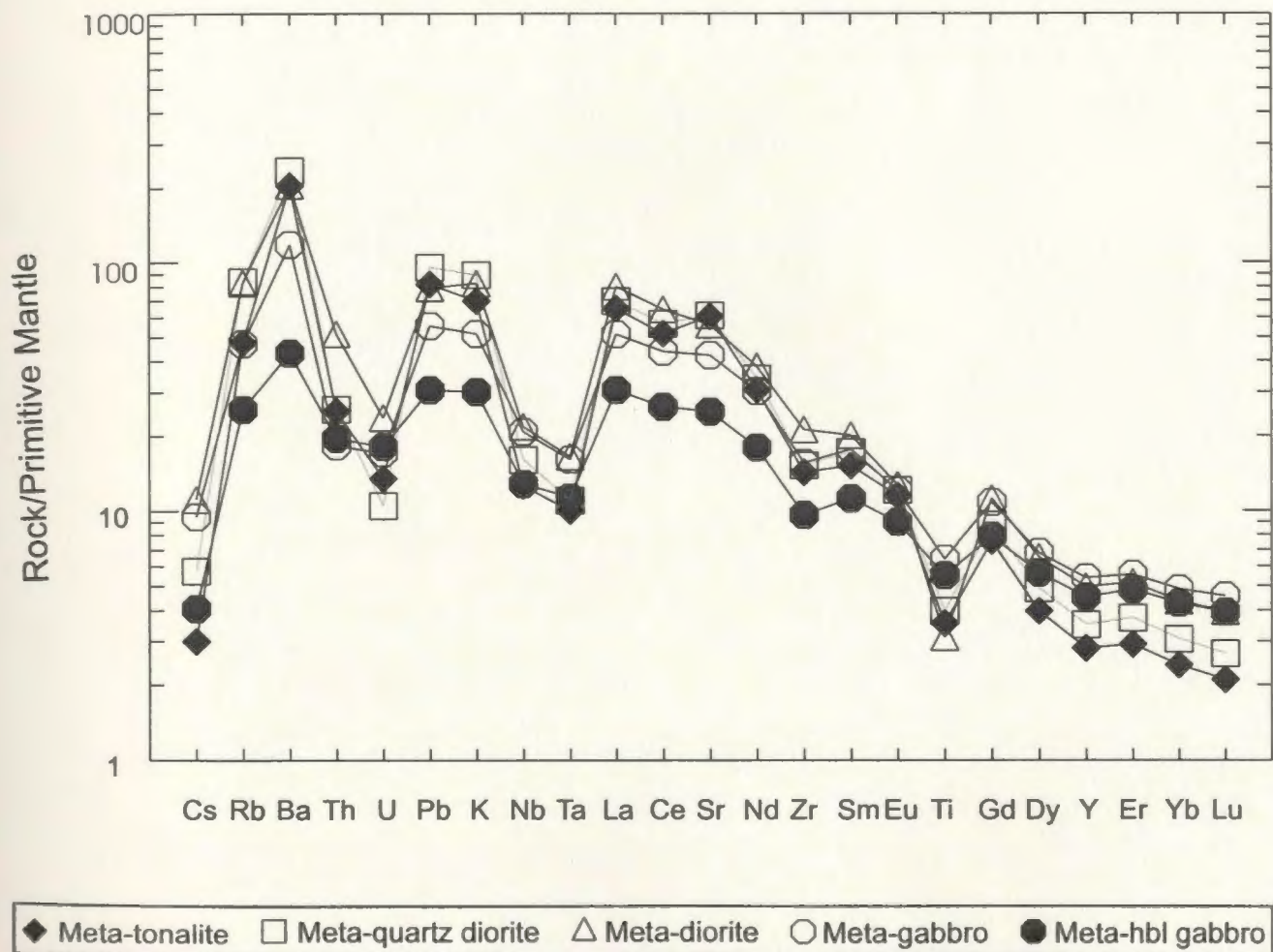
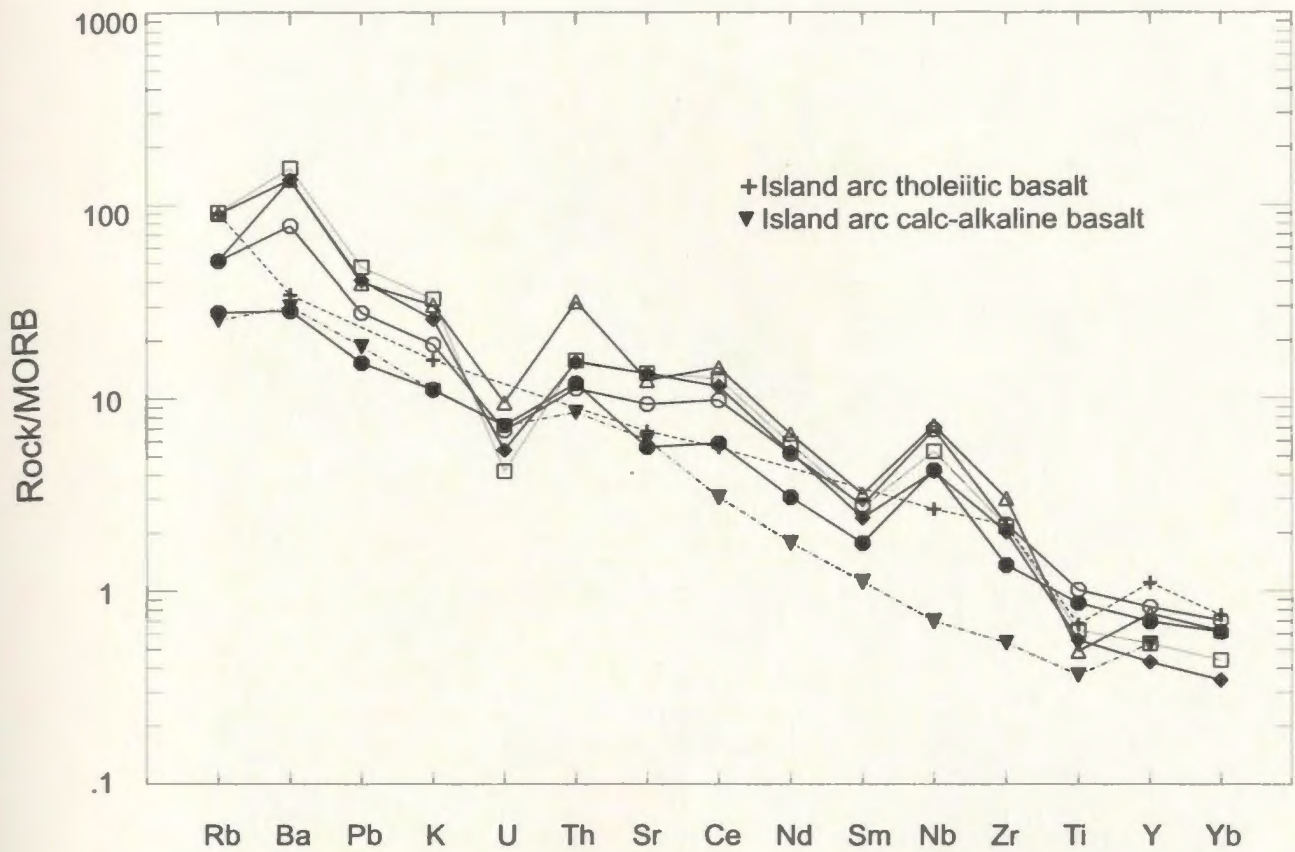
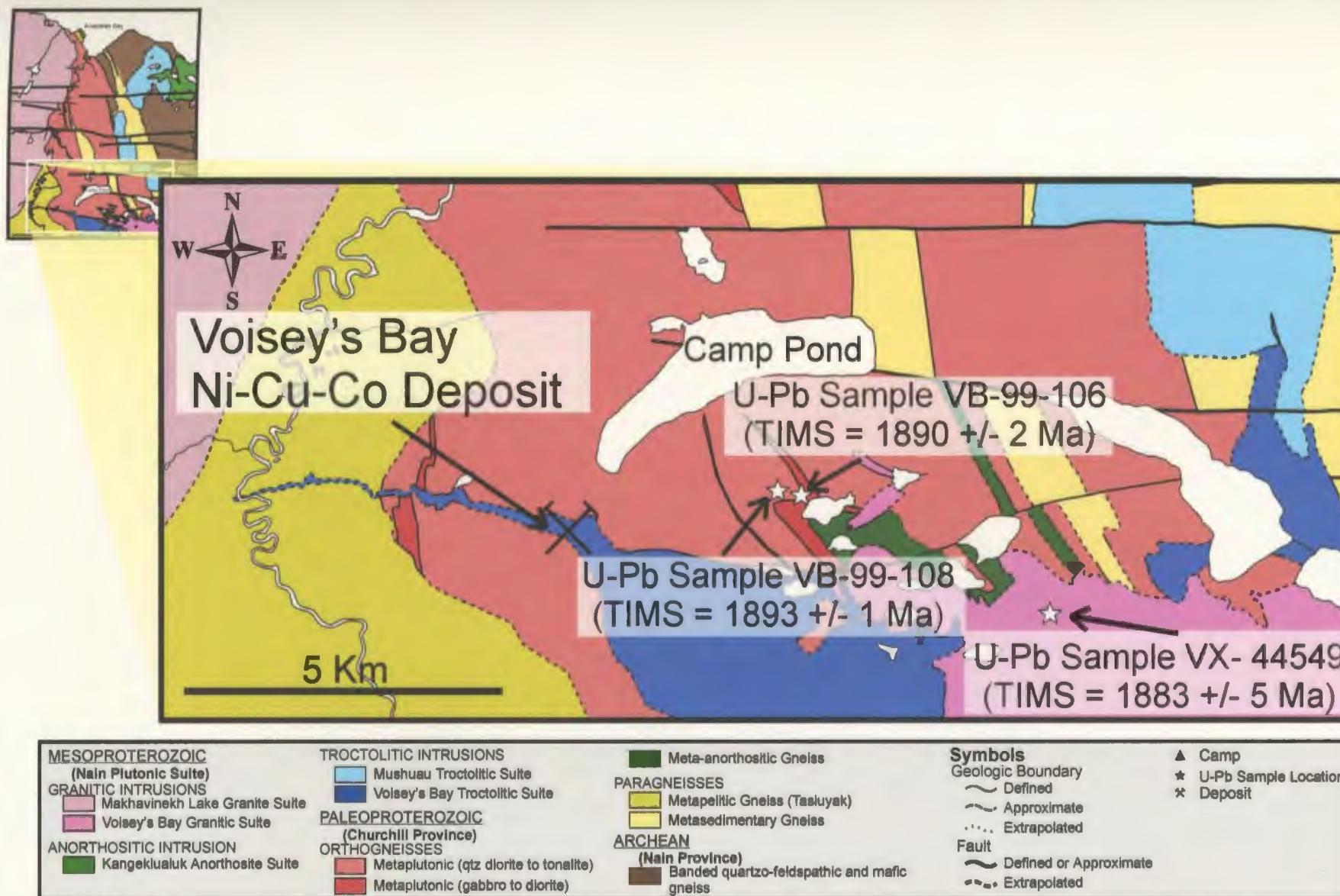


Figure 2.10. Primitive-mantle normalized extended trace element spider-diagrams for the average of each group of the Paleoproterozoic metaplutonic rocks from Voisey's Bay, Labrador. Normalizing values from Sun and McDonough (1989).



◆ Meta-tonalite □ Meta-quartz diorite △ Meta-diorite ○ Meta-gabbro ● Meta-hbl gabbro

Figure 2.11. Mid-ocean ridge basalt (MORB) normalized extended trace element spider-diagrams for the average of each group of the Paleoproterozoic metaplutonic rocks from Voisey's Bay, Labrador. Normalizing values from McCulloch and Gamble (1990). Island arc tholeiitic basalt data from Ewart (1982) and island arc calc-alkaline basalt from Sun (1980).



2-55 **Figure 2.12.** Simplified geologic map of Voisey's-Anaktalak Bay area, Labrador (simplified after Map 1, back pocket). Showing the location of the U-Pb zircon samples.

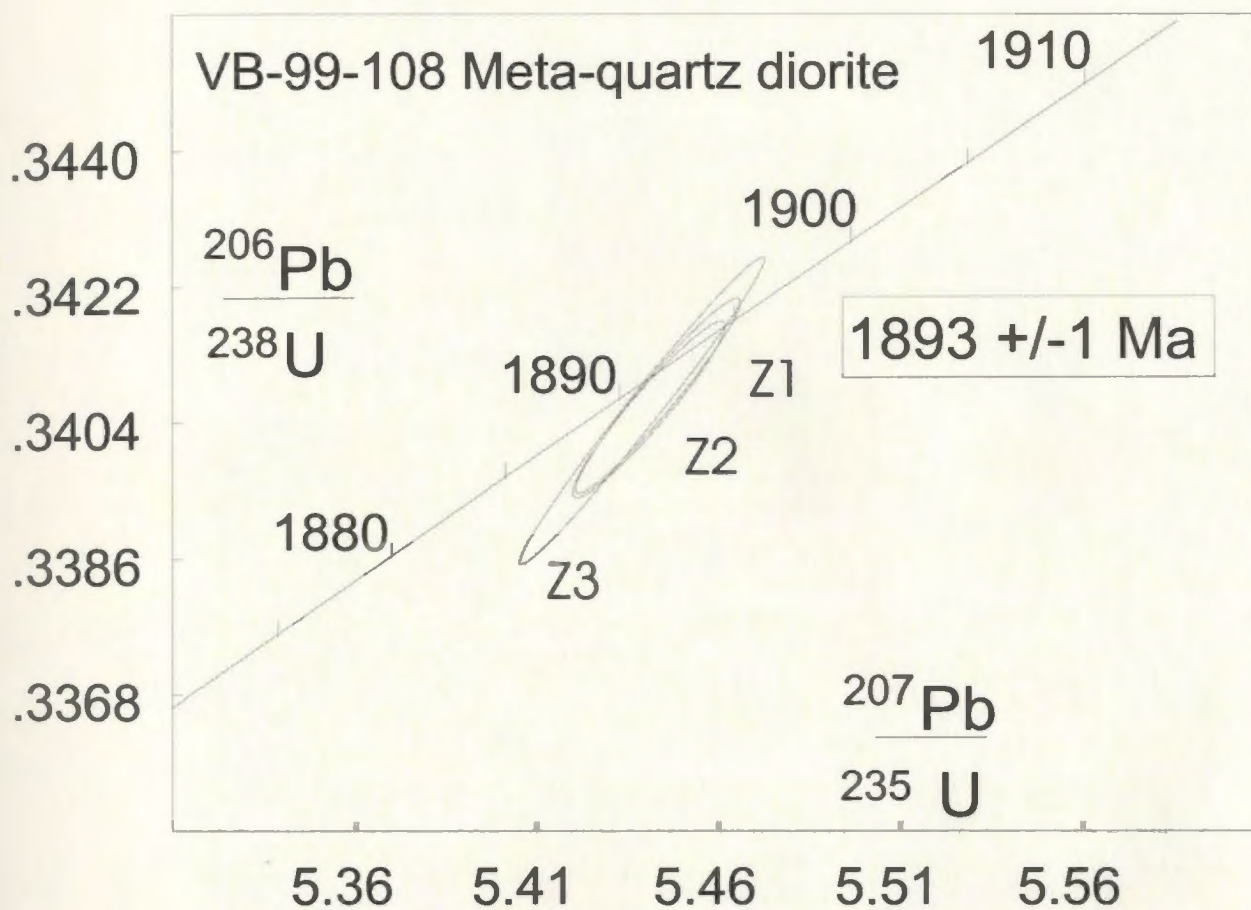


Figure 2.13. U-Pb concordia plot for the sample of meta-quartz diorite VB-99-108 from Voisey's Bay, Labrador.

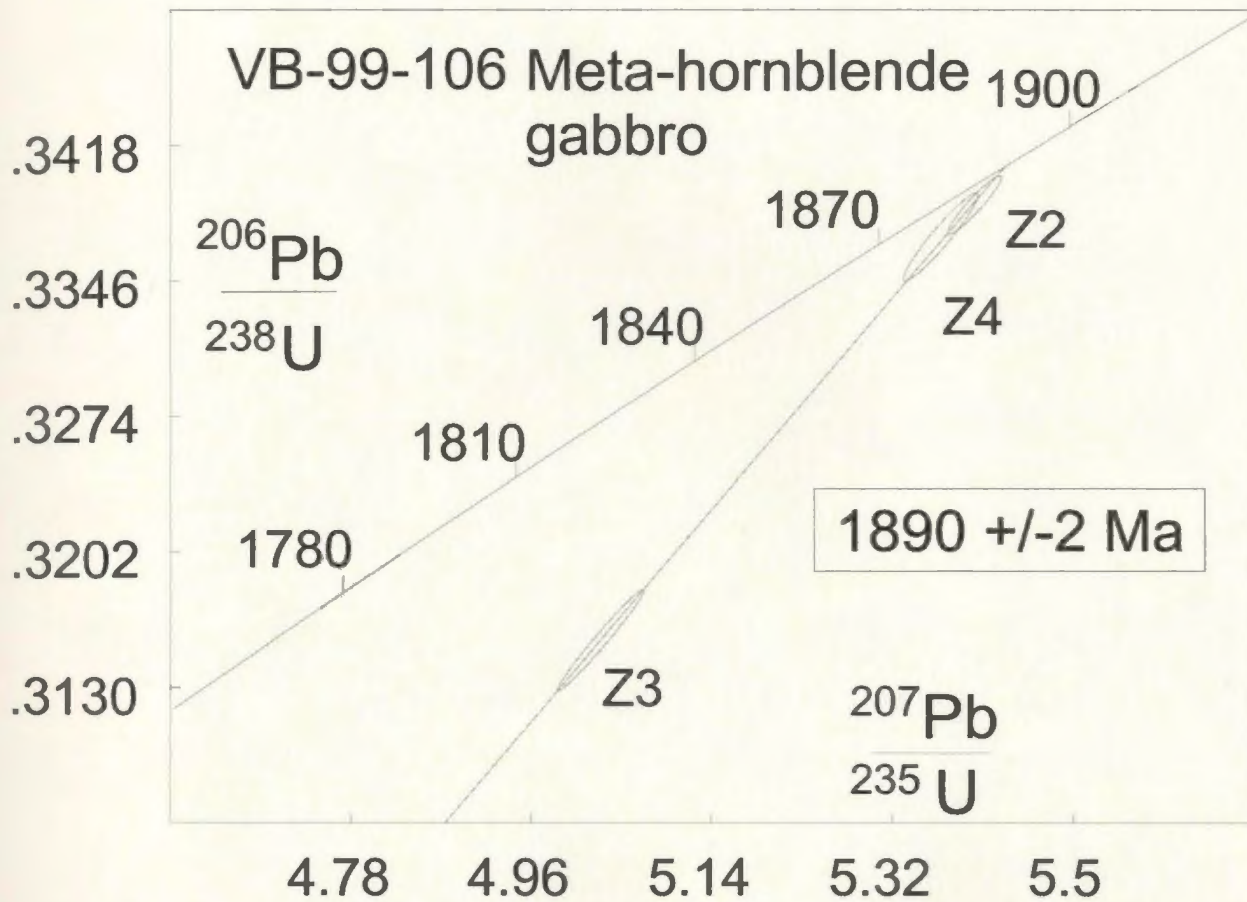


Figure 2.14. U-Pb concordia plot for the sample of meta-hornblende gabbro VB-99-106 from Voisey's Bay, Labrador.

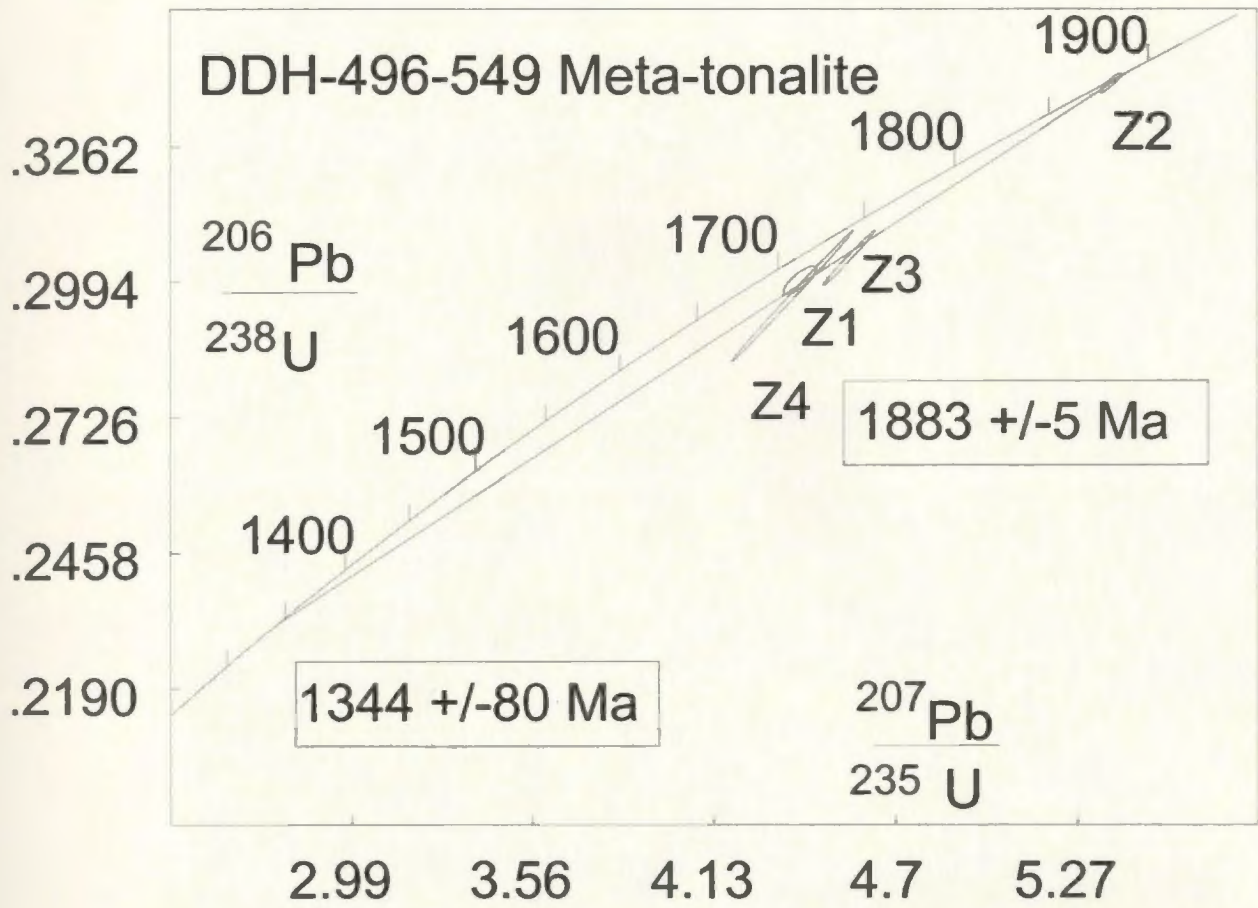
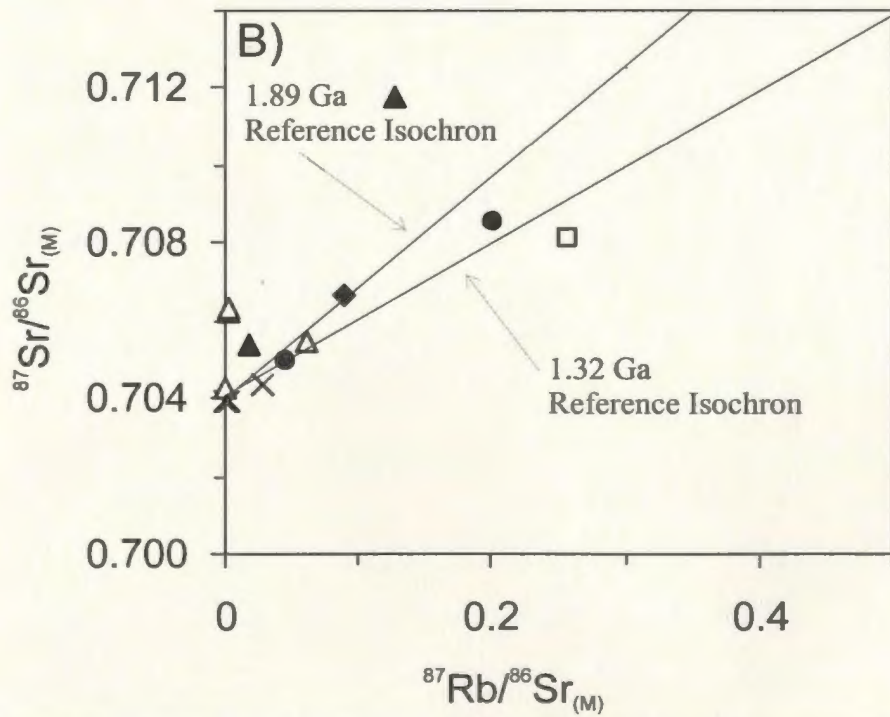
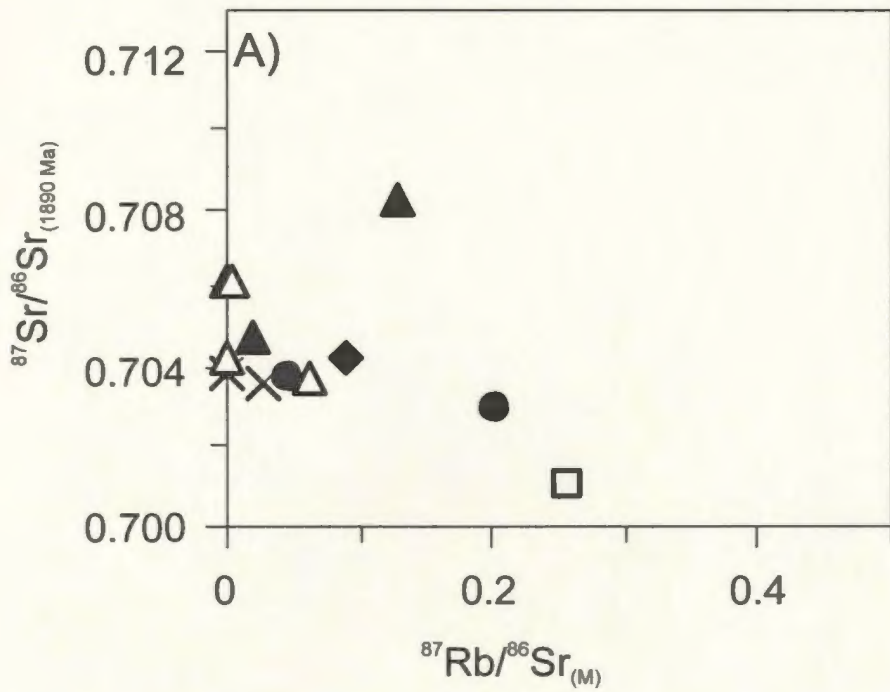
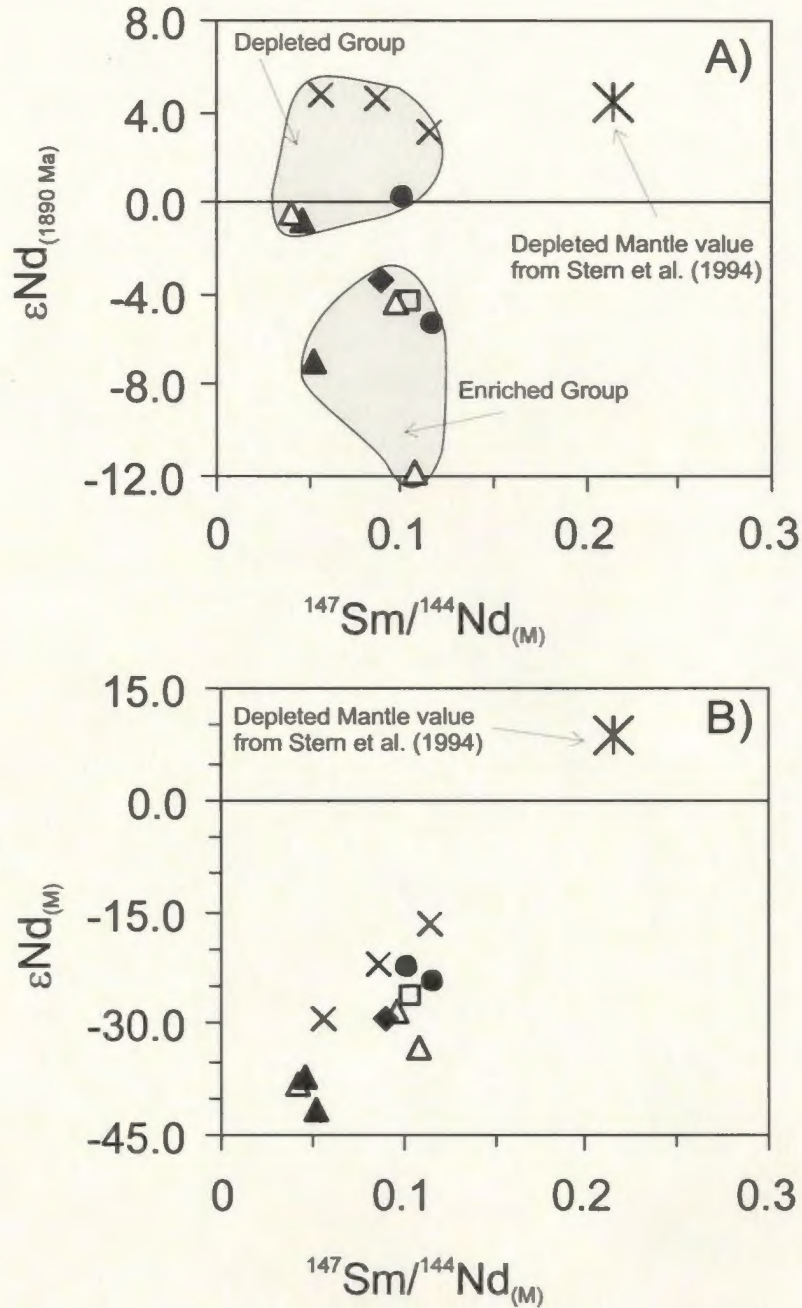


Figure 2.15. U-Pb concordia plot for the sample of meta-tonalite DDH-496-549 from Voisey's Bay, Labrador.



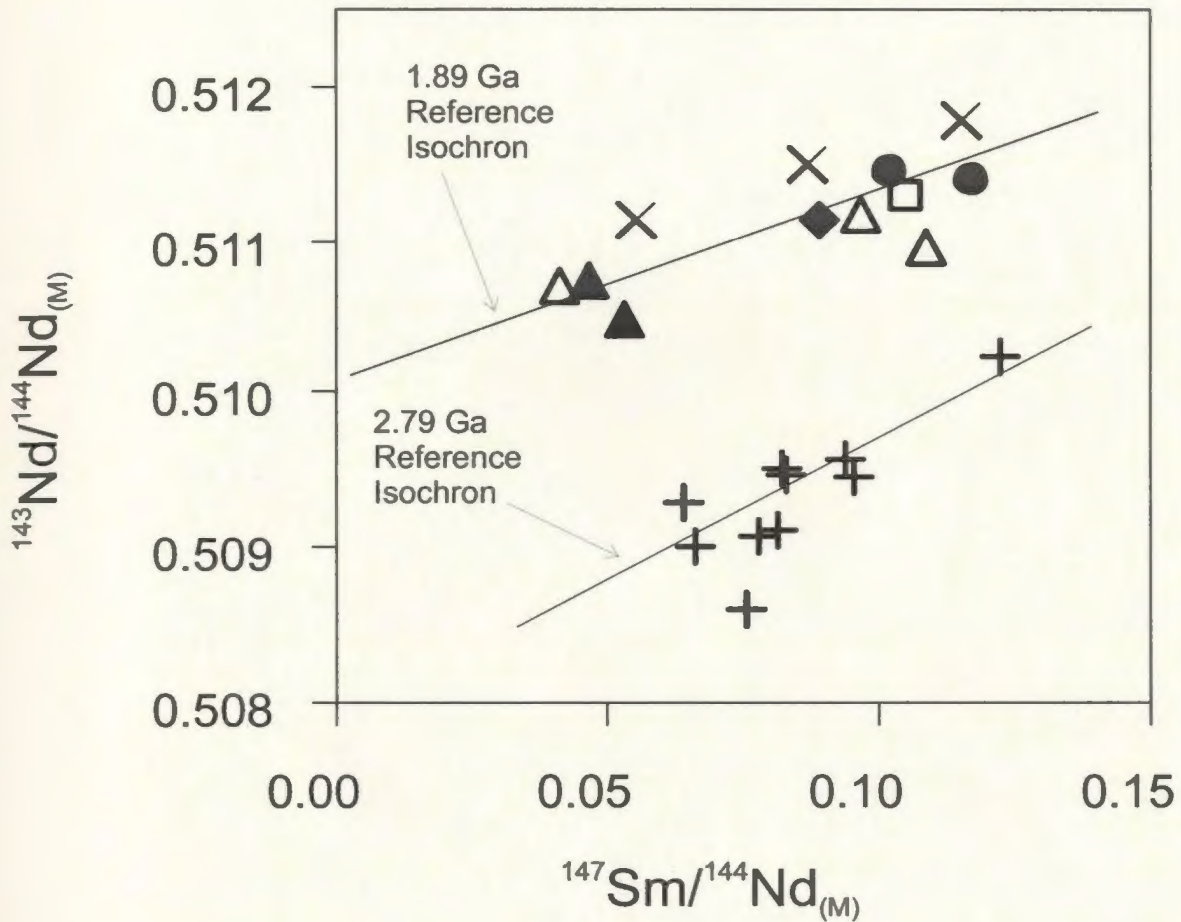
Paleoproterozoic Metaplutonic Suite		
This Study	◆ Meta-tonalite	□ Meta-quartz diorite
Amelin et al. (2000)	× "Enderbite"	▲ Quartzo-feldspathic gneisses
		● Meta-hornblende gabbro
		△ Mafic gneisses

Figure 2.16. Rb-Sr isotopic data for the Paleoproterozoic metaplutonic rocks from Voisey's Bay, Labrador. A) $^{87}\text{Rb}/^{86}\text{Sr}$ versus $^{87}\text{Sr}/^{86}\text{Sr}$ (1890 Ma or initial). B) Rb/Sr isochron diagram showing measured $^{87}\text{Rb}/^{86}\text{Sr}$ versus $^{87}\text{Sr}/^{86}\text{Sr}$ ratios. Isochrons for 1.89 and 1.32 Ga, with an initial $^{87}\text{Sr}/^{86}\text{Sr}$ of 0.704, are shown for reference.



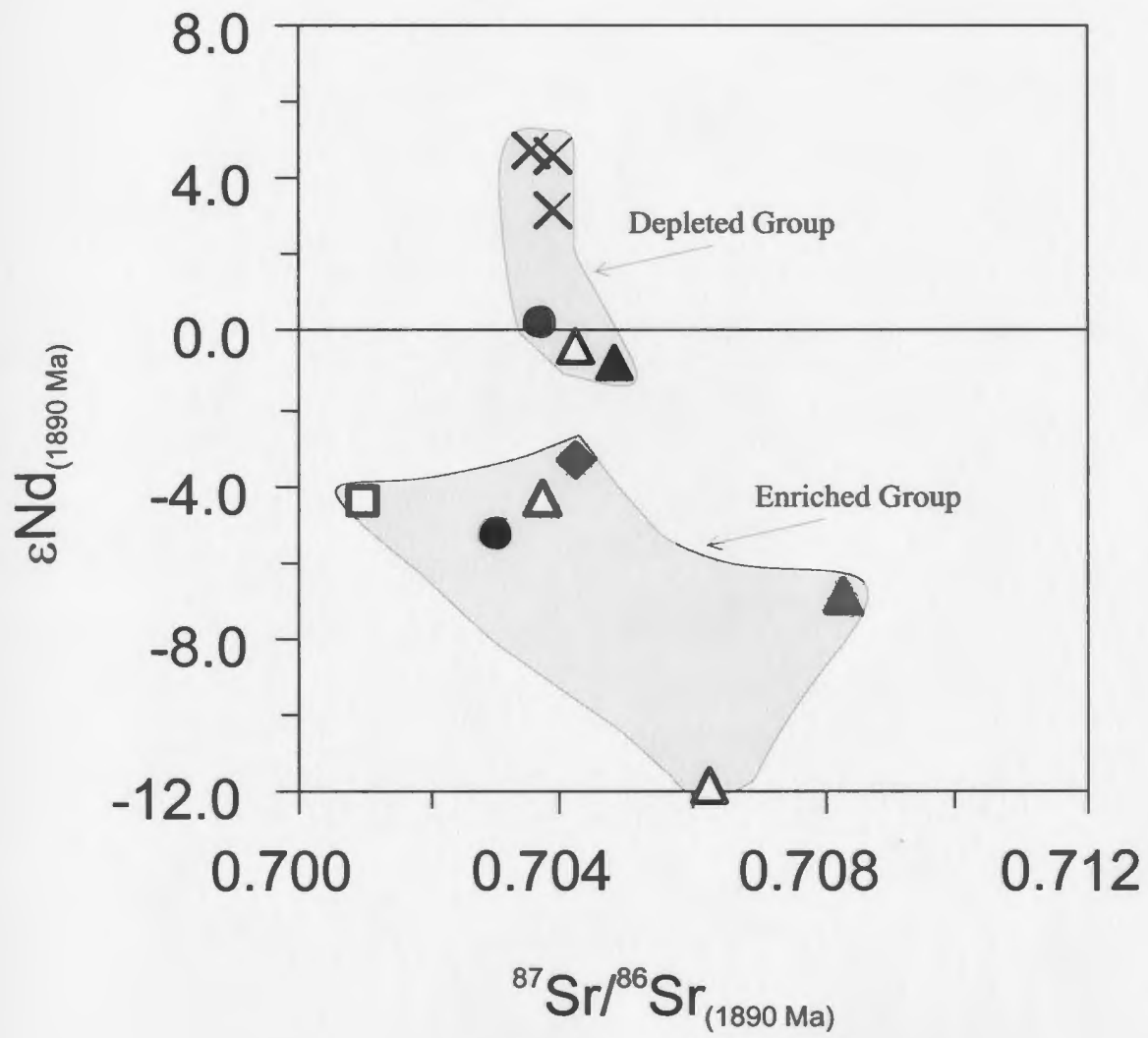
Paleoproterozoic Metaplutonic Suite			
This Study	◆ Meta-tonalite	□ Meta-quartz diorite	● Meta-hornblende gabbro
Amelin et al. (2000)	× "Enderbite"	▲ Quartzo-feldspathic gneisses	△ Mafic gneisses

Figure 2.17. Sm-Nd isotopic data for the Paleoproterozoic metaplutonic rocks from Voisey's Bay, Labrador. A) $^{147}\text{Sm}/^{144}\text{Nd}$ (measured) versus $\epsilon\text{Nd}_{(1890 \text{ Ma})}$. B) $^{147}\text{Sm}/^{144}\text{Nd}$ (measured) versus ϵNd (measured). Depleted mantle values from Stern et al. (1994) are shown for reference.



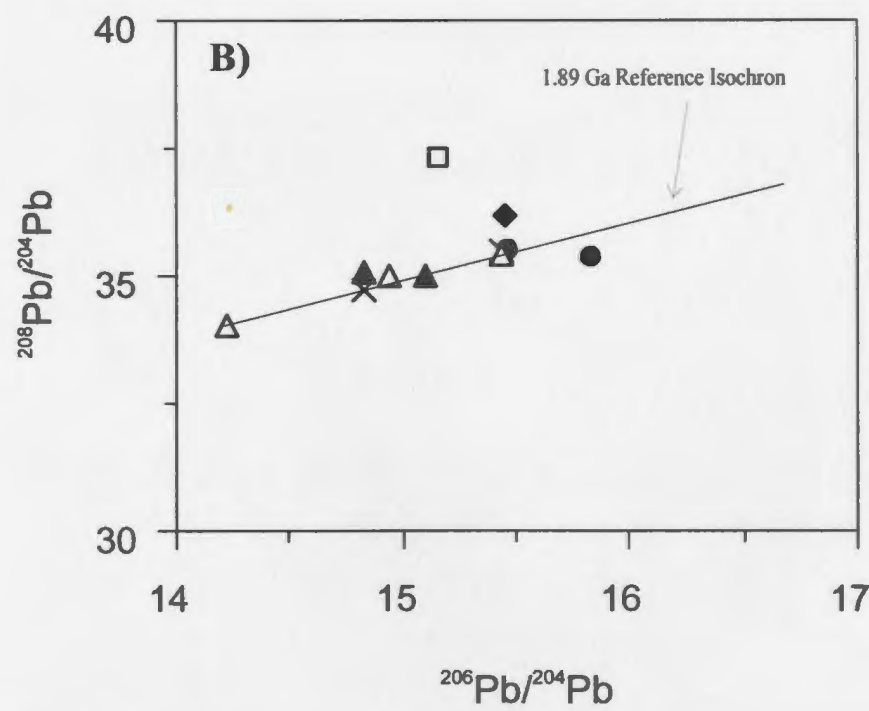
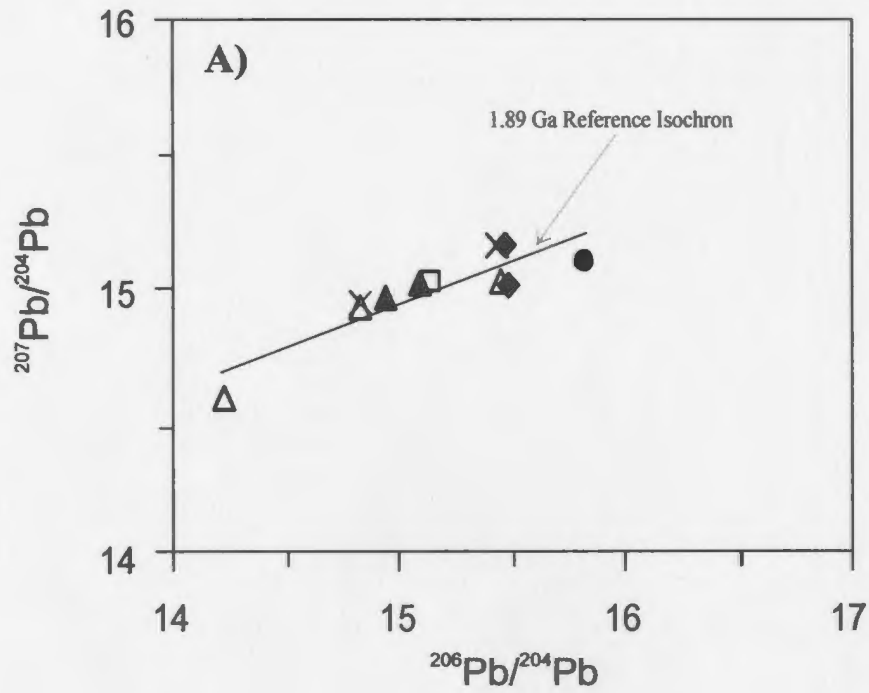
Paleoproterozoic Metaplutonic Suite			
This Study	◆ Meta-tonalite	□ Meta-quartz diorite	● Meta-hornblende gabbro
Amelin et al. (2000)	× "Enderbite"	▲ Quartzo-feldspathic gneisses	△ Mafic gneisses
Archean Nain Orthogneisses			
Collerson et al. (1989)	+ Quartzo-feldspathic orthogneisses		

Figure 2.18. $^{147}\text{Sm}/^{144}\text{Nd}$ versus $^{143}\text{Nd}/^{144}\text{Nd}$ diagram for Paleoproterozoic metaplutonic rocks from Voisey's Bay, Labrador. Compositions of rocks in this study, and for the "enderbite", "Nain" quartzo-feldspathic and mafic gneisses of Amelin et al. (2000) fall along a 1.89 Ga reference isochron. In comparison, Archean Nain quartzo-feldspathic gneisses from the Saglek-Hebron region of Labrador (after Collerson et al., 1989) fall along a 2.79 Ga reference isochron.



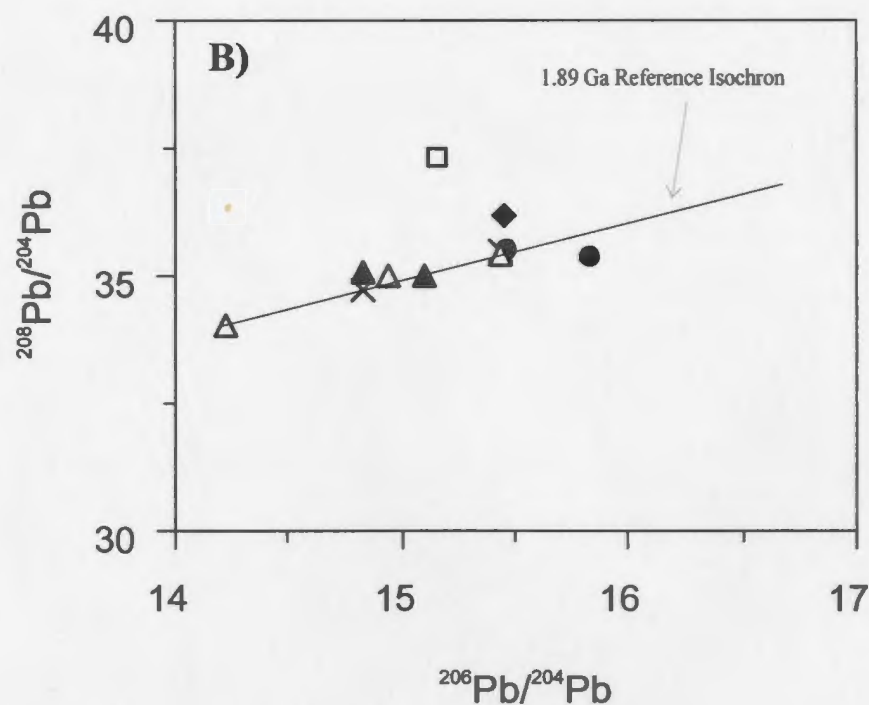
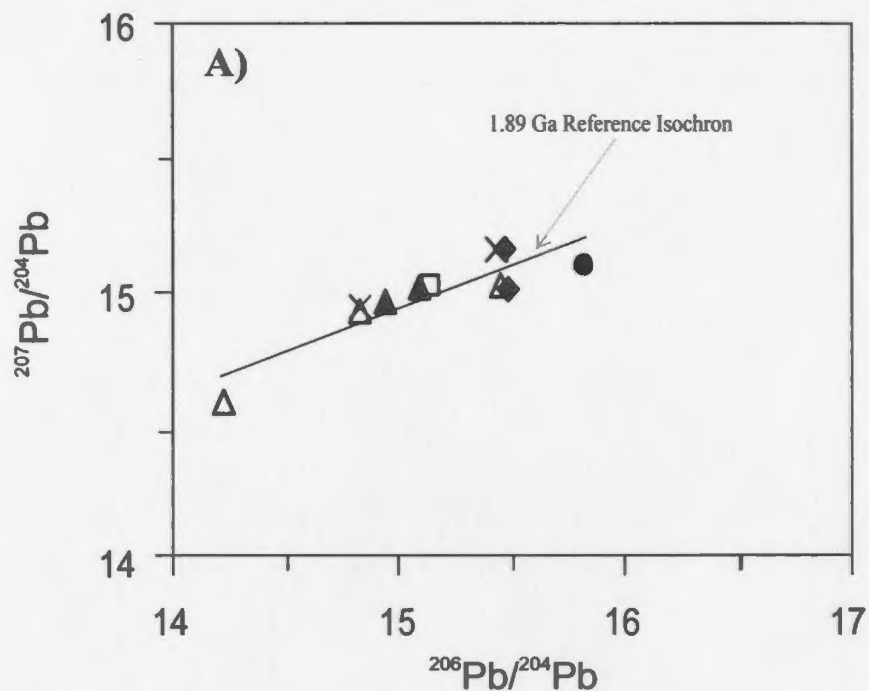
Paleoproterozoic Metaplutonic Suite				
This Study	◆ Meta-tonalite	□ Meta-quartz diorite	● Meta-hornblende gabbro	
Amelin et al. (2000)	× "Enderbite"	▲ Quartzo-feldspathic gneisses	△ Mafic gneisses	

Figure 2.19. $^{87}\text{Sr}/^{86}\text{Sr}_{(1890 \text{ Ma})}$ versus $\epsilon Nd_{(1890 \text{ Ma})}$ for the Paleoproterozoic metaplutonic rocks from Voisey's Bay, Labrador.



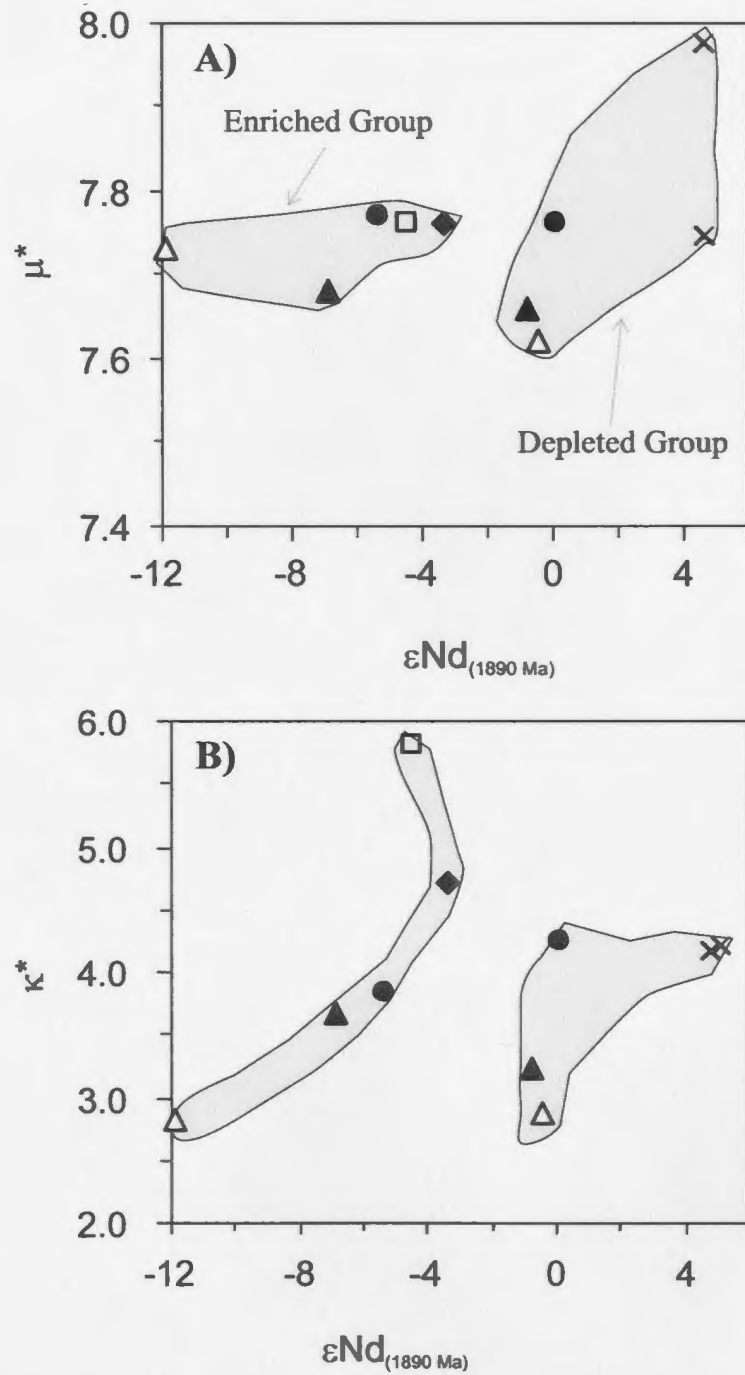
Paleoproterozoic Metaplutonic Suite		
This Study	◆ Meta-tonalite	□ Meta-quartz diorite
Amelin et al. (2000)	× "Enderbite"	▲ Quartzo-feldspathic gneisses
		● Meta-hornblende gabbro
		△ Mafic gneisses

Figure 2.20. $^{206}\text{Pb}/^{204}\text{Pb}$ versus A) $^{207}\text{Pb}/^{204}\text{Pb}$ and B) $^{208}\text{Pb}/^{204}\text{Pb}$ diagram for Paleoproterozoic metaplutonic rocks from Voisey's Bay, Labrador. Much of the data fall along a 1.89 Ga reference isochron.



Paleoproterozoic Metaplutonic Suite		
This Study	◆ Meta-tonalite	◻ Meta-quartz diorite
Amelin et al. (2000)	× "Enderbite"	▲ Quartzo-feldspathic gneisses
		● Meta-hornblende gabbro
		△ Mafic gneisses

Figure 2.20. $^{206}\text{Pb}/^{204}\text{Pb}$ versus A) $^{207}\text{Pb}/^{204}\text{Pb}$ and B) $^{208}\text{Pb}/^{204}\text{Pb}$ diagram for Paleoproterozoic metaplutonic rocks from Voisey's Bay, Labrador. Much of the data fall along a 1.89 Ga reference isochron.



Paleoproterozoic Metaplutonic Suite			
This Study	◆ Meta-tonalite	□ Meta-quartz diorite	● Meta-hornblende gabbro
Amelin et al. (2000)	× "Enderbite"	▲ Quartzo-feldspathic gneisses	△ Mafic gneisses

Figure 2.21. $\epsilon Nd_{(1890 \text{ Ma})}$ versus A) μ^* and B) κ^* for the Paleoproterozoic metaplutonic rocks from Voisey's Bay, Labrador. μ^* is the time intergrated $^{238}\text{U}/^{204}\text{Pb}$ of the mantle and crustal sources of the sample. κ^* is the time intergrated $^{232}\text{Th}/^{238}\text{U}$ of the mantle and crustal sources of the sample.

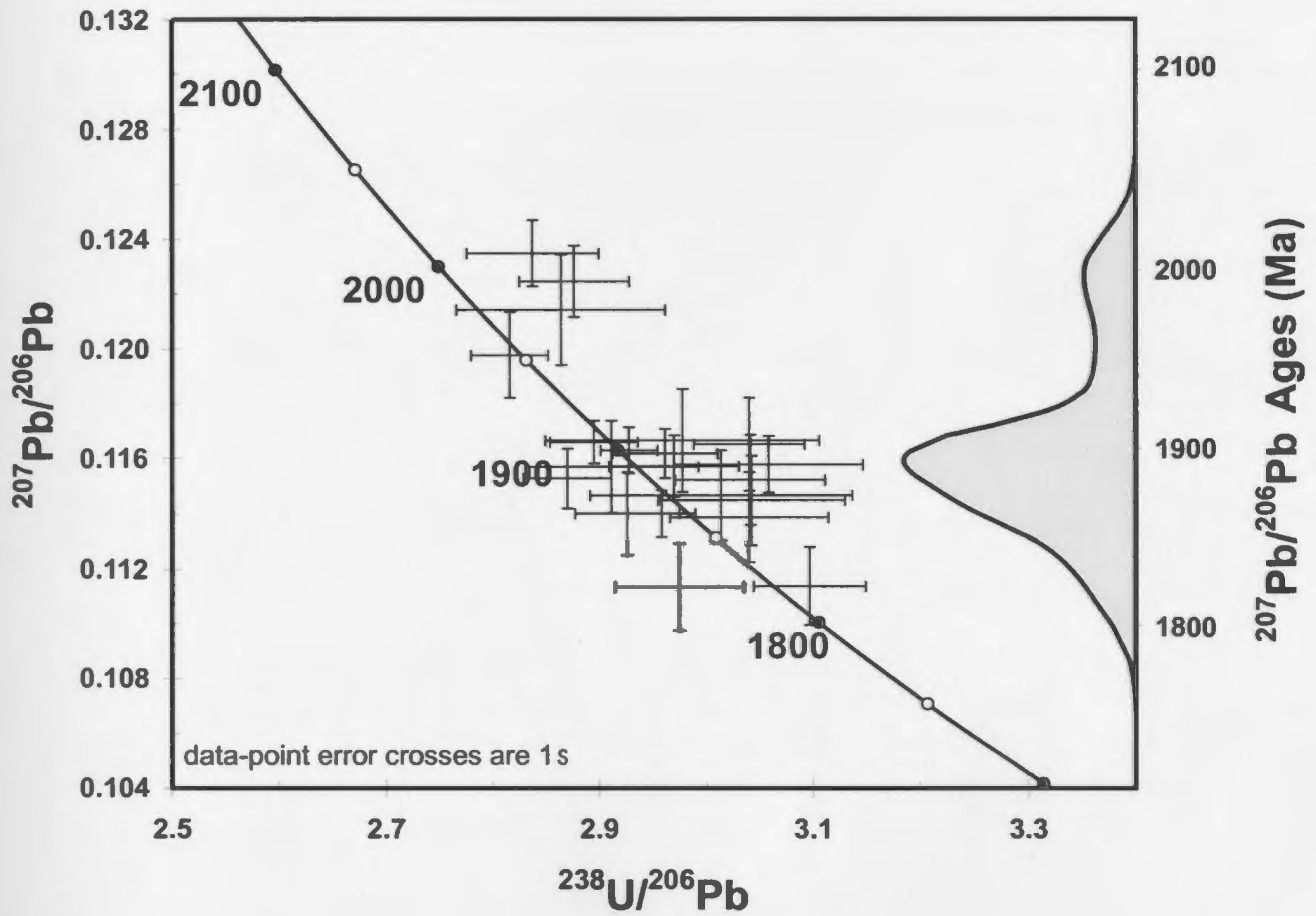
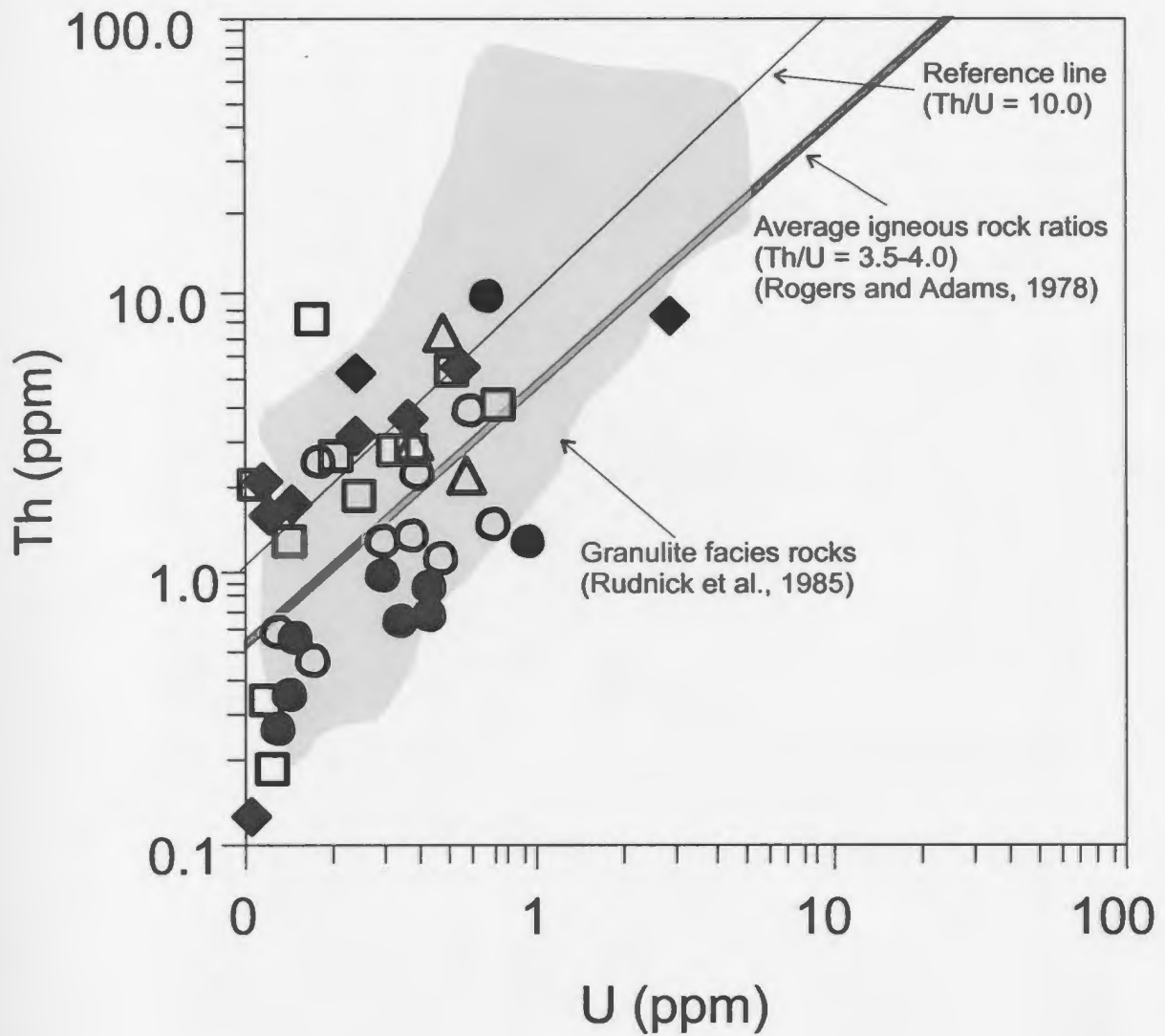
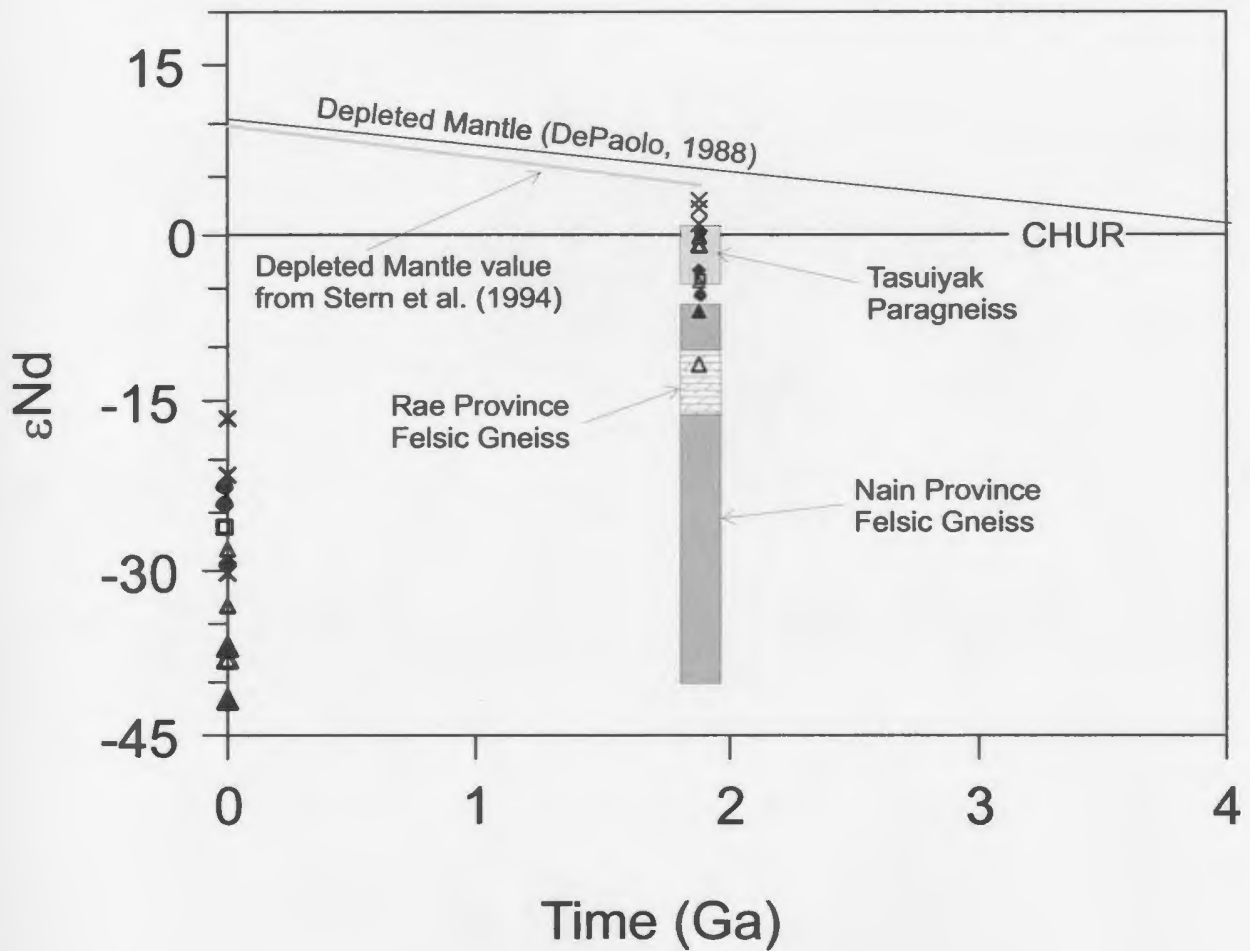


Figure 2.22. U-Pb versus Pb/Pb plot for the LAM-ICP-MS zircon analysis of the Paleoproterozoic metaplutonic rocks from Voisey's Bay, Labrador. A histogram of the Pb/Pb ages is plotted along the right side of the graph.



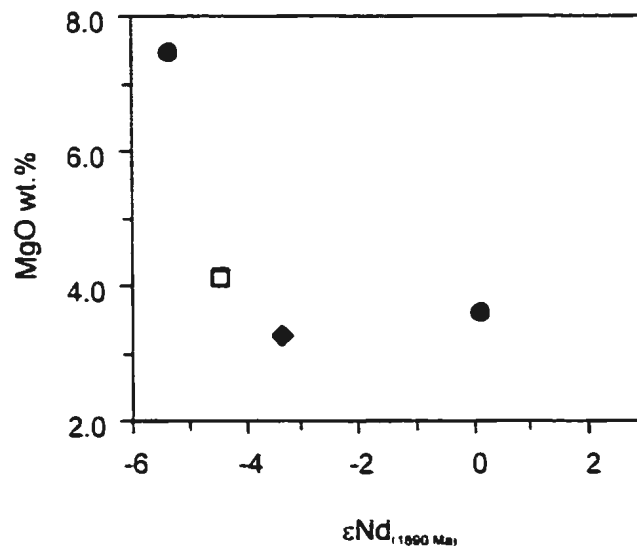
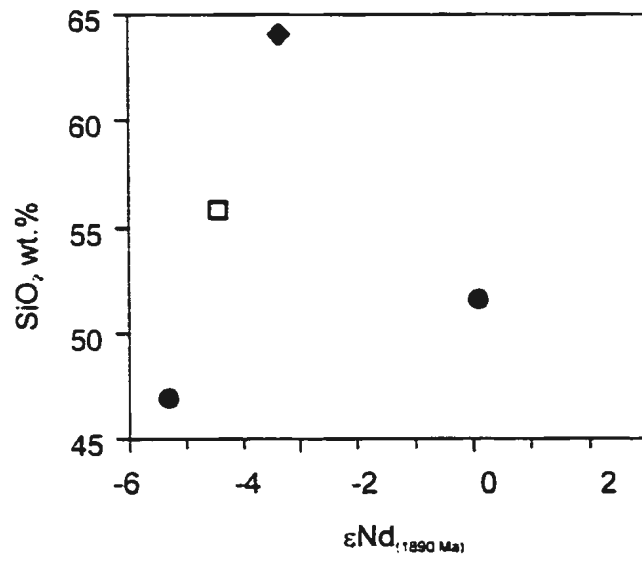
◆ Meta-tonalite □ Meta-quartz diorite △ Meta-diorite ○ Meta-gabbro ● Meta-hbl gabbro

Figure 2.24. U (ppm) versus Th (ppm) diagram for the Paleoproterozoic metaplutonic rocks from Voisey's Bay, Labrador. The average granulite facies rock ratios from Rudnick et al. (1985), the average igneous rock ratio from Rogers and Adams (1978) and the ratio line of 10 are shown for reference.



Paleoproterozoic Metaplutonic Suite			
This Study	◆ Meta-tonalite	□ Meta-quartz diorite	● Meta-hornblende gabbro
Amelin et al. (2000)	× "Enderbite"	▲ Quartzo-feldspathic gneisses	△ Mafic gneisses

Figure 2.25. Time versus ϵNd for the Paleoproterozoic metaplutonic rocks from Voisey's Bay, Labrador. Showing ϵNd values of present day and at 1890 Ma. Depleted mantle values from Stern et al. (1994) and DePaolo (1988) are shown for reference. Nain Province felsic gneiss data from Collerson et al. (1989), Schiotte et al. (1993) and Campbell (1997). Rae Province felsic gneiss data from Campbell (1997). Tasiuyak paragneiss data from Theriault and Ermanovics (1997) and Amelin et al. (2000).



Paleoproterozoic Metaplutonic Suite
 This Study ◆ Meta-tonalite □ Meta-quartz diorite ● Meta-hornblende gabbro

Figure 2.26. εNd_(1890 Ma) versus A) SiO₂ (wt.%) and B) MgO (wt.%) for the Paleoproterozoic metaplutonic rocks from Voisey's Bay, Labrador.

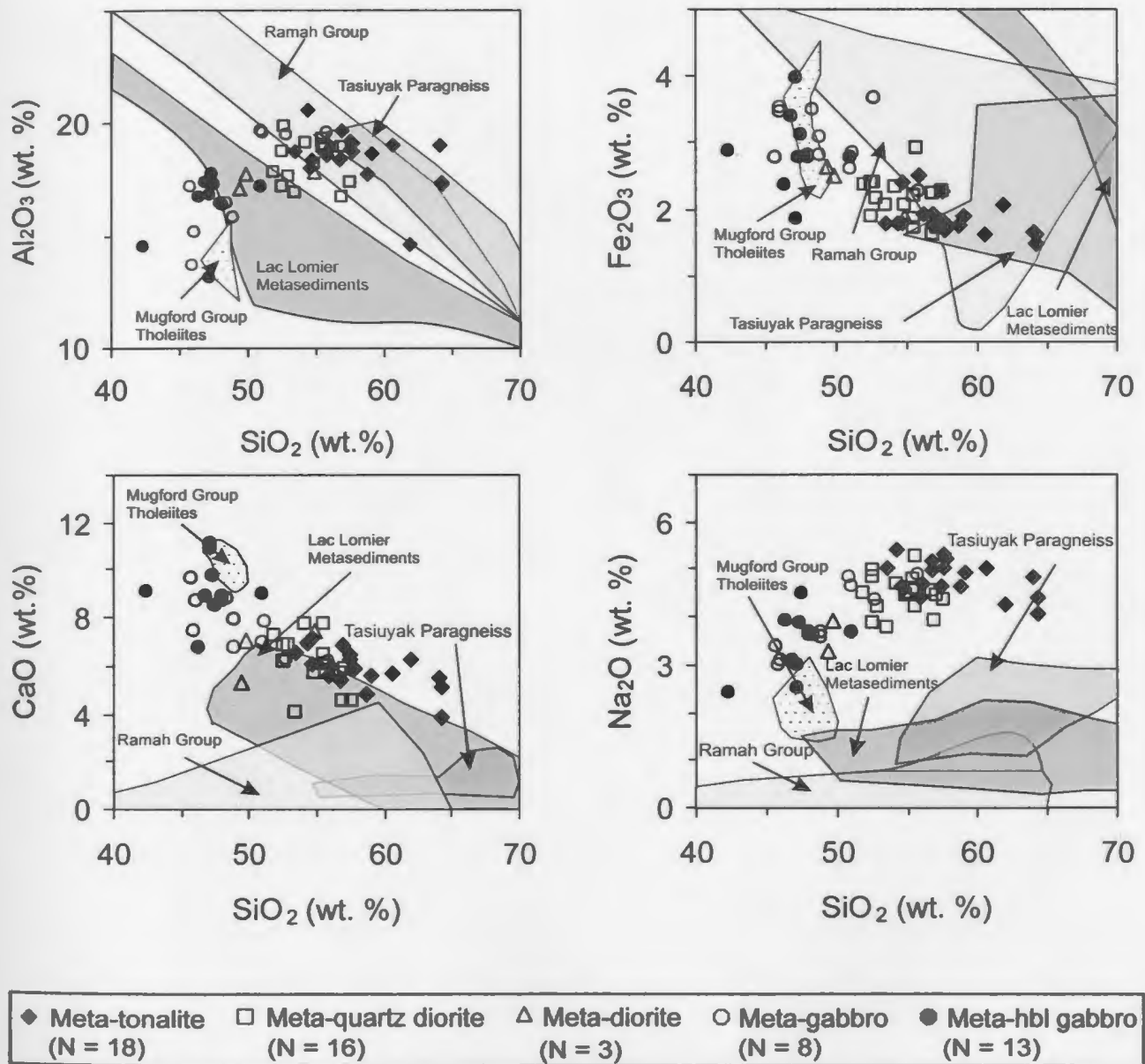


Figure 2.27. SiO₂ versus selected major element (Harker) diagrams for Paleoproterozoic metaplutonic rocks from Voisey's Bay, Labrador. For comparison, fields for various Paleoproterozoic supracrustal rocks are shown. Data for the Tasiuyak paragneiss, Ramah Group and Lac Lomier metasediments are from Theriault and Ermanovics (1997). Mugford Group tholeiites are from Hamilton (1994).

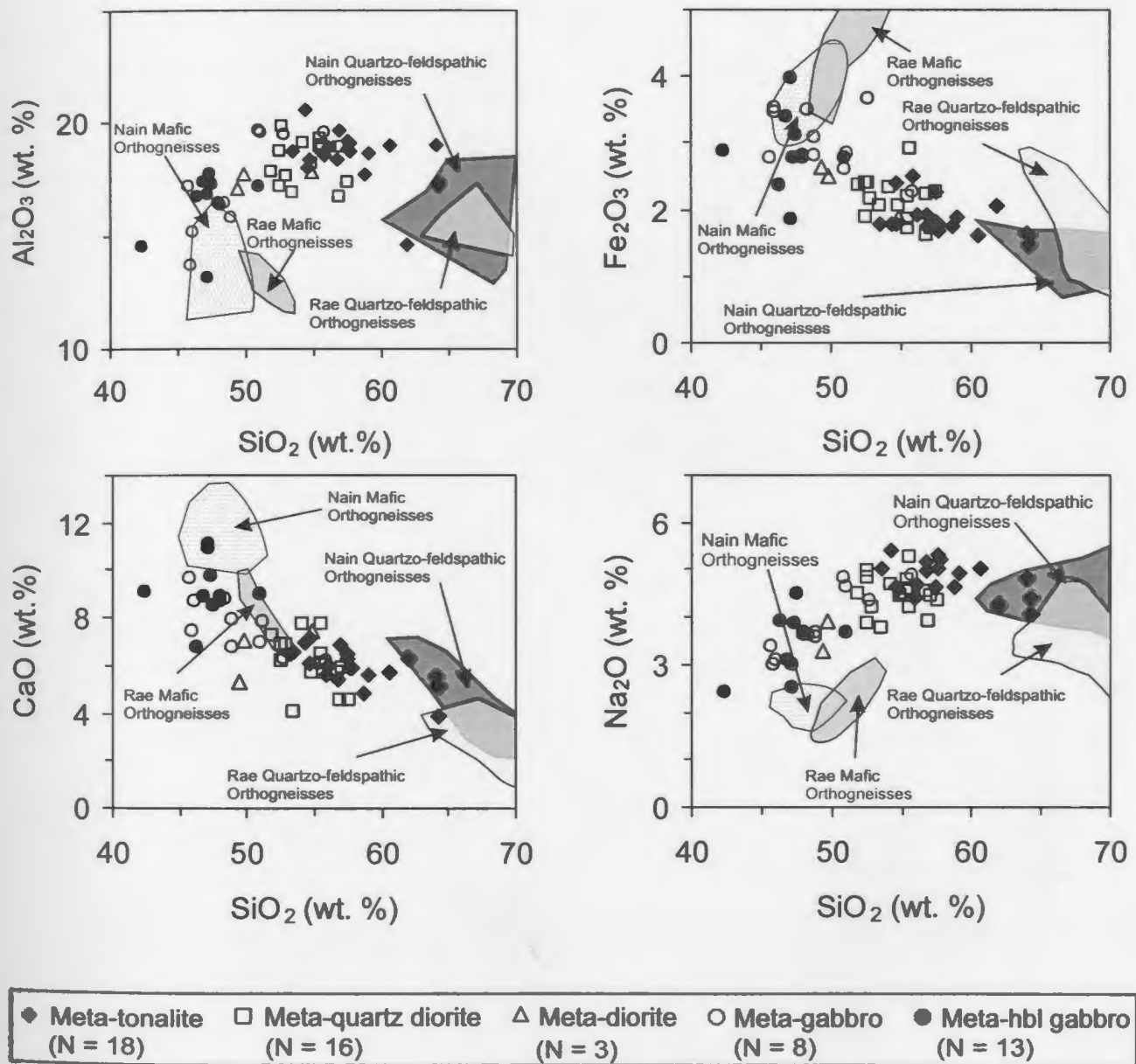
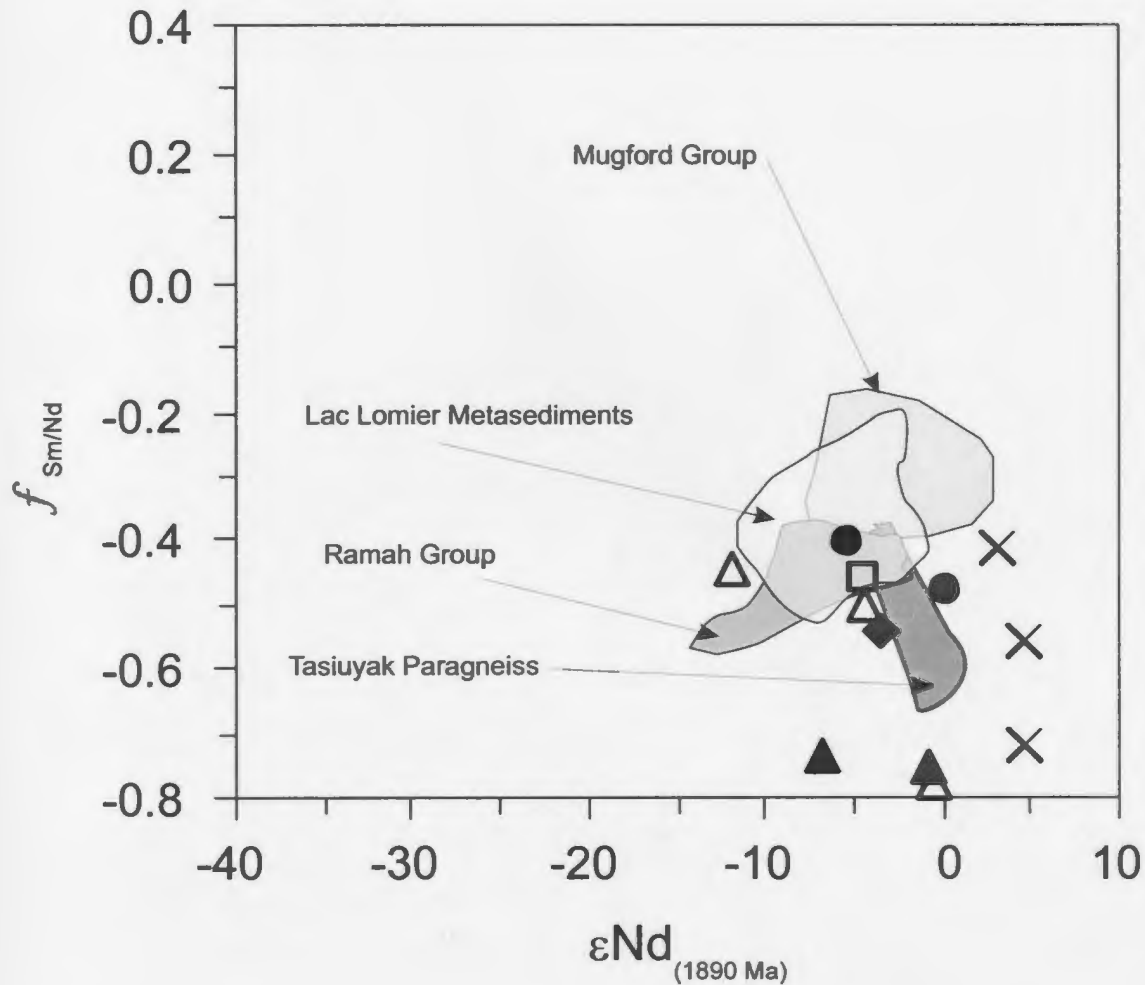
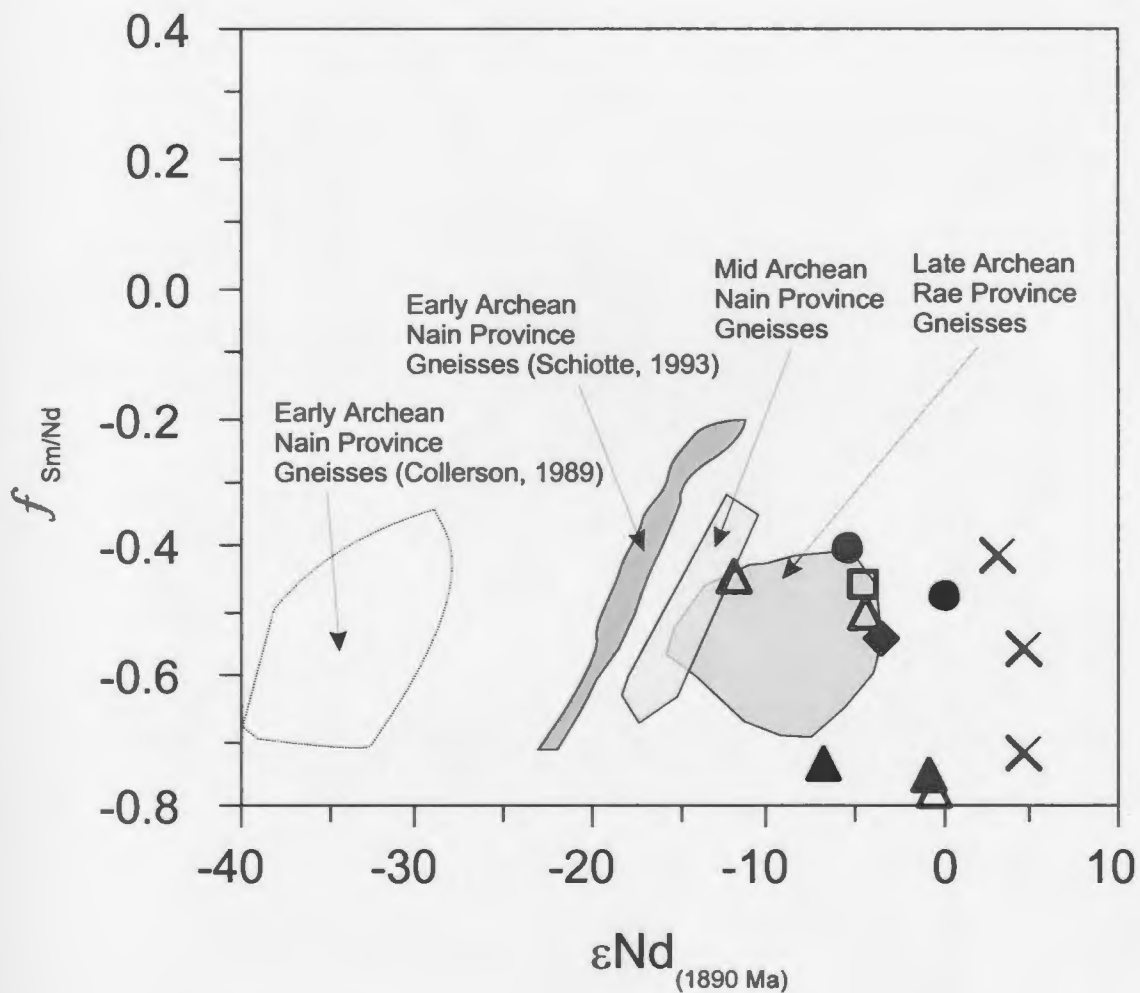


Figure 2.28. SiO_2 versus selected major element (Harker) diagrams for Paleoproterozoic metaplutonic rocks from Voisey's Bay, Labrador. For comparison, fields of the Archean quartzo-feldspathic and mafic orthogneisses of both the Nain Province and Rae craton are shown. Some of the Nain Archean mafic orthogneiss and all of the Rae Archean (felsic and mafic) data are after Campbell (1997).



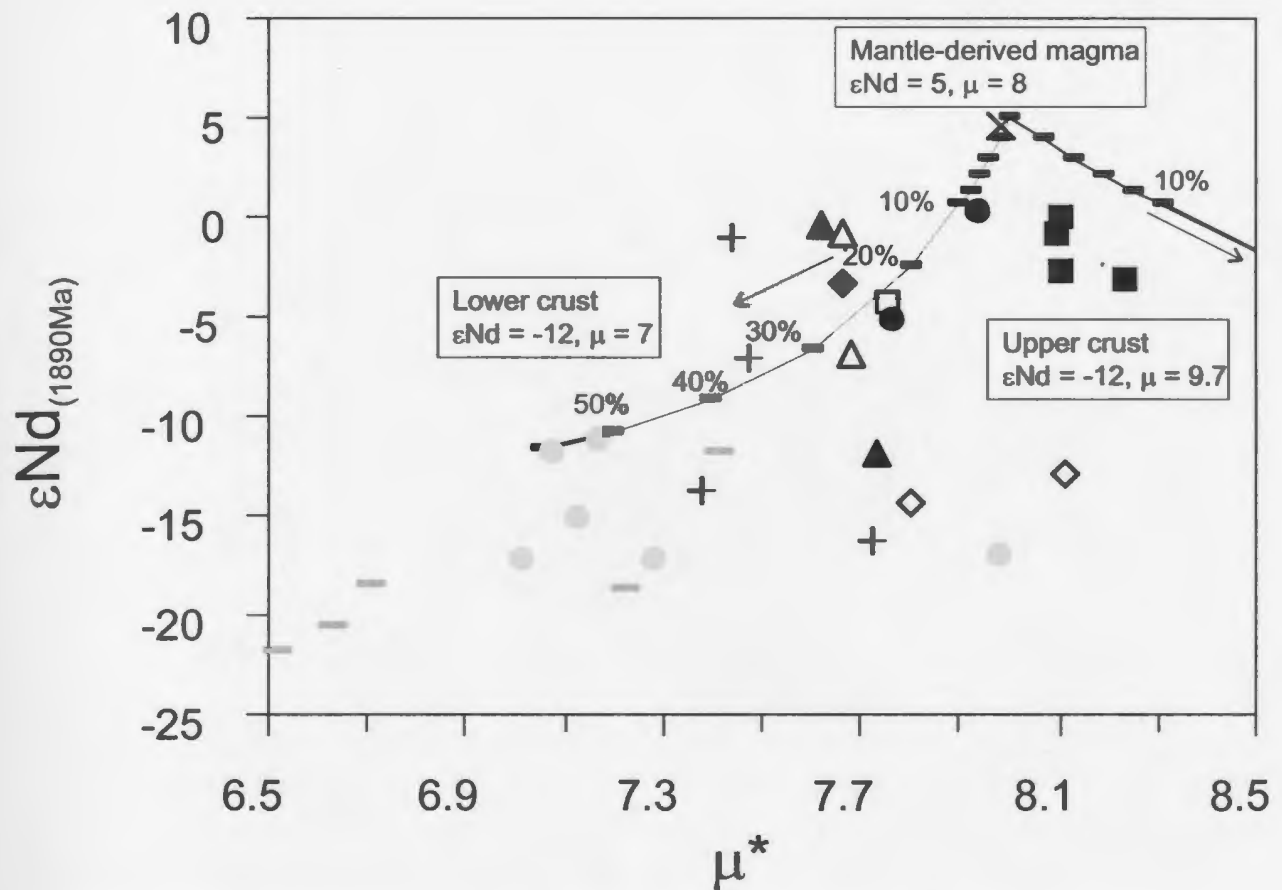
Paleoproterozoic Metaplutonic Suite			
This Study	◆ Meta-tonalite	□ Meta-quartz diorite	● Meta-hornblende gabbro
Amelin et al. (2000)	× "Enderbite"	▲ Quartzo-feldspathic gneisses	△ Mafic gneisses

Figure 2.29. ϵNd versus $f_{\text{Sm/Nd}}$ (fractionation factor) diagram for Paleoproterozoic metaplutonic rocks from Voisey's Bay, Labrador, compared to other Paleoproterozoic supracrustal units in the region: Mugford Group tholeiites from an area north of Saglek Bay (Hamilton, 1993), and the Lac Lomier metasediments, Ramah group and the Tasiuyak paragneiss from the North River-Nutak area (Theriault and Ermanovics, 1997). The Tasiuyak paragneiss field also contains data from the Voisey's Bay area (Amelin et al, 2000). The $f_{\text{Sm/Nd}}$ values for the mineral separates of the metaplutonic suite from Amelin et al.(2000) are not directly comparable to the whole rock compositions because minerals exhibit crystal-chemical controls of Sm/Nd partitioning.



Paleoproterozoic Metaplutonic Suite			
This Study	◆ Meta-tonalite	□ Meta-quartz diorite	● Meta-hornblende gabbro
Amelin et al. (2000)	× "Enderbite"	▲ Quartzo-feldspathic gneisses	△ Mafic gneisses

Figure 2.30. ϵNd versus $f_{Sm/Nd}$ (fractionation factor) diagram for Paleoproterozoic metaplutonic rocks from Voisey's Bay, Labrador, compared to other major units in the region: Early Archean Nain Province gneisses from the Saglek area (Collerson et al., 1989), Mid-Archean and Early Archean Nain Province gneisses from south of Okak (Schiotte et al., 1993) and Late Archean Rae Province gneisses from the North River-Nutak area (Theriault and Ermanovics, 1993) and west of the Burwell Domain (Campbell, 1997). The $f_{Sm/Nd}$ values for the mineral separates of the metaplutonic suite from Amelin et al. (2000) are not directly comparable to the whole rock compositions because minerals exhibit crystal-chemical controls of Sm/Nd partitioning.



Paleoproterozoic Metaplutonic Suite			
This Study	◆ Meta-tonalite	□ Meta-quartz diorite	● Meta-hornblende gabbro
Amelin et al. (2000)	× "Enderbite"	▲ Quartzo-feldspathic gneisses	△ Mafic gneisses
Paleoproterozoic Supracrustal units			
Amelin et al. (2000)	■ Tasiuyak paragneiss		
Archean Felsic Orthogneisses			
Campbell et al. (1997)	+ Nain orthogneisses	◇ Rae orthogneisses	
Schiotte et al. (1993)	— Mid-Archean quartzo-feldspathic Nain gneisses	● Early Archean quartzo-feldspathic Nain gneisses	

Figure 2.31. μ^* versus $\epsilon Nd_{(1890\text{ Ma})}$ diagram for Paleoproterozoic metaplutonic rocks from Voisey's Bay, Labrador. Mixing lines are plotted between an assumed composition of mantle-derived magma ($\epsilon Nd = 5$, $Nd = 10$ ppm, $\mu^* = 8.0$, $Pb = 10$ ppm); Archean upper crust ($\epsilon Nd = -12$, $Nd = 32$ ppm, $\mu^* = 9.7$, $Pb = 20$ ppm); and the Archean Lower crust ($\epsilon Nd = -12$, $Nd = 32$ ppm, $\mu^* = 7.0$, $Pb = 10$ ppm). End member compositions for the mixing model are those used by Arndt and Todt (1994) for the 1.9 Ga Trans-Hudson Batholiths, with Nd isotopic compositions and concentrations from Chauval et al. (1987), and Pb concentrations from Taylor and McLennan (1985). Tick marks on mixing lines represent 2% increments of crustal contamination of the mantle-derived magma except where noted.

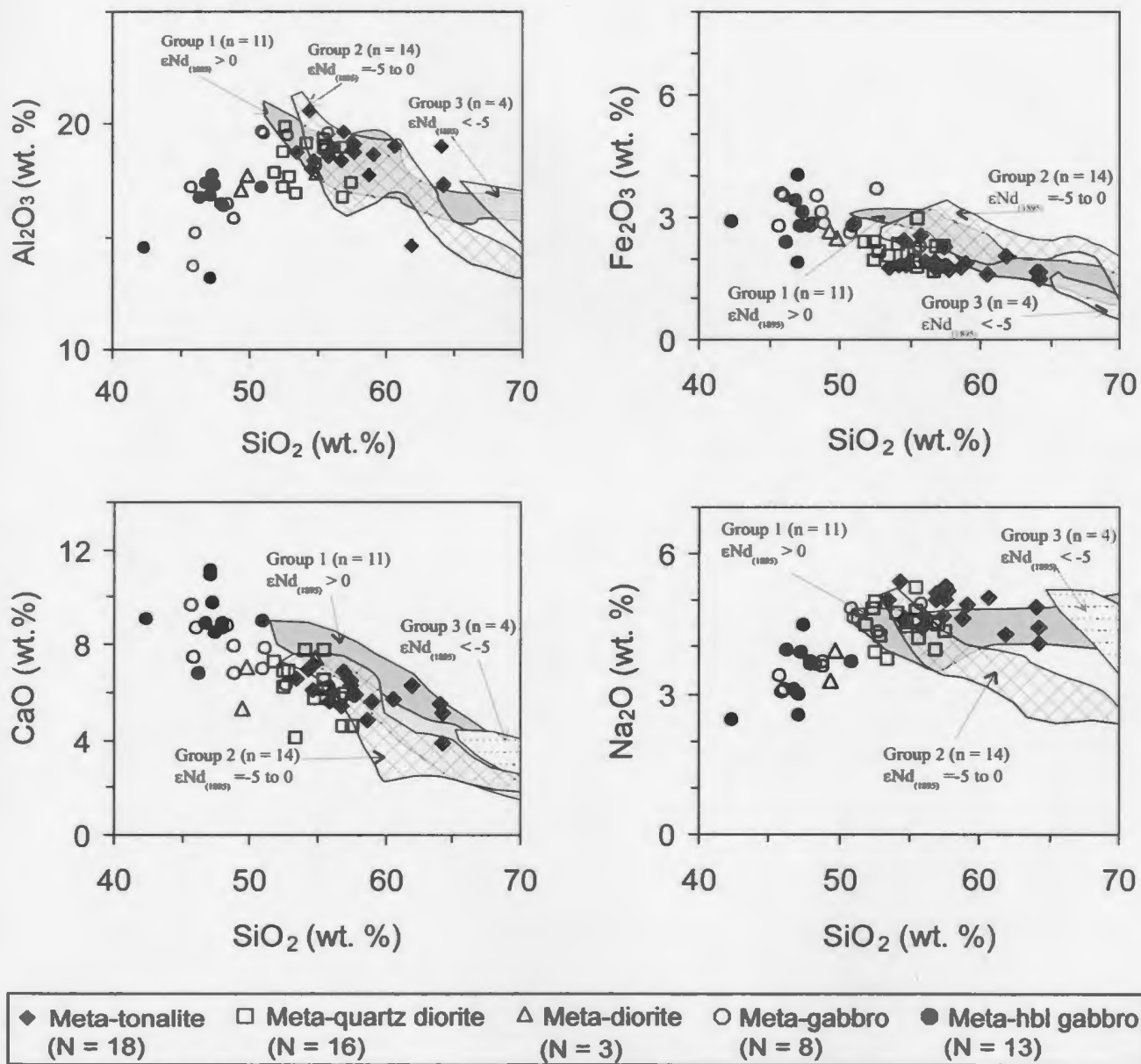


Figure 2.32. Selected major element versus SiO_2 (Harker) diagram for Paleoproterozoic metaplutonic rocks from Voisey's Bay, Labrador. Fields for calc-alkaline Paleoproterozoic metaplutonic rocks in the Burwell Domain of the Torngat Orogen are shown (data after Campbell, 1997). Units are subdivided based on ϵNd isotopic values.

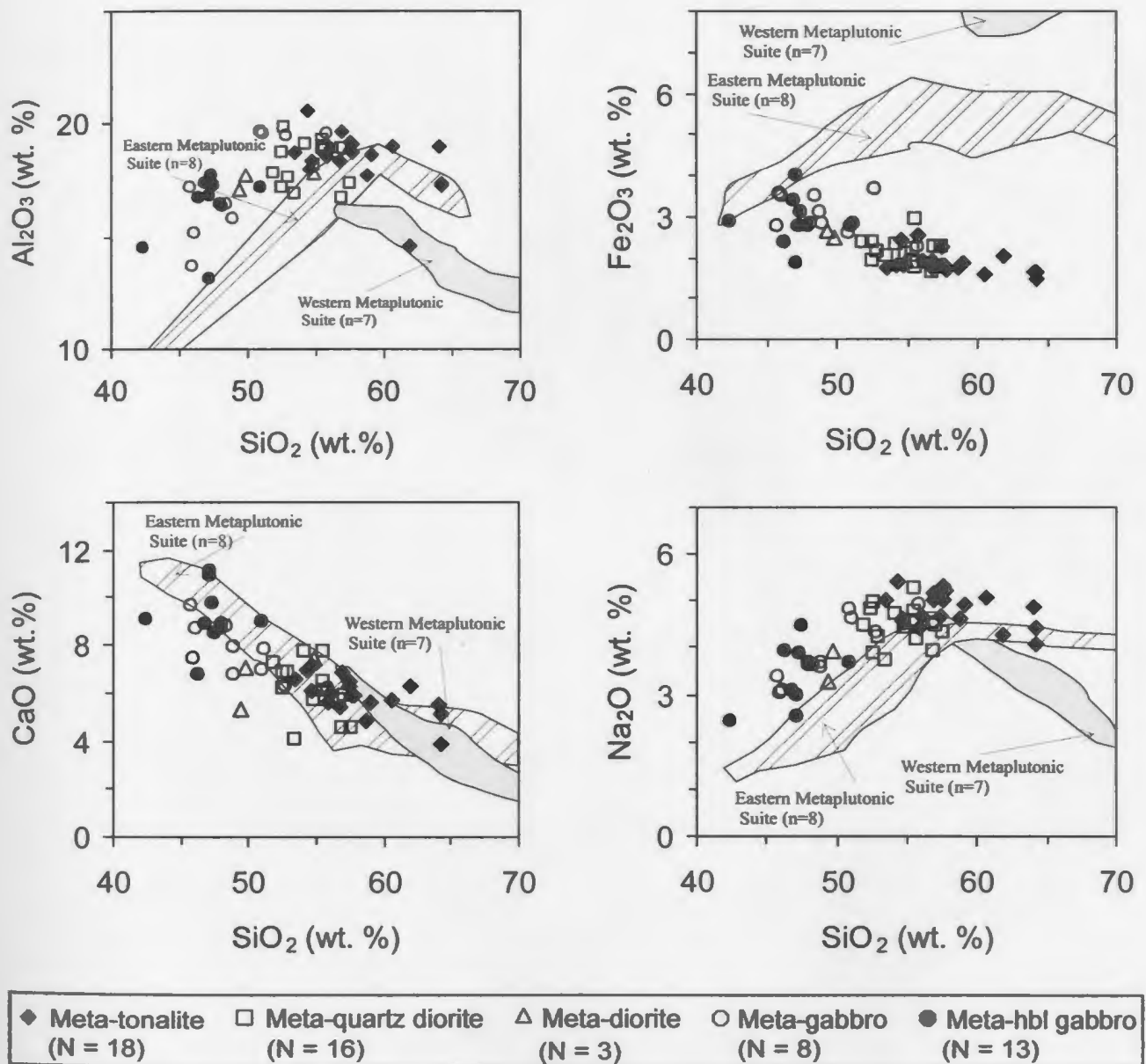


Figure 2.33. Selected major element versus SiO₂ (Harker) diagram for Paleoproterozoic metaplutonic rocks from Voisey's Bay, Labrador. Fields for the eastern and western Paleoproterozoic metaplutonic suites in the southern sections (North River-Nutak area) of the Torngat Orogen are shown for comparison (data after Theriault and Ermanovics, 1997).

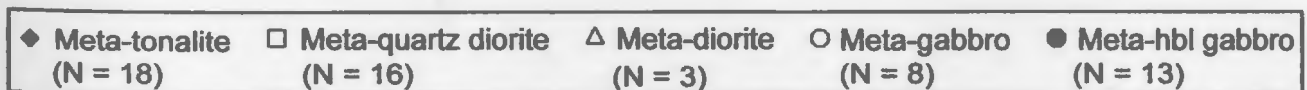
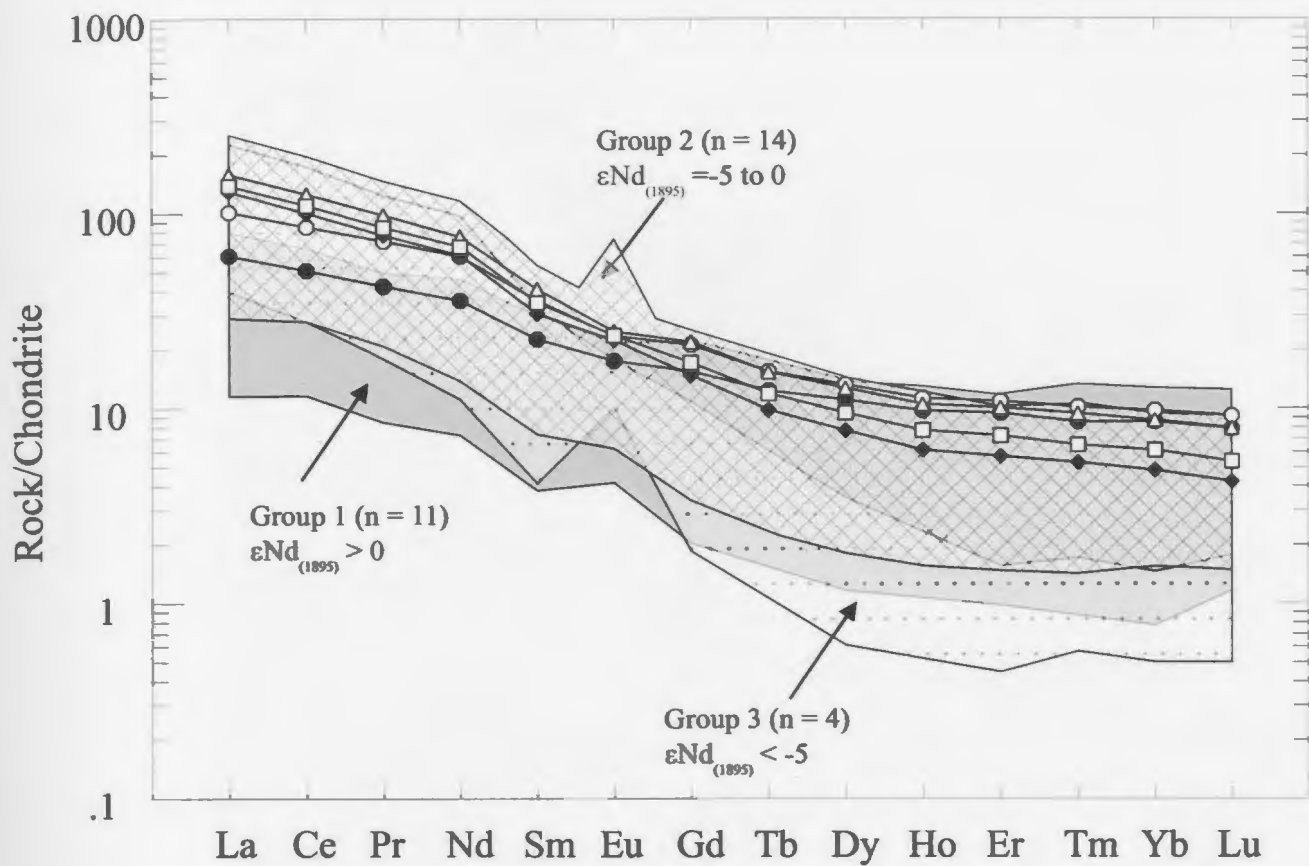


Figure 2.34. Chondrite normalized REE spider-diagrams for Paleoproterozoic metaplutonic rocks from Voisey's Bay, Labrador. Fields for the Paleoproterozoic metaplutonic rocks in the Burwell Domain of the Torngat Orogen are shown for comparison (data after Campbell, 1997). Units are subdivided based on ϵNd isotopic values.

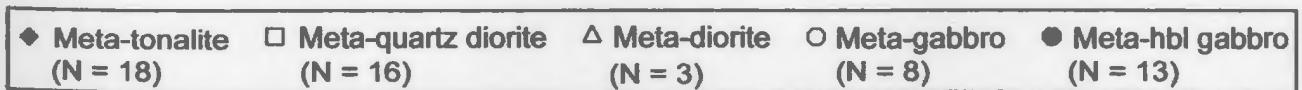
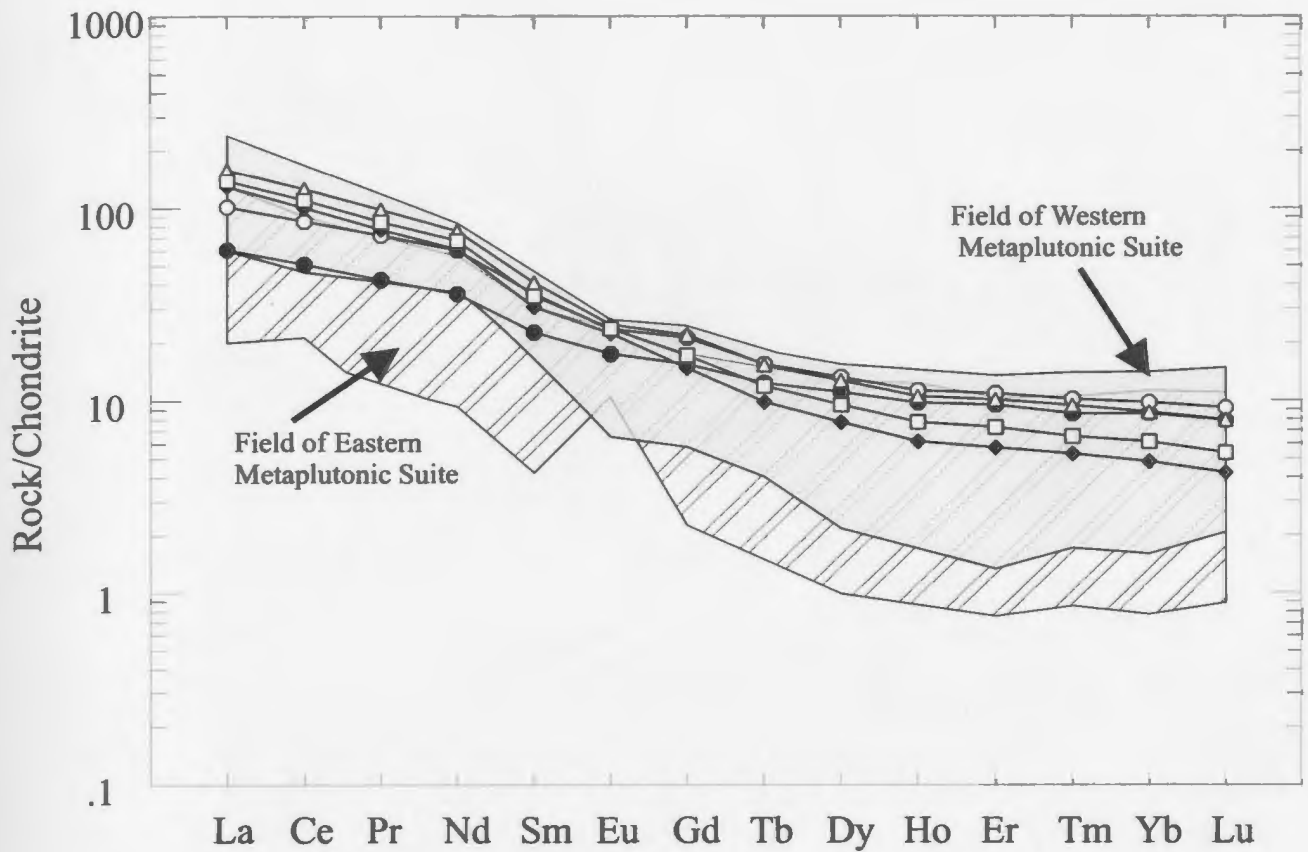
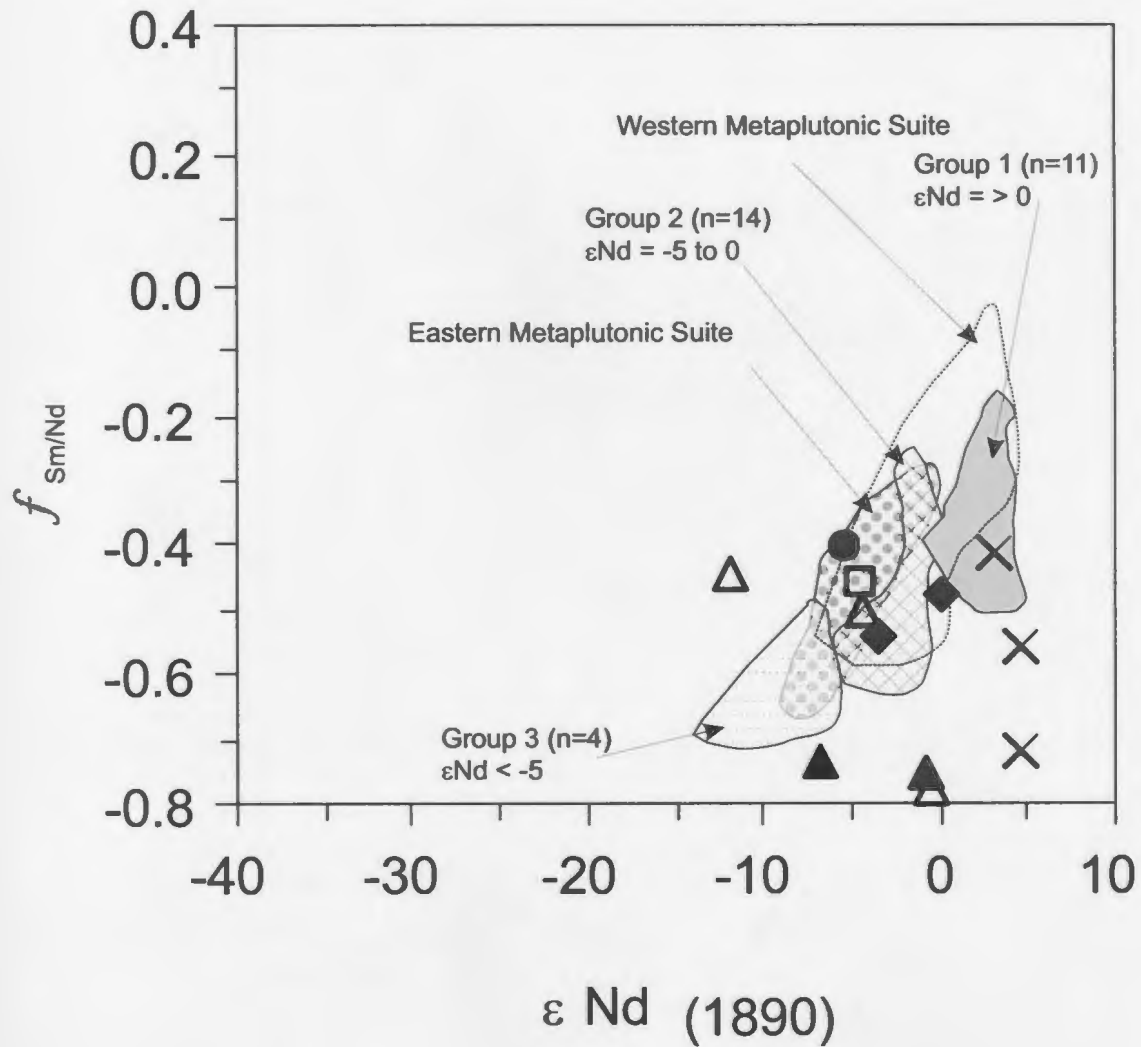


Figure 2.35. Chondrite normalized REE spider-diagrams for Paleoproterozoic metaplutonic rocks from Voisey's Bay, Labrador. Fields for the eastern and western Paleoproterozoic metaplutonic suites in the southern section (North River-Nutak area) of the Torngat Orogen are shown for comparison (data after Theriault and Ermanovics, 1997).



Paleoproterozoic Metaplutonic Suite			
This Study	◆ Meta-tonalite	□ Meta-quartz diorite	● Meta-hornblende gabbro
Amelin et al. (2000)	× "Enderbite"	▲ Quartzo-feldspathic gneisses	△ Mafic gneisses

Figure 2.36. $f_{Sm/Nd}$ versus ϵNd diagram for Paleoproterozoic metaplutonic rocks from Voisey's Bay, Labrador, compared to other metaplutonic units in the Torngat Orogen: Eastern and Western metaplutonic suite from the North River-Nutak area (Theriault and Ermanovics, 1993), the metaplutonic suites form the Burwell domain (labeled group 1 to 3, after Campbell, 1997).

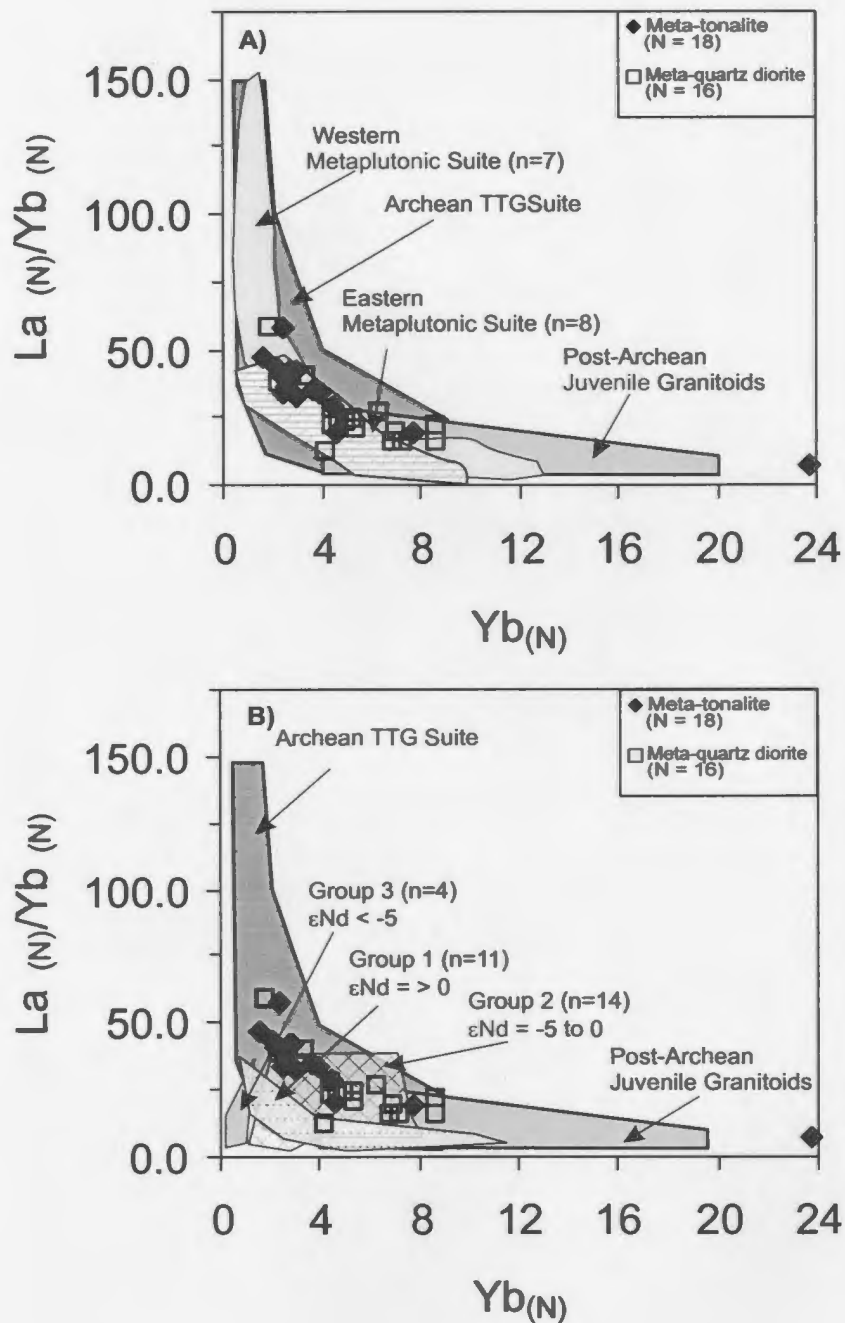


Figure 2.37. $Yb_{(N)}$ versus $La_{(N)}/Yb_{(N)}$ diagram for the Paleoproterozoic metaplutonic rocks from Voisey's Bay, Labrador. Fields for the Archean TTG suites and post-Archean juvenile granitoids are drawn for reference (after Martin, 1994). A) Comparison to the eastern and western metaplutonic suites in the southern section of the Torngat orogen (data after Theriault and Ermanovics, 1997). B) Comparison to the Paleoproterozoic calc-alkaline Metaplutonic rocks in the Burwell Domain of the Torngat Orogen (data after Campbell, 1997). These rocks are subdivided into groups based on ϵNd isotopic values.

Table 2.1 - Major element analyses of Paleoproterozoic metaplutonic rocks of the Voisey's Bay Area, Labrador

(Wt. %)	Meta-tonalite								
	DDH-496-511	DDH-496-532	DDH-496-535	DDH-496-549	DDH-497-217	DDH-497-219	DDH-497-220	DDH-497-223	DDH-497-225
SiO ₂	58.71	54.67	56.84	64.03	54.30	53.50	57.73	57.53	57.60
TiO ₂	0.50	0.65	0.76	0.58	0.71	0.68	0.62	0.68	0.66
Al ₂ O ₃	17.78	18.39	19.63	19.01	20.58	18.73	19.14	18.88	18.73
Fe ₂ O ₃ *	1.75	1.80	1.91	1.65	1.79	1.77	1.67	1.81	1.79
FeO	2.87	2.81	2.94	2.35	2.93	2.96	2.58	2.76	2.63
MnO	0.07	0.06	0.07	0.06	0.07	0.06	0.06	0.07	0.06
MgO	1.82	3.59	3.48	3.25	2.81	3.75	2.72	3.00	3.12
CaO	4.83	6.13	6.84	5.50	6.91	6.53	5.87	6.23	5.88
Na ₂ O	4.61	4.59	5.16	4.84	5.39	5.03	5.20	5.30	5.04
K ₂ O	1.49	2.17	1.62	2.18	0.96	1.21	1.48	1.53	2.08
P ₂ O ₅	0.18	0.40	0.45	0.34	0.46	0.43	0.38	0.41	0.41
Sum	95.12	95.81	100.13	104.22	97.28	95.06	97.81	98.60	98.46

(Wt. %)	Meta-tonalite								
	DDH-497-227	DDH-497-231	VB-99-076	VB-99-082	AR-00-004	AR-00-017	AR-00-032	AR-00-053	AR-00-054
SiO ₂	59.03	64.24	56.79	61.90	54.59	57.46	64.23	55.84	56.10
TiO ₂	0.68	0.56	0.61	0.93	0.96	0.97	0.58	0.93	0.78
Al ₂ O ₃	18.65	17.33	18.41	14.58	17.98	19.18	17.27	18.58	18.92
Fe ₂ O ₃ *	1.87	1.48	1.74	2.05	2.41	2.27	1.63	2.52	1.93
FeO	2.76	1.98	2.54	3.70	4.00	3.21	2.56	3.33	2.67
MnO	0.06	0.04	0.06	0.17	0.08	0.08	0.05	0.09	0.07
MgO	2.94	1.85	3.37	1.97	4.78	4.58	3.49	4.39	3.44
CaO	5.64	3.91	5.46	6.27	7.15	6.46	5.08	5.55	5.95
Na ₂ O	4.91	4.05	4.99	4.25	4.62	4.65	4.40	4.41	4.68
K ₂ O	2.08	3.53	2.27	0.86	1.64	2.82	1.75	3.78	3.07
P ₂ O ₅	0.34	0.23	0.33	0.32	0.61	0.54	0.19	0.58	0.49
Sum	99.38	99.66	96.98	97.32	99.39	102.76	101.52	100.47	98.60

Major element data by X-Ray fluorescence. Analytical method given in Appendix 1.

Fe₂O₃* and FeO recalculated from Fe₂O₃T (total) using the procedure of LeMaitre (1976).

Oxides normalized to 100 % (anhydrous). Actual analysis totals are reported in "Sum" column.

Table 2.1 - (continued)

Meta-quartz diorite									
(Wt. %)	DDH- 496-527	DDH- 496-530	DDH- 496-536	DDH- 496-542	DDH- 496-547	DDH- 496-202	DDH- 497-203	DDH- 497-208	DDH- 497-210
SiO ₂	54.19	55.48	54.86	55.47	57.11	56.80	56.91	57.54	53.50
TiO ₂	0.90	0.77	0.75	0.70	0.64	0.55	0.80	0.81	0.94
Al ₂ O ₃	19.15	19.34	18.17	18.90	18.96	18.92	16.74	17.35	16.93
Fe ₂ O ₃ *	2.32	2.18	2.07	1.84	1.72	1.62	2.23	2.25	2.04
FeO	3.81	3.48	3.13	2.79	2.45	2.34	2.93	2.67	2.70
MnO	0.10	0.09	0.08	0.08	0.07	0.06	0.07	0.07	0.07
MgO	4.31	3.93	3.46	3.24	3.24	3.02	3.56	3.59	3.25
CaO	7.73	7.73	5.72	6.51	5.92	5.67	4.54	4.52	4.03
Na ₂ O	4.70	4.76	4.43	4.59	4.46	4.53	3.92	4.32	3.75
K ₂ O	1.68	1.79	2.62	2.38	3.01	2.82	4.27	4.76	4.59
P ₂ O ₅	0.63	0.64	0.46	0.49	0.42	0.39	0.46	0.44	0.47
Sum	100.06	100.70	96.28	97.64	98.54	97.40	96.83	98.75	92.70

Meta-quartz diorite										Meta-diorite	
(Wt. %)	DDH- 497-221	VB-99- 077	VB-99- 107	VB-99- 108	AR-00- 008	AR-00- 009	AR-00- 050	VB-99- 089	VB-99- 092		
SiO ₂	55.56	52.61	51.93	55.63	52.54	52.90	52.49	49.77	49.35		
TiO ₂	0.65	0.64	0.85	1.05	0.97	0.91	0.78	1.13	0.01		
Al ₂ O ₃	18.98	19.81	17.78	18.85	17.21	17.67	18.72	17.77	17.12		
Fe ₂ O ₃ *	1.73	2.38	2.38	2.93	2.39	2.16	1.90	2.49	2.65		
FeO	2.66	4.58	4.09	3.75	4.09	3.66	3.21	4.63	4.04		
MnO	0.06	0.10	0.10	0.10	0.12	0.09	0.06	0.10	0.10		
MgO	2.44	5.37	4.80	4.08	4.31	4.94	3.36	5.05	4.96		
CaO	6.05	6.90	7.28	5.66	6.89	6.89	6.22	7.07	5.28		
Na ₂ O	5.28	4.95	4.47	4.18	3.85	4.22	4.84	3.90	3.26		
K ₂ O	1.57	0.15	1.61	4.31	2.25	1.95	1.37	1.65	4.03		
P ₂ O ₅	0.39	0.23	0.52	0.56	0.34	0.54	0.49	0.34	0.50		
Sum	95.79	99.33	96.13	101.57	95.39	96.42	93.86	94.24	93.06		

Table 2.1 - (continued)

(Wt. %)	M. diorite	Meta-gabbro							
	DDH- 496-526	DDH- 496-501	DDH- 496-540	DDH- 497-213	DDH- 497-228	VB-99- 090	VB-99- 080	AR-00- 057	AR-00- 059
SiO ₂	54.91	52.74	46.06	48.40	48.88	48.91	45.93	55.79	51.14
TiO ₂	0.73	1.73	1.32	1.69	1.07	1.19	1.49	0.90	1.09
Al ₂ O ₃	17.81	19.47	15.19	16.47	15.84	15.79	13.65	19.57	19.55
Fe ₂ O ₃ *	1.90	3.65	3.48	3.48	3.08	2.80	3.53	2.26	2.84
FeO	3.23	6.70	7.46	7.23	6.45	5.50	7.47	2.99	5.10
MnO	0.09	0.14	0.29	0.20	0.13	0.13	0.17	0.08	0.12
MgO	3.98	4.30	7.74	4.65	7.27	5.28	6.89	3.94	4.35
CaO	7.39	6.27	8.69	8.74	7.90	6.81	7.44	6.14	7.84
Na ₂ O	4.54	4.34	3.08	3.61	3.56	3.65	3.02	4.89	4.63
K ₂ O	1.46	1.15	1.51	1.12	1.08	1.50	1.70	3.29	1.15
P ₂ O ₅	0.51	0.31	0.35	0.72	0.25	0.41	0.49	0.51	0.30
Sum	96.96	101.05	95.54	96.66	95.97	92.35	92.17	100.87	98.61

(Wt. %)	Meta-hornblende gabbro								
	AR-00- 065	AR-00- 068	DDH- 496-516	DDH- 497-211	DDH- 497-212	DDH- 497-215	VB-99- 078	VB-99- 083	VB-99- 085
SiO ₂	50.92	45.74	47.17	48.06	47.97	47.31	42.36	47.20	47.49
TiO ₂	1.04	1.34	2.03	1.11	1.07	1.34	1.29	0.36	1.13
Al ₂ O ₃	19.64	17.19	13.10	16.33	16.44	17.74	14.49	16.85	17.30
Fe ₂ O ₃ *	2.62	2.76	3.97	2.82	2.77	2.77	2.89	1.86	3.12
FeO	4.67	5.83	9.68	6.33	6.06	6.01	7.29	4.43	6.17
MnO	0.13	0.12	0.18	0.15	0.15	0.14	0.14	0.08	0.11
MgO	3.39	6.50	10.23	6.72	6.43	5.62	8.42	6.50	4.05
CaO	6.90	9.63	10.91	8.87	8.66	9.75	9.10	11.10	8.53
Na ₂ O	4.81	3.40	2.53	3.61	3.66	3.85	2.43	2.99	4.47
K ₂ O	1.03	1.36	1.02	0.51	0.68	0.58	1.12	0.73	0.71
P ₂ O ₅	0.42	0.83	0.20	0.29	0.28	0.61	0.43	0.13	0.61
Sum	95.96	95.26	101.66	95.00	94.41	95.97	90.32	92.43	94.01

Table 2.1 - (continued)

(Wt. %)	Meta-hbl gabbro			
	VB-99- 106C	VB-99- 106F	VB-99- 091	AR-00- 02
SiO ₂	50.99	46.88	46.34	51.55
TiO ₂	0.95	1.16	0.58	0.73
Al ₂ O ₃	17.20	17.32	16.74	16.42
Fe ₂ O ₃ *	2.77	3.40	2.35	3.02
FeO	6.08	7.37	4.54	5.27
MnO	0.16	0.18	0.11	0.10
MgO	7.10	7.44	6.17	3.58
CaO	8.97	8.85	6.77	6.04
Na ₂ O	3.66	3.08	3.92	4.97
K ₂ O	0.48	1.38	1.51	1.03
P ₂ O ₅	0.06	0.15	0.22	0.34
Sum	97.53	98.67	89.47	93.65

Table 2.2 - Trace element analyses of Paleoproterozoic metaplutonic rocks of the Voisey's Bay Area, Labrador.

(ppm)	Meta-tonalite								
	DDH-496-511	DDH-496-532	DDH-496-535	DDH-496-549	DDH-497-217	DDH-497-219	DDH-497-220	DDH-497-223	DDH-497-225
Li	21	15	16	16	14	14	15	13	14
S	1165	106	139	156	45	108	64	64	116
Cl	54	164	147	528	179	120	104	270	252
Sc	<LD	<LD	<LD	<LD	10.2	12.8	<LD	<LD	10.3
V	54.0	81.0	93.0	60.9	88.8	83.9	72.6	78.4	75.8
Cr	24.2	17.7	25.0	<LD	24.6	18.6	38.2	21.0	21.9
Ni	<LD	8.9	11.5	7.5	15.1	13.9	<LD	10.3	10.3
Cu	44.0	14.6	42.6	30.8	<LD	44.7	<LD	23.4	52.0
Zn	20.7	29.1	32.1	13.8	32.0	41.2	31.1	32.9	34.4
Ga	24.9	22.2	24.3	23.5	25.0	23.8	24.7	25.8	22.1
As	<LD	<LD	<LD	25.5	<LD	<LD	<LD	26.6	<LD
Rb	11.2	18.3	12.7	37.2	6.3	9.5	8.8	20.5	22.7
Sr	626	1451	1423	1236	1550	1507	1317	1353	1383
Y	9.8	9.2	9.1	8.4	6.7	7.6	6.1	7.7	7.8
Zr	43.2	147.7	74.1	146.7	<LD	73.4	80.5	107.2	134.5
Nb	9.5	6.2	6.6	7.5	5.4	6.1	5.7	5.3	6.9
Mo	0.2	0.2	0.2	0.9	0.3	0.4	0.3	0.2	0.5
Cs	<LD	<LD	<LD	0.2	<LD	<LD	<LD	<LD	<LD
Ba	944	2570	1348	1139	982	1116	1151	1221	1616
La	34.4	38.4	38.9	47.4	35.3	39.4	34.4	37.0	43.8
Ce	65.2	78.3	75.9	97.4	70.8	79.4	67.8	75.2	89.0
Pr	6.3	8.7	9.1	10.7	8.4	9.4	7.9	8.8	10.6
Nd	22.1	33.8	35.6	40.7	32.8	37.0	31.0	34.8	41.1
Sm	3.18	5.39	5.66	5.93	5.34	6.09	4.97	5.50	6.60
Eu	1.15	1.75	1.83	1.52	1.80	1.85	1.69	1.71	1.89
Gd	2.36	3.41	3.89	3.56	3.20	3.64	3.05	3.25	3.99
Tb	0.32	0.39	0.39	0.39	0.35	0.41	0.33	0.36	0.42
Dy	1.87	1.95	2.01	1.97	1.83	2.10	1.66	1.86	2.13
Ho	0.37	0.33	0.34	0.34	0.31	0.34	0.28	0.31	0.36
Er	1.09	0.85	0.88	0.89	0.80	0.88	0.70	0.83	0.90
Tm	0.17	0.11	0.11	0.12	0.14	0.16	0.08	0.14	0.10
Yb	1.15	0.64	0.67	0.73	0.57	0.64	0.52	0.61	0.68
Lu	0.17	0.09	0.11	0.10	0.06	0.07	0.07	0.06	0.08
Hf	0.34	0.79	0.79	0.77	0.24	0.37	0.36	0.44	1.32
Ta	0.36	0.24	0.28	0.50	0.24	0.27	0.25	0.22	0.30
Tl	<LD	<LD	<LD	<LD	0.06	0.10	0.07	0.18	0.14
Pb	9.6	13.1	12.3	16.7	10.4	11.6	11.8	10.7	13.0
Bi	0.03	0.03	0.03	0.04	0.03	0.04	<LD	<LD	<LD
Th	1.23	1.75	1.58	5.54	0.18	0.18	0.04	0.08	0.17
U	0.04	0.15	0.12	0.55	0.08	0.06	0.01	<LD	<LD

Trace element data by X-ray fluorescence and Inductively Coupled Plasma-Mass Spectrometry. Analytical details given in Appendix 1. LD = limit of detection.

Table 2.2 - (continued)

(ppm)	Meta-tonalite								
	DDH- 497-227	DDH- 497-231	VB-99- 076	VB-99- 082	AR-00- 004	AR-00- 017	AR-00- 032	AR-00- 053	AR-00- 054
Li	12	7	18	13	23	13	10	10	15
S	69	243	93	331	423	74	185	57	37
Cl	237	153	287	427	493	298	237	420	342
Sc	11.1	<LD	<LD	<LD	<LD	<LD	<LD	<LD	<LD
V	83.9	58.1	67.1	88.1	112.7	93.1	72.2	87.1	87.3
Cr	14.6	<LD	<LD	15.2	41.6	40.8	23.1	66.5	26.1
Ni	9.1	<LD	9.6	<LD	23.0	15.0	<LD	24.3	16.0
Cu	16.0	60.6	66.6	76.3	517.8	14.5	27.2	85.9	21.2
Zn	26.3	27.9	22.8	13.0	46.1	40.1	7.3	49.0	36.2
Ga	21.6	18.7	19.9	19.5	25.4	24.2	22.6	23.1	19.7
As	<LD	<LD	<LD	<LD	<LD	<LD	<LD	<LD	<LD
Rb	21.3	40.1	72.3	20.2	24.4	40.6	28.0	70.3	65.1
Sr	1284	907	1213	507	1301	1544	589	1088	1347
Y	7.9	7.6	7.1	61.6	15.9	11.8	6.8	20.9	12.6
Zr	140.6	246.8	119.0	282.9	386.9	126.1	121.7	296.2	235.7
Nb	6.0	5.8	7.2	21.4	9.1	9.6	4.2	21.1	9.7
Mo	0.1	0.1	0.3	3.5	0.4	0.3	0.3	0.4	0.5
Cs	<LD	<LD	0.4	<LD	<LD	0.1	0.1	0.2	0.3
Ba	1433	1798	1303	248	874	1966	905	1551	1832
La	35.7	30.9	37.2	67.6	47.8	49.0	52.0	56.7	51.0
Ce	72.5	61.8	76.8	142.3	115.0	100.2	99.3	119.3	101.5
Pr	8.8	7.6	8.6	15.5	15.5	11.6	9.9	14.5	11.9
Nd	33.5	29.2	32.3	58.6	59.8	45.1	34.2	56.2	45.1
Sm	5.51	4.69	5.14	11.85	9.80	7.16	4.72	9.45	7.07
Eu	1.51	1.37	1.51	2.41	2.10	1.96	1.20	2.18	1.77
Gd	3.31	2.96	3.21	11.57	6.14	4.21	2.95	6.29	4.37
Tb	0.36	0.33	0.38	1.83	0.67	0.50	0.34	0.79	0.50
Dy	1.91	1.75	1.93	11.38	3.46	2.52	1.81	4.46	2.64
Ho	0.32	0.31	0.33	2.26	0.57	0.43	0.31	0.82	0.46
Er	0.86	0.78	0.91	6.55	1.49	1.14	0.79	2.22	1.20
Tm	0.14	0.10	0.13	0.94	0.22	0.17	0.10	0.32	0.18
Yb	0.64	0.61	0.76	5.92	1.11	0.92	0.59	1.92	0.99
Lu	0.07	0.07	0.11	0.84	0.15	0.12	0.08	0.28	0.14
Hf	0.65	2.09	0.66	3.92	0.90	1.45	0.65	2.70	1.67
Ta	0.27	0.25	0.31	1.06	0.27	0.39	0.22	0.98	0.35
Tl	0.19	0.25	0.51	<LD	0.17	0.26	0.16	0.48	0.50
Pb	11.5	13.0	11.9	8.1	9.2	13.5	11.6	16.2	16.9
Bi	0.03	<LD	0.03	0.04	0.03	0.03	0.01	0.02	0.03
Th	0.17	0.13	2.12	8.55	0.08	3.14	4.47	5.22	3.59
U	0.06	0.11	0.11	2.82	0.05	0.24	0.09	0.24	0.37

Table 2.2 - (continued)

(ppm)	Meta-quartz diorite								
	DDH- 496-527	DDH- 496-530	DDH- 496-536	DDH- 496-542	DDH- 496-547	DDH- 496-202	DDH- 497-203	DDH- 497-208	DDH- 497-210
Li	16	14	14	15	14	15	15	18	16
S	336	300	153	396	170	278	149	96	221
Cl	264	164	202	282	221	641	237	312	446
Sc	21.9	<LD	<LD	<LD	<LD	<LD	19.0	10.8	9.3
V	120.7	105.0	79.3	84.8	63.9	65.5	93.8	76.0	82.3
Cr	25.0	24.0	35.5	<LD	12.6	14.1	81.1	77.1	63.3
Ni	11.0	10.9	11.9	9.6	<LD	<LD	30.3	29.1	31.0
Cu	44.0	41.4	20.2	42.6	18.1	22.6	53.5	11.8	131.6
Zn	41.7	44.3	41.8	25.4	27.6	22.6	28.4	32.7	37.3
Ga	21.3	21.0	22.7	18.8	22.3	20.3	22.5	21.1	21.3
As	<LD	<LD	<LD	<LD	<LD	<LD	<LD	<LD	<LD
Rb	18.7	17.3	26.7	30.2	36.0	43.5	110.7	111.4	143.1
Sr	1533	1634	1427	1451	1478	1593	929	869	643
Y	18.8	20.3	16.3	14.9	11.4	25.2	9.9	11.7	12.6
Zr	103.9	8.8	161.5	95.7	155.3	147.7	92.2	301.9	474.3
Nb	10.6	7.3	10.5	9.3	9.3	12.4	9.9	13.1	17.1
Mo	0.5	0.7	0.3	0.4	0.3	0.7	0.9	0.7	1.1
Cs	<LD	<LD	<LD	<LD	<LD	0.2	0.4	0.2	0.2
Ba	1455	1635	2081	2660	2282	2504	1275	1402	1101
La	63.5	51.1	48.1	41.6	46.3	52.5	42.0	37.7	43.9
Ce	133.9	112.8	94.1	90.4	98.3	117.0	87.0	76.9	93.1
Pr	15.0	13.2	11.2	10.3	11.4	12.8	9.9	8.9	11.1
Nd	58.1	53.4	43.4	40.4	44.7	50.0	37.5	33.7	42.3
Sm	9.32	9.22	7.18	6.65	7.10	8.28	6.15	5.57	7.03
Eu	2.30	2.15	2.00	1.89	2.10	1.91	1.64	1.53	1.64
Gd	6.05	6.33	5.27	4.74	4.47	5.50	3.86	3.57	4.55
Tb	0.73	0.81	0.59	0.60	0.52	0.82	0.49	0.45	0.57
Dy	3.90	4.41	3.19	3.33	2.72	4.90	2.75	2.56	3.25
Ho	0.69	0.80	0.58	0.61	0.48	0.95	0.50	0.46	0.58
Er	1.86	2.16	1.60	1.65	1.31	2.81	1.39	1.31	1.57
Tm	0.26	0.29	0.23	0.23	0.18	0.38	0.18	0.22	0.22
Yb	1.57	1.74	1.33	1.34	1.12	2.15	1.19	1.12	1.23
Lu	0.22	0.24	0.21	0.19	0.16	0.27	0.15	0.13	0.15
Hf	0.99	0.60	0.56	0.97	1.43	1.43	1.01	1.79	1.67
Ta	0.43	0.34	0.41	0.47	0.47	0.54	0.47	0.57	0.50
Tl	<LD	<LD	<LD	<LD	<LD	<LD	0.76	0.76	0.99
Pb	12.8	13.5	16.5	14.3	14.7	19.8	20.4	21.0	21.9
Bi	0.02	0.03	0.03	0.03	0.03	0.04	0.03	0.04	0.03
Th	5.10	1.26	0.66	1.79	2.73	3.97	2.52	0.19	0.12
U	0.52	0.15	0.09	0.25	0.33	0.74	0.21	0.13	0.07

Table 2.2 - (continued)

(ppm)	Meta-quartz diorite						Meta-diorite		
	DDH- 497-221	VB-99- 077	VB-99- 107	VB-99- 108	AR-00- 008	AR-00- 009	AR-00- 050	VB-99- 089	VB-99- 092
Li	14	17	14	12	29	16	21	19	14
S	87	118	70	81	213	72	42	61	83
Cl	162	319	455	547	545	480	221	448	595
Sc	11.4	<LD							
V	74.8	92.7	78.3	97.3	124.1	96.9	83.0	125.0	92.1
Cr	17.8	<LD	39.2	81.5	31.1	17.6	28.3	79.6	79.4
Ni	<LD	<LD	15.1	23.7	<LD	<LD	9.3	16.9	35.2
Cu	35.2	41.2	9.0	34.9	28.6	16.4	15.7	30.2	12.4
Zn	30.3	29.8	57.8	41.9	34.7	36.3	35.3	41.8	44.2
Ga	25.6	22.4	25.2	22.2	23.5	25.1	23.3	24.3	19.5
As	<LD	<LD	<LD	<LD	<LD	<LD	<LD	<LD	<LD
Rb	10.1	40.4	30.4	82.9	63.1	31.7	7.5	46.3	84.8
Sr	1363	623	1042	912	938	1666	1404	897	961
Y	7.1	8.7	24.4	21.9	18.0	11.6	7.2	15.7	21.5
Zr	78.9	75.1	91.9	369.1	185.9	96.5	113.1	90.5	543.1
Nb	4.9	5.0	11.1	22.0	13.3	7.0	6.5	10.5	23.9
Mo	0.3	0.2	0.2	0.6	0.8	0.3	0.2	0.6	0.4
Cs	<LD	0.3	<LD	0.2	0.3	0.1	0.1	0.4	0.2
Ba	1448	544	633	1491	1125	1556	1579	941	2368
La	33.6	19.2	42.1	69.7	40.8	51.4	42.0	29.3	75.9
Ce	66.5	41.8	91.4	144.0	91.0	106.6	74.4	60.2	158.8
Pr	8.0	5.0	11.6	15.8	10.2	12.3	8.5	7.5	17.4
Nd	32.4	19.4	47.4	58.4	38.9	47.4	31.8	29.4	62.7
Sm	5.30	3.53	9.18	9.46	6.60	7.44	4.91	5.51	9.89
Eu	1.62	1.06	2.01	1.95	1.53	2.11	1.58	1.63	2.12
Gd	3.21	2.73	6.88	6.61	4.50	4.51	2.97	4.16	6.58
Tb	0.35	0.37	0.88	0.85	0.63	0.52	0.31	0.54	0.83
Dy	1.82	2.16	4.95	4.72	3.48	2.60	1.58	3.14	4.61
Ho	0.31	0.41	0.90	0.88	0.66	0.43	0.26	0.58	0.84
Er	0.78	1.16	2.34	2.48	1.90	1.11	0.68	1.61	2.37
Tm	0.10	0.16	0.31	0.36	0.29	0.15	0.11	0.27	0.33
Yb	0.58	1.04	1.82	2.17	1.71	0.85	0.47	1.37	2.02
Lu	0.06	0.15	0.23	0.32	0.24	0.11	0.07	0.17	0.29
Hf	0.23	1.11	0.62	2.41	2.25	0.37	0.35	1.00	3.20
Ta	0.23	0.20	0.30	0.55	0.55	0.27	0.21	0.56	0.87
Tl	0.04	<LD	0.16	0.55	0.43	0.23	0.10	0.38	0.49
Pb	11.3	8.6	9.4	14.8	9.2	11.0	9.7	9.2	14.2
Bi	<LD	0.02	<LD	0.03	0.02	0.02	0.04	0.04	0.03
Th	0.04	0.33	1.14	8.04	2.65	2.01	0.28	2.20	7.25
U	<LD	0.12	<LD	0.17	0.38	0.11	0.09	0.57	0.48

Table 2.2 - (continued)

(ppm)	M. diorite	Meta-gabbro							
	DDH- 496-526	DDH- 496-501	DDH- 496-540	DDH- 497-213	DDH- 497-228	VB-99- 090	VB-99- 080	AR-00- 057	AR-00- 059
Li	18	20	15	22	12	16	17	17	11
S	261	131	240	240	786	94	128	70	854
Cl	207	<LD	630	239	330	604	708	264	241
Sc	<LD	17.2	43.7	27.3	21.3	<LD	<LD	15.7	17.2
V	70.0	160.0	268.6	275.9	198.6	153.2	208.8	97.0	166.4
Cr	26.5	128.6	262.0	51.0	185.7	115.3	137.7	38.5	73.7
Ni	8.4	72.0	64.4	<LD	62.2	23.4	36.1	15.3	18.9
Cu	20.9	<LD	30.3	145.2	141.1	51.3	72.8	34.2	81.1
Zn	26.8	73.1	129.1	93.1	68.4	54.6	80.8	43.1	50.7
Ga	24.2	35.9	22.0	21.4	25.4	23.8	20.0	22.5	26.4
As	<LD	<LD	<LD	<LD	<LD	<LD	<LD	<LD	<LD
Rb	17.7	13.6	26.5	14.8	12.2	41.3	61.5	62.0	14.3
Sr	1493	492	550	575	574	831	644	1388	737
Y	26.8	22.0	26.4	37.6	16.5	24.3	25.9	11.7	32.4
Zr	32.3	171.6	85.4	204.1	122.3	117.8	169.7	231.5	135.1
Nb	8.9	18.0	8.9	17.6	6.9	15.3	16.2	10.6	14.7
Mo	0.5	0.2	0.4	1.1	0.2	0.7	0.7	0.7	0.8
Cs	0.2	<LD	0.2	0.1	<LD	0.2	0.5	0.3	0.2
Ba	745	306	320	552	332	941	851	1760	599
La	50.8	32.6	15.7	33.4	17.1	35.6	36.2	38.6	48.9
Ce	106.5	74.3	39.7	72.0	40.2	76.4	78.7	78.8	102.3
Pr	13.1	8.4	5.5	9.3	5.4	9.6	10.6	9.7	12.5
Nd	50.6	33.1	24.0	39.3	22.0	38.2	43.0	37.1	48.8
Sm	9.32	6.86	5.38	8.34	4.53	7.42	8.36	6.07	9.20
Eu	1.96	1.55	1.77	2.29	1.32	1.72	1.68	1.68	1.84
Gd	7.37	5.81	5.44	7.74	3.82	5.76	7.07	3.88	7.42
Tb	0.94	0.81	0.74	1.11	0.53	0.78	0.88	0.44	1.03
Dy	5.34	4.49	4.73	6.86	3.24	4.58	5.31	2.34	6.17
Ho	1.01	0.82	0.96	1.39	0.63	0.86	1.00	0.41	1.19
Er	2.82	2.25	2.88	3.96	1.80	2.44	2.85	1.06	3.29
Tm	0.39	0.32	0.42	0.61	0.26	0.38	0.42	0.14	0.47
Yb	2.33	1.95	2.68	3.51	1.58	2.10	2.52	0.89	2.94
Lu	0.35	0.28	0.44	0.51	0.21	0.27	0.36	0.13	0.43
Hf	0.96	1.61	2.04	0.95	0.80	1.54	3.14	1.21	1.92
Ta	0.41	0.92	0.43	0.84	0.31	0.65	0.78	0.35	0.70
Tl	<LD	<LD	<LD	0.14	0.08	0.24	0.43	0.33	0.11
Pb	12.1	9.3	9.0	8.5	5.9	7.5	5.9	13.9	8.9
Bi	0.05	0.02	0.03	0.07	0.04	<LD	<LD	0.00	0.02
Th	2.94	2.45	1.31	1.06	0.20	1.24	3.71	0.58	2.17
U	0.38	0.18	0.38	0.47	0.07	0.30	0.60	0.13	0.40

Table 2.2 - (continued)

(ppm)	Meta-hornblende gabbro								
	AR-00-065	AR-00-068	DDH-496-516	DDH-497-211	DDH-497-212	DDH-497-215	VB-99-078	VB-99-083	VB-99-085
Li	13	14	11	13	18	17	26	12	8
S	216	240	1469	101	108	59	328	43	58
Cl	308	681	449	108	248	169	821	798	530
Sc	<LD	19.4	30.8	27.6	31.9	23.9	28.0	46.1	<LD
V	125.8	132.8	337.4	215.9	202.6	227.2	221.2	154.6	166.0
Cr	113.4	69.7	315.1	117.9	101.8	65.3	98.9	82.9	18.2
Ni	16.7	27.8	198.2	23.1	17.8	10.0	39.4	31.5	<LD
Cu	27.2	120.0	53.8	11.9	8.9	8.4	65.6	<LD	12.1
Zn	47.0	63.4	67.1	54.0	57.1	54.1	25.9	<LD	46.7
Ga	22.5	24.1	21.7	24.1	24.4	22.0	22.1	17.5	24.6
As	<LD	<LD	<LD	<LD	<LD	<LD	<LD	<LD	<LD
Rb	8.9	26.9	12.8	3.3	12.0	6.0	28.6	11.0	6.9
Sr	849	1802	279	517	557	589	572	317	808
Y	19.9	15.4	19.8	17.1	16.0	28.8	13.1	13.2	33.9
Zr	256.2	142.2	133.1	80.1	64.9	149.8	31.5	12.0	297.5
Nb	11.3	17.9	11.7	6.7	6.6	12.6	5.3	1.8	16.4
Mo	0.4	0.9	0.7	0.4	0.4	0.7	0.5	0.2	1.2
Cs	0.5	0.0	<LD	<LD	<LD	<LD	0.5	<LD	<LD
Ba	1026	1097	258	204	231	252	291	172	312
La	45.1	30.0	14.7	11.8	13.2	22.0	16.5	8.9	66.8
Ce	109.1	63.0	37.9	25.8	28.2	50.2	34.7	17.6	144.7
Pr	14.5	8.0	4.9	3.5	3.7	6.4	4.8	2.3	16.1
Nd	59.4	32.3	21.4	15.4	16.4	27.3	20.8	9.6	60.6
Sm	10.05	6.07	4.86	3.59	3.65	5.91	4.14	2.18	10.42
Eu	2.48	1.75	1.58	1.26	1.21	1.73	1.39	0.67	2.08
Gd	6.34	5.07	4.81	3.61	3.63	5.45	3.84	2.54	8.17
Tb	0.74	0.65	0.69	0.53	0.53	0.81	0.47	0.37	1.13
Dy	3.90	3.92	4.12	3.25	3.28	4.92	2.86	2.57	6.60
Ho	0.68	0.75	0.76	0.67	0.67	0.99	0.54	0.52	1.26
Er	1.79	2.10	2.08	1.89	1.87	2.81	1.45	1.60	3.52
Tm	0.25	0.29	0.28	0.26	0.28	0.38	0.18	0.27	0.48
Yb	1.33	1.90	1.68	1.72	1.71	2.45	1.18	1.37	2.89
Lu	0.18	0.29	0.24	0.25	0.23	0.35	0.16	0.17	0.41
Hf	1.70	2.88	1.87	0.86	0.72	1.64	1.25	0.55	4.81
Ta	0.32	0.66	0.60	0.36	0.36	0.57	0.31	0.12	0.73
Tl	0.24	0.05	<LD	<LD	0.07	<LD	0.19	0.10	<LD
Pb	6.4	7.9	4.1	3.3	3.5	4.1	4.1	3.2	7.1
Bi	0.04	<LD	0.03	<LD	0.02	<LD	<LD	0.03	0.02
Th	1.43	0.46	0.57	0.25	0.35	0.85	1.22	0.68	9.91
U	0.72	0.18	0.15	0.13	0.14	0.43	0.92	0.44	0.69

Table 2.2 - (continued)

(ppm)	Meta-hbl gabbro			
	VB-99- 106C	VB-99- 106F	VB-99- 091	AR-00- 02
Li	9	19	19	7
S	74	101	78	515
Cl	520	1133	313	1414
Sc	44.1	32.8	<LD	0.0
V	247.9	262.1	86.0	73.4
Cr	113.4	0.4	<LD	19.6
Ni	18.2	<LD	<LD	252.4
Cu	4.4	31.2	14.4	154.9
Zn	37.2	41.8	17.9	35.9
Ga	20.6	18.7	19.6	26.5
As	<LD	<LD	<LD	0.0
Rb	3.3	27.3	42.4	20.5
Sr	436	406	542	1192
Y	19.0	22.5	10.7	9.6
Zr	58.2	114.2	66.8	117.7
Nb	9.2	8.4	6.1	7.7
Mo	0.6	0.9	0.7	0.3
Cs	<LD	<LD	0.3	0.0
Ba	199	387	537	678
La	10.3	17.5	16.9	34.4
Ce	22.6	40.7	37.0	62.1
Pr	3.2	5.5	4.3	8.2
Nd	13.8	21.4	17.2	32.6
Sm	3.17	4.73	3.15	5.44
Eu	1.11	1.46	1.01	1.75
Gd	3.26	4.77	2.55	3.68
Tb	0.54	0.71	0.36	0.44
Dy	3.46	4.65	2.16	2.38
Ho	0.74	0.94	0.42	0.44
Er	2.07	2.74	1.22	1.14
Tm	0.30	0.40	0.18	0.18
Yb	2.08	2.50	1.15	1.04
Lu	0.30	0.38	0.17	0.14
Hf	1.36	1.80	1.03	0.55
Ta	0.49	0.40	0.27	0.29
Tl	0.02	0.21	0.33	0.12
Pb	5.1	6.6	4.8	31.0
Bi	<LD	0.03	0.02	0.06
Th	0.63	0.93	0.23	0.31
U	0.34	0.30	0.10	0.22

Table 2.3. U-Pb TIMS data for the metaplutonic samples from Voisey's Bay, Labrador.

Fractions ^a	weight mg	U ppm	Pb _{rad} ppm ^b	Pb _{com} pg ^c	-----Corrected atomic ratios ^{d,e} -----						Age (Ma)				
					$\frac{^{206}\text{Pb}^c}{^{204}\text{Pb}}$	$\frac{^{206}\text{Pb}}{^{206}\text{Pb}}$	$\frac{^{206}\text{Pb}}{^{238}\text{U}}$	+/-	$\frac{^{207}\text{Pb}}{^{235}\text{U}}$	+/-	$\frac{^{207}\text{Pb}}{^{206}\text{Pb}}$	+/-	$\frac{^{206}\text{Pb}}{^{238}\text{U}}$	$\frac{^{207}\text{Pb}}{^{235}\text{U}}$	$\frac{^{207}\text{Pb}}{^{206}\text{Pb}}$
Meta-quartz-diorite (VB-99-108) UTM: 6243436E, 557528N															
Z1 clr sml abr	0.0430	188	70.3	42	4091	0.1553	0.34076	106	5.4439	186	0.11587	12	1890	1892	1893
Z2 clr lgr abr	0.0330	179	66.2	44	2852	0.1450	0.34058	96	5.4415	172	0.11588	12	1889	1891	1894
Z3 clr lgr abr	0.6800	121	44.5	4	40098	0.1342	0.34056	166	5.4395	276	0.11584	10	1889	1891	1893
Meta-hornblende gabbro (VB-99-106c) UTM: 6243393E, 557673N															
Z2 clr best abr	0.0500	133	49.0	124	1149	0.1527	0.33864	126	5.4018	218	0.11569	16	1880	1885	1891
Z3 clr lgr abr	0.0160	166	55.2	6	9218	0.1117	0.34551	218	5.0298	352	0.11562	16	1768	1824	1890
Z4 clr sml abr	0.0100	181	65.2	3	14551	0.1258	0.33694	190	5.3683	300	0.11555	20	1872	1880	1889
Meta-tonalite (DDH-496-549) UTM: 6243135E, 559780N															
Z1 clr euh abr	0.0040	95	33.9	49	143	0.2741	0.29962	226	4.4023	414	0.10656	60	1689	1713	1741
Z2 clr euh abr	0.0500	54	20.4	121	486	0.1927	0.33843	156	5.3764	274	0.11522	24	1879	1881	1883
Z3 clr lrg mti-f abr	0.0220	117	41.7	36	1366	0.2528	0.30401	442	4.5568	664	0.10871	18	1711	1741	1778
Z4 clr sml abr	0.0070	86	29.9	4	2691	0.2624	0.29649	1060	4.3787	1566	0.10711	22	1674	1708	1751

^aZ, zircon; clr, clear; sml, small; abr, abraded; lgr, large; euh, euhedral; mti-f, multi-faceted

^bTotal radiogenic Pb after correction for blank, common Pb, and spike.

^cmeasured

^dratios corrected for fractionation, spike, 5-10 picogram laboratory blank, initial common Pb at the age of the sample calculated from the model of Stacey and Kramers (1975) and 1 picogram U blank

^eTwo sigma uncertainties are calculated with an error propagation program, refer to the last two digits and are reported after the ratios.

Table 2.4. Rb-Sr and Sm-Nd TIMS data for metaplutonic rocks from Voisey's Bay, Labrador.

Sample no.	Location	Rock Type ^a	Rb (ppm)	Sr (ppm)	⁸⁷ Sr/ ⁸⁶ Sr (m)	2σ ^b (+/-)	⁸⁷ Rb/ ⁸⁶ Sr (m)	2σ ^b (+/-)	⁸⁷ Sr/ ⁸⁶ Sr (1890 Ma)	2σ ^b (+/-)
VB-99-108	GPS Hill	Meta-qtz dio	83.63	915.80	0.708074	7	0.25811	12	0.70104	12
AR-00-02	Discovery Hill	Meta-hbl gbr	19.43	1192.50	0.704929	14	0.04605	3	0.70368	3
DDH-496-549	DDH-496	Meta-ton	38.80	1234.82	0.706669	14	0.08880	6	0.70426	6
VB-99-106F	GPS Hill	Meta-hbl gbr	29.00	404.62	0.708536	25	0.20259	6	0.70302	6

Sample no.	Location	Rock Type ^a	Nd (ppm)	Sm (ppm)	¹⁴³ Nd/ ¹⁴⁴ Nd ^b (m)	2σ ^c (+/-)	¹⁴⁷ Sm/ ¹⁴⁴ Nd (m)	2σ ^c (+/-)	¹⁴³ Nd/ ¹⁴⁴ Nd ^d (1890 Ma)	2σ ^c (+/-)	εNd (1890 Ma)
VB-99-108	GPS Hill	Meta-qtz dio	56.75	9.67	0.511272	25	0.10520	9	0.509962	9	-4.4
AR-00-02	Discovery Hill	Meta-hbl gbr	32.93	5.45	0.511470	41	0.10224	6	0.510198	7	0.13
DDH-496-549	DDH-496	Meta-ton	40.40	5.87	0.511141	9	0.08964	13	0.510030	1	-3.3
VB-99-106F	GPS Hill	Meta-hbl gbr	22.01	4.19	0.511384	32	0.11765	13	0.509920	1	-5.3

^a qtz dio, quartz-diorite; ton, tonalite; hbl gbr, hornblende gabbro

^b measured and corrected for mass fractionation

^c Errors refer to last one or two digits and are propagated to include reproducibility of standard analysis and run errors

^d calculated using present day chondritic uniform reservoir with ¹⁴³Nd/¹⁴⁴Nd = 0.512638 & ¹⁴⁷Sm/¹⁴⁴Nd = 0.1967

Table 2.5. Pb isotope MC-ICP-MS data for metaplutonic rocks from Voisey's Bay, Labrador.

Sample no.	Location	Rock Type ^a	²⁰⁸ Pb/ ²⁰⁴ Pb	2σ ^b	²⁰⁷ Pb/ ²⁰⁴ Pb	2σ ^b	²⁰⁶ Pb/ ²⁰⁴ Pb	2σ ^b	μ ^c	κ ^d
			(m) ^e	(+/-)	(m) ^e	(+/-)	(m) ^e	(+/-)		
VB-99-108	GPS Hill	Meta-qtz dio	15.160	2	15.008	2	37.277	6	7.76	5.81
AR-00-02	Discovery Hill	Meta-hbl gbr	15.475	1	15.145	2	35.507	5	7.94	4.24
DDH-496-549	DDH-496	Meta-ton	15.448	1	15.000	2	36.196	4	7.66	4.72
VB-99-106F	GPS Hill	Meta-hbl gbr	15.834	2	15.106	2	35.352	6	7.77	3.84

^a qtz dio, quartz-diorite; ton, tonalite; hbl gbr, hornblende gabbro

^b Errors refer to last digit and are propagated to include reproducibility of standard analysis and run errors

^c μ^c is the time-integrated ²³⁸U/²⁰⁴Pb of the mantle & crustal sources of the samples

^d κ^d is the time-integrated ²³²Th/²³⁸U of the mantle & crustal sources of the samples

^e m, measured and correction for mass fractionation

Table 2.6. LAM-ICP-MS U-Pb data for the igneous zircons from the metaplutonic rocks from Voisey's Bay, Labrador.

SAMPLE	Spot no	CONCORDIA RATIOS ^{a,b}										AGES Ma					Plotted Ratios				
		²⁰⁷ Pb		²⁰⁶ Pb		Rho ^c	²⁰⁷ Pb		2 σ %	2 σ %	2 σ %	²⁰⁷ Pb		206Pb	207Pb	1σ	²³⁸ U		²⁰⁷ Pb		
		²³⁸ U	(+/-)	²³⁸ U	(+/-)		²⁰⁸ Pb	(+/-)				²⁰⁷ Pb/ ²⁰⁶ Pb	²⁰⁸ Pb/ ²⁰⁶ Pb				²⁰⁷ Pb/ ²⁰⁶ Pb	²³⁸ U	1σ	²³⁸ U	1σ
DDH-496-549	my17a11	5.5251	0.0535	0.3517	0.0028	0.81	0.1146	0.0006	1.93	1.59	1.13	1904.5	8.3	1942.5	13.4	1873.3	10.2	3.096	0.052	0.111	0.001
DDH-496-549	my17a12	5.9011	0.0478	0.3730	0.0027	0.72	0.1151	0.0007	1.62	1.47	1.17	1961.4	7.0	2043.5	12.9	1881.7	10.5	2.926	0.049	0.114	0.001
DDH-496-549	my04b27	5.7013	0.0417	0.3735	0.0027	0.72	0.1138	0.0006	1.48	1.47	1.10	1931.6	6.3	2045.7	12.8	1860.8	10.0	2.911	0.081	0.116	0.001
DDH-496-549	my04b29	5.5456	0.0427	0.3668	0.0030	0.76	0.1124	0.0006	1.54	1.64	1.11	1907.7	6.6	2014.1	14.2	1839.1	10.0	3.042	0.087	0.114	0.001
DDH-496-549	ja0962	5.8602	0.0333	0.3651	0.0018	0.78	0.1153	0.0004	1.14	0.98	0.71	1955.4	4.9	2006.4	8.4	1885.0	8.4	2.870	0.041	0.115	0.001
DDH-496-549	ja0966	5.7709	0.0322	0.3576	0.0019	0.86	0.1157	0.0003	1.12	1.07	0.59	1942.1	4.8	1971.5	9.1	1891.3	5.3	2.961	0.049	0.116	0.000
DDH-496-549	ja0967	5.5888	0.0223	0.3455	0.0013	0.71	0.1161	0.0003	0.80	0.74	0.59	1914.4	3.4	1913.2	6.1	1896.7	5.3	2.927	0.027	0.116	0.000
VB-99-108	ja09a40	5.4318	0.0213	0.3405	0.0014	0.77	0.1148	0.0003	0.78	0.84	0.55	1889.9	3.4	1888.9	6.9	1876.5	5.0	2.958	0.032	0.114	0.000
VB-99-108	my12c06	6.4478	0.0737	0.4031	0.0039	0.83	0.1140	0.0007	2.29	1.95	1.29	2038.8	10.0	2183.4	18.1	1864.4	11.7	2.974	0.060	0.111	0.001
VB-99-108	my04b05	5.9688	0.0513	0.3817	0.0032	0.91	0.1159	0.0004	1.72	1.66	0.71	1971.3	7.5	2084.4	14.8	1893.3	6.4	3.058	0.088	0.116	0.001
VB-99-108	my04b07	5.8130	0.0399	0.3584	0.0023	0.87	0.1162	0.0004	1.42	1.28	0.71	1918.1	6.1	1974.6	10.9	1897.9	8.4	2.969	0.061	0.116	0.001
VB-99-108	my04b08	5.5547	0.0436	0.3583	0.0026	0.73	0.1150	0.0006	1.57	1.43	1.10	1909.1	6.7	1974.2	12.2	1879.2	9.9	3.040	0.074	0.114	0.001
VB-99-108	my04b12	5.8024	0.0430	0.3579	0.0025	0.72	0.1158	0.0006	1.53	1.40	1.11	1916.5	6.6	1972.3	11.9	1893.1	10.0	3.041	0.070	0.115	0.001
VB-99-108	my04b13	5.3587	0.0331	0.3470	0.0019	0.62	0.1143	0.0006	1.24	1.10	1.03	1878.3	5.3	1920.1	9.1	1869.3	9.3	3.040	0.052	0.117	0.001
VB-99-108	my04b15	5.9425	0.0640	0.3878	0.0041	0.73	0.1139	0.0009	2.15	2.13	1.57	1967.5	9.4	2112.5	19.2	1863.1	14.2	3.013	0.122	0.115	0.001
VB-99-108	my04b16	6.1738	0.0809	0.4000	0.0055	0.90	0.1153	0.0007	2.62	2.75	1.22	2000.8	11.4	2169.3	25.3	1884.7	11.0	2.977	0.128	0.117	0.001
VB-99-106C	ja09a31	5.6669	0.0330	0.3480	0.0019	0.80	0.1171	0.0003	1.17	1.12	0.52	1926.3	5.0	1925.2	9.3	1911.7	4.7	2.895	0.041	0.117	0.000

^aMeasured masses: Hg, 202; Tl, 203,205; Pb, 206, 207; Bi, 209; U, 233, 238; U, 233, 238; Np, 237; Oxides, 249, 253, 254.

^bConstants used to correct measured ratios for mass fractionation and calculate ages: ²⁰⁹Bi/²⁰⁵Tl = 0.7500, ²⁰⁵Tl/²³⁷Np = 2.5500, ²⁰⁹Bi/²³⁷Np = 1.6500, λ²³⁵U = 9.85E-10, λ²³⁸U = 1.55E

^cPropagated errors

Table 2.7. LAM-ICP-MS U-Pb zircon data for the inherited zircon cores of the metaplutonic rocks from Voisey's Bay, Labrador.

SAMPLE	Spot no.	CONCORDIA RATIOS ^{a,b}					AGES Ma					Plotted Ratios									
		$\frac{^{207}\text{Pb}}{^{235}\text{U}}$	$\frac{^{206}\text{Pb}}{^{238}\text{U}}$	Rho ^c	$\frac{^{207}\text{Pb}}{^{206}\text{Pb}}$	$\frac{^{206}\text{Pb}}{^{207}\text{Pb}}$	$\frac{^{207}\text{Pb}}{^{235}\text{U}}$	$\frac{^{206}\text{Pb}}{^{238}\text{U}}$	$\frac{^{207}\text{Pb}}{^{206}\text{Pb}}$	$\frac{^{238}\text{U}}{^{206}\text{Pb}}$	$\frac{^{207}\text{Pb}}{^{206}\text{Pb}}$	$\frac{^{238}\text{U}}{^{206}\text{Pb}}$	$\frac{^{207}\text{Pb}}{^{206}\text{Pb}}$								
VB-99-106c	ja09a07	6.8593	0.0275	0.3654	0.0016	0.44	0.1180	0.0006	0.94	0.87	0.96	1955.2	4.1	2007.8	7.5	1926.1	8.6	2.816	0.036	0.120	####
VB-99-106c	ja09a16	6.1578	0.0348	0.3685	0.0018	0.74	0.1225	0.0005	1.13	0.98	0.78	1998.5	4.9	2022.2	8.5	1993.4	6.9	2.837	0.062	0.123	####
VB-99-106c	ja09a22	6.0674	0.0361	0.3682	0.0022	0.76	0.1208	0.0005	1.19	1.22	0.84	1985.6	5.2	2020.8	10.6	1968.4	7.4	2.876	0.052	0.122	####
VB-99-106c	ja09a23	6.0130	0.0310	0.3720	0.0020	0.73	0.1187	0.0005	1.03	1.09	0.78	1977.7	4.5	2039.0	9.5	1937.3	7.0	2.864	0.098	0.121	####

^aMeasured masses: Hg, 202; Tl, 203,205; Pb, 206, 207; Bi, 209; U, 233, 238; U, 233, 238; Np, 237; Oxides, 249, 253, 254.

^bConstants used to correct measured ratios for mass fractionation and calculate ages. $^{209}\text{Bi}/^{205}\text{Tl} = 0.7500$, $^{205}\text{Tl}/^{237}\text{Np} = 2.5500$, $^{209}\text{Bi}/^{237}\text{Np} = 1.6500$, $\lambda^{235}\text{U} = 9.85\text{E}-10$, $\lambda^{238}\text{U} = 1.55\text{E}-$

^cPropagated errors



Plate 2.1. Field appearance of Paleoproterozoic metaplutonic rocks from Voisey's Bay, Labrador. A) Relatively pristine meta-quartz diorite. B) Highly foliated meta-tonalite.



Plate 2.2. Field appearance of Paleoproterozoic metaplutonic rocks from Voisey's Bay, Labrador. A) Relatively undeformed meta-gabbro in drill core. B) Relatively undeformed meta-gabbro in outcrop.



Plate 2.3. Outcrop-scale lithological variations in Paleoproterozoic metaplutonic rocks from Voisey's Bay, Labrador. A) Meta-gabbro. B) Weathered meta-tonalite.

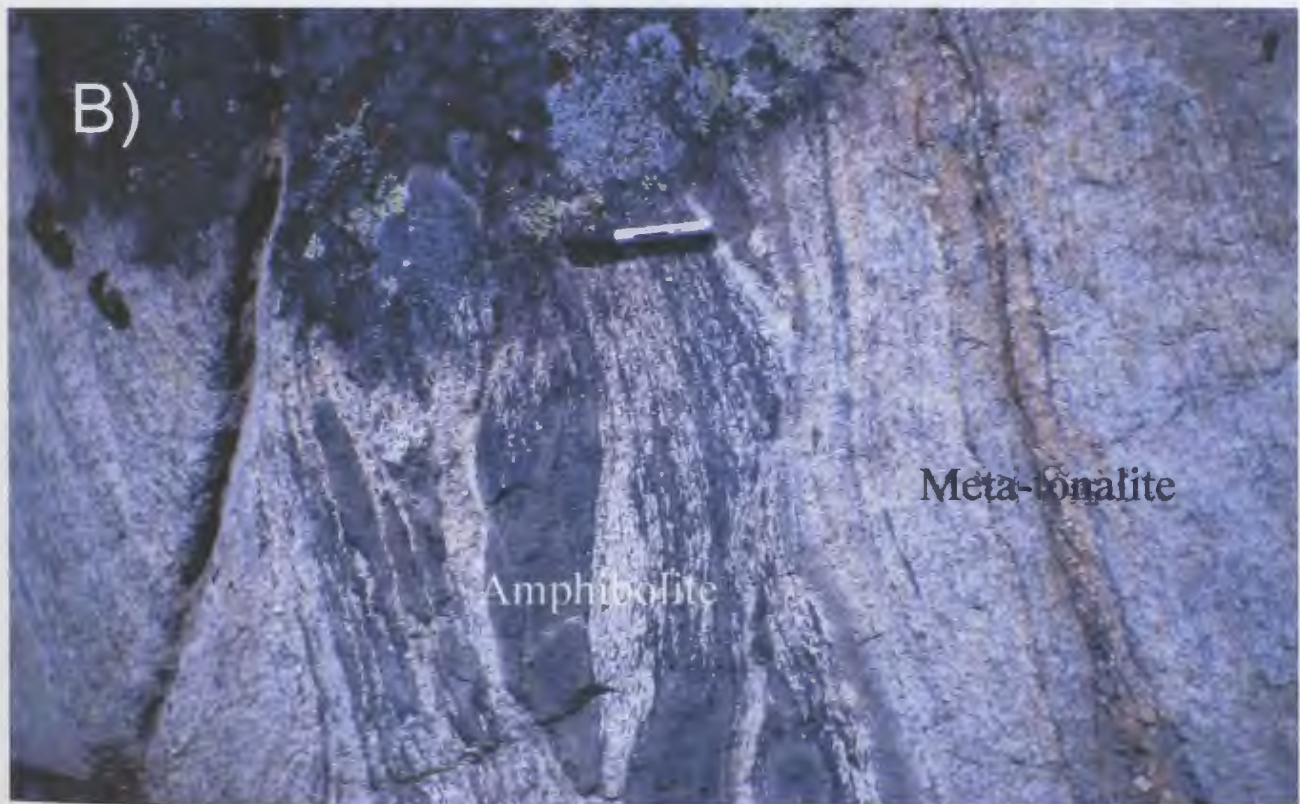
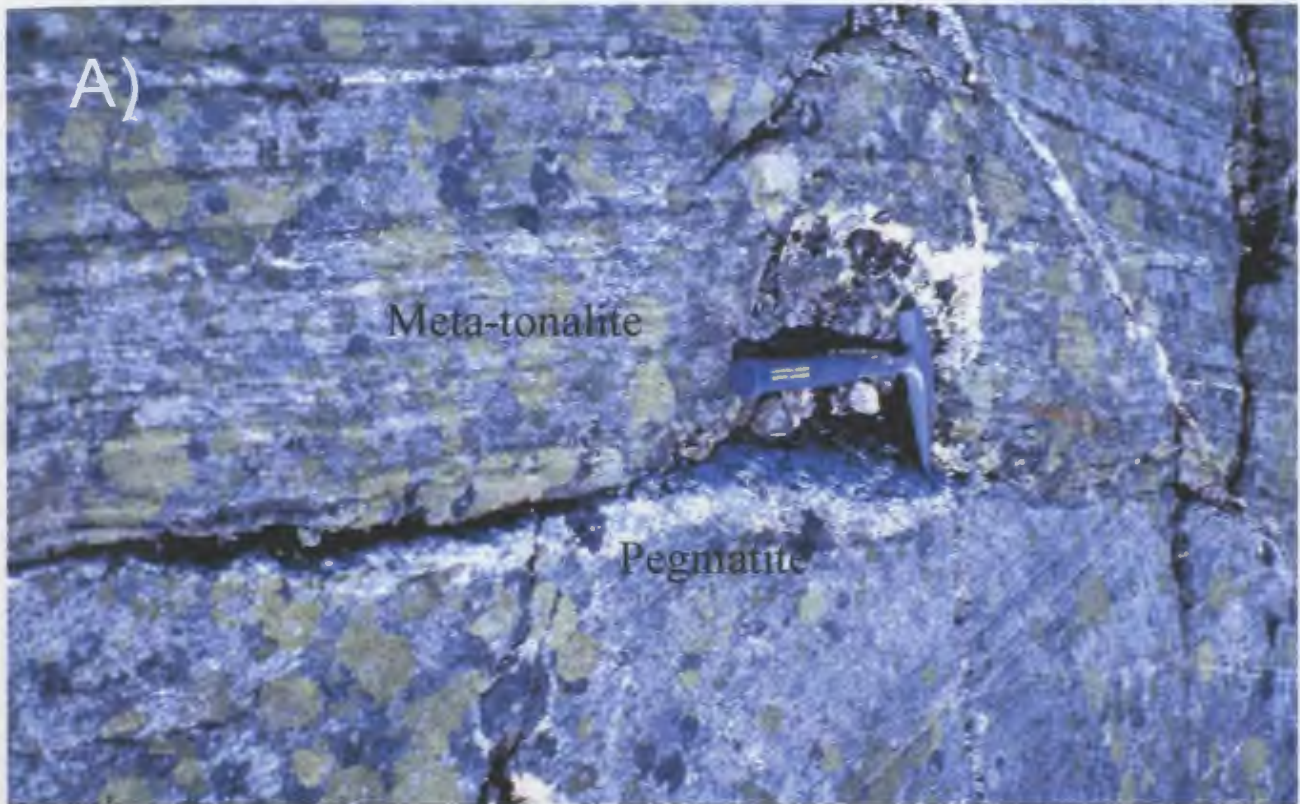


Plate 2.4. Field relationships of Paleoproterozoic metaplutonic rocks from Voisey's Bay, Labrador. A) Cross-cutting pegmatite veins in meta-tonalite. B) Tectonically interleaved and deformed amphibolite dykes in meta-tonalite.



Plate 2.5. Field appearance of metasedimentary rocks from Voisey's Bay, Labrador. A) Metapelite. B) Tightly folded quartz-rich metasediments.



Plate 2.6. Field relationships of meta-anorthosite rocks that are layered with the Paleoproterozoic metaplutonic rocks from Voisey's Bay, Labrador. A) Foliated meta-anorthosite in contact with meta-gabbro. B) Tightly folded meta-anorthosite.

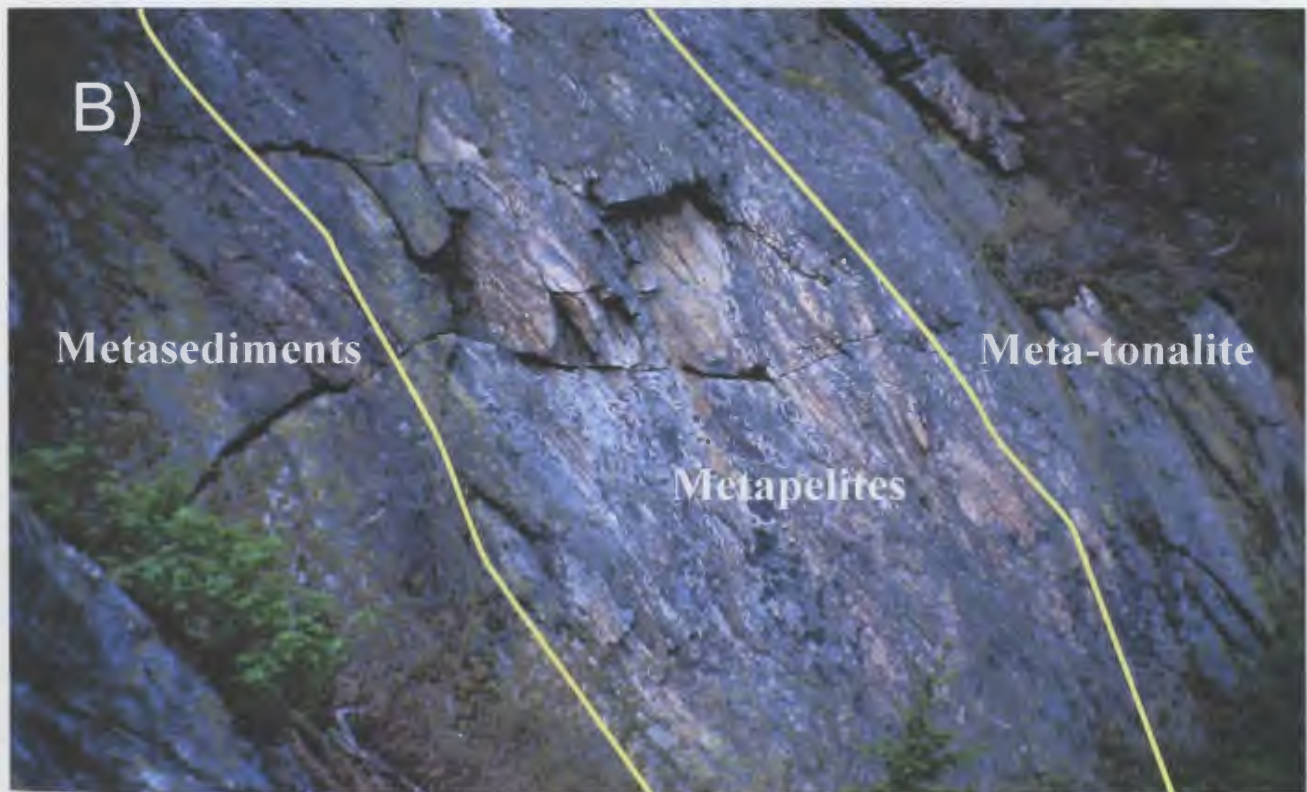


Plate 2.7. Field relationships between the meta-sedimentary unit and the Paleoproterozoic metaplutonic rocks from Voisey's Bay, Labrador. A) Meta-gabbro in contact with quartzite. B) Meta-tonalite in contact with metapelites.



Plate 2.8. Contact relationships between the Nain Province gneisses and the Paleoproterozoic metaplutonic rocks from Voisey's Bay, Labrador. A) Contact in drill core between banded orthogneisses and meta-gabbro. B) Contact in outcrop between quartzo-feldspathic orthogneisses and meta-gabbro.

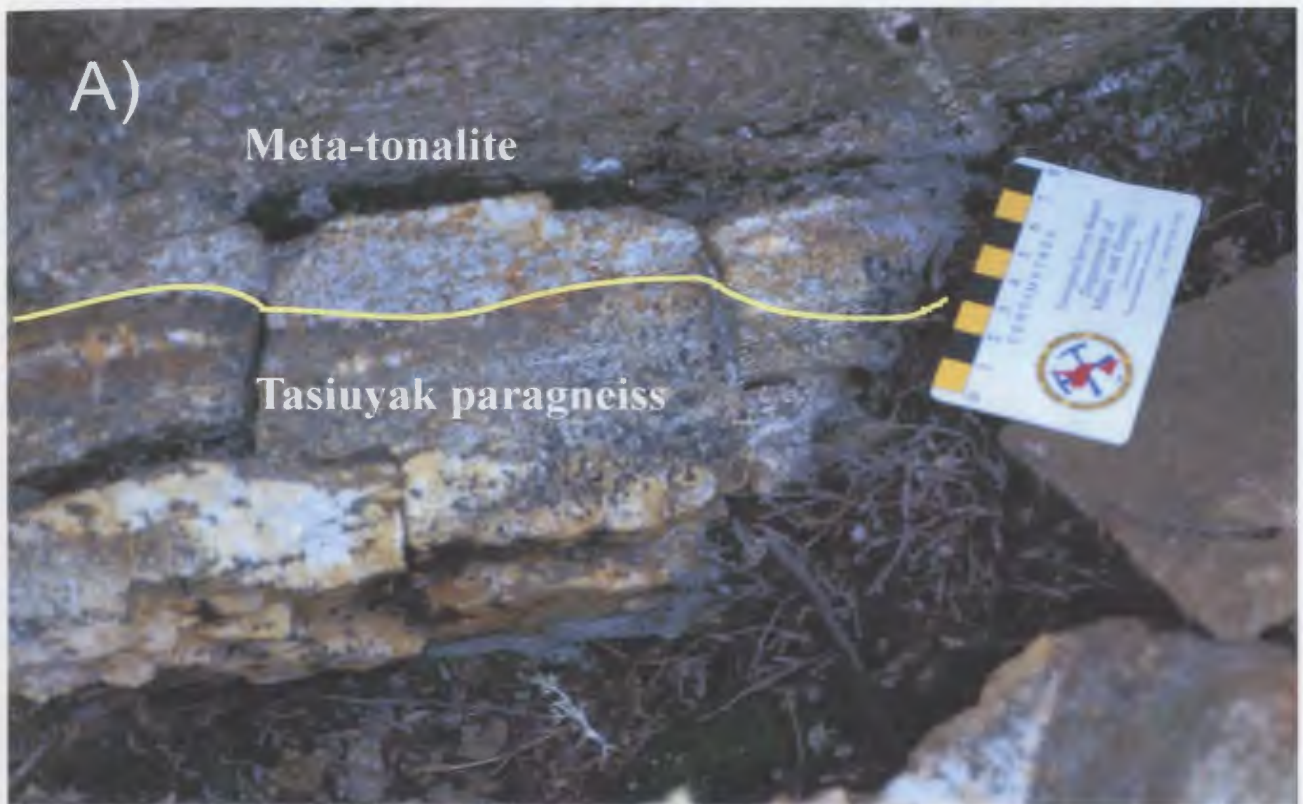


Plate 2.9. Contact relationships between the Tasiuyak paragneiss and the Paleoproterozoic metaplutonic rocks from Voisey's Bay, Labrador. A) Contact between meta-tonalite and Tasiuyak paragneiss in outcrop. B) Contact between weathered meta-tonalite and Tasiuyak paragneisses in outcrop.

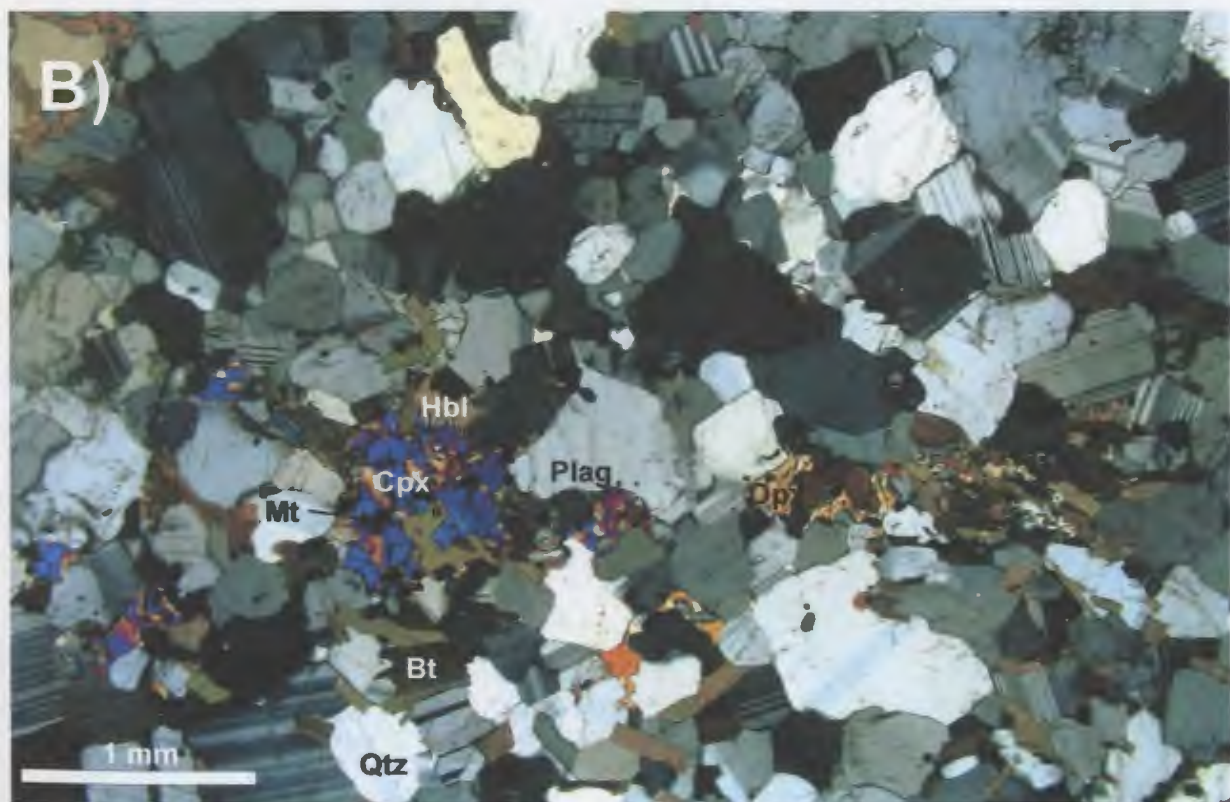
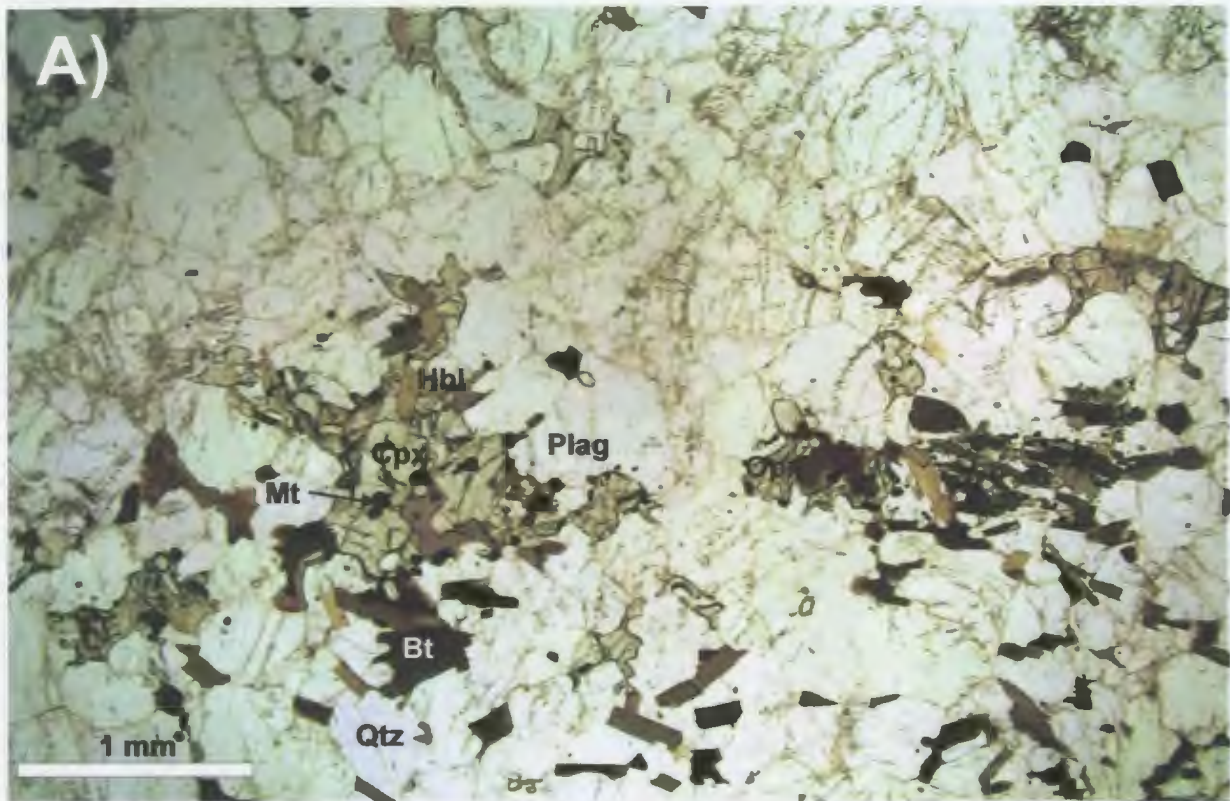


Plate 2.10. Photomicrographs of a felsic (tonalitic) sample of the Paleoproterozoic metaplutonic suite from Voisey's Bay, Labrador. A) Plane polarized light. B) Cross polarized light.

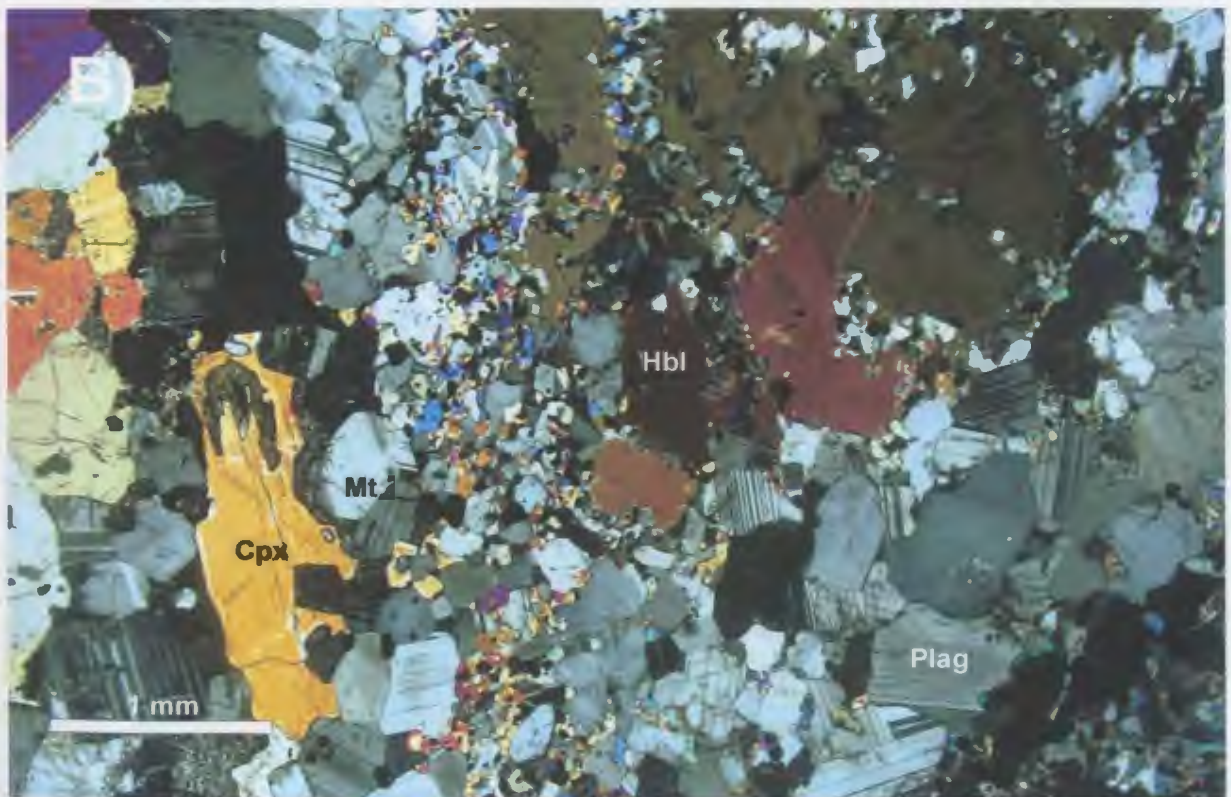
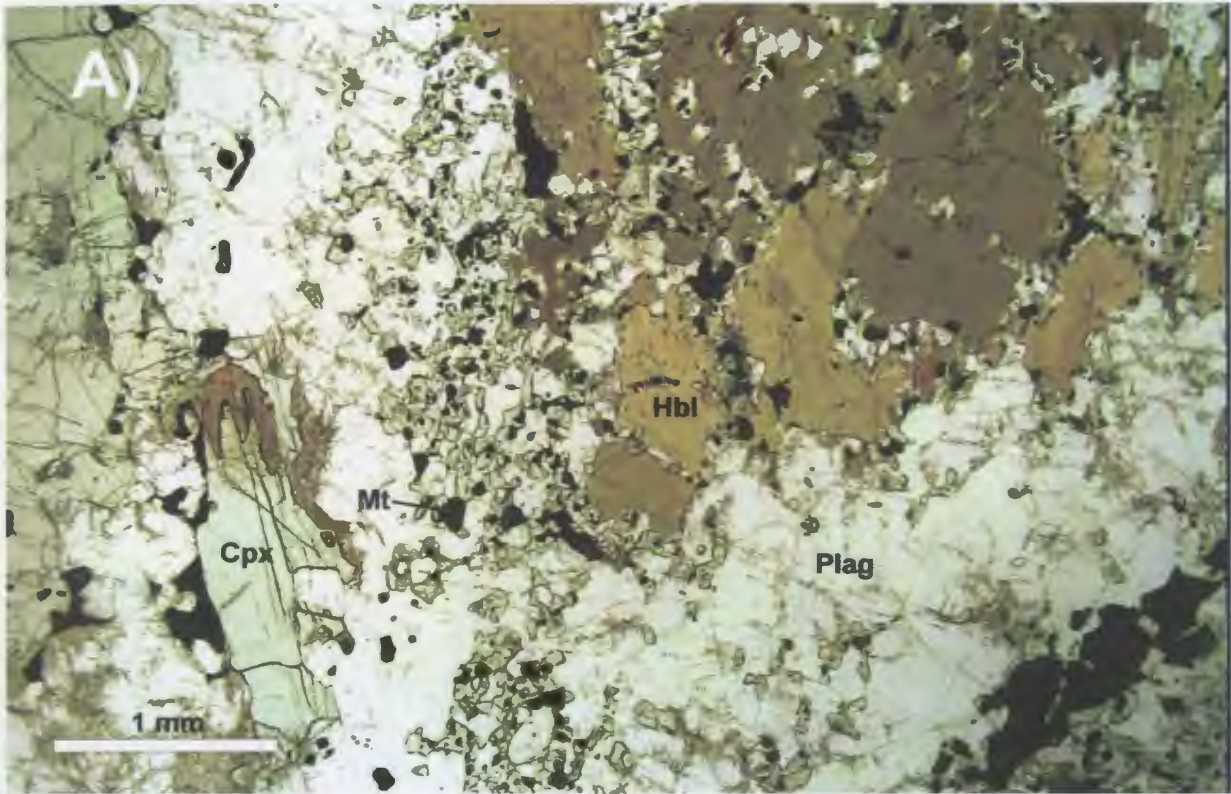


Plate 2.11. Photomicrographs of a mafic (meta-hornblende gabbro) sample of the Paleoproterozoic metaplutonic suite from Voisey's Bay, Labrador. A) Plane polarized light. B) Cross polarized light.



Plate 2.12. U-Pb sample VB-99-108 (meta-quartz diorite) from Voisey's Bay, Labrador. A) Field appearance. B) Photomicrograph in cross polarized light.

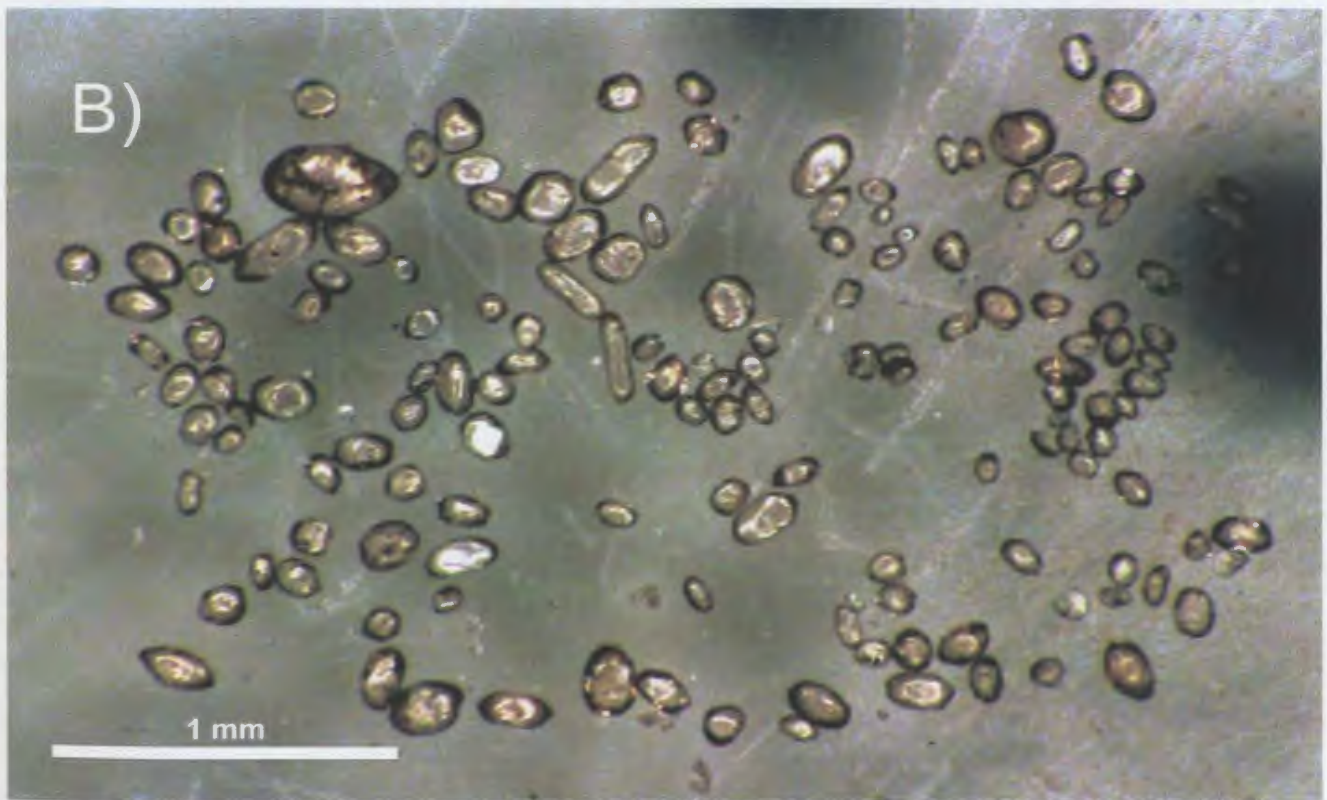
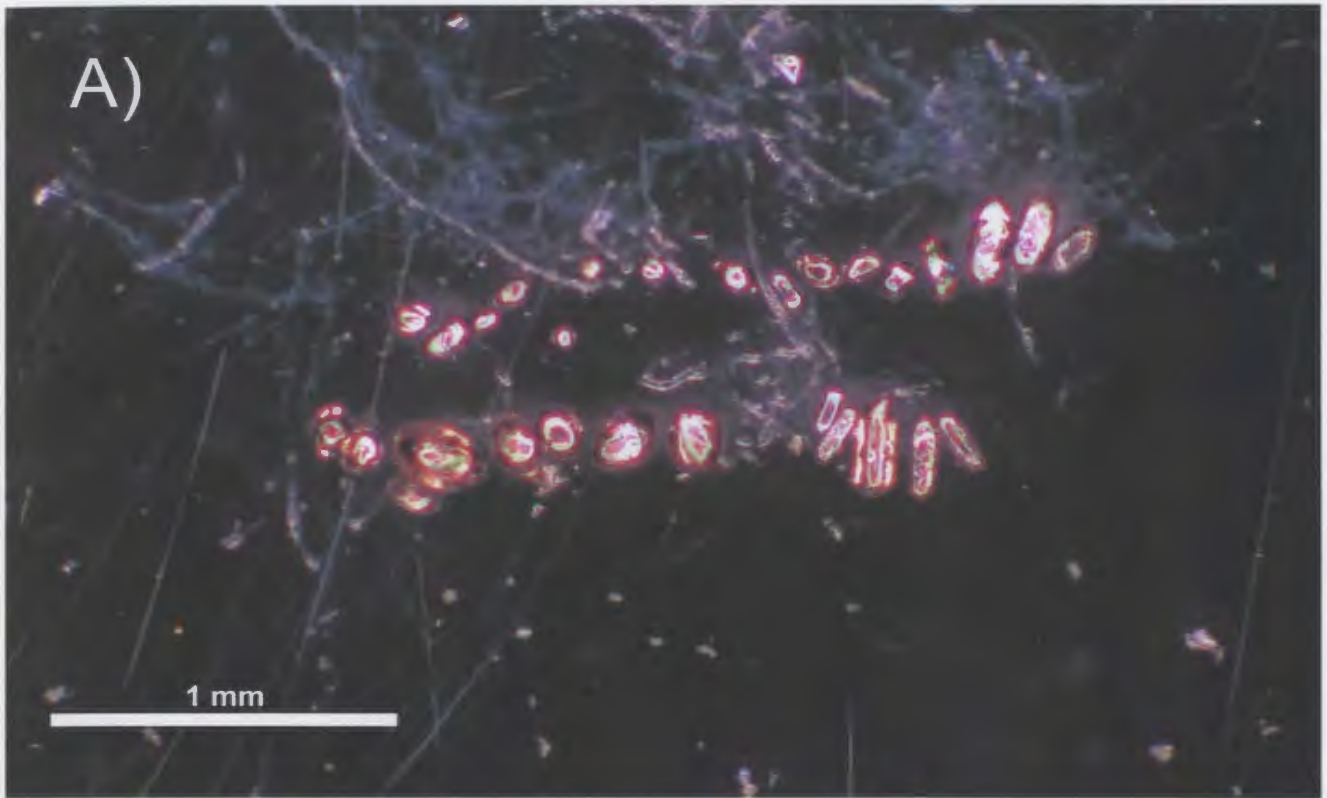


Plate 2.13. Zircons from the Paleoproterozoic meta-quartz diorite sample VB-99-108. A) Selected zircon morphology analyzed in the U-Pb dating. B) General zircon population.

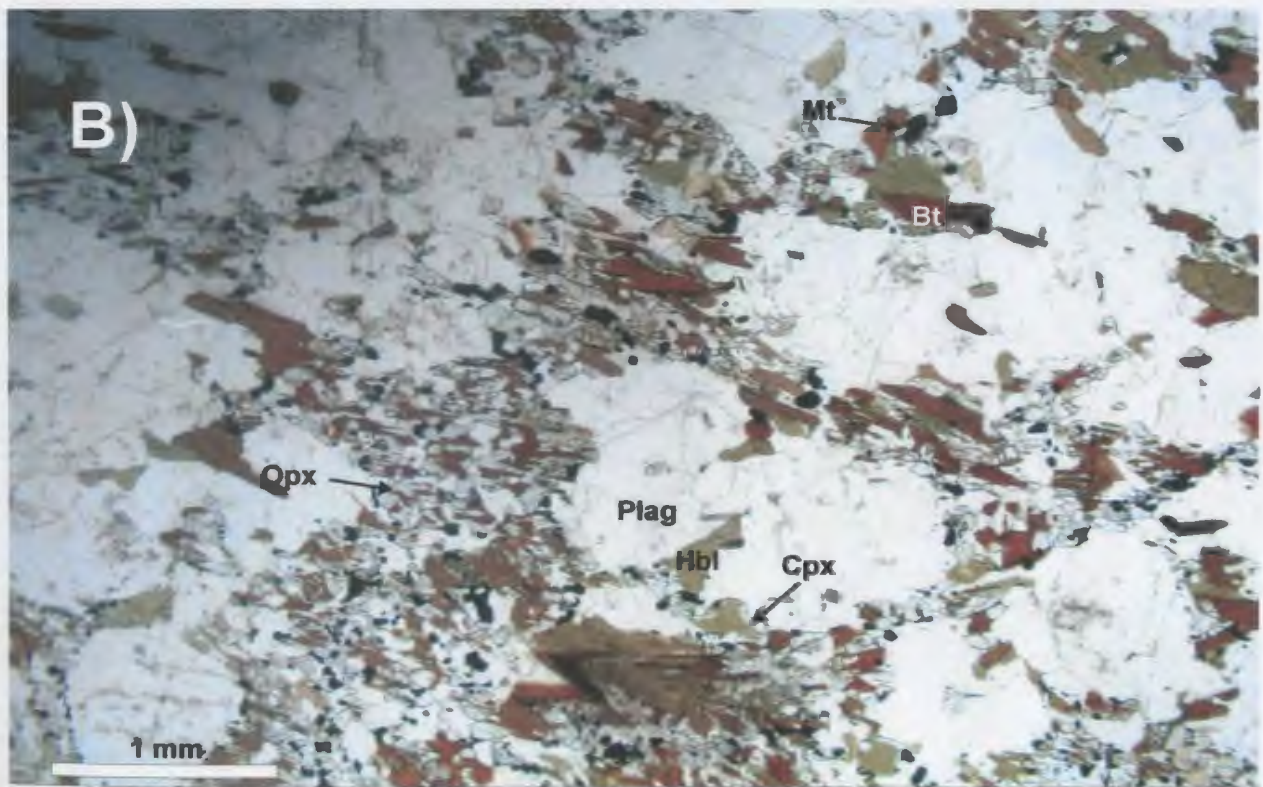


Plate 2.14. U-Pb sample VB-99-106c (meta-hornblende gabbro) from Voisey's Bay, Labrador. A) Field appearance (coarser grained material was selected for dating). B) Photomicrograph in plane polarized light.

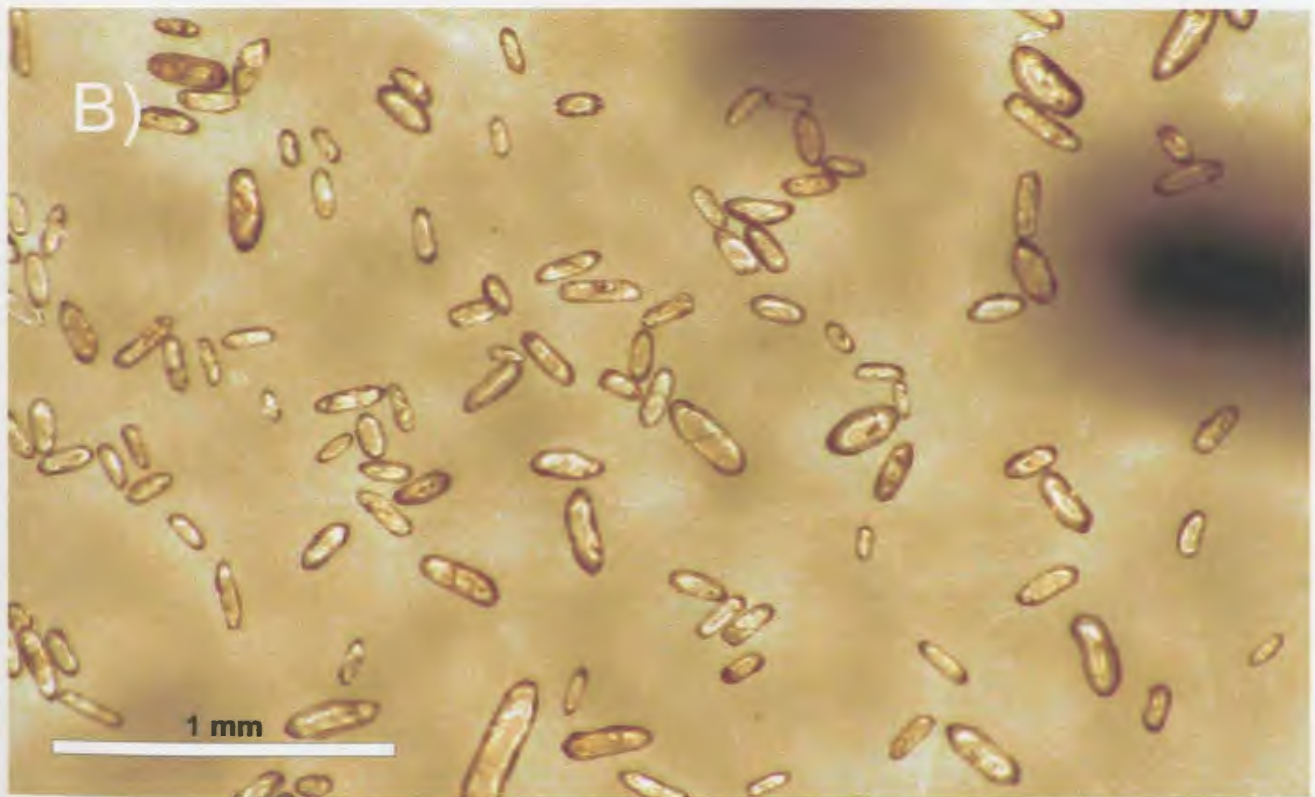
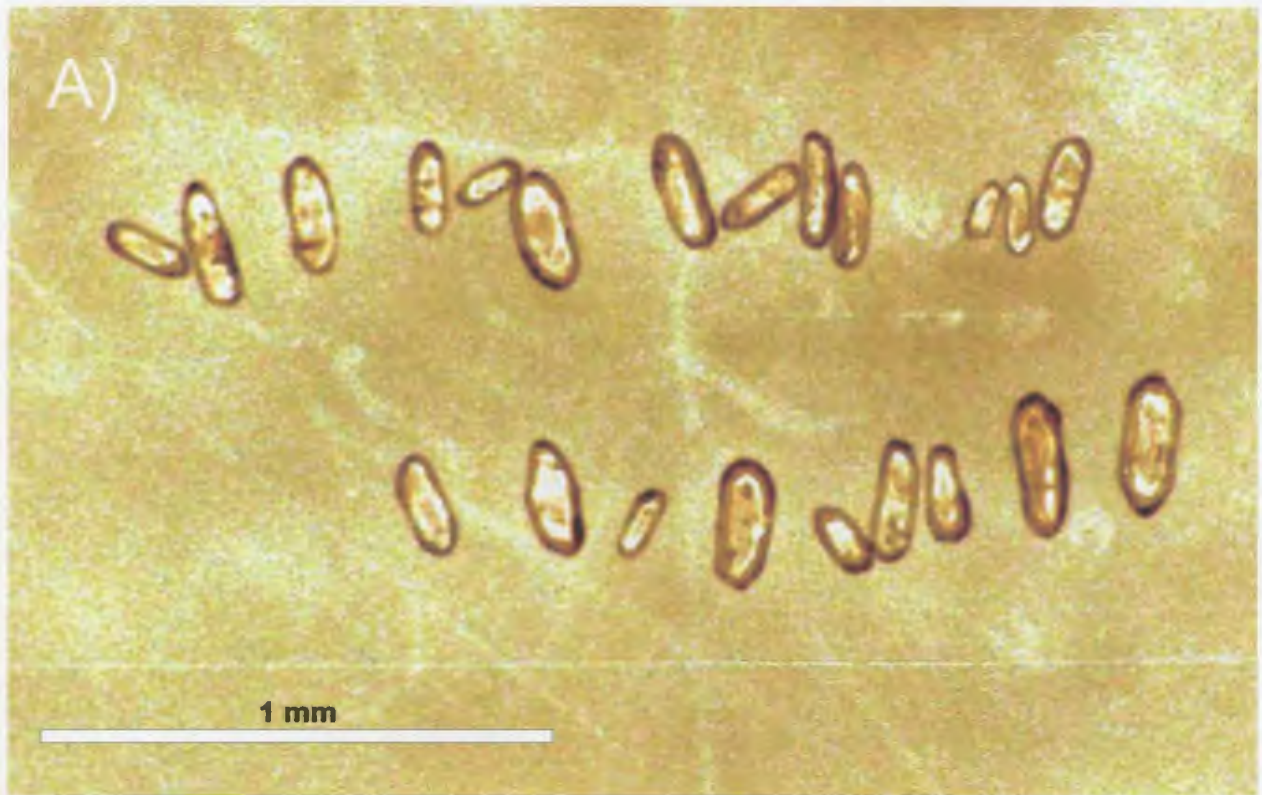


Plate 2.15. Zircons from the Paleoproterozoic meta-hornblende gabbro sample VB-99-106c. A) Selected zircon morphology analyzed in the U-Pb dating. B) General zircon population.

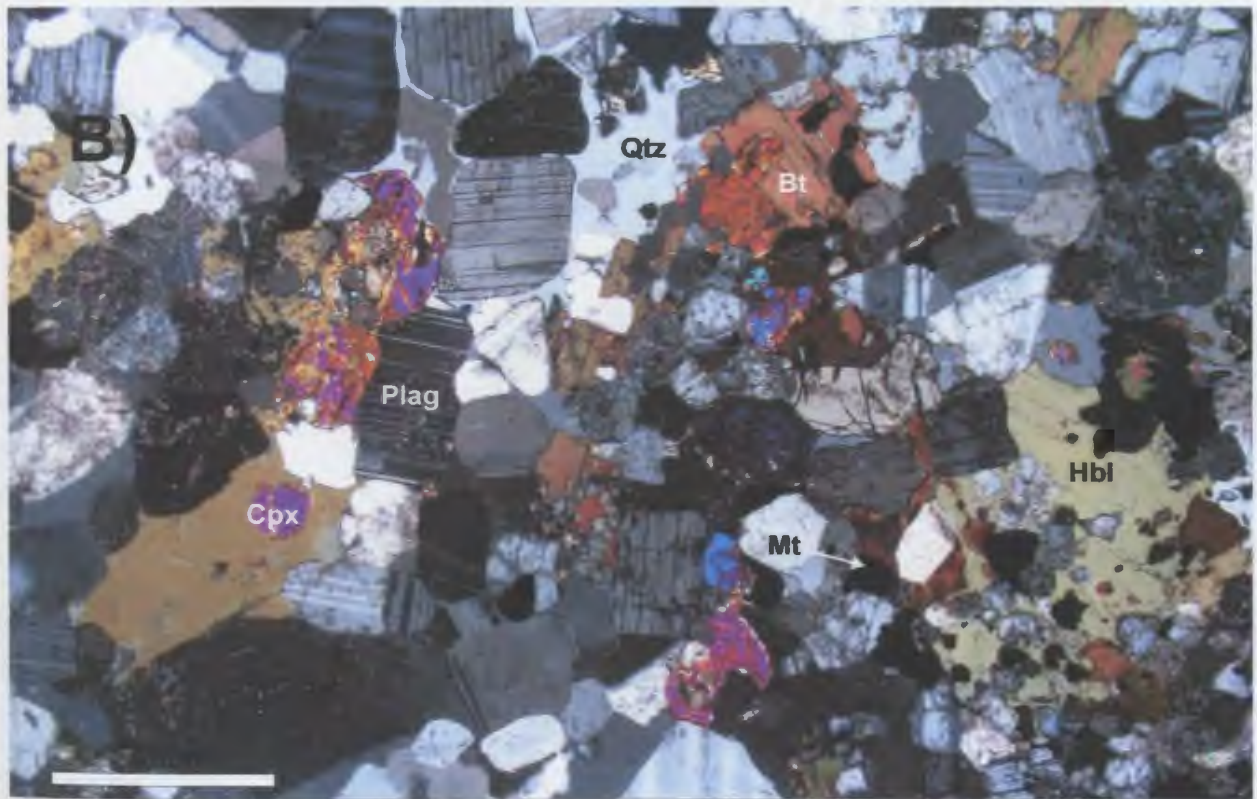
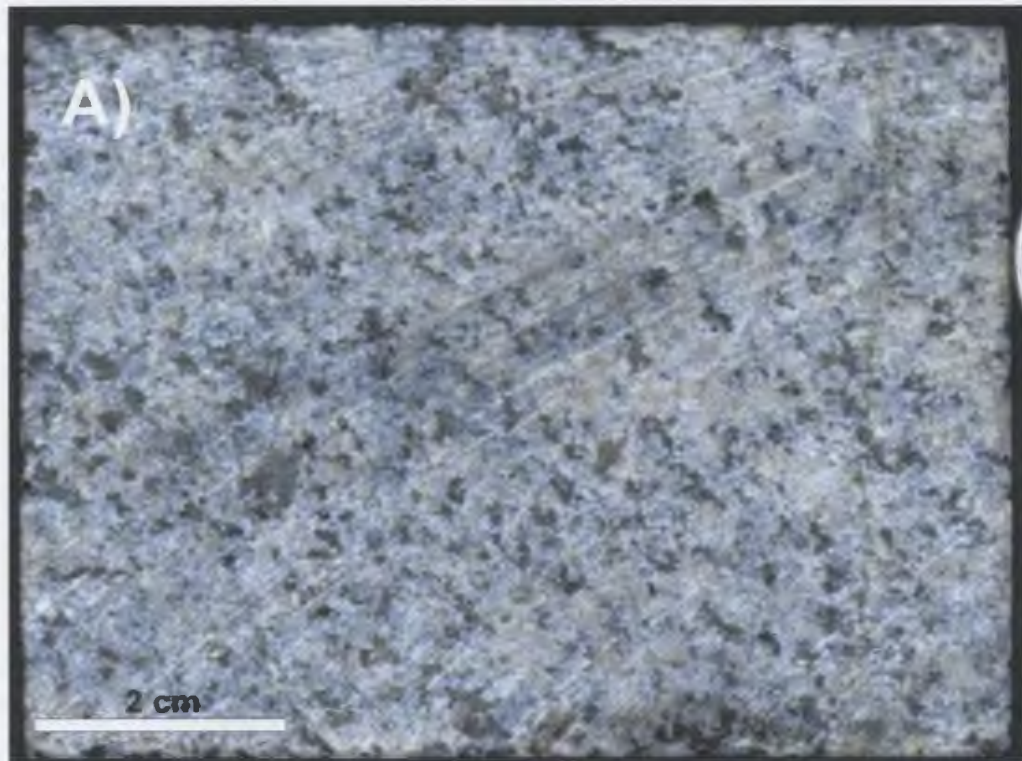


Plate 2.16. U-Pb sample DDH-496-549 (meta-tonalite) from Voisey's Bay, Labrador. A) Drill core sample. B) Photomicrograph in cross polarized light.

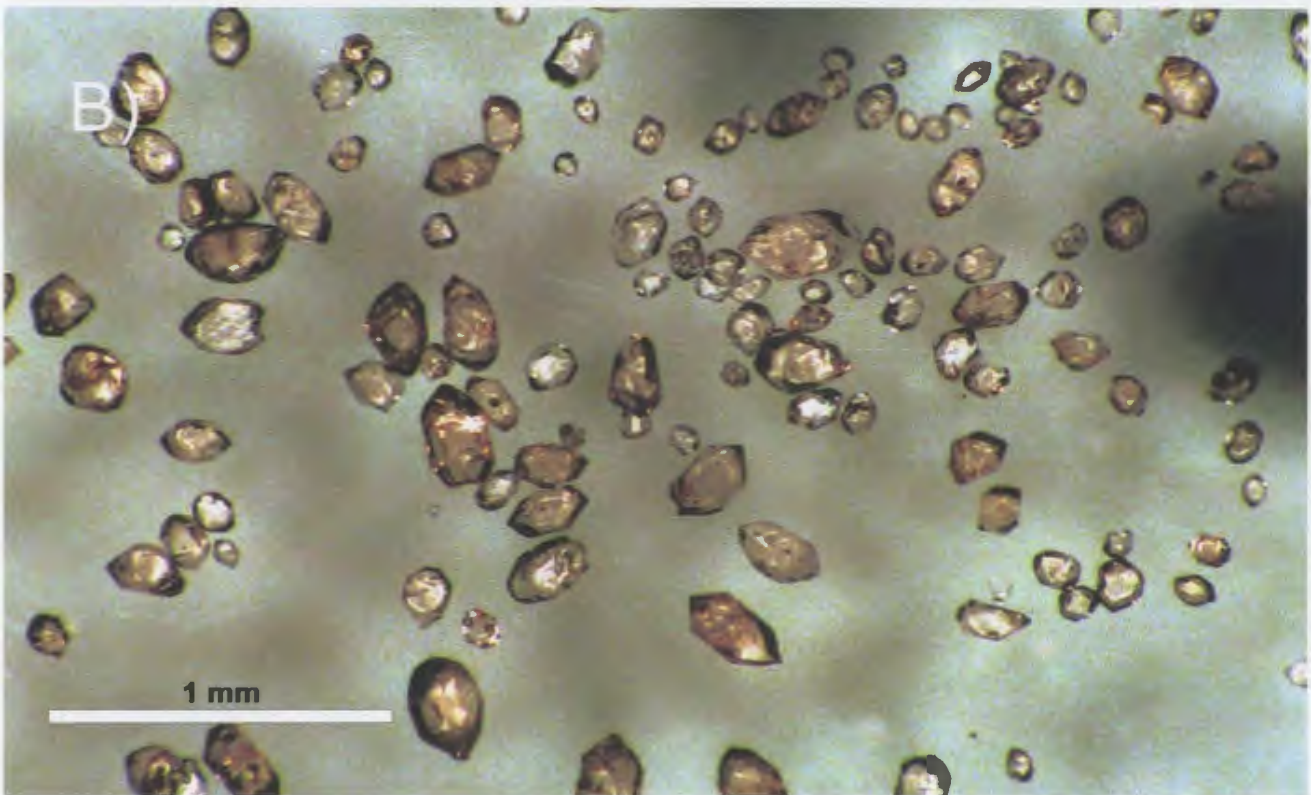
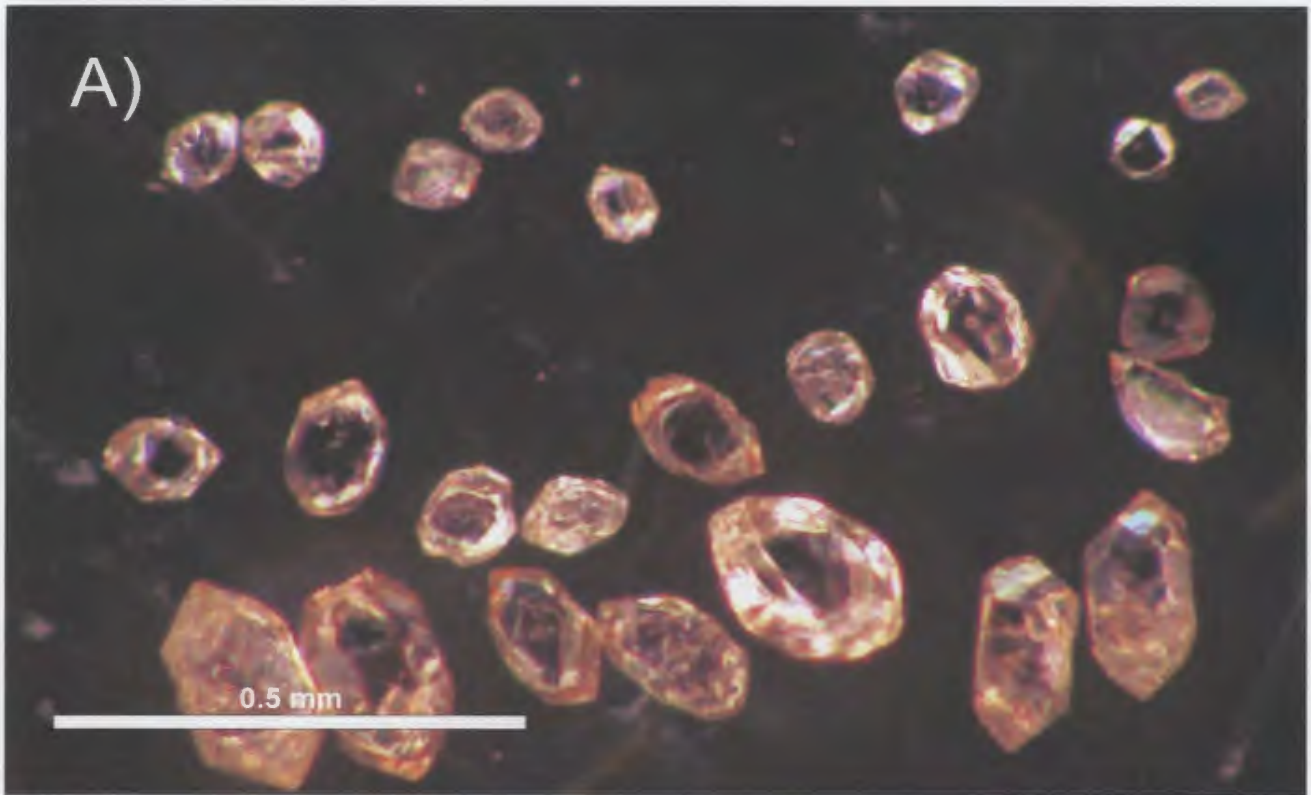


Plate 2.17. Zircons from the Paleoproterozoic meta-tonalite sample DDH-496-549. A) Selected zircon morphology analyzed in the U-Pb dating. B) General zircon population.

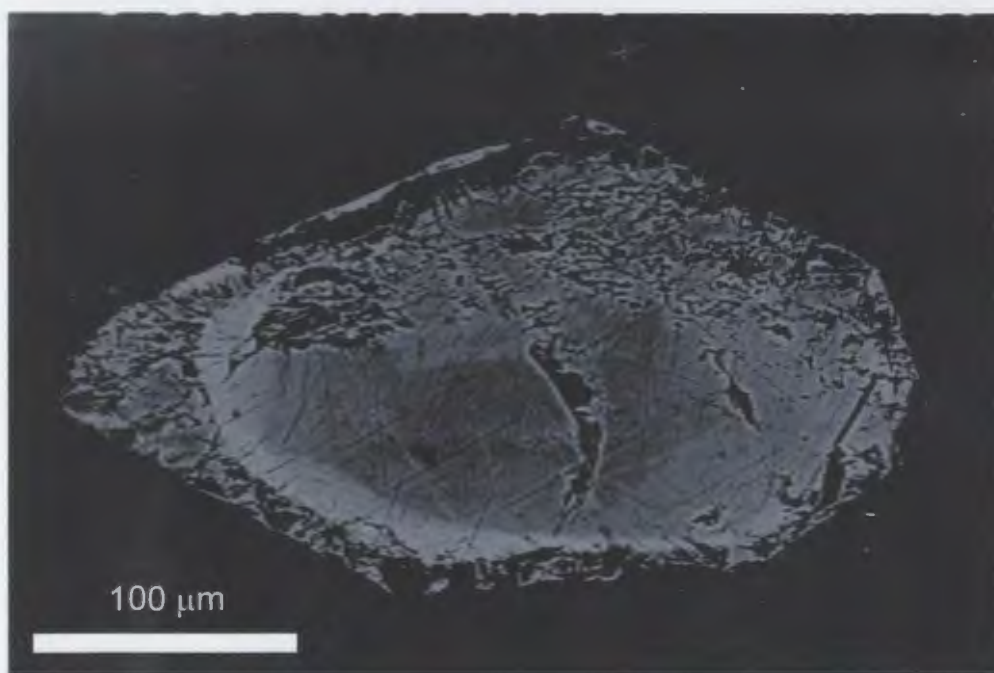
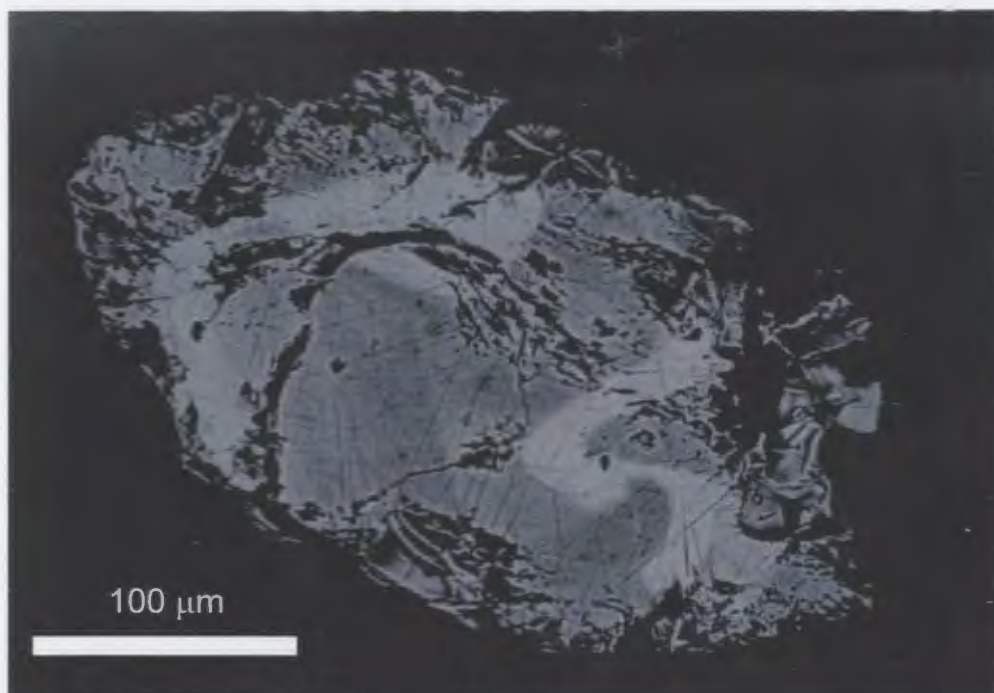


Plate 2.18. Back-scattered electron images of potential inherited cores in zircons from sample VB-99-106c of the Paleoproterozoic metaplutonic suite in Voisey's Bay, Labrador.

Chapter 3

A New Perspective on the Role of the Paleoproterozoic Metaplutonic Suite in Voisey's Bay Ni-Cu-Co Mineralization, Labrador, Canada

3.1 ABSTRACT

The Voisey's Bay Ni-Cu-Co deposit of Northern Labrador represents a new class of magmatic ore, one hosted by a troctolitic member of an anorthosite-mangerite-charnockite-granite suite. Addition of silica and/or sulfur to the troctolite magma by crustal contamination is considered to have been critical in triggering sulfide precipitation. Within the Voisey's Bay area, there are three potential crustal contaminants: the heterogeneous Archean orthogneisses of the Nain Province, the Paleoproterozoic Tasiuyak paragneiss of the Churchill Province and the Paleoproterozoic metaplutonic suite (previously referred to as the enderbite gneisses). New field, geochemical and isotopic evidence indicate that the Paleoproterozoic metaplutonic rocks may have played a larger role in the crustal contamination of Voisey's Bay parental magma than was previously recognised. Recent mapping indicates that the unit covers a sizeable geographic area encompassing most parts of the ore system. The trace element chemistry of the rocks is distinctive and markedly similar to the Voisey's Bay deposit, specifically in possessing Th-U and Nb-Ta depletions and elevated La/Sm ratios (2.92 to 11.02) with a range of Th/Nb ratios (0.004 to 1.065). The sulfur content of the

metaplutonic suite reaches levels of 0.1 weight percent and these rocks are interleaved with newly discovered sulfide-rich paragneisses, which present a possible larger source of additional sulfur. The Paleoproterozoic metaplutonic rocks define two distinct isotopic groups: an enriched group with $\epsilon\text{Nd}_{(1320 \text{ Ma})}$ of -11.1 and -11.2 , $^{87}\text{Sr}/^{86}\text{Sr}_{(1320 \text{ Ma})}$ ratios between 0.7032 and 0.7050 and μ^* values of 7.66 to 7.77; and a more depleted group which exhibits $\epsilon\text{Nd}_{(1320 \text{ Ma})}$ values between -2.8 to -6.8 , $^{87}\text{Sr}/^{86}\text{Sr}_{(1320 \text{ Ma})}$ ratios between 0.7038 and 0.7041 and μ^* values 7.75 to 7.98.

Trace element and isotopic data from the Voisey's Bay intrusion and conduit rocks can be most readily explained by 5-10 percent contamination of a picritic basalt magma with the enriched group of the metaplutonic rocks. Contamination by the Tasiuyak paragneiss would produce more subtle effects on the compositions in the intrusion.

This new evidence indicates that the Paleoproterozoic metaplutonic rocks played a key role in the crustal contamination of the Voisey's Bay intrusion, which may have led to sulfur saturation and precipitation of sulfides. Metaplutonic contamination may be an essential element in the formation of similar deposits in the region and elsewhere.

3.2 INTRODUCTION

Crustal contamination of mantle-derived magmas may increase their concentration of sulfur or silica, promoting sulfide saturation and triggering precipitation of Ni sulfide ores (Naldrett, 1973; MacLean, 1969; Irvin, 1975 and others). This is thought to have occurred in the recently discovered Voisey's Bay Ni-Cu-Co sulfide deposit, of Northern Labrador (Naldrett et al., 1996a; Amelin, 2000; Li et al. 2000, and others). This deposit is very unusual in that it is hosted by troctolitic rocks that are part of an anorthosite-mangerite-charnockite-granite complex, the 1350-1290 Ma Nain Plutonic Suite. The association of troctolites with major Ni sulfide mineralization was not confirmed until the Voisey's Bay deposit was discovered and studies have just begun to determine the critical factors in the ore genesis (Ryan et al., 1995; Naldrett et al., 1996a; Ryan, 1997). Initial results favoured crustal contamination of the troctolite magma by the sulfur and graphite-rich Tasiuyak paragneiss as being critical in triggering sulfide precipitation (Amelin et al., 2000; Li et al. 2000, Naldrett et al., 2000a, b; and others). The most compelling evidence is the presence of small (0.5-10 cm), partially digested, metasedimentary gneiss inclusions in the troctolitic units, particularly in the breccia associated with the sulfide mineralization (Li and Naldrett, 2000). However, the Paleoproterozoic metaplutonic suite of the Voisey's Bay area may have also played an important, but yet undefined role.

The Paleoproterozoic metaplutonic suite has been referred to as enderbites or enderbitic orthogneisses (Evans-Lamswood et al., 2000; Lightfoot and Naldrett, 1999; Li and Naldrett, 1999; Amelin et al., 1999; and others). Rawlings et al. (Chapter 2) showed however that the previously defined enderbitic unit is actually part of a much more extensive series of Paleoproterozoic (i.e. c. 1890 Ma) metaplutonic rocks. In addition, the

term enderbite is ambiguous as it describes both orthopyroxene-bearing tonalites (igneous) and granulite facies tonalites (metamorphic rock) (i.e. Newton, 1992; Percival, 1990; Stern and Dawoud, 1991; Raith et al., 1999; and others). Thus the term metaplutonic suite is preferred.

The Paleoproterozoic metaplutonic rocks have been largely ignored or dismissed in crustal contamination models of the Voisey's Bay ores for various reasons. Perhaps the most significant has been the belief that the metaplutonic rocks are rather limited in geographic extent. Recent geological mapping Rawlings et al. (Chapter 2) showed, however, that the metaplutonic rocks represent a unit of considerable volume in the area, and almost completely host the Voisey's Bay ore and related troctolitic bodies. Thus, this paper considers the geological and geochemical evidence that the metaplutonic suite was important in the genesis of Voisey's Bay Ni-Cu-Co ores.

3.3 REGIONAL GEOLOGY

The regional geology of northern Labrador is characterized by the tectonic contact between the Proterozoic and reworked Archean (Rae) rocks of the southeastern Churchill Province in the west and the Archean rocks of the Nain Province in the east (Figure 3.1). The ca. 1333 Ma Voisey's Bay nickel-copper-cobalt sulfide deposit is hosted by a troctolite-gabbro intrusion emplaced in relatively close proximity to the 1.85 Ga tectonic boundary of the Churchill-Nain provinces. In the Voisey's Bay area, there are three main gneissic units. To the west is the Tasiuyak gneiss complex, comprising interlayered garnet-sillimanite and sulfide-, graphite-bearing paragneiss belonging to the Churchill Province. To the east are heterogeneous, quartzo-feldspathic gneisses alternating with

amphibolitic and gabbroic gneisses, all belonging to the Nain Province. The Nain Province gneisses have been cross cut by at least two sets of mafic dykes, subjected to several deformational events and contain numerous tectonic fabrics. Sandwiched between the Tasiuyak paragneiss and Nain Province orthogneisses is the ca. 1890 metaplutonic unit, composed of a relatively homogenous belt of massive to foliated meta-gabbroic, meta-dioritic and meta-tonalitic gneisses (Figure 3.2). This unit is interleaved and deformed with belts of various metasedimentary units (dominantly metapelites and quartzites), anorthosite, and amphibolite. Much of the tectonic suture in the area, is concealed by the extensive (~19,000 km²) Nain Plutonic Suite (NPS) which intruded from 1.35 to 1.29 Ga (Emslie et al., 1994, Berg et al., 1994). The NPS is dominantly anorthosite and granite with minor troctolite, diorite and gabbro (Ryan et al., 1995). The NPS was intruded by at least two separate suites of diabase dykes of poorly defined age (Wiebe, 1985).

The Voisey's Bay Intrusion (VBI) is one of the oldest known troctolitic intrusions in the NPS with a U-Pb age of 1332.7 ± 1 Ma (Amelin et al., 1999). The intrusion comprises two sulfide-poor magma chambers termed the Eastern Deeps chamber and Western Deeps chamber (Figure 3.3). The mineralization is dominantly located in two sulfide-rich conduit dikes, the Ovoid conduit and the Eastern Deeps feeder, which likely exploit the structure of the chambers but may not be synchronous with their emplacement (Evans-Lamswood et al., 2000). The subvertical Ovoid conduit consists of four zones of mineralization, which are termed, from east to west: the Ovoid, the Mini-Ovoid, the Reid Brook zone, and the Discovery Hill zone (Figure 3.3). Sulfide deposition is interpreted as filling a swell, or a bulge in the conduit and thus the location of mineralization is related

to dyke geometry, rather than gravitational settling (Evans-Lamswood, 1999; Evans-Lamswood et al., 2000). The subhorizontal Eastern Deeps Feeder contains mineralization at the base of the Eastern Deeps chamber, which is significantly different than the Ovoid and other mineralization to the west. However like the Ovoid, the Eastern Deeps mineralization did not occur by crystal settling to the base of the Eastern Deeps chamber. Instead the Eastern Deeps conduit simply intersected the Eastern Deeps chamber close to a structural low (Evans-Lamswood et al., 2000). Subsequent to the mineralising event, subhorizontal, sheet-like bodies of granite and syenite intruded the Voisey's Bay troctolite-gabbro.

3.4 PREVIOUS GEOCHEMICAL STUDIES

Although most studies of the Voisey's Bay mineralization have implicated the Tasiuyak paragneiss as the key contaminant in triggering sulfide precipitation, the details of proposed models are in sharp disagreement with one another. Amelin et al. (2000) and Lambert et al. (1999, 2000) used radiogenic isotopes to determine the magmatic history of the Voisey's Bay ore system. Radiogenic isotopes can be a particularly useful tool in tracing the interaction of magmas with the continental crust, particularly when there is a large isotopic contrast between the igneous units (in this case, troctolitic magma) and basement rocks (country rock gneisses) (DePaolo, 1988; Emslie et al., 1994). Amelin et al. (2000) reported that the Voisey's Bay Intrusion (VBI) preserved evidence for extensive crustal contamination, yet with remarkable isotopic homogeneity, in terms of initial isotopic ratios of Sr ($^{87}\text{Sr}/^{86}\text{Sr} = 0.7034$ to 0.7038), Nd ($\epsilon\text{Nd} = -1$ to -2) and Pb

($^{206}\text{Pb}/^{204}\text{Pb} = 15.34$ to 15.54 , $^{207}\text{Pb}/^{204}\text{Pb} = 15.10$ to 15.18 , $^{208}\text{Pb}/^{204}\text{Pb} = 35.24$ to 35.56).

To reconcile this unusual isotopic evidence, they suggested a two-stage model in which an isotopically enriched, low-Mg basalt was (1) produced from an enriched mantle source, or through $\leq 10\%$ contaminations of lower-middle crust, and (2) became somewhat more enriched by contamination at a higher crustal level with 8-13% Tasiuyak gneiss. The authors claimed that crustal contamination of the isotopically more depleted, high-Mg picritic basalt did not produce reasonable fits to the Voisey's Bay Sr-Nd-Pb data.

Lambert et al. (1999, 2000) addressed the Re-Os isotopic systematics of the Voisey's Bay deposit. They found that the sulfide-rich samples had radiogenic and heterogeneous initial Os isotopes ($\gamma_{\text{Os}} = 200$ to 1100), suggesting interaction of parent magma with crustal sources. Lambert et al. (2000) proposed a two-stage crustal contamination model but with important differences from that of Amelin et al. (2000). In their preferred Re-Os model, a primitive, high-Mg picritic basalt is contaminated with ca. 1% lower to middle crust similar in composition to the Nain orthogneisses. In the upper crust, the basalt selectively assimilated sulfide and carbon components of the Tasiuyak gneiss through a melting-devolatilization process, rather than assimilating the bulk Tasiuyak as in the model of Amelin et al. (2000). According to Lambert et al. (2000), selective sulfide assimilation is more consistent with the heterogeneous Os and homogenous Sr, Nd and Pb isotope compositions of the Voisey's Bay intrusion. This is because osmium is usually concentrated largely in sulfide minerals whereas Sr, Nd, and Pb are largely in the silicate phases. Lambert et al. (2000) cited high Mg, olivine-bearing

melatroctolite inclusions in parts of the intrusion as evidence that picritic basalts were parental to the magmatic system.

Mineral, whole rock and stable isotope composition data have also been used to address the nature of the proposed interaction of the Tasiuyak paragneiss with the Voisey's Bay troctolite magma. Li and Naldrett (2000) examined the petrographic evidence of mineral reactions in the partially digested gneiss inclusions of the breccia units of the intrusion. They concluded that there was selective silicate-oxide contamination with much of the SiO_2 and K_2O and some of the Na_2O in the inclusions being added to the magma, and some of the FeO and MgO from the magma being added to the inclusions. Felsification would have decreased the sulfide capacity of the magma promoting sulfide precipitation.

Li et al. (2000) studied the whole rock trace element compositions of the Voisey's Bay intrusion, in particular the La/Sm versus Th/Nb variations. On the basis of these data, they suggested that the bulk of the Voisey's Bay intrusion formed from a picritic basalt parent magma that was contaminated by lower to middle crustal gneiss. This first-stage of contamination increased the La/Sm ratios of the Voisey's Bay troctolites. As the contaminated magma ascended into the upper crust, a second contamination event took place, this involving the Tasiuyak paragneiss. In an important distinction to the model of Amelin et al. (2000), the second-stage contamination affected only the conduit and breccia rocks. The distinction between the Voisey's Bay rocks affected by Tasiuyak contamination, and those that were not, was made on the basis of elevated Th/Nb ratios, which approach the high values seen in the Tasiuyak.

Ripley et al. (1999, 2000) measured the S and O isotope compositions of the Voisey's Bay intrusion and Tasiuyak paragneiss. The Tasiuyak paragneiss is characterized by $\delta^{34}\text{S}$ of -0.9 to -17.0 per mil and $\delta^{18}\text{O}$ of 8.3 to 16.1 per mil. Normal troctolite of the Voisey's Bay intrusion, in contrast, has $\delta^{34}\text{S}$ of -0.5 to $+1.8$ per mil and $\delta^{18}\text{O}$ of -5.4 to -7.7 per mil, which are mantle-like values, suggesting no interaction with the Tasiuyak paragneiss. As lower-middle crustal orthogneisses also commonly have mantle-like S and O isotope values, these data cannot address the model for early crustal contamination based on other geochemical data. In conduit rocks and breccia units there is evidence of contamination by the Tasiuyak paragneiss, as $\delta^{34}\text{S}$ are more negative (as low as -4.1 per mil in the Reid Brook zone) and $\delta^{18}\text{O}$ are elevated (up to 9.3 per mil). Gneiss inclusions are depleted in ^{18}O relative to the Tasiuyak paragneiss, suggesting loss of a siliceous ^{18}O -rich component during their partial digestion.

Despite differences in detail, the existing data clearly indicate that the parental mafic magma of the Voisey's Bay intrusion was contaminated by crustal rocks. In addition, part of the magmatic system, the sulfide-bearing conduit dike rocks, subsequently interacted with Tasiuyak paragneiss. An important question, addressed in this paper, is whether the Paleoproterozoic metaplutonic suite was responsible for the first-stage contamination of the Voisey's Bay intrusion. If so, a related question is whether contamination by the metaplutonic suite was a necessary element in producing the nickel-sulfide ores.

Contamination of the Voisey's Bay parental magmas by the metaplutonic suite has been considered by previous workers but rejected on several grounds, or dismissed as having little relevance to sulfide precipitation. The arguments have included:

- (1) The unlikelihood that all phases of the Voisey's Bay intrusion would have come in contact with the metaplutonic unit, given its small size (Li et al., 2000)
- (2) The low sulfur content of the metaplutonic suite (Ripley et al. 1999)
- (3) Unrealistically large amounts of contamination by the metaplutonic unit, which would be required to explain certain trace element characteristics of the Voisey's Bay intrusion, such as the La/Sm ratio (Li et al., 2000).
- (4) Sr-Nd-Pb isotope systematics indicate that Tasiuyak gneiss was the main contaminant of the major phases of the Voisey's Bay intrusion (Amelin et al., 2000).

The remainder of this paper addresses each of these points using new data for the metaplutonic suite, and evaluates existing data in light of the new observations.

3.5 GEOGRAPHIC DISTRIBUTION OF THE PALEOPROTEROZOIC METAPLUTONIC SUITE

Existing geological maps of the Voisey's Bay area (Evans-Lamswood et al., 2000; Ryan, 2000) show the metaplutonic suite (referred to as enderbitic gneiss) as a small lithological unit (<10 Km long and <5 Km wide) that hosts the sulfide mineralization and associated troctolitic rocks of the Ovoid and Discovery Hill zones but not much of the Eastern Deeps. New mapping for this study, however, extends the Paleoproterozoic

metaplutonic unit far beyond what was previously recognised, from Anaktalak Bay to Voisey's Bay, with an area of some 20 km long × 10 Km wide (Figure 3.2). In particular the boundary between the metaplutonic suite and the Nain gneisses to east is placed much further eastward than previously determined. Thus, the metaplutonic rocks are much more voluminous in the Voisey's Bay area than is the Tasiuyak paragneiss, and host almost the entire ore deposit. An important implication of the new mapping with regards to isotopic studies discussed later, is that several samples described as Archean "Nain gneisses" in previous work (Amelin et al. 2000, Lambert et al. 2000) are now included in the Paleoproterozoic metaplutonic suite. The new mapping has also identified a previously unknown metasedimentary unit tectonically interleaved within the metaplutonic suite. The unit varies from semipelitic to pelitic and, like the Tasiuyak paragneiss, is sulfide-rich.

3.6 SULFUR CONTENT OF PALEOPROTEROZOIC METAPLUTONIC SUITE

Sulfide saturation at Voisey's Bay may have been achieved by addition of external sources of sulfur or silica to the parental magma. Ripley et al. (1999) noted that sulfur contents of the Tasiuyak paragneiss (mostly >500 ppm with domains up to 5400 ppm) are much higher than the metaplutonic suite (mostly <300 ppm). Thus, if external sulfur was added to the Voisey's Bay intrusion to trigger sulfide precipitation, the Tasiuyak paragneiss would have been a more likely source. A large-scale geochemical survey of the metaplutonic suite is consistent with this view. Sulfur contents range from 37 to 2153 ppm with a mean of 268.7 and a median of 127.7 (Figure 3.4). Bulk assimilation of a

given volume of metaplutonic rocks by invading troctolitic magma would add less external sulfur than an equivalent volume of Tasiuyak paragneiss.

It is possible, however, that sulfur was liberated from the metaplutonic and Tasiuyak country rocks by breakdown of sulfide minerals rather than by whole rock assimilation. In the conduit dikes at Voisey's Bay where the case for Tasiuyak contamination is mostly compelling because of the presence of partially digested xenoliths, $\delta^{34}\text{S}$ and γ_{O_2} systematics of most of the sulfides can be explained by mixing of a hypothetical primitive troctolite magma with sulfide from the metaplutonic suite (Figure 3.5). On the Reid Brook zone, which is the one part of the Voisey's Bay mineralization system actually hosted by Tasiuyak paragneiss, can a strong case be made for a Tasiuyak sulfur source (Ripley et al. 1999). Finally, the Paleoproterozoic metaplutonic rocks are tectonically interleaved with metasedimentary to metapelitic rocks. These lithologies may have been an additional source of external sulfur to the invading troctolitic magma.

3.7 TRACE ELEMENT GEOCHEMISTRY

Trace element characteristics of the Voisey's Bay intrusion (VBI) provide compelling evidence for contamination of their parent magmas by the metaplutonic suite. The primitive-mantle normalized spider diagram patterns of the VBI and conduit troctolitic rocks, the Paleoproterozoic metaplutonic, Tasiuyak paragneiss and Archean orthogneisses are plotted in figure 3.6. The VBI and the Ovoid-mini-ovoid conduit rocks display similar primitive-mantle normalized trace element patterns with enrichments in several large ion lithophile elements (LILE: Pb, Sr, Ba, K) and the light rare earth elements, and depletions

in Cs and Rb relative to Ba. They have two very distinctive features, large, negative Th-U and Nb-Ta anomalies (Figure 3.6).

The trace element geochemistry of the Paleoproterozoic metaplutonic rocks is characterised by many of the same features as seen in the troctolites: pronounced enrichment in light rare earth elements (LREE) and Pb, Sr, Ba, K and depletion in Cs and Rb relative to Ba. They also exhibit the distinct negative Th-U and Nb-Ta anomalies. This comparison strongly suggests that the troctolites in both the VBI and conduit dikes inherited their trace element compositions largely from the metaplutonic suite by contamination.

The Archean orthogneisses are similar in composition to the Paleoproterozoic metaplutonic rocks and troctolites in that they exhibit high concentrations of LREE, similar LILE enrichments and negative Nb-Ta anomalies. However, these rocks display a different kind of Th-U anomaly with uranium much more depleted than thorium. This argues against the Archean gneisses being an important contaminant of the troctolitic rocks.

The Tasiuyak paragneiss exhibits a trace element pattern quite different from the VBI conduit troctolite rocks. In particular, the paragneiss does not exhibit a negative Th-U anomaly, Rb is not depleted relative to Ba and the HREE pattern is concave-upward. These differences strongly suggest that the Tasiuyak paragneiss was not the primary (first-stage) contaminant of the Voisey's Bay intrusion. The data do not rule out a role for the Tasiuyak as second-stage contaminant in the conduit dikes. However, again, as for the S- and Os- isotope data, the trace element data allow a role for the metaplutonic suite in the second-stage contamination of the conduit dikes as well.

On figure 3.7, the ratios of La/Sm versus Th/Nb are plotted for the various potential country rock contaminants and the trends of the VBI troctolites and breccia rocks (from Li et al., 2000). The more mafic compositions of the Paleoproterozoic metaplutonic suite have La/Sm ratios between 3.0 and 7.0 and Th/Nb ratios of less than 0.1 to 0.4. The felsic components of the metaplutonic units are characterised by higher La/Sm ratios ranging from 5.0 to 9.0 and broader Th/Nb ratios ranging from less than 0.1 to 0.8. The Archean quartzo-feldspathic orthogneisses belonging to the Nain province display La/Sm values from 10.0 to 14.0 and a wide range of Th/Nb ratios of 0.1 to 2.0. The Tasiuyak paragneiss has La/Sm ratios from 4.0 to 8.0 and Th/Nb ratios of 0.2 to 2.0. The VBI troctolite rocks have La/Sm ratios between 3.0 and 4.0 and Th/Nb values of less than 0.1. These compositions can be modelled with 7% contamination of a picritic basalt composition (from Noril'sk and West Greenland after Lightfoot and Hawkesworth, 1997) by a meta-quartz diorite from the metaplutonic suite. The Voisey's Bay basal breccia trend extends from the main group of the troctolites toward higher La/Sm and Th/Nb ratios, which as Li et al. (2000) pointed out, is compatible with the gneiss inclusions in the breccias being extensively altered Tasiuyak. The new data from this study indicate that some metaplutonic rocks also have high La/Sm and Th/Nb ratios like the Tasiuyak gneiss, and could explain the ratios observed in the mineralized troctolite.

3.8 Nd-Sr-Pb ISOTOPIC DATA

Neodymium, strontium and lead isotopic systems in whole rock samples of the Paleoproterozoic metaplutonic unit were analysed in order to evaluate the possible role of the unit in contamination of the Voisey's Bay Intrusion (VBI) and conduit rocks. The Nd

and Sr isotopic data were calculated for an age of 1320 +/- 15 Ma, encompassing the 1333 Ma igneous crystallization age of the Voisey's Bay intrusion and the 1305 Ma age for thermal and/or fluid disturbance (Amelin et al., 2000). The latter event probably involved contact metamorphism caused by emplacement of the Voisey's Bay granite-syenite intrusion (Amelin et al. 1999). The lead isotopic data are presented as time integrated $^{238}\text{Pb}/^{204}\text{Pb}$ (μ^*) and $^{232}\text{Th}/^{238}\text{U}$ (κ^*) of the mantle and crustal sources for each of the samples.

For the purpose of comparing the isotopic signatures of the Voisey's Bay troctolite with potential crustal contaminants, the isotopic data for this study are combined with previous data. The latter include data for the Tasiuyak gneisses, VBI, Voisey's Bay basal breccia, and the metaplutonic suite from Amelin et al. (2000). In addition, data reported by Amelin et al. (2000) as Nain quartzo-feldspathic and mafic gneisses are now thought to be part of the metaplutonic suite based on the results of Rawlings et al. (Chapter 2), and are treated as such here. Most of the data from Amelin et al. (2000) are analyses of mineral separates rather than whole rocks. The metaplutonic suite is divided into depleted and enriched groups, based on their Nd isotopic composition relative to CHUR at the time of their crystallization, 1890 Ma (Rawlings et al., Chapter 2). Data for quartzo-feldspathic Archean orthogneisses of the Nain Province are a combination of results from Collerson et al. (1989) and Campbell (1997). Data for mafic Archean Nain Province orthogneisses are from Campbell (1997).

$^{87}\text{Sr}/^{86}\text{Sr}$ versus ϵNd isotopic data for the Voisey's Bay intrusion and potential contaminants are shown in figure 3.8. The Voisey's Bay intrusion exhibits a distinctive

trend of decreasing $\epsilon\text{Nd}_{(1.320 \text{ Ma})}$ from about 0 to -4 with only a very slight increase in $^{87}\text{Sr}/^{86}\text{Sr}_{(1.320 \text{ Ma})}$ from 0.703-0.704 in figure 3.8. The depleted metaplutonic group defines a linear trend that overlaps and extends the VBI trend to more negative ϵNd values. The enriched group defines a field with still more negative ϵNd values, again in line with the array of VBI data. Amelin et al. (2000) reported six analyses from the Voisey's Bay breccia in the feeder dikes. Four of the six plot at the negative ϵNd end of the VBI trend, near and within the field for the depleted metaplutonic group. The other two samples, feldspar separates, plot with significantly more negative ϵNd values and are closely related with the enriched metaplutonic group. Amelin et al. (2000) speculate that the two anomalous feldspar separates inherited the pre-magmatic isotopic composition of their sources. If so, their sources were similar to enriched metaplutonic rocks.

The remarkable coherence of Nd-Sr isotopic data between the VBI and breccia rocks, and the metaplutonic suite is strong evidence that the metaplutonic suite contaminated and modified the composition of both the VBI and conduit dikes. In contrast the Tasiuyak paragneiss defines a field that is separate and distinct from the Voisey's Bay troctolite samples and breccia samples. The Tasiuyak gneisses have $\epsilon\text{Nd}_{(1.320 \text{ Ma})}$ between -8 and -10 and elevated $^{87}\text{Sr}/^{86}\text{Sr}_{(1.320 \text{ Ma})}$ ratios of 0.712-0.717. The failure of the Voisey's Bay troctolite and the breccia to trend toward the Tasiuyak suggests that the unit did not significantly contaminate the VBI or conduit dikes. The Archean orthogneisses have a large, distinct isotopic range with $\epsilon\text{Nd}_{(1.320 \text{ Ma})}$ between -16 and -52 (with the most of the samples from -40 to -52 and are Early Archean while the more depleted values are Late Archean) and $^{87}\text{Sr}/^{86}\text{Sr}_{(1.320 \text{ Ma})}$ ratios ranging from 0.7026

to 0.8359. However, it should be noted that isotopic data for the Archean orthogneisses in the immediate area of the deposit is not currently available. The Archean Nain orthogneiss could potentially have different isotopic characteristics, although due to complex history of these gneisses, they are likely isotopically heterogeneous as well. The Nd-Sr isotopic heterogeneity of the Archean orthogneisses argues against their being the contaminant of the VBI, which is characterized by isotopic homogeneity.

The Pb isotope data of the Voisey's Bay troctolite and the Voisey's Bay basal breccia, Paleoproterozoic metaplutonic suite, Archean orthogneisses, Tasiuyak Paragneiss, are presented in figure 3.9 expressed as μ^* versus $\epsilon\text{Nd}_{(1320 \text{ Ma})}$ and in figure 3.10 expressed as κ^* versus $\epsilon\text{Nd}_{(1320 \text{ Ma})}$.

The Voisey's Bay intrusion and the Voisey's Bay breccia define a restricted field of Pb isotopes compositions with μ^* values of 7.75 to 8.05 and κ^* values of 4.1 to 4.24. There is not a systematic-correlation of either μ^* or κ^* with ϵNd . The depleted group of metaplutonic rocks overlap the Voisey's Bay intrusion and breccia in Pb isotopes, with μ^* values of 7.75 to 7.98 and κ^* values between 4.08 and 4.24. The enriched group of Paleoproterozoic metaplutonic rocks have somewhat lower μ^* values of 7.62 to 7.77 and a large range of κ^* from 4.12 to 5.81. The Tasiuyak paragneiss exhibits high μ^* from 8.09 to 8.14 and a wide range of κ^* from 3.94 to 5.42. The Archean orthogneisses have low μ^* values ranging from 7.38 to 7.72 and very low κ^* values ranging from 1.13 to 2.37.

In order to quantify the extent of crustal contamination of the Voisey's Bay intrusion and conduit dikes by the metaplutonic suite, the chemical and isotopic

composition of the primitive, mantle-derived parental magma must be determined. The most isotopically primitive magmatic components known for the NPS are ca. 1280 Ma low P basaltic dykes (Wiebe, 1985 and Carlson et al., 1993), which was used by Amelin et al. (2000) for their modelling. Corrected to 1320 Ma, these dykes have $\epsilon\text{Nd}_{(1320 \text{ Ma})}$ values ranging from 0.03 to -1.2, $^{87}\text{Sr}/^{86}\text{Sr}$ ratios ranging from 0.7028 to 0.7031, μ^* values ranging from 7.53 to 7.54 and κ^* values ranging from 4.00 to 4.01. Using the composition of the low P, basaltic dykes as the primitive melt, none of the country rock gneisses, including the metaplutonic suite, provide credible mixing models for the Voisey's Bay intrusion and breccias (Figure 3.11 and 3.12). For the metaplutonic suite, two contamination models were constructed, one for the depleted group and another for the enriched group. The compositions used for the two groups have the same concentrations of Nd, Sr, and Pb but different isotopic ratios, which are the averages for the samples in this study and Amelin et al. (2000).

In the Nd-Sr isotope plot (Figure 3.11), both metaplutonic model curves intersect the Voisey's Bay troctolite data, but on the Nd-Pb plot (Figure 3.12), they largely do not. Model curves for the Tasiuyak paragneiss were constructed using the isotopic composition for the Tasiuyak of Amelin et al. (2000), the concentrations of Sr and Nd are averages of the data reported by Theriault and Ermanovics, (1997) and the concentration of Pb are from the measured Tasiuyak paragneiss in this study. On the Nd-Sr plot (Figure 3.11), the Tasiuyak model curve has a trend of increasing $^{87}\text{Sr}/^{86}\text{Sr}$ with decreasing ϵNd that is much more steep than the Voisey's troctolite data unless, as noted by Amelin et al. (2000), the Pb concentrations are increased by factors of 2-5 times the observed values.

Model curves for Archean orthogneiss were constructed with the isotopic composition and concentration from the Nain province tonalitic gneisses of Campbell (1997), as this is the only complete set of isotopic data available for the Nain Province tonalitic gneisses. The average middle crust model curves were created using the same isotopic composition and concentrations from Rudnick and Fountain (1995), and are the same Amelin et al. (2000) used. Model mixing curves for the average middle crust and Archean orthogneisses do not provide credible matches to the Voisey's Bay troctolite data in figure 3.12.

Crustal contamination models for the metaplutonic suite that use a more primitive picritic, parental magma explain the isotopic signature of the Voisey's Bay intrusive suite very well. Li et al. (2000) and Lambert et al. (2000) have previously suggested a picritic parental magma for the VBI based on trace element ratios and Os-isotopes, respectively. Both groups of workers cited melatroctolite inclusions in Voisey's conduit rocks that contain primitive olivines suggesting a picritic magma source. In addition, similar magmatic sulfide deposits hosted in mafic and ultra-mafic rocks are often believed to be derived from primitive mantle-derived magmas such as high-Mg basalts, picrites or komatiites (Naldrett, 1989). The comparatively high-temperature of the Mg-rich magmas makes their capacity for melting and assimilating country rock gneisses much greater than normal, low-Mg basalts. For the modelling, the isotopic values of picritic magmas associated with the Noril'sk magmatic district in Russia were used, in particular the Tuklonsky picrite, which is believed to be most representative of the parental magma in the Noril'sk area (Wooden et al., 1993). The accepted isotopic values, recalculated to 1320 Ma, are $\epsilon\text{Nd}_{(1320 \text{ Ma})} = 3.2$ (from a range of 3.2 to 0.8), $^{87}\text{Sr}/^{86}\text{Sr}$ ratio = 0.7031 (from

a range of 0.7028 to 0.7032), $\mu^* = 7.83$ (from a range of 7.83 to 8.12). These values are between bulk earth and depleted mantle at 1.32 Ga. The concentrations of Nd, Sr and Pb assumed for the primitive, starting magma are based on measured values for the Tuklonsky picrite reported by Wooden et al. (1993).

Mixing models for the picritic parent are plotted on figure 3.13 for $^{87}\text{Sr}/^{86}\text{Sr}$ versus $\epsilon\text{Nd}_{(1320 \text{ Ma})}$ and in figure 3.14 for μ^* versus $\epsilon\text{Nd}_{(1320 \text{ Ma})}$. The models for the metaplutonic suite show good matches to the data for the Voisey's Bay intrusion and breccia. For the enriched group of the metaplutonic suite the model would suggest contamination at levels of 5 to 10 percent based on Nd-Sr data and 4 to 7 percent based on the Nd-Pb data. This is consistent with the estimates of 5 to 10 percent given earlier in the paper based on La/Sm ratios. Thus, contamination of a picritic basalt by the enriched metaplutonic suite is the preferred model for the origin of the VBI. The data suggest that the same model is applicable to the conduit dikes. The depleted group of Paleoproterozoic metaplutonic rocks may have also contaminated the picritic parent magma of the VBI but it could not have acted alone. To explain the Nd-Sr isotopic signature of the VBI, levels of contamination exceeding 50 percent would be needed, which is thermodynamically unrealistic.

The Tasiuyak paragneiss, Archean orthogneiss and middle crust models do not provide good matches to the Nd-Pb data for either the VBI or breccias (Figure 3.14). The failure of the breccias to show a strong compositional effect of Tasiuyak contamination is particularly surprising as they contain abundant gneissic inclusions interpreted as having a Tasiuyak parentage (Li and Naldrett, 2000). Unlike in the low-Mg basalt parent model

(figure 3.12), increasing the lead concentrations of the hypothetical Tasiuyak contaminant will not provide a better fit to the Voisey's Bay troctolite data. This is because the μ^* values of the Tasiuyak and assumed mafic parent in figure 3.14 are similar. The average middle crust and Archean quartzo-feldspathic gneisses have μ^* values too low to explain the Voisey's Bay intrusion and breccia data without lowering their concentrations of Pb. The average middle crust would need to have its Pb concentration lowered from 15.3 ppm to an unrealistic 3 ppm. The Archean quartzo-feldspathic gneisses would only require its Pb concentrations be lowered from 20 ppm to 3 ppm.

The use of mixing models to identify a potential crustal contaminant in magmatic systems, and quantify the extent of their involvement, is limited by certain uncertainties. The most significant uncertainty is the original composition of the parental melt, since choosing different isotopic values for the starting material can greatly alter the position of a mixing curve in isotopic space. However, when data for different isotopic systems point to the same contaminant and the same degree of contamination, the result is more robust. In this case, both Nd-Sr and Nd-Pb isotopic systematics support the conclusion that the enriched group of Paleoproterozoic metaplutonic suite was most likely involved as a crustal contaminant of the VBI, at a level of 5 to 10 percent.

3.9 DISCUSSION AND CONCLUSION

Crustal contamination is widely believed to play a critical role in promoting sulfur saturation in mafic magmatic systems, in some cases triggering magmatic sulfide precipitation. In order to understand magmatic Ni-Cu-Co ore genesis and discover similar

new deposits it is particularly important to determine the composition and amount of a crustal contaminant in the magmatic system. In the Voisey's Bay Ni-Cu-Co deposit the issue is particularly critical as the deposit is hosted by a troctolite in an anorthosite-mangerite-charnockite-granite complex, a setting that would not have been predicted by current models of Ni sulfide ore genesis. This paper presents several lines of evidence that the Paleoproterozoic metaplutonic rocks of the region played a significant role in the ore genesis as a crustal contaminant of the Voisey's Bay primitive troctolitic magma.

In previous work, the Paleoproterozoic metaplutonic rocks were ruled out as a potential contaminant for various reasons, many of which upon further study are no longer valid based on the results of this study. In particular it is now known that they comprise a unit of sizable volume that hosts all the parts of the nickel deposit except the westernmost Reid Brook zone. They also contain domains with sulfur values as high as 0.1 wt %, and so could have led to sulfur saturation of the Voisey's Bay magmas not only by adding silica but also sulfur. In the eastern portions of the deposit, Ripley et al. (1999) recognised that oxygen isotopes were consistent with a metaplutonic rock, crustal contamination origin and, to reconcile the high- $\delta^{18}\text{O}$ values in some samples, suggested that the Paleoproterozoic metaplutonic rocks might have been interlayered with paragneiss. This suggestion has been confirmed by the mapping of this study: the Paleoproterozoic metaplutonic rocks are tectonically interlayered with paragneisses, metasediments, amphibolites and meta-anorthosites.

Other reasons for dismissing the Paleoproterozoic metaplutonic rocks as a potential crustal contaminant include the perception that large amounts of contamination

were required (Li et al., 2000). However, the modelling results presented here suggest that 5 to 10 percent contamination was sufficient. The trace element pattern of the Paleoproterozoic metaplutonic rocks provides perhaps the most compelling evidence for their involvement in the contamination of the Voisey's Bay intrusion. The metaplutonic rocks have a trace element pattern that is markedly similar to the Voisey's Bay troctolites and breccias, and different than the other gneisses in the region. The distinctive Th-U depletion of this pattern is unusual in mafic rocks like the Voisey's Bay troctolites and is the "smoking gun" of the metaplutonic contamination. The data do not constrain the depth of crustal contamination and so cannot confirm the 2-stage crustal contamination model of Li et al. (2000) and Lambert et al. (2000), in which lower-middle crustal contamination was followed by upper crustal contamination. However, as the metaplutonic suite seems to be the main constant for both the VBI and conduit rocks, there is no necessity for two stages of contamination.

While presenting a strong case for the Paleoproterozoic metaplutonic rocks as the main crustal contaminant of the Voisey's Bay intrusion, the data also cast doubt on the significance of the Tasiuyak paragneiss in ore genesis. While the presence of gneiss inclusions resembling Tasiuyak gneiss is certainly ubiquitous in the breccia of the conduit dikes to the deposit, there is little evidence for a change in composition of the conduit rocks as a result of gneiss digestion. Sulfur isotope data appear to show little effects of Tasiuyak contamination only in the Reid Brook zone, which is the only part of the deposit hosted by the Tasiuyak. The Sr-Nd-Pb data present no strong case for significant silicate dissolution of the Tasiuyak in the conduit dikes. Taken together, the evidence does not rule out a role for the Tasiuyak paragneiss in promoting sulfide precipitation at Voisey's

Bay, but indicates that the metaplutonic suite may have played a more important role.

Determining the precise processes that led to sulfide saturation will require more detailed study of the metaplutonic suite and the Ni-Cu-Co ore deposit.

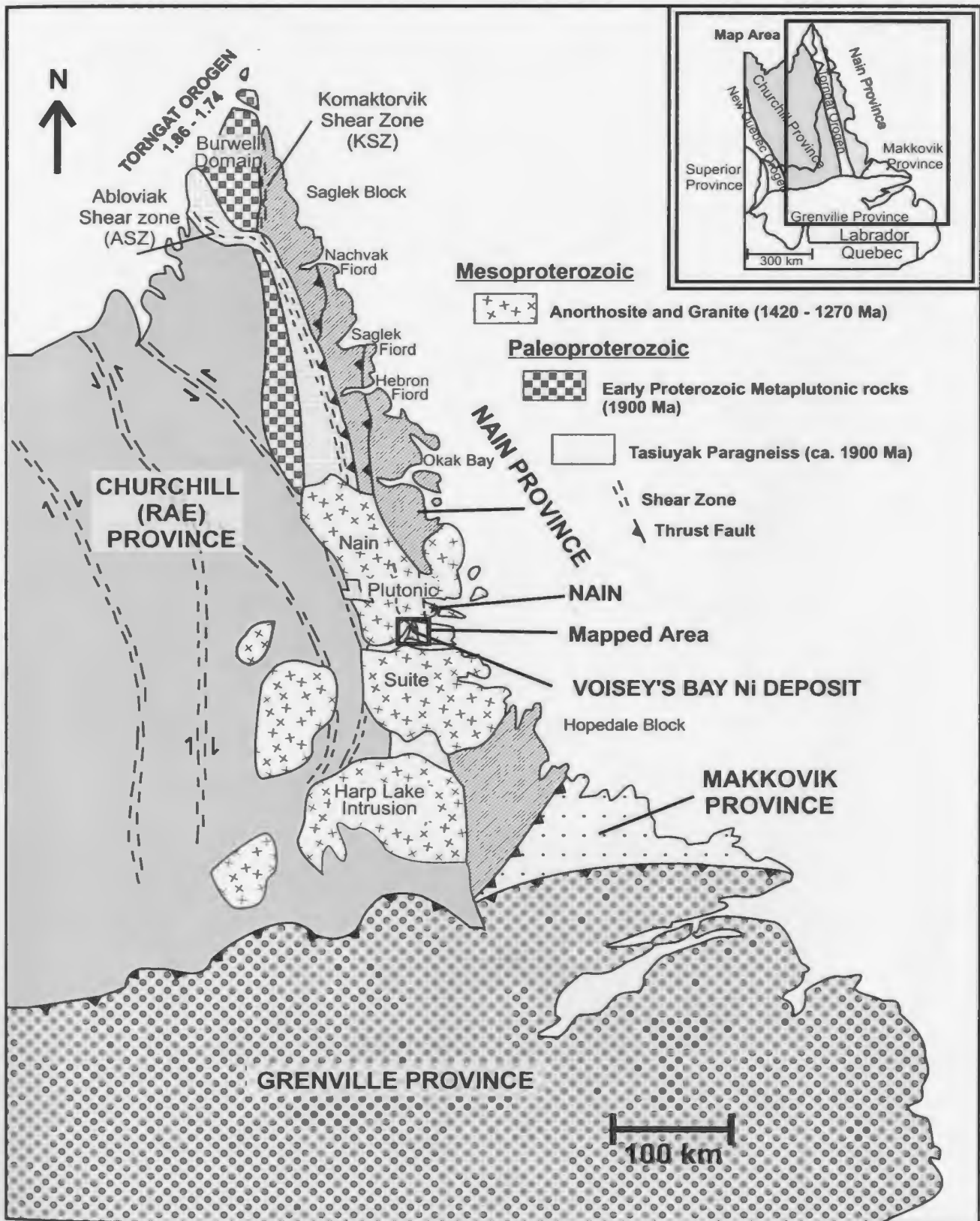


Figure 3.1. Simplified geologic map of Labrador, showing the lithotectonic elements, the Voisey's Bay Ni-Cu-Co deposit and the area mapped for this paper (modified after van Kranendonk and Wardle, 1996, and Wardle et al., 1997).

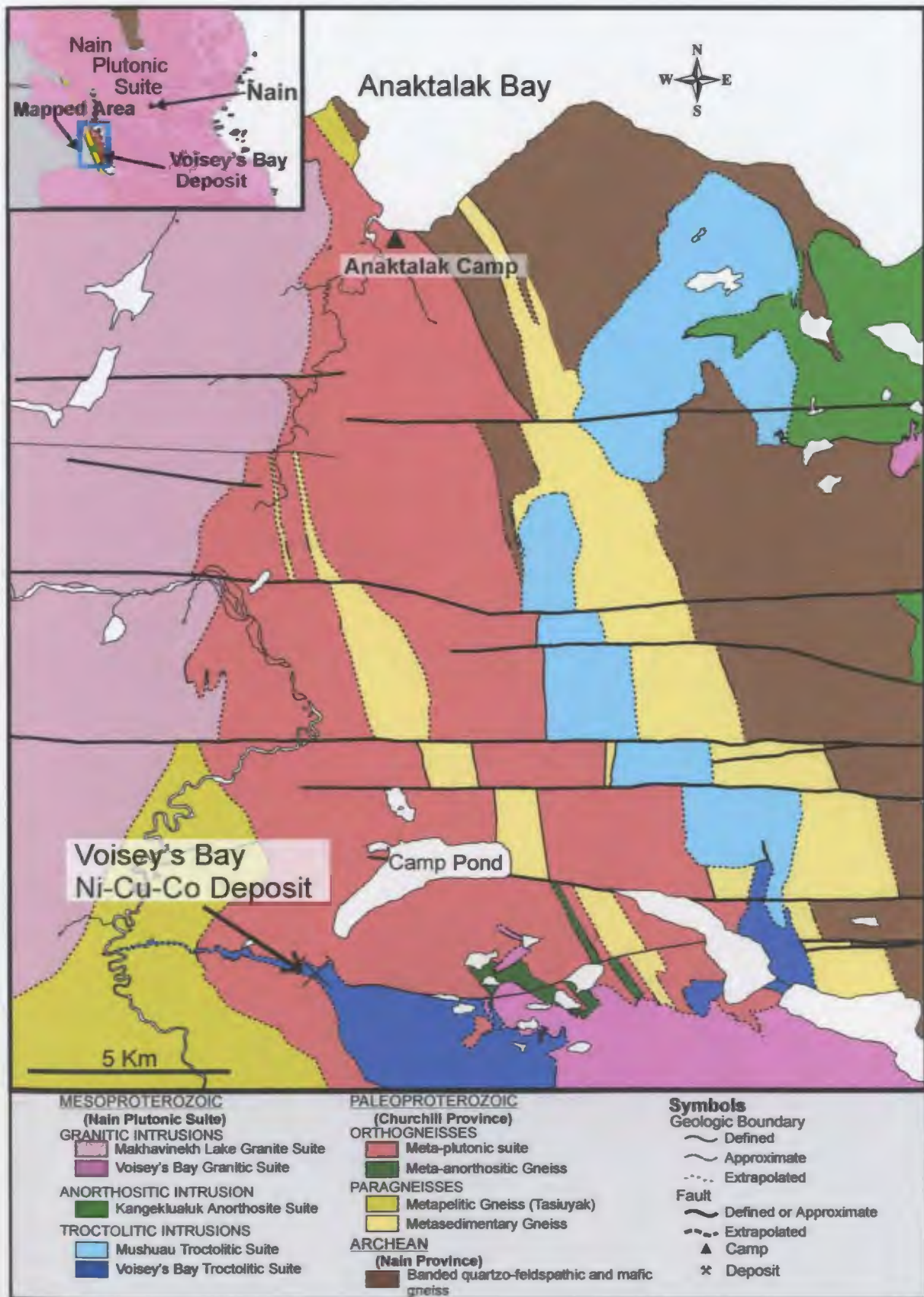


Figure 3.2. Simplified geologic map of Voisey's-Anaktalak Bay area, Labrador (simplified after Map 1, back pocket). Major geologic units are outlined.

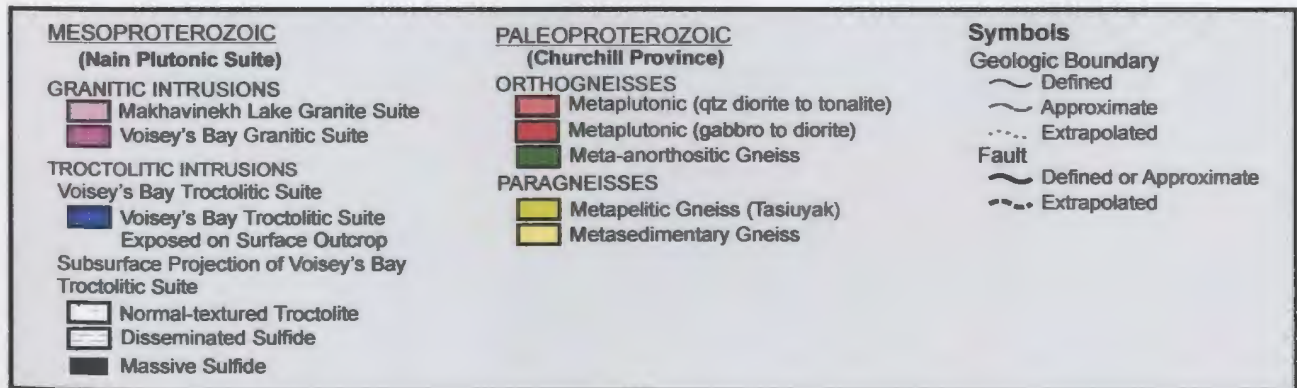
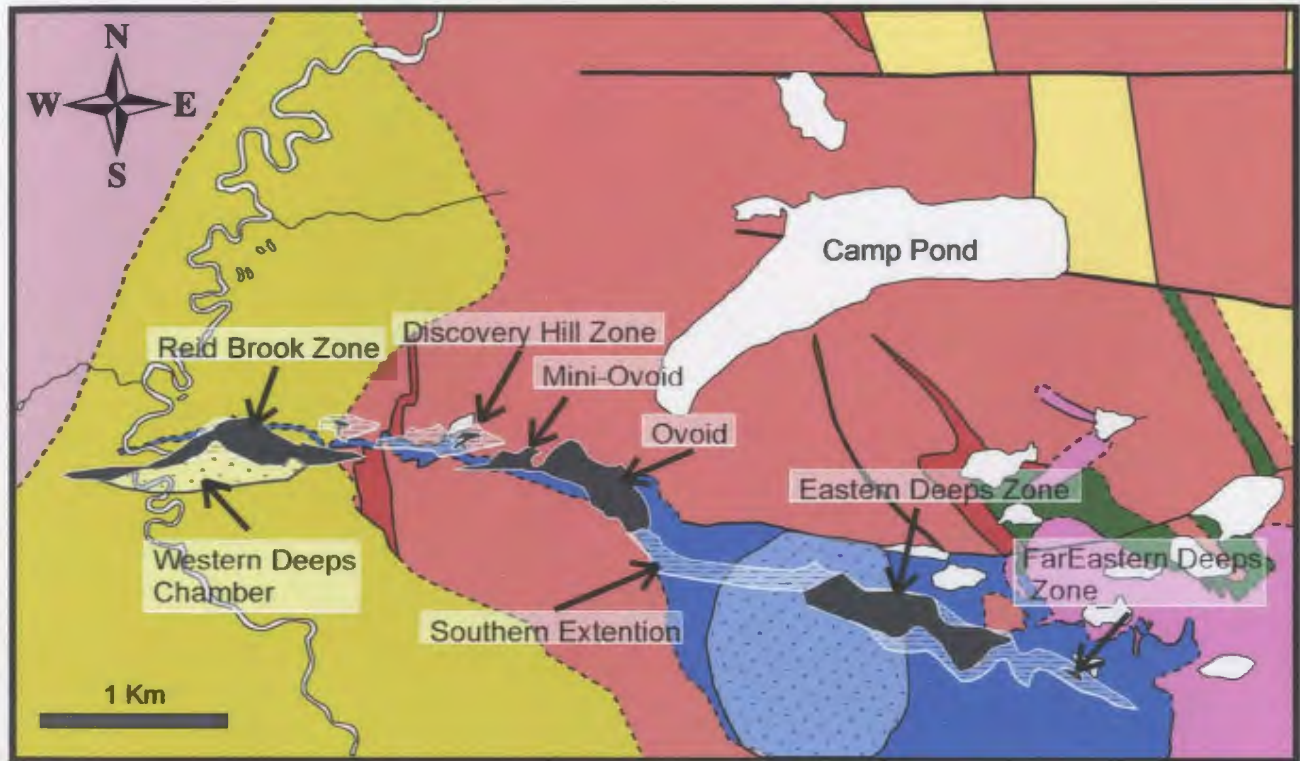


Figure 3.3. Simplified geologic map of Voisey's Bay deposit area, Labrador (simplified after Map 1, back pocket). Showing the surface projection of the subsurface Voisey's Bay Troctolite intrusion and associated mineralization from Evans-Lamswood et al. (2000).

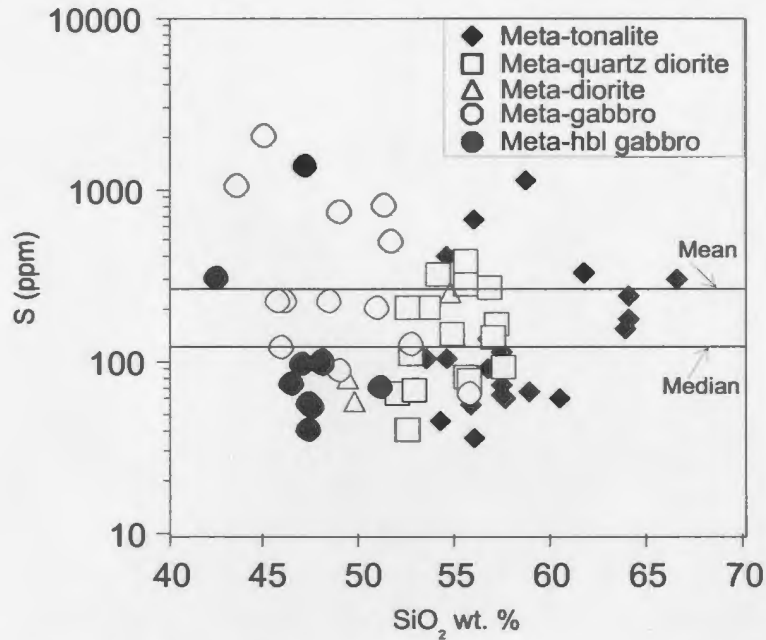


Figure 3.4. Plot of SiO_2 versus sulfur for the various lithologies of the Paleoproterozoic metaplutonic suite from Voisey's Bay, Labrador.

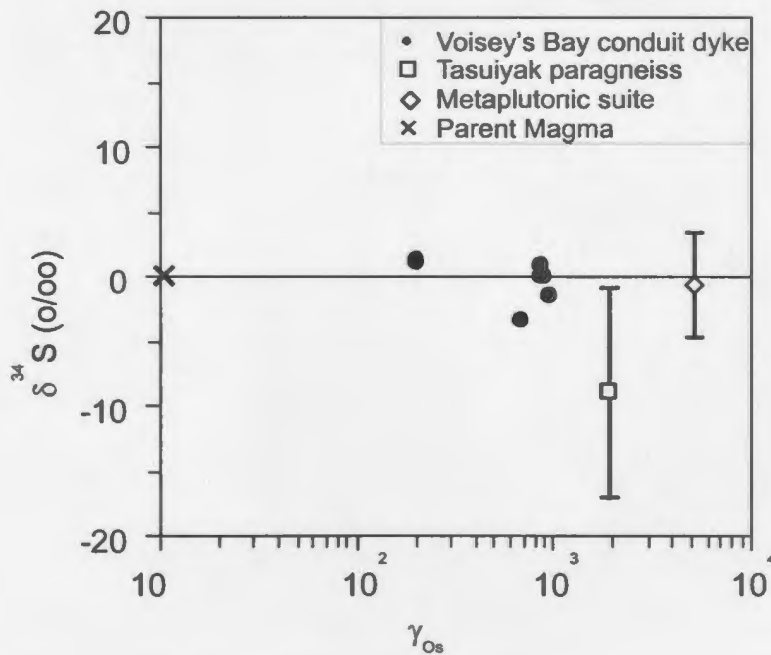


Figure 3.5. γ_{Os} versus $\delta^{34}\text{S}$ in sulfides from conduit dykes (Reid Brook, Discovery Hill, Eastern Deeps) at Voisey's Bay, a sulfide from a metaplutonic rock, and a sulfide from a Tasiuyak paragneiss. Os- isotopic data from Lambert et al. (2000). Metaplutonic sample is incorrectly described as from "Nain gneiss". S- isotope data from metaplutonic and Tasiuyak samples are ranges of whole rock values for these units as the sulfides have not been measured. Parent magma is assumed $\gamma_{\text{Os}} = 10$, $\delta^{34}\text{S} = 0$.

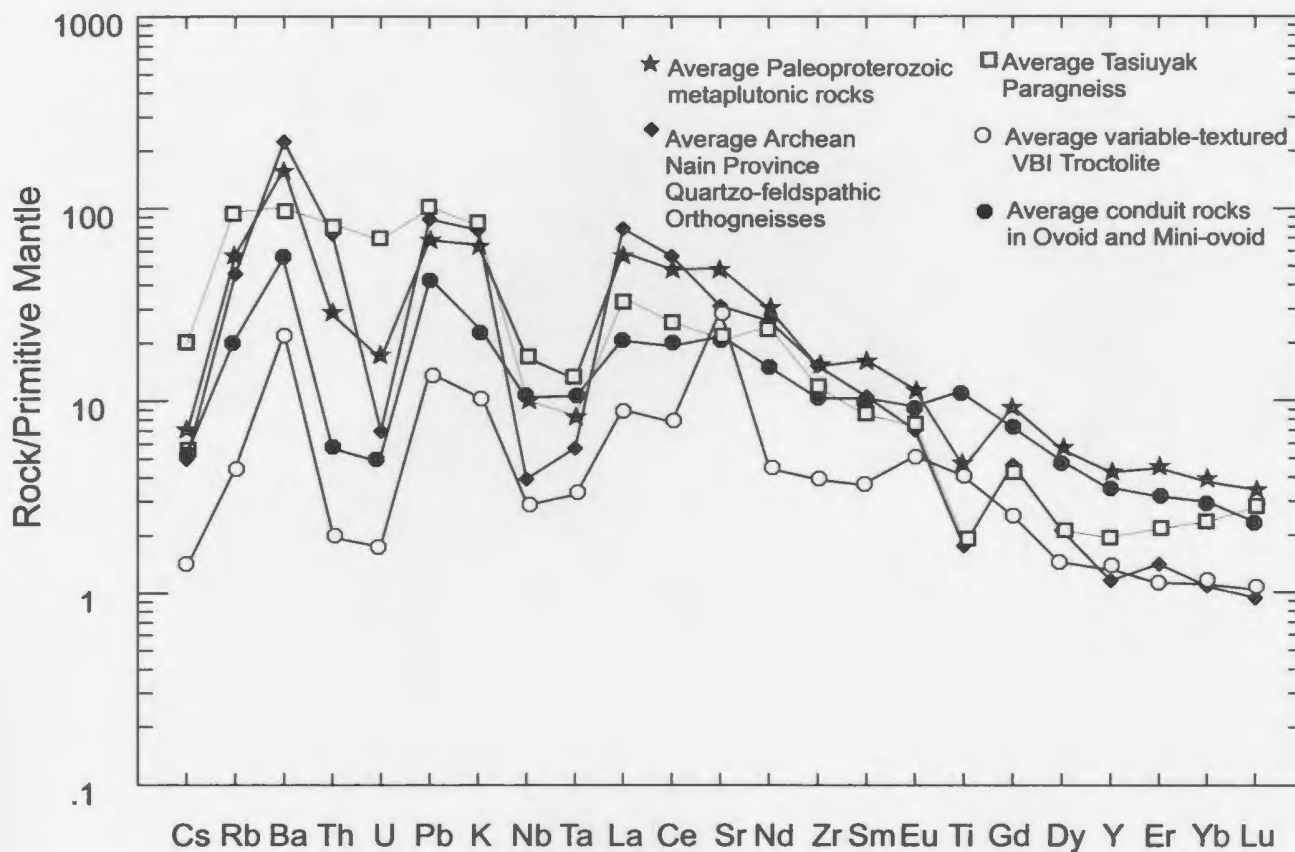


Figure 3.6. Primitive mantle normalized spider diagrams of the average Paleoproterozoic metaplutonic rock, Archean Nain Province orthogneiss, Tasiuyak paragneiss, variable-textured Voisey's Bay intrusion (VBI) troctolite and combined mineralized ovoid and mini-ovoid conduit rocks. Metaplutonic and Archean orthogneiss data are from this study. Tasiuyak paragneiss, variable-textured VBI troctolite and ovoid-mini-ovoid conduit data are after Lightfoot and Naldrett (1999).

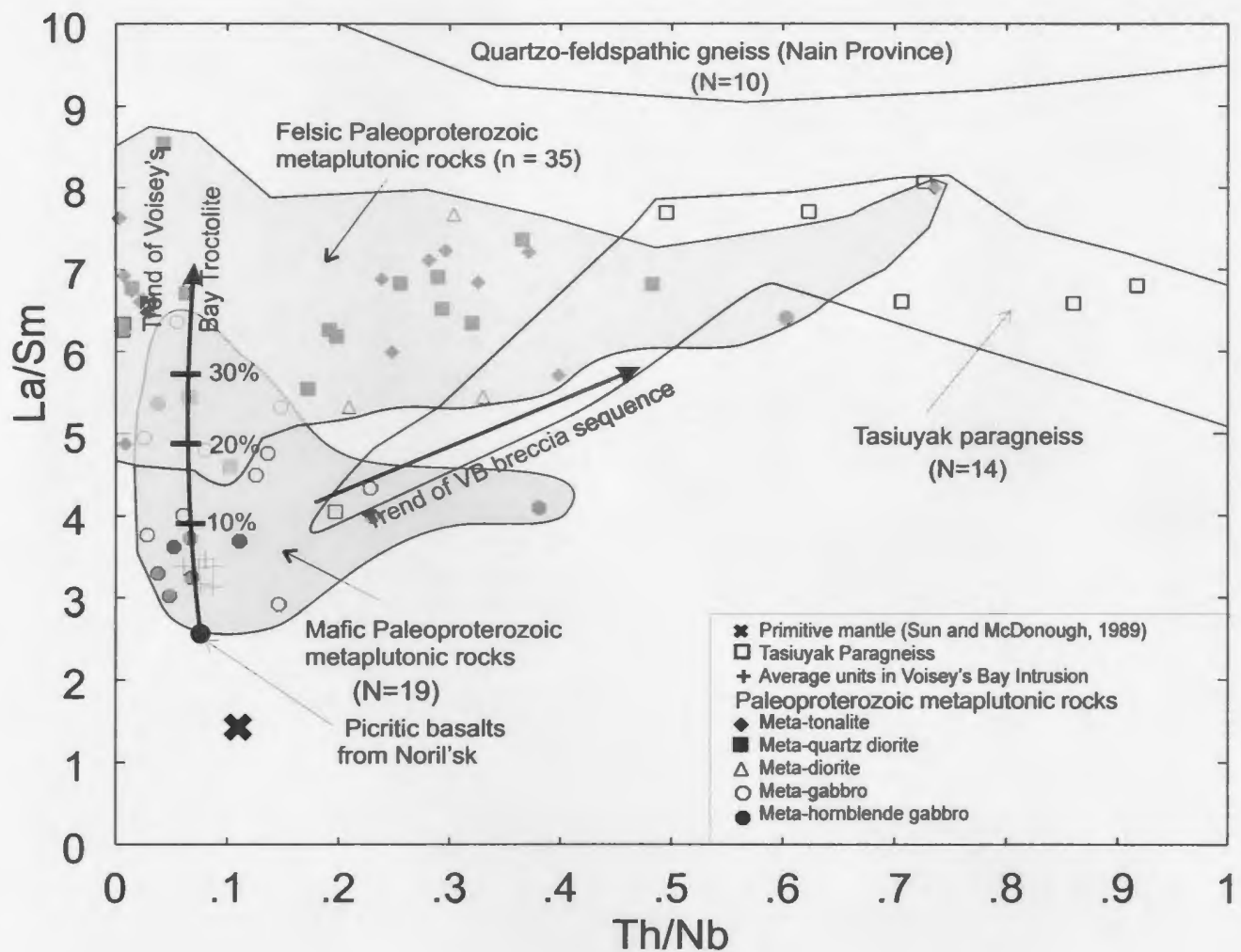


Figure 3.7. Plot of La/Sm versus Th/Nb for the Voisey's Bay intrusion (VBI), Tasiuyak paragneiss, Archean quartzo-feldspathic orthogneisses, Paleoproterozoic metaplutonic rocks. VBI troctolite data are after Li et al. (2000), crosses represent average values of VBI units and arrows represent trends of the breccia unit and troctolite. Quartzo-feldspathic Nain gneisses are from Li et al. (2000). Tasiuyak data are combined from this study and Theriault and Ermanovics (1997). Starting composition used in the modeling is a Noril'sk picritic basalt from Wooden et al. (1993).

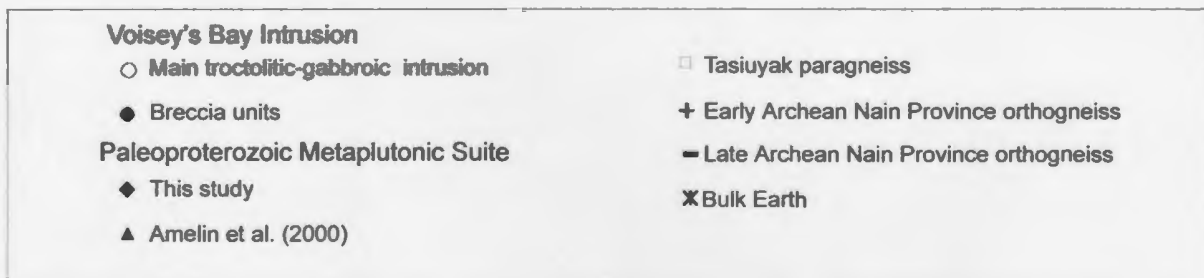
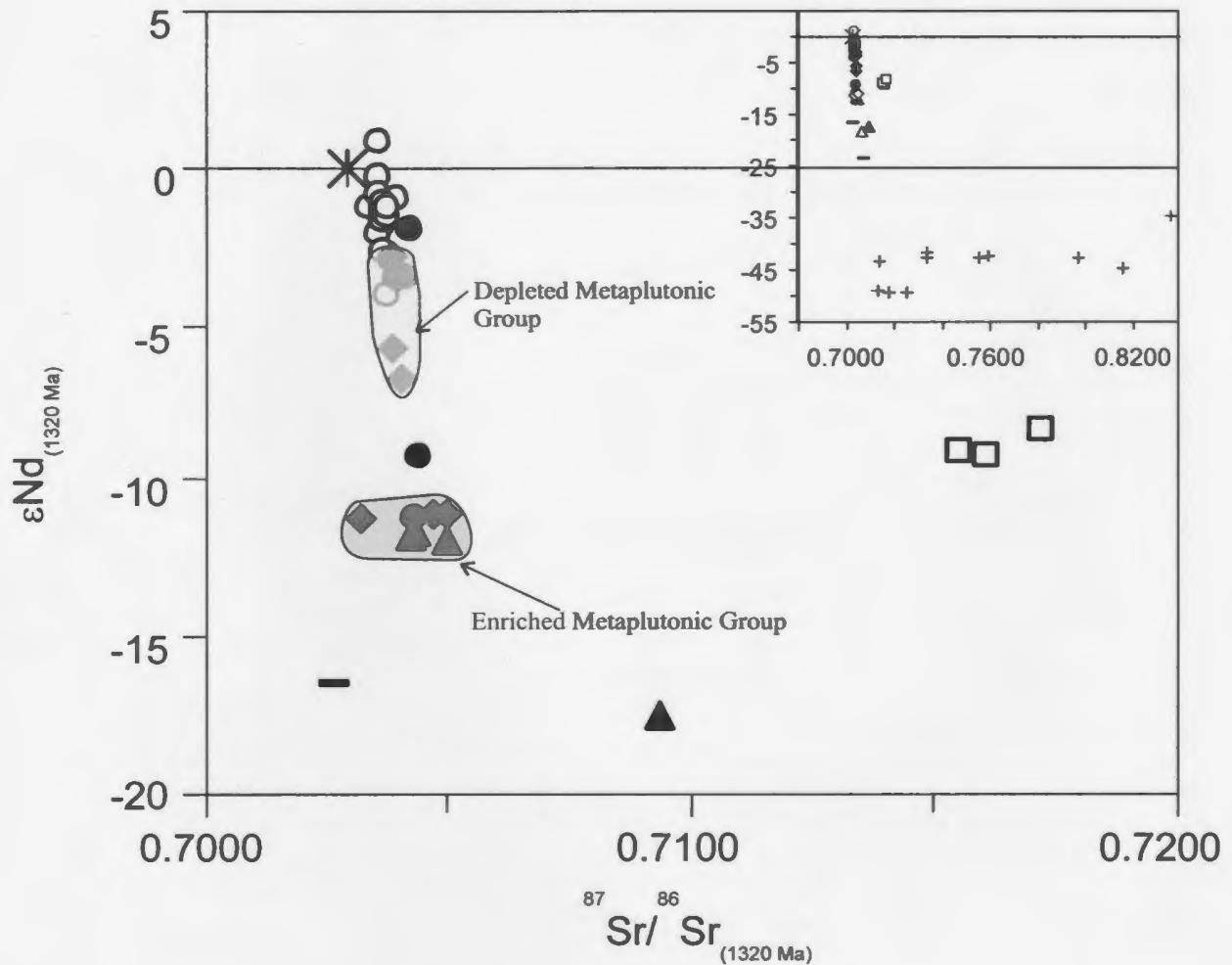


Figure 3.8. $^{87}\text{Sr}/^{86}\text{Sr}_{(1320\text{ Ma})}$ versus $\epsilon\text{Nd}_{(1320\text{ Ma})}$ diagram for the Voisey's Bay intrusion (Amelin et al., 2000) and potential crustal contaminants. The Paleoproterozoic metaplutonic suite data are combined from this study and Amelin et al. (2000). They are subdivided into depleted and enriched groups, based on their isotopic composition at the time of their formation (1890 Ma). One anomalous metaplutonic sample is not included in either group. The Early Archean Nain Province gneisses of the Saglek area are from Collerson et al. (1989) and Late Archean Nain Province felsic gneisses east of the Burwell Domain are from Campbell (1997). Bulk earth value is from DePaolo (1988). Inset diagram shows full range of data.

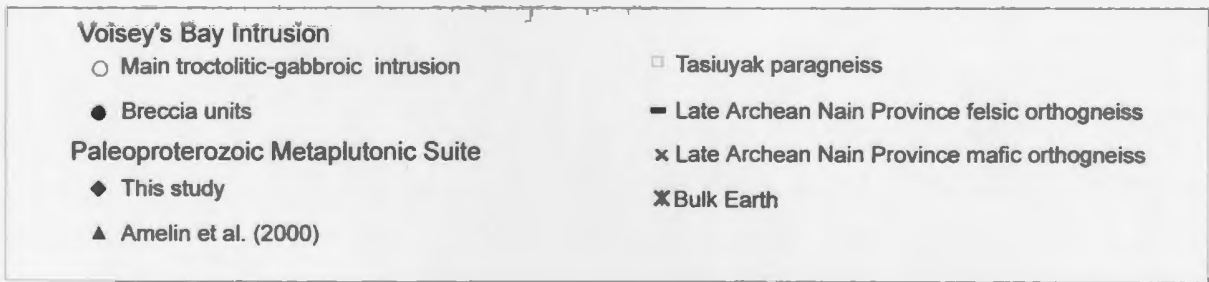
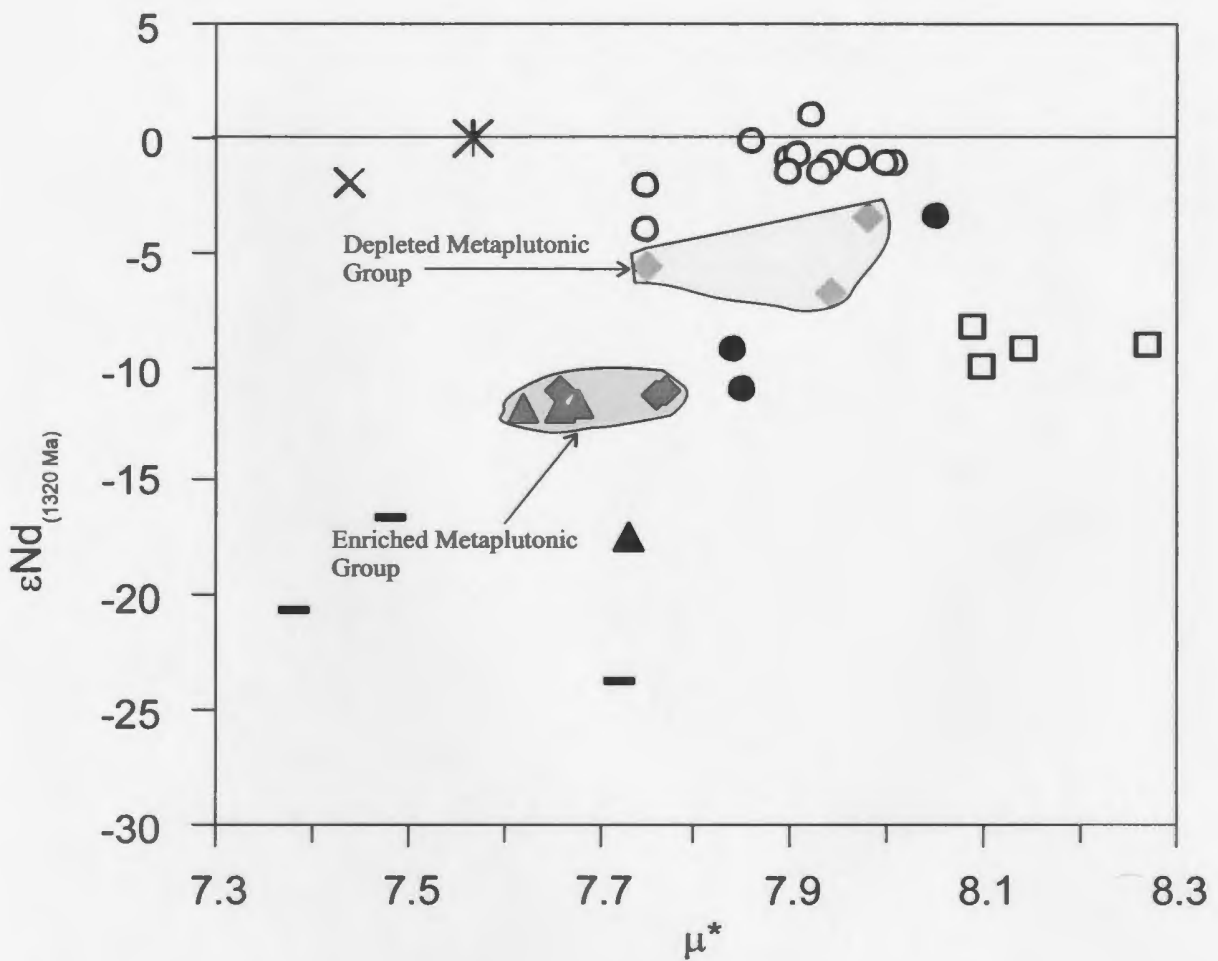


Figure 3.9. μ^* versus $\epsilon Nd_{(1320\text{ Ma})}$ diagram for the Voisey's Bay intrusion and potential crustal contaminants. The Paleoproterozoic metaplutonic suite data are combined from this study and Amelin et al. (2000). Data sources are the same as in figure 3.8. In addition, the Late-Archean Nain Province mafic orthogneisses data are from Campbell (1997).

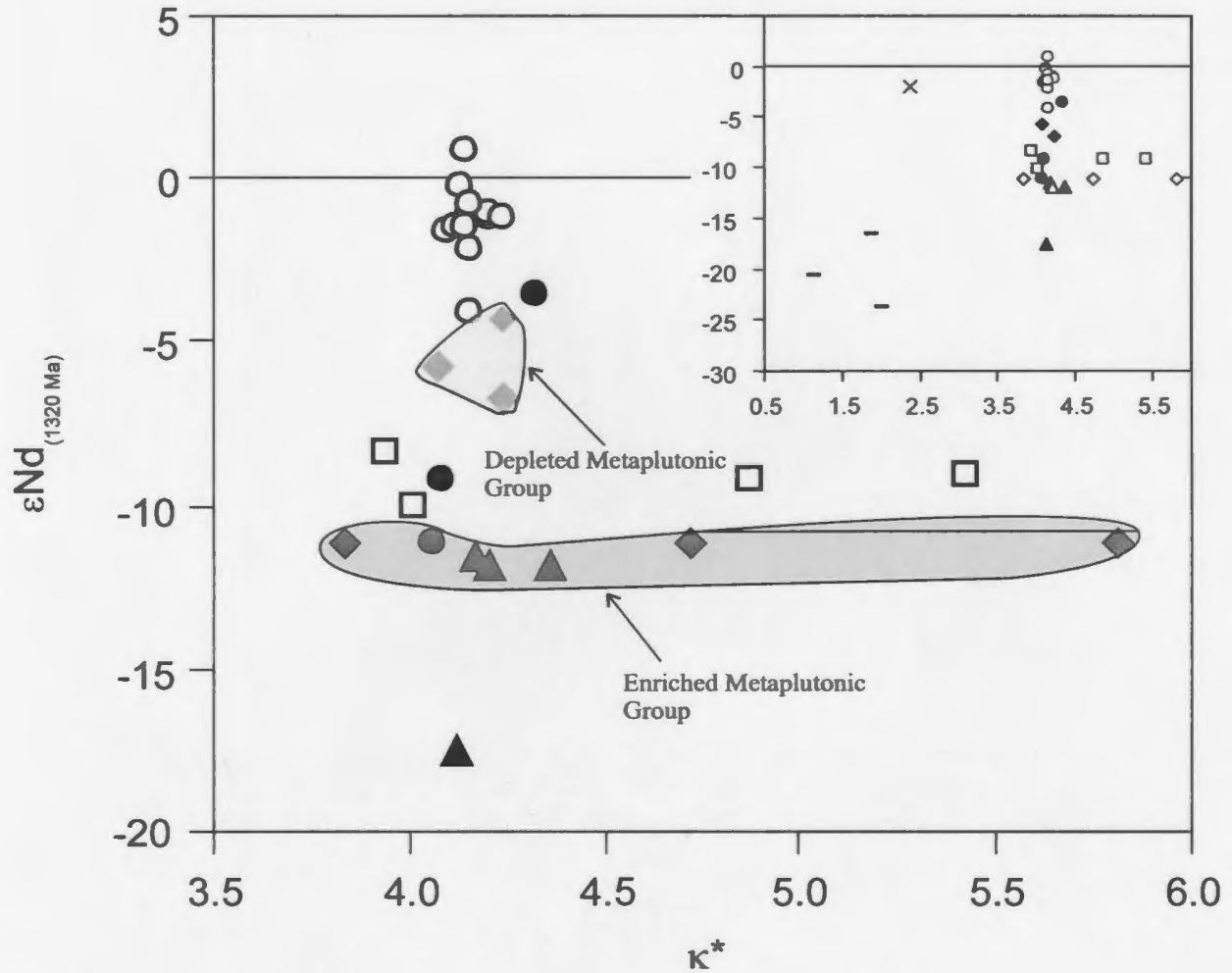


Figure 3.10. κ^* versus $\epsilon Nd_{(1320 \text{ Ma})}$ diagram for the Voisey's Bay intrusions and potential crustal contaminants. Data sources are the same as in Figure 3.9. Inset diagram shows full range of data.

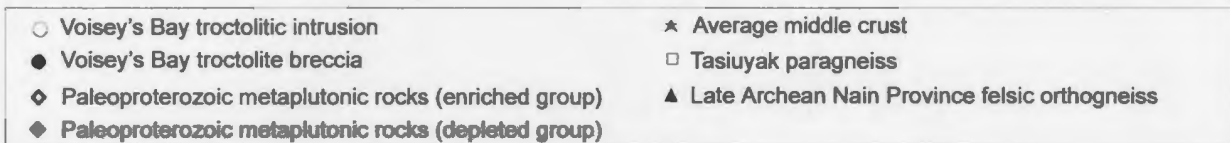
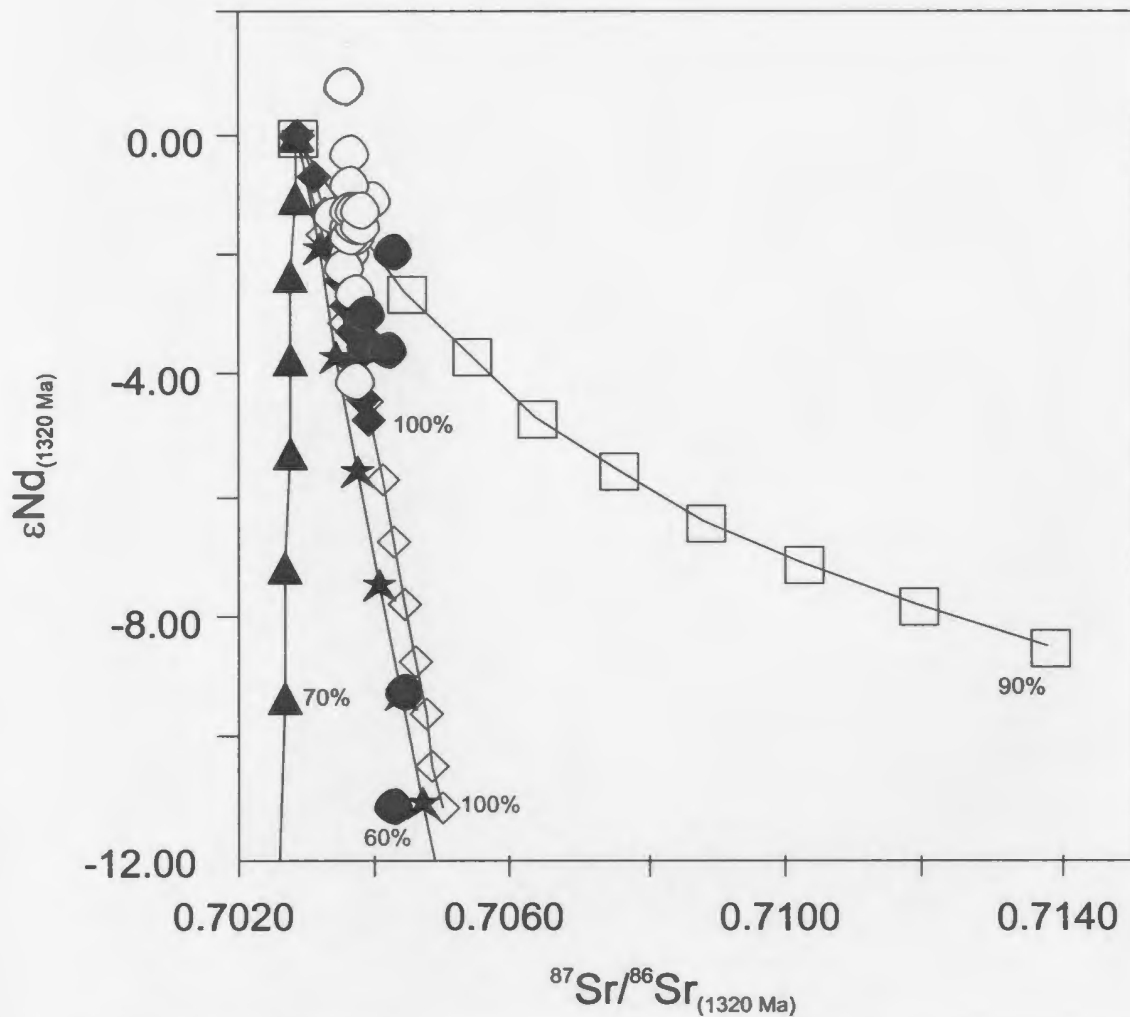
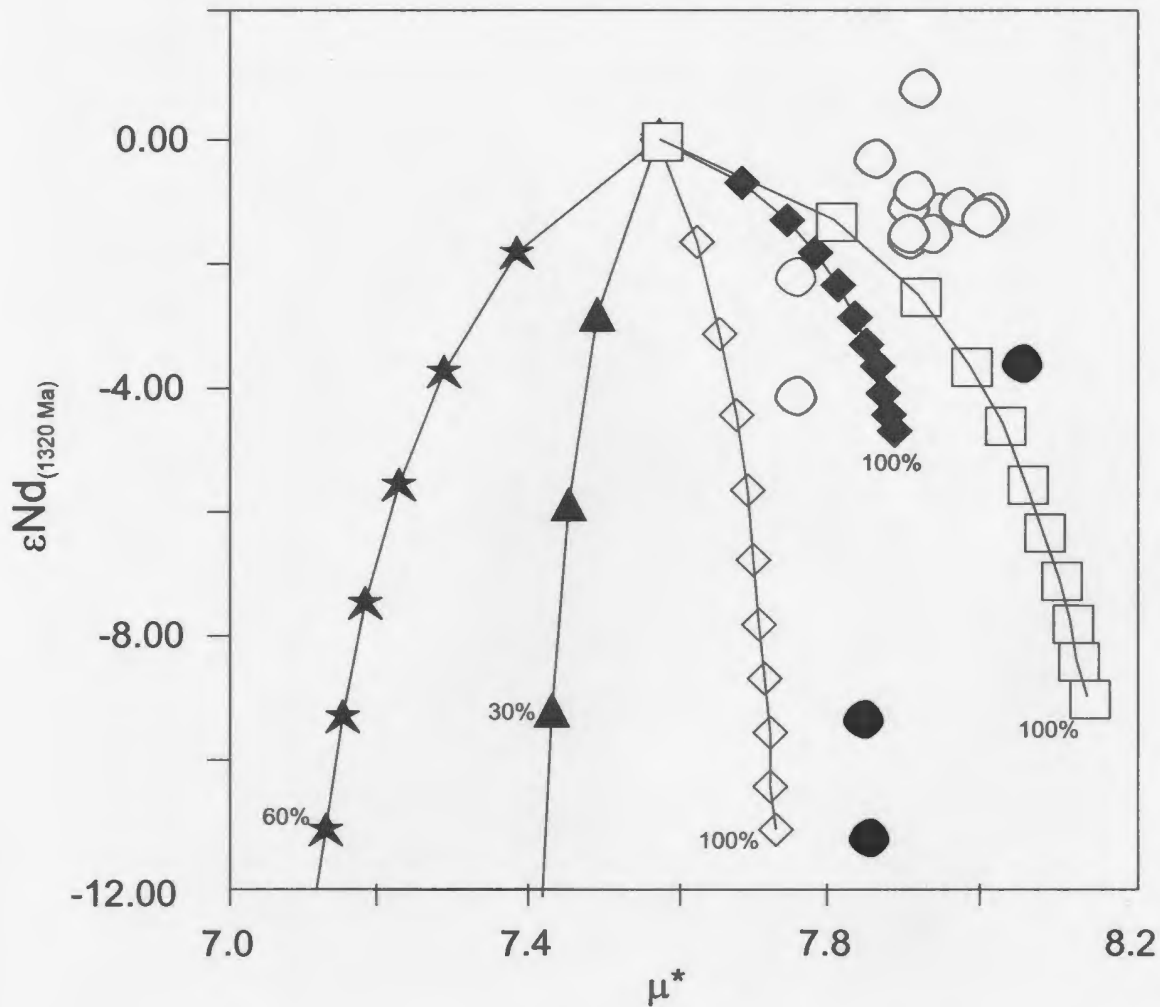
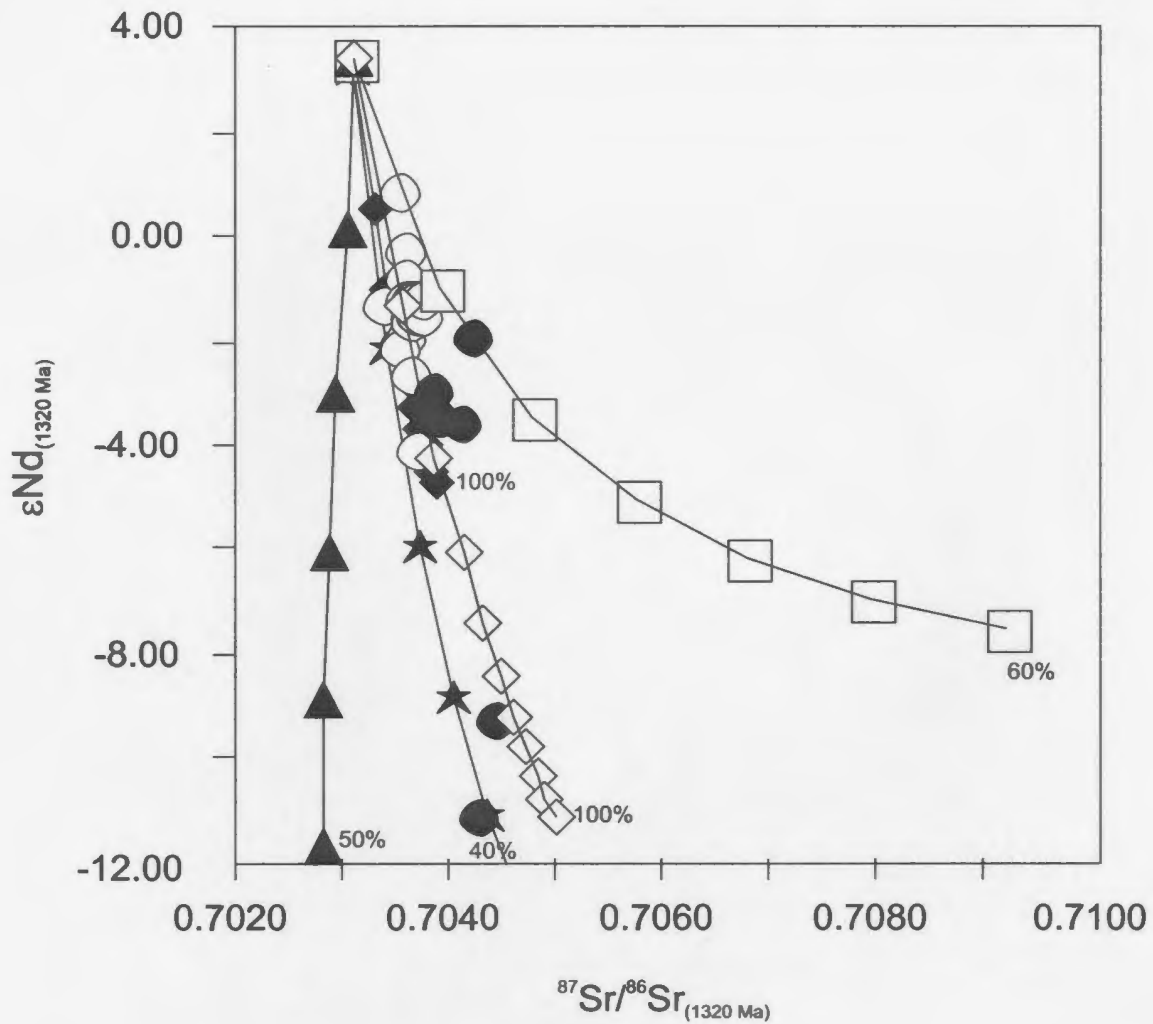


Figure 3.11. Plot of $^{87}\text{Sr}/^{86}\text{Sr}$ versus $\epsilon\text{Nd}_{(1320 \text{ Ma})}$ of the Voisey's Bay intrusion (VBI) in comparison with mixing models between the basaltic parental magma end-member similar to the Nain basaltic dykes (23.3 ppm Nd, 363 ppm Sr, $\epsilon\text{Nd}_{(1320 \text{ Ma})} = 0$, $^{87}\text{Sr}/^{86}\text{Sr}_{(1320 \text{ Ma})} = 0.70294$) and the potential contaminants: Tasiuyak paragneiss (37.4 ppm Nd, 197.2 ppm Sr, $\epsilon\text{Nd}_{(1320 \text{ Ma})} = -9$, $^{87}\text{Sr}/^{86}\text{Sr}_{(1320 \text{ Ma})} = 0.716$), Archean quartzo-feldspathic gneiss (Nain Province; 10 ppm Nd, 500 ppm Sr, $\epsilon\text{Nd}_{(1320 \text{ Ma})} = -23.7$, $^{87}\text{Sr}/^{86}\text{Sr}_{(1320 \text{ Ma})} = 0.70263$), the enriched group of Paleoproterozoic metaplutonic rocks (35.5 ppm Nd, 760 ppm Sr, $\epsilon\text{Nd}_{(1320 \text{ Ma})} = -11.13$, $^{87}\text{Sr}/^{86}\text{Sr}_{(1320 \text{ Ma})} = 0.705$), the depleted group of Paleoproterozoic metaplutonic rocks (35.5 ppm Nd, 760 ppm Sr, $\epsilon\text{Nd}_{(1320 \text{ Ma})} = -4.72$, $^{87}\text{Sr}/^{86}\text{Sr}_{(1320 \text{ Ma})} = 0.70391$) and the average middle crust (24 ppm Nd, 281 ppm Sr, $\epsilon\text{Nd}_{(1320 \text{ Ma})} = -18.3$, $^{87}\text{Sr}/^{86}\text{Sr}_{(1320 \text{ Ma})} = 0.70624$). Mixing curves are marked at intervals of 10 percent contamination.



- | | |
|--|---|
| ○ Voisey's Bay troctolitic intrusion | ★ Average middle crust |
| ● Voisey's Bay troctolite breccia | □ Tasiuyak paragneiss |
| ◇ Paleoproterozoic metaplutonic rocks (enriched group) | ▲ Late Archean Nain Province felsic orthogneiss |
| ◆ Paleoproterozoic metaplutonic rocks (depleted group) | |

Figure 3.12. Plot of μ^* versus $\epsilon Nd_{(1320\text{ Ma})}$ of the Voisey's Bay intrusion (VBI) in comparison with mixing models between the basaltic parental magma end-member similar to the Nain basaltic dykes (23.3 ppm Nd, 3 ppm Pb, $\epsilon Nd_{(1320\text{ Ma})} = 0$, $\mu^* = 7.57$) and the potential contaminants: Tasiuyak paragneiss (37.4 ppm Nd, 18.7 ppm Pb, $\epsilon Nd_{(1320\text{ Ma})} = -9$, $\mu^* = 8.14$), Archean quartzo-feldspathic gneiss (Nain Province; 10 ppm Nd, 31 ppm Pb, $\epsilon Nd_{(1320\text{ Ma})} = -23.7$, $\mu^* = 7.38$), enriched group of Paleoproterozoic metaplutonic rocks (35.5 ppm Nd, 14.8 ppm Pb, $\epsilon Nd_{(1320\text{ Ma})} = -11.13$, $\mu^* = 7.73$), the depleted group of Paleoproterozoic metaplutonic rocks (35.5 ppm Nd, 14.8 ppm Pb, $\epsilon Nd_{(1320\text{ Ma})} = -4.72$, $\mu^* = 7.89$) and the average middle crust (24 ppm Nd, 15.3 ppm Pb, $\epsilon Nd_{(1320\text{ Ma})} = -18.3$, $\mu^* = 7.07$). Mixing curves are marked at intervals of 10 percent contamination.



- | | |
|--|---|
| ○ Voisey's Bay troctolitic intrusion | ★ Average middle crust |
| ● Voisey's Bay troctolite breccia | □ Tasiuyak paragneiss |
| ◇ Paleoproterozoic metaplutonic rocks (enriched group) | ▲ Late Archean Nain Province felsic orthogneiss |
| ◆ Paleoproterozoic metaplutonic rocks (depleted group) | |

Figure 3.13. Plot of $^{87}\text{Sr}/^{86}\text{Sr}$ versus $\epsilon\text{Nd}_{(1320\text{ Ma})}$ of the Voisey's Bay intrusion (VBI) in comparison with mixing models using picritic parental magma end-member similar Tuklonsky Picrite (Noril'sk, Russia) (8.08 ppm Nd, 276 ppm Sr, $\epsilon\text{Nd}_{(1320\text{ Ma})} = 3.2$, $^{87}\text{Sr}/^{86}\text{Sr}_{(1320\text{ Ma})} = 0.70313$. The mixing curves have the same parameters as in figure 3.11. All mixing curves are marked at intervals of 10 percent contamination.

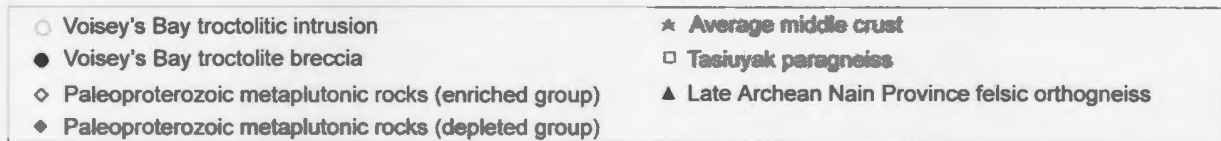
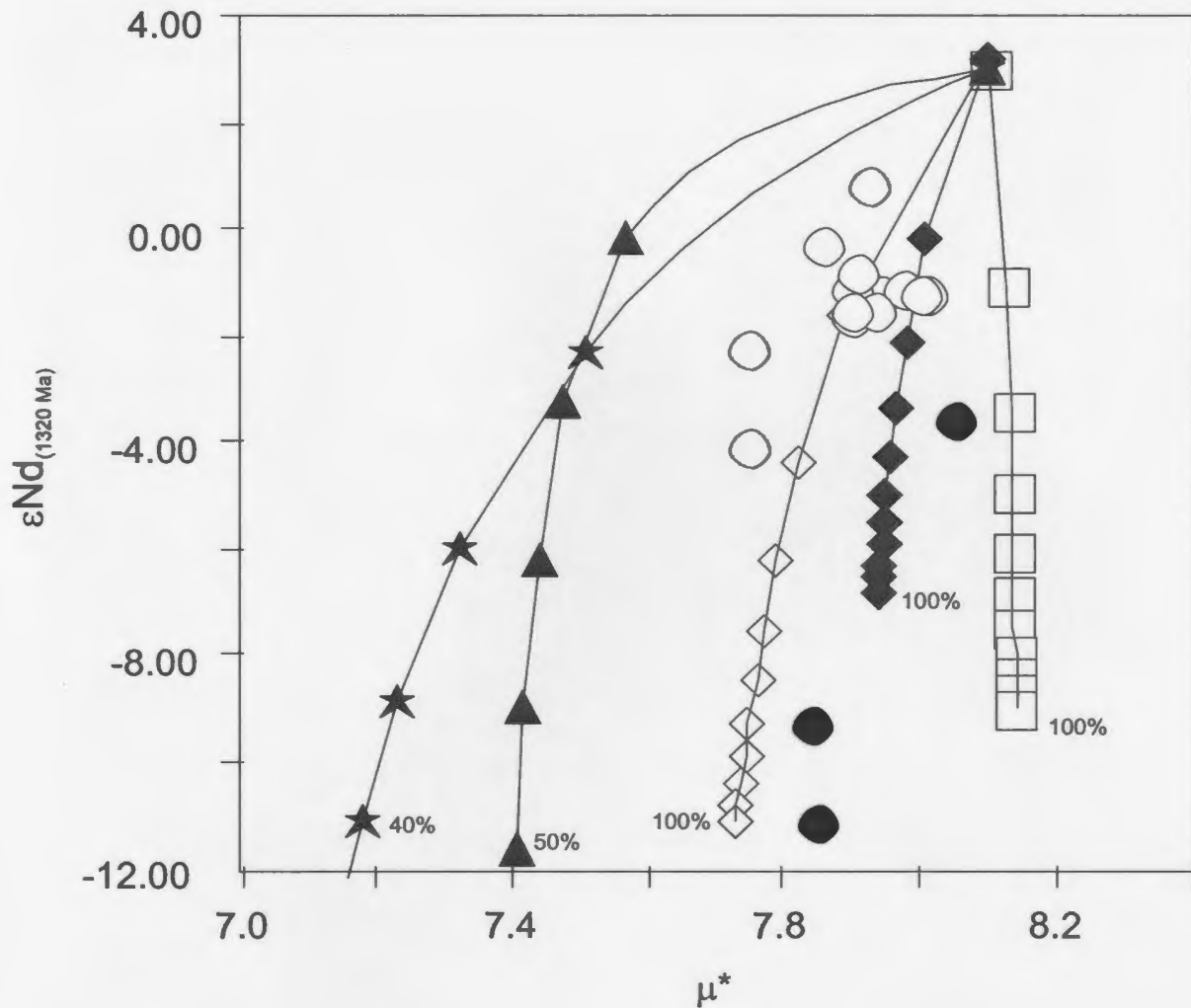


Figure 3.14. Plot of μ^* versus $\epsilon Nd_{(1320 \text{ Ma})}$ of the Voisey's Bay intrusion (VBI) in comparison with mixing models using picritic parental magma end-member similar Tukulnsky Picrite (Noril'sk, Russia; 8.08 ppm Nd, 1.26 ppm Pb, $\epsilon Nd_{(1320 \text{ Ma})} = 3.2$, $\mu^* = 7.83$). The mixing curves have the same parameters as in figure 3.12. All mixing curves are marked at intervals of 10 percent contamination.

Chapter 4

Summary and Conclusion

4.1 INTRODUCTION

The main goals of this thesis, as presented in chapter 1, were to define and characterise the Paleoproterozoic metaplutonic rocks in the Voisey's Bay area, Labrador; focussing on: (a) interpretation of the petrogenetic history of the metaplutonic suite in hopes of constraining the Paleoproterozoic tectonic setting of the region, and (b) evaluation of the role that the metaplutonic suite might have played in crustal contamination and genesis of the Voisey's Bay Ni-Cu-Co deposit. To achieve these goals, certain criteria were met, which included: providing a detailed geological map, petrology, geochronology, geochemistry and isotopic geochemistry studies of the metaplutonic rocks.

4.2 SUMMARY

In order to fulfil the main goals of this research project, a detailed (1:10,000) geological map of the Paleoproterozoic metaplutonic rocks and adjacent rocks in the map area was completed in conjunction with major and trace element geochemistry, U-Pb TIMS geochronology, U-Pb LAM-ICP-MS and isotopic geochemistry (Sm-Nd, Rb-Sr and Pb-Pb). This section will briefly summarise the main findings of the two papers (Chapter 2 and 3) of this thesis.

4.2.1 Chapter 2 – *Southern extension of the Torngat Orogen: Remnants of a calc-alkaline batholith in the Voisey's Bay area, Labrador.*

This paper focuses on the characterization and definition of the Paleoproterozoic metaplutonic suite in the Voisey's Bay area through the use of geochemistry, field geology, geochronology and isotopic composition studies. This is important for several reasons including: (1) this unit is an important component of the Torngat Orogen, and hereby increasing our understanding of the most southerly contact of the Nain-Rae cratons; and (2) this unit provides an opportunity to evaluate Paleoproterozoic subduction zone processes and interpret those processes relative to modern analogues.

The Paleoproterozoic metaplutonic suite defines a belt of calc-alkaline rocks consisting of a relatively undifferentiated, mafic to intermediate batholith. This suite is metamorphosed at upper amphibolite to granulite facies, presumably related to one major deformational event. The metaplutonic rocks are classified into five compositions: 1) meta-tonalite, 2) meta-quartz-diorite, 3) meta-diorite, 4) meta-gabbro and 5) meta-hornblende gabbro, though meta-quartz diorite is the dominant phase. These rocks are interlayered and deformed with metasedimentary rocks (dominantly metapelite and quartzite), amphibolite and minor meta-anorthosites.

The ca. 1890 Ma meta-gabbro to meta-quartz diorite compositions define a magmatic series that probably evolved through fractional crystallization. The slightly younger meta-tonalites (1883 \pm 5 Ma), appear to have evolved along a different magmatic trend. All compositions of the Paleoproterozoic metaplutonic suite display large enrichments in Ba, light-rare-earth-elements (LREEs), Sr, Zr and Hf, in conjunction with pronounced depletions in Th-U and Nb-Ta. The REE patterns are fractionated with

LREE to HREE, and this fractionation increases with silica content. This indicates that the meta-tonalites had more residual garnet in their source regions than the other compositions in the suite.

The $\epsilon_{\text{Nd}}(1890 \text{ Ma})$ of the metaplutonic suite varies between 0.13 and -5.3, suggesting interaction between the primary magma and the continental crust. The $^{206}\text{Pb}/^{204}\text{Pb}$ isotopic ratios ranged from 15.160 to 15.834; while the $^{207}\text{Pb}/^{204}\text{Pb}$ values ranged from 15.000 to 15.145. These values are consistent with contamination by the lower crust.

U-Pb zircon LAM-ICP-MS (laser ablation microscopy-inductively coupled plasma-mass spectrometry) analysis identified a population of inherited cores in one sample of meta-hornblende gabbro. The population is 50 to 100 Ma years older than the igneous population. No inherited Archean cores were found in any of the three samples.

The main conclusions of this study are summarized below. These rocks represent a relatively undifferentiated, mafic to intermediate, calc-alkaline batholith that formed above a Paleoproterozoic subduction zone. The meta-gabbro to meta-quartz diorite compositions evolved along an igneous fractionation trend. These primitive parent magmas to these rocks likely formed by partial melting of the mantle wedge but interacted with continental crust either in the source region or lower crust. The slightly younger meta-tonalites evolved along a different magmatic trend than the remainder of the metaplutonic suite and likely evolved from partial melting of subducting oceanic crust in the Paleoproterozoic subduction zone. The magmatism in the Voisey's Bay area was contemporaneous and similar in composition with calc-alkaline activity along the northern (Burwell Domain) and southern (North River-Nutak) segments of the Torngat

Orogen. This calc-alkaline magmatism may have formed along a single, 500 km long, convergent plate margin. In conclusion, both slab and wedge melting were important in forming the calc-alkaline activity of the Torngat Orogen, this suggests that the transition from slab-dominated Archean magmatism to wedge-dominated post-Archean magmatism may have occurred progressively through the Paleoproterozoic.

4.2.2 Chapter 3 – *A new perspective on the role of Paleoproterozoic metaplutonic rocks in the Voisey's Bay Ni-Cu-Co Mineralization, Labrador, Canada.*

The main focus of this paper was to consider geochemical and geological evidence that the Paleoproterozoic metaplutonic suite was important in the genesis of the Voisey's Bay Ni-Cu-Co deposit. Previous data clearly indicated that the parental mafic magma of the Voisey's Bay intrusion was contaminated by crustal rocks; however, these studies largely failed to address the role of the metaplutonic suite primarily due to the belief that this unit was geographically quite a small unit. Recent mapping, as part of this thesis (Map 1), showed that the metaplutonic suite is a much larger unit and is more voluminous in the Voisey's Bay area than the Tasiuyak paragneiss, which was the favoured crustal contaminant of the primitive Voisey's Bay magma.

Recent geochemical data support the role of the Paleoproterozoic metaplutonic rocks as a crustal contaminant. The Paleoproterozoic metaplutonic trace element chemistry is distinctive and markedly similar to the Voisey's Bay troctolite intrusion and breccia unit, particularly the presence of Th-U and Nb-Ta depletions and enriched La/Sm ratio (2.92 to 11.02) with a range of Th/Nb ratios (0.004 to 1.065). The metaplutonic suite

contains domains with sulfur values as high as 0.1 weight percent, and thus could have led to sulfur saturation of the Voisey's Bay magmas by adding either sulfur or silica. This unit is also interleaved with sulfide-rich paragneisses, which may have provided an additional source of sulfur.

The Paleoproterozoic metaplutonic suite defines two isotopically distinct groups: an enriched group with $\epsilon\text{Nd}_{(1320 \text{ Ma})}$ of -11.1 and -11.2 , $^{87}\text{Sr}/^{86}\text{Sr}_{(1320 \text{ Ma})}$ ratios between 0.7032 and 0.7050 and μ^* values of 7.66 to 7.77 ; and a more depleted group which exhibits $\epsilon\text{Nd}_{(1320 \text{ Ma})}$ values between -2.8 to -6.8 , $^{87}\text{Sr}/^{86}\text{Sr}_{(1320 \text{ Ma})}$ ratios between 0.7038 and 0.7041 and μ^* values 7.75 to 7.98 .

The trace element and isotopic compositions of the Voisey's Bay troctolite and breccia can be readily explained by 5 to 10 percent contamination of a picritic basalt magma with the enriched group of the metaplutonic rocks. The Tasiuyak paragneiss produced more subtle effects on the composition of the intrusion and probably thus played a more diminished role in crustal contamination.

New evidence from this study indicates that the Paleoproterozoic metaplutonic rocks played a key role in the crustal contamination of the Voisey's Bay troctolitic intrusion, potentially leading to sulfur saturation and precipitation of sulfides. Contamination by the metaplutonic suite may be an essential element in the formation of similar deposits in the region and elsewhere.

4.3 DIRECTIONS FOR FURTHER STUDY

Although this thesis presents a large variety of data, there exists much that can be completed in terms of future studies and research. In terms of tectonic and structural studies of formation of the Torngat orogeny, several key issues remain to be addressed. Firstly the identification, through detailed field mapping of the continuation of Paleoproterozoic metaplutonic rocks to the north or south of Voisey's Bay area is important. This may provide much needed insight into the intrusive contacts of the suite and thus constrain the orientation of subduction. In addition, a detailed metamorphic study of these rocks may shed light on the pressure-temperature-time path evolution of these rocks, and thus, the tectonic evolution of area. A more detailed isotopic study (particularly Sm-Nd) is also needed to constrain the petrogenesis of these rocks. In particular, this study should focus on whether the isotopic characteristics vary across the plutonic body (both east to west and north to south) in order to further decipher which Archean craton was being subducted in the area during the Paleoproterozoic, in addition to determining potential crustal contaminants.

In terms of the metallogenic evolution of the area, a more detailed study of the role of the metaplutonic rocks in crustal contamination of the Voisey's Bay intrusion is essential. This would focus on, evaluating the Paleoproterozoic metaplutonic rocks as a potential contaminant by further detailed studies, such as Re-Os, Sm-Nd, and detailed sulfur isotopic studies to provide further clues to the development of sulfide mineralization. In addition to the meta-plutonic suite, the Archean Nain orthogneisses have not been seriously evaluated in terms of a potential contaminant, primarily due to

the limited availability of isotopic data on these gneisses in the region. As this deposit is brought into development and mining begins, immense knowledge will be gained due to the ability to see the nature of the underground contacts and the analysis of the units at depth, which is presently limited to drill core.

References

- Amelin, Y., Li, C. and Naldrett, A.J. 1999. Geochronology of the Voisey's Bay intrusion, Labrador, Canada, by precise U-Pb dating of coexisting baddeleyite, zircon and apatite. *Lithos*, **47**: 33-51.
- Amelin, Y., Li, C., Valeyv, O. and Naldrett, A.J. 2000. Nd-Pb-Sr isotope systematics of the crustal assimilation in the Voisey's Bay and Mushuau intrusions, Labrador, Canada. *Economic Geology*, **95**: 815-80.
- Arnt, N.T. and Todt, W. 1994. Formation of 1.9-Ga-old Trans-Hudson continental crust: Pb isotopic data. *Chemical Geology*, **118**: 9-26.
- Barker, F. (editor). 1979. Trondhjemites, dacites, and related rocks. Elsevier Scientific Publication Co., 659 pp.
- Berg, J.H., Emslie, R.F., Hamilton, M.A., Morse, M.A., Ryan, A.B. and Wiebe, R.A. 1994. Anorthositic, granitoid and related rocks of the Nain Plutonic Suite. Guidebook to a field excursion to the Nain area, August 4-10, 1994: IGCP Projects 290 and 315, 69 pp.
- Bertrand, J.M., Roddick, J.C., van Kranendonk, M.J. and Ermanovics, I. 1993. U-Pb geochronology of deformation and metamorphism across a central transect of the Early Proterozoic Torngat Orogen, North River map area, Labrador. *Canadian Journal of Earth Sciences*, **30**: 1470-1489.
- Brace, T.D. and Wilton, D.H.C. 1991. Geology, geochemistry and metallogeny of the Archean Florence Lake Group and associated ultramafic and trondhjemitic rocks, southern Nain Province, central Labrador. *Canadian Mineralogist*, **28**: 419-430.
- Brenan, J.M. and Li, C. 2000. Constraints on oxygen fugacity during sulfide segregation in the Voisey's Bay intrusion, Labrador, Canada. *Economic Geology*, **95**: 901-915.
- Bridgwater, D., Rossing, M., Schiotte, L. and Austrheim, H. 1989. The effect of fluid controlled element mobility during metamorphism on whole rock isotope systems, some theoretical aspects and possible examples. *In* Fluid movements; element transport and the composition of the deep crust. *Edited by* D. Bridgwater. NATO ASI Series. Series C: Mathematical and Physical Sciences, 281, pp. 277-298.
- Cadman, A.C., Heaman, L., Tarney, J., Wardle, R.J. and Krogh, T.E. 1993. U-Pb geochronology and geochemical variations within two Proterozoic mafic dyke swarms, Labrador. *Canadian Journal of Earth Sciences*, **30**: 1490-1504.
- Calon, T.J. and Jamison, W. 1992. Structural evolution of the Eastern Boderland of the Torngat Orogen, Kiki Lake transect, Saglek Fiord area, northern Labrador. Eastern Canadian Shield Onshore-Offshore Transect (ECSOOT) Transect Meeting, LITHOPROBE Report 32, pp. 90-112.
- Calon, T.J. and Jamison, W. 1994. Structural evolution of the Eastern Boderland of the Torngat Orogen, Kiki Lake transect, Saglek Fiord area, northern Labrador. Eastern Canadian Shield Onshore-Offshore Transect (ECSOOT) Transect Meeting, LITHOPROBE Report 36, pp. 89-90.

- Campbell, L.M. 1997. Isotopic and geochemical investigations of Precambrian continental crust in the Torngat Orogen, northeastern Canada: constraints on the mechanisms of Precambrian crust formation and on the Early Proterozoic assembly of Northeastern Laurentia. Ph.D. Thesis. University of Colorado. 193 pp.
- Carlson, R.W., Weibe, R.A. and Kalamarides, R.I. 1993. Isotopic study of basaltic dikes in the Nain Plutonic Suite: evidence for enriched mantle source. *Canadian Journal of Earth Sciences*, **30**: 1141-1146.
- Chauval, C., Arndt, N.T., Kielinczuk, S. and Thom, A. 1987. Formation of Canadian 1.9 Ga old continental crust. I: Nd isotopic data. *Canadian Journal of Earth Sciences*, **24**: 396-406.
- Collerson, K.D. 1991. New field and isotopic constraints on the evolution of early Archean gneisses in Northern Labrador. Eastern Canadian Shield Onshore-Offshore Transect (ECSOOT) Transect Meeting, LITHOPROBE Report 27, pp. 96-101.
- Collerson, K.D., McCulloch, M.T. and Nutman, A.P. 1989. Sr and Nd isotope systematics of polymetamorphic Archean gneisses from southern West Greenland and northern Labrador. *Canadian Journal of Earth Sciences*, **26**: 446-466.
- Connelly, J.N. and Ryan, B. 1992. U-Pb constraints on the thermotectonic history of the Nain area. Eastern Canadian Shield Onshore-Offshore Transect (ECSOOT) Transect Meeting, LITHOPROBE Report 32, pp. 137-144.
- Connelly, J.N. and Ryan, B. 1994. Late Archean and Paleoproterozoic events in the central Nain craton. Eastern Canadian Shield Onshore-Offshore Transect (ECSOOT) Transect Meeting, LITHOPROBE Report 36, pp. 53-61.
- Connelly, J.N. and Ryan, B. 1996. Late Archean evolution of the Nain Province, Nain, Labrador: imprint of a collision. *Canadian Journal of Earth Sciences*, **33**: 1325-1342.
- Davies, D.W. 1982. Optimum linear regression and error estimations applied to U-Pb data. *Canadian Journal of Earth Sciences*, **19**: 2141-2149.
- DePaolo, D.J. 1988. Neodymium Isotope Geochemistry: an Introduction. Springer-Verlag, 187 pp.
- DePaolo, D.J. and Wasserburg, G.J. 1976. Nd isotopic variations and petrogenetic models. *Geophysical Research Letters*, **2**: 249-252.
- Dickin, A.P. Radiogenic Isotope Geology. Cambridge University Press, 490 pp.
- Emslie, R.F. 1975. Pyroxene megacrysts from anorthositic rocks: new clues to the sources and evolution of the parent magmas. *Canadian Mineralogist*, **13**: 138-145.
- Emslie, R.F. and Hegner, E. 1993. Reconnaissance isotopic geochemistry of anorthosite-mangerite-charnockite-granite (AMCG) complexes, Grenville Province, Canada. *Geochemical Geology*, **106**: 279-298.
- Emslie, R.F. and Loveridge, W.D. 1992. Fluorite bearing early and middle Proterozoic granites, Okak Bay area, Labrador: geochronology, geochemistry and petrogenesis. *Lithos*, **28**: 87-109.

- Emslie, R.F. and Stirling, J.A.R. 1993. Rapakivi and related granitoids of the Nain Plutonic Suite: geochemistry, mineral assemblages and fluid equilibria. *Canadian Mineralogist*, **31**: 821-847.
- Emslie, R.F., Hamilton, M.A. and Theriault, R.J. 1994. Petrogenesis of a mid-Proterozoic anorthosite-mangerite-charnockite-granite (AMCG) complex: isotopic and chemical evidence from the Nain Plutonic Suite. *The Journal of Geology*, **102**: 539-558.
- Ermanovics, I. 1993. Geology of the Hopedale Block, southern Nain Province, and the adjacent Proterozoic terranes, Labrador, Newfoundland. Geological Survey of Canada, Memoir 431, 161 pp.
- Ermanovics, I. and Raudsepp, M. 1979. Geology of the Hopedale block of the eastern Nain Province, Labrador. *In* Current research, Part B. Geological Survey of Canada Paper, 79-1B, pp. 341-348.
- Ermanovics, I. and van Kranendonk, M.J. 1990. The Torngat Orogen in the North-River-Nutak transect area of Nain and Churchill provinces. *Geoscience Canada*, **17**:293-296.
- Ermanovics, I.F., van Kranendonk, M.J., Corriveau, L., Mengel, F., Bridgwater, D. and Sherlock, R. 1989. The boundary zone of the Nain-Churchill provinces in the North River-Nutak map area, Labrador. *In* Current research, Part C, Canadian Shield. Geological Survey of Canada Paper, 89-1C, pp. 385-394.
- Evans-Lamswood, D.M. 1999. Physical and geometric controls on the distribution of magmatic and sulfide-bearing phases within the Voisey's Bay Nickel-Copper-Cobalt deposit, Voisey's Bay, Labrador. MSc Thesis. Memorial University of Newfoundland, 265 pp.
- Evans-Lamswood, D.M., Butt, D.P., Jackson, R.S., Lee, D.V., Muggridge, M.G., Wheeler, R.I. and Wilton, D.H.C. 2000. Physical controls associated with the distribution of sulfides in the Voisey's Bay Ni-Cu-Co Deposit, Labrador. *Economic Geology*, **95**: 749-769.
- Ewart, A. 1982. The mineralogy and petrology of Tertiary-Recent orogenic volcanic rocks: with special reference to the andesitic-basaltic compositional range. *In* Andesites. *Edited by* R.S. Thorpe. 25-27.
- Farmer, G.L. and Ball, T.T. 1993. Origin and significance of Nd isotopic provinces within the Precambrian crust of the conterminous United States. *In* The Geology of North America Vol. C-2, Precambrian: Conterminous U.S. The geological Society of America: 614-636.
- Faure, G. 1986. Principles of Isotope Geology, 2nd edition. John Wiley and Sons, 589 pp.
- Feininger, T. and Ermanovics, I. 1994. Geophysical interpretation of the Torngat Orogen along the North River-Nutak transect, Labrador. *Canadian Journal of Earth Sciences*, **31**: 722-727.
- Finn, G.C. 1989. Rb-Sr geochronology of the Archean Maggo gneiss from the Hopedale block, Nain Province, Labrador. *Canadian Journal of Earth Sciences*, **26**: 2512-2522.
- Gariépy, C. and Dupré, B. 1991. Pb isotopes and crust-mantle evolution. *In* Applications of radiogenic isotope systems to problems in geology. Mineralogical Association Of Canada- Short course handbook. *Edited by* L. Heaman and J.N. Ludden, **19**: 191-224.
- Gower, C.F., Flanagan, M.J., Kerr, A. and Bailey, D.G. 1982. The geology of the Kaipokok-Big River area, Central Mineral Belt, Labrador. Newfoundland Department of Mines and Energy, Mineral Development Division, Report 82-7, 77 pp.

- Gower, C.F., James, D.T., Nunn, G.A.G. And Wardle, R.J. 1995. The Eastern Grenville Province. *In* The Geology and Mineral Deposits of Labrador: A guide for the Exploration Geologist (Compiled by R.J. Wardle and D.H.C. Wilton). Newfoundland Department of Natural Resources – Center for Earth Resources Research Report, 73-101.
- Hamilton, M.A. 1994. Tholeiitic and weakly alkalic basaltic volcanism of the Mugford Group, northern Labrador: preliminary geochemical results. *In* Current Research, Part C. Geological Survey of Canada, Report 1994-1C, pp. 333-342.
- Hamilton, M.A. 1997. U-Pb geochronological results from Mesoproterozoic Nain Plutonic Suite, Labrador, and implications for the origin and emplacement of massif anorthosites and related rocks. COPENA conference Abstracts and proceedings, Trondheim, Norway, 2 pp.
- Hamilton, M.A., Emslie, R.F. and Ryan, B. 1998. U-Pb evidence for Paleoproterozoic anorthositic and granitoid magmatism predating the emplacement of Mesoproterozoic Nain Plutonic Suite, Labrador. GAC MAC Annual Meeting, Quebec City, 1998. Electronic Program with Abstracts.
- Heir, K.S. 1965. Radioactive elements in continental crust. *Nature*, **208**: 479-480.
- Heir, K.S. 1973. Geochemistry of granulite facies rocks and problems with their origin. *Philosophical Transactions of the Royal Society of London. Series A: Mathematical and Physical Sciences*, A273: 429-442.
- Hoffman, P.F. 1988. United plates of America, the birth of a craton: Early Proterozoic assembly and growth of Laurentia. *Annual Review of Earth and Planetary Sciences*, **16**: 543-603.
- Hoffman, P.F. 1990. Dynamics of the assembly of northeast Laurentia in Geon 18 (1.9 – 1.8 Ga). *Geoscience Canada*, **17**: 222-226.
- Horn, I., Rudnick, R.L., McDonough, W.F. 2000. Precise elemental and isotope ratio determination by simultaneous solution nebulization and laser ablation-ICP-MS: application to U-Pb geochronology. *Chemical Geology*, **164**: 281-301.
- Irvine, T.N. and Barager, W.R.A. 1971. A guide to the chemical classification of the common volcanic rocks. *Canadian Journal of Earth Sciences*, **8**: 523-528.
- Jacobsen, S.B. 1988. Isotopic constraints on crustal growth and recycling. *Earth and Planetary Science Letters*, **90**: 315-329.
- Jaffey, A.H., Flynn, K.F., Glendenin, L.E., Bentley, W.C. and Essing, A.M. 1971. Precision measurements of half-lives of ^{235}U and ^{238}U . *Physics Review C*, **4**: 1889-1906.
- James, D.T. 1993. Geology of the Ashuanipi Complex in western Labrador. Newfoundland Department of Mines and Energy, Open File Maps 93-17 and 93-18.
- James, D.T. 1995. The Superior Province. *In* The Geology and Mineral Deposits of Labrador: A guide for the Exploration Geologist (Compiled by R.J. Wardle and D.H.C. Wilton). Newfoundland Department of Natural Resources – Center for Earth Resources Research Report, pp. 24-25.

- James, D.T. 1997. The Archean Hunt River greenstone belt, Hopedale Block, eastern Labrador (NST 13/7 and 13N.10): Geology and exploration potential. *In* Current Research. Newfoundland Department of Mines and Energy, Geological Survey Branch, Report 97-1 pp. 9-27.
- James, D.T., Connelly, J.N., Wasteneys, H.A. and Kinfoil, G.J. 1996a. Paleoproterozoic lithotectonic divisions of the southeastern Churchill Province, western Labrador. *Canadian Journal of Earth Sciences*, **33**: 216-230.
- James, D.T., Miller, R.R., Patey, R.P. and Thibodeau, S. 1996b. Geology and mineral potential of the Archean Florence Lake greenstone belt, Hopedale Block (Nain Province), eastern Labrador. *In* Current Research. Newfoundland Department of Mines and Energy, Geological Survey Branch, Report 96-1: pp. 85-17.
- James, D.T., Krogh, T., Kamo, S. 1997. Evolution of Archean supracrustal sequences in the Hopedale Block, southern Nain Province (Labrador): Preliminary U-Pb geochronological data. Eastern Canadian Shield Onshore-Offshore Transect (ECSOOT) Transect Meeting, LITHOPROBE Report 61, pp. 135-156.
- Jenner, G.A., Longerich, H.P., Jackson, S.E. and Fryer, B.J. 1990. ICP-MS—A powerful tool for high-precision trace-element analysis in Earth sciences: evidence from analysis of selected U.S.G.S. reference samples. *Chemical Geology*, **83**: 133-148.
- Jensen, L.S. 1976. A new cation plot for classifying subalkalic volcanic rocks. Ontario Division of Mines, Miscellaneous Paper 66.
- Kamo, S.J., Gower, C.F. and Krogh, T.E. 1989. Birthdate for the Iapetus Ocean? A precise U-Pb badellyite age for the Long Range dykes, southeast Labrador. *Geology*, **17**: 602-605.
- Korstgaard, J.A., Ryan, B., Wardle, R.J. 1987. The boundary between Proterozoic and Archean crustal blocks in central west Greenland and northern Labrador. *In* Evolution of the Lewisian and Comparable Precambrian High Grade Terrains. *Edited by* R.G. Park, J. Tarney, Geological Society Special Publication, **27**: 247-259.
- Krogh, T.E. 1973. A low-contamination method for hydrothermal decomposition of zircon and extraction of U and Pb for isotopic age determination. *Geochemica and Cosmochimica Acta*, **37**: 485-494.
- Krogh, T.E. 1982. Improved accuracy of U-Pb zircon ages by the creation of more concordant systems using an air abrader. *Geochemica and Cosmochimica Acta*, **46**: 637-649.
- Lambert, D.D., Foster, J.G., Frick, L.R., Li, C. and Naldrett, A.J. 1999. Re-Os isotopics systematics of the Voisey's Bay Ni-Cu-Co magmatic ore system Labrador, Canada. *Lithos*, **47**: 69-88.
- Lambert, D.D., Frick, L.R., Foster, J.G., Li, C. and Naldrett, A.J. 2000. Re-Os isotope systematics of the Voisey's Bay Ni-Cu-Co magmatic sulfide system Labrador, Canada: II. Implications for parental magma chemistry, ore genesis and metal redistribution. *Economic Geology*, **95**: 867-888.
- Le Maitre, R.W. 1976. Some problems of the projection of chemical data into mineralogical classifications. *Contributions to Mineralogy and Petrology*, **56**: 181-189.

- Le Maitre, R.W. (editor). 1989. *A Classification of Igneous Rocks and Glossary of Terms*. Blackwell, Oxford. 193 pp.
- Li, C., Lightfoot, P.C., Amelin, Y. and Naldrett, A.J. 2000. Contrasting petrological and geochemical relationships in the Voisey's Bay and Mushuau intrusions, Labrador, Canada: implications for ore genesis. *Economic Geology*, **95**: 771-799.
- Li, C. and Naldrett, A.J. 2000. Melting reactions of gneissic inclusions with enclosing magma at the Voisey's Bay, Labrador, Canada: implications with respect to ore genesis. *Economic Geology*, **95**: 801-814.
- Lightfoot, P.C. and Hawkesworth C.J. 1997. Flood basalt and magmatic Ni, Cu, and PGE sulphide mineralization: comparative geochemistry of the Noril'sk (Siberian traps) and West Greenland sequences. *American Geophysical Union Geophysical Monograph*, **100**: 357-380.
- Lightfoot, P.C. and Naldrett, A.J. 1999. Geological and geochemical relationships in the Voisey's Bay intrusion, Nain Plutonic Suite, Labrador, Canada. *Geological Association of Canada Short Course Notes*, **13**: 1-30.
- Longerich, H.P. 1989a. Mass spectrometric determinations of the temperature of an argon inductively coupled plasma from the formation of the singly charged monoxide rare earths and their dissociation energies. *Journal of analytical atomic spectrometry*, **4**: 491-497.
- Longerich, H.P. 1989b. The effects of nitric acid, acetic acid and ethanol on inductively coupled plasma-mass spectrometric ion signals as a function of nebulizer gas flow, with implications on matrix suppression and enhancements. *Journal of analytical atomic spectrometry*, **4**: 665-677.
- Longerich, H.P. 1989c. Automatic shutoff circuit for use on a Sciex-Perkin Elmer ELAN ICP-MS. *ICP Information Newsletter*, **15**: 157-160.
- Longerich, H.P. 1993. Application of a new tested LiF200 crystal of X-ray fluorescence analysis of geological samples. *X-ray Spectrometry*, **22** (2): 114-118.
- Longerich, H.P. 1995. Analysis of pressed pellets of geological samples using wavelength-dispersive X-ray fluorescence spectrometry. *X-ray Spectrometry*, **24**: 123-125.
- Longerich, H.P., Strong, D.F. and Kantipuly, C.J. 1986. Progress in evaluation of instrumental and other parameters affecting chemical and isotopic analysis by inductively coupled plasma-mass spectrometry (ICP-MS). *Canadian Journal of Spectroscopy*, **31**(5): 111-121.
- Longerich, H.P., Jenner, G.A., Fryer, B.J. and Jackson, S.E. 1990. Inductively coupled plasma-mass spectrometry analysis of geological samples: a critical evaluation based on case studies. *Chemical Geology*, **83**: 105-118.
- Loveridge, W.D., Ermanovics, I.F. and Sullican, R.W. 1987. U-Pb ages on zircon from the Maggo Gneiss, the Kanairiktok Plutonic suite and the Island Harbour Plutonic Suite, coastal of Labrador, Newfoundland. In *Radiogenic Age and Isotopic Studies*, Report 1. Geological Survey of Canada, Paper 87-2, pp. 56-65.

- Maclean, W.H. 1969. Liquidus phase relations in the FeS-FeO-Fe₃O₄-SiO₂ systems and their application in geology. *Economic geology*, **64**: 865-884.
- McCulloch, M.T. and Gamble, J.A. Geochemical and geodynamical constraints on subduction zone magmatism. *Earth and Planetary Science Letters*, **120**: 358-374.
- Manhes G., Allegre C.J., Dupre B. and Hamelin B. 1980. Lead isotope study of basic-ultrabasic layered complexes: speculations about the age of the Earth and primitive mantle characteristics. *Earth Planetary Science Letters*, **47**: 370-382.
- Martin H. 1994. The Archean grey gneisses and the genesis of continental crust. *In Archean crustal evolution. Edited by K.C. Condie. Elsevier. pp. 205-261.*
- Mengel, F. C. 1984. Preliminary results of mapping in the Ramah Group and adjacent gneisses south of Saglek Fiord, northern Labrador. *In Current research. Government of Newfoundland and Labrador. Department of Mines and Energy, Mineral Development Division, 84-1: 21-29.*
- Mengel, F. 1985. Nain-Churchill province boundary: a preliminary report on a cross-section through the Hudsonian Front in the Saglek Fiord area, northern Labrador. *In Current research. Government of Newfoundland and Labrador. Department of Mines and Energy. Mineral Development Division, 85-1: 33-42.*
- Mengel, F. and Rivers, T. 1990. The synmetamorphic P-T-t path of granulite-facies gneisses from the Torngat Orogen, and its bearing on their tectonic history. *Geoscience Canada, 17-4: 288-293.*
- Mengel, F.C. 1988. Thermotectonic evolution of the Proterozoic-Archean boundary in the Saglek area, northern Labrador. Ph.D. thesis. Memorial University of Newfoundland, 355 pp.
- Mengel, F., Rivers, T. and Reynolds, P. 1991. Lithotectonic elements and tectonic evolution of Torngat Orogen, Saglek Fiord, northern Labrador. *Canadian Journal of Earth Sciences, 28-9: 1407-1423.*
- Morse, S.A. 1969. The Kiglapait Layered Intrusion, Labrador. *Geological Society of America Memoir. 112, 204 pp.*
- Naldrett, A.J. 1973. Nickel sulfide deposits: Classification, composition and genesis. *Economica Geology 75th Anniversary Volume. pp. 628-685.*
- Naldrett, A.J. 1989. *Magmatic Sulfide Deposits. N.Y. Oxford, Clarendon Press-Oxford University Press, 186 pages.*
- Naldrett, A.J., Asif, M., Kristic, S. and Li, C. 2000a. The composition of mineralization of the Voisey's Bay Ni-Cu sulfide deposit, with special reference to platinum-group elements. *Economic Geology, 95: 845-865.*
- Naldrett, A.J. and MacDonald, A.J. 1980. Tectonic settings of the Ni-Cu sulfide ores: their importance in genesis and exploration. *In The Continental Crust and Its Mineral Deposits. Edited by D.W. Stangway. Geological Association of Canada Special Paper 20: pp. 633-657.*

- Naldrett, A.J., Federenko, V.A., Mohammed, A., Lin, S., Kunilov, V.E., Stekhin, A.I., Lightfoot, P.C. and Gorbachev, N.S. 1996b. Controls on the composition of Ni-Cu sulfide deposits as illustrated by those at Noril'sk, Siberia. *Economic Geology*, **91**: 751-773.
- Naldrett, A.J., Keats, H., Sparkes, K. and Moore, R. 1996. Geology of the Voisey's Bay Ni-Cu-Co Deposit, Labrador, Canada. *Exploration and Mining Geology*, **5**: 169-179.
- Naldrett, A.J., Singh, J., Krstic, S. and Li, C. 2000b. The mineralogy of the Voisey's Bay Ni-Cu-Co deposit, northern Labrador, Canada; influence of oxidation state on textures and mineral compositions. *Economic Geology*, **95**: 889-900.
- Newton, R.C. 1992. An overview of chernokite. *Precambrian Research*, **55**:399-405.
- Nutman, A.P. and Collerson, K.D. 1991. Very early Archean crustal-accretion complexes preserved in North Atlantic craton. *Geology*, **19**: 791-794.
- Nutman, A.P., Fryer, B.J. and Bridgwater, D. 1989. The early Archean Nulliak (supracrustal) assemblage, northern Labrador. *Canadian Journal of Earth Sciences*, **26**: 2159-2168.
- Percival, J.A. 1990. Archean tectonic setting of granulite terranes of the Seperior Province, Canada: a view from the bottom. *In Granulites and Crustal Differentiation. Edited by D. Vielzeuf and P. Vidal*, pp. 171-193.
- Pearce, J.A., Harris, N.B.W. and Tindel, A.G. 1984. Trace element discrimination diagrams for tectonic interpretation of granitic rocks. *Journal of Petrology*, **25**: 956-983.
- Potts, P.J., Tindle, A.G. and Webb, P.J. 1992. *Geochemical Reference Material Compositions*. CRC Press Inc., Boca Raton, 313 pages.
- Raith, M.M., Sriantappa, C., Buhl, D. and Koehler, H. 1999. The Nilgiri enderbites, South India: nature and age constraints on protolith formation, high-grade metamorphism and cooling history. *Precambrian Research*, **98**: 129-150.
- Ripley, E.M. 1981. Sulfur isotopic abundances of the Dunka Road Cu-Ni deposit, Duluth Complex, Minnesota. *Economic Geology*, **76**: 610-620.
- Ripley, E.M. 1986. Applications of stable isotope studies to problems of magmatic sulfide ore genesis with special reference to the Duluth Complex, Minnesota. *In Geology and Metallogeny of Copper Deposits. Edited by G.H. Friedrich, A.D. Genkin, A.J. Naldrett, J.D. Ridge and R.H. Sillitoe*. Society of Geology Applied to Ore Deposits Special Publication 4. Springer-Verlag, Heidelberg, pp. 25-42.
- Ripley, E.M. 1990a. Platinum-group element geochemistry of Cu-Ni mineralization in the Basal Zone of the Babbit deposit, Duluth Complex, Minnesota. *Economic Geology*, **85**: 830-841.
- Ripley, E.M. 1990b. Se/S ratios of the Virginia Formation and the Cu-Ni sulfide mineralization in the Babbit area, Duluth Complex, Minnesota. *Economic Geology*, **85**: 1935-1940.
- Ripley, E.M., Park, Y., Li, C. and Naldrett, A.J. 1999. Sulfur and oxygen isotopic evidence of country rock contamination in the Voisey's Bay Ni-Cu-Co deposit, Labrador, Canada. *Lithos*, **47**: 53-68.

- Ripley, E.M., Park., Y., Li, C. and Naldrett, A.J. 2000. Oxygen isotope studies of the Voisey's Bay Ni-Cu-Co deposit, Labrador, Canada. *Economic Geology*, **95**: 831-844.
- Rivers, T. 1997. Lithotectonic elements of the Grenville Province: review and tectonic implications. *Precambrian research*, **86**: 117-154.
- Rivers, T., Martingole, J., Gower, C.F. and Davidson, A. 1989. New tectonic divisions of the Grenville Province, southeast Canadian Shield. *Tectonics*, **8**: 63-84.
- Rivers, T., Mengel, F., Scott, D.J., Campbell, L.M. and Goulet, N. 1996. Torngat Orogen: a Paleoproterozoic example of a narrow doubly vergent collisional orogen. *In* Precambrian crustal evolution in the North Atlantic region. *Edited by* T.S. Brewer. Geological Society of London Special Publications, **112**: 117-136.
- Rollinson, H.R. 1993. *Using Geochemical Data: evaluation, presentation, interpretation*. Longman Scientific and Technical, John Wiley and Sons, 352 pp.
- Rogers, J.J.W. and Adams J.A.S. 1978. Th: Abundances in common igneous rocks. *In* Handbook of Geochemistry. *Edited by* K.H. Wedepohl. Springer-Verlag, pp 1-12.
- Rudnick, R.L. and Fountain, D.M. 1995. Nature and composition of the continental crust: A lower crustal perspective. *Reviews of Geophysics*, **33**: 267-309.
- Rudnick, R.L. and Goldstein, S.L. 1990. The Pb isotopic compositions of lower crustal xenoliths and the evolution of lower crustal Pb. *Earth and Planetary Science Letters*, **98**: 192-207.
- Rudnick, R.L., McLennan, S.M. and Taylor, S.R. 1985. Large ion lithophile elements in rocks from high-pressure granulite facies terrains. *Geochimica et Cosmochimica Acta*, **49**: 1645-1655.
- Ryan, B. 1983. The Nain-Churchill boundary in the Hebron area of northern Labrador: summary report. *In* Preliminary current research reports. Government of Newfoundland and Labrador, Department of Mines and Energy, Mineral Development Division, **83**: 3-4.
- Ryan, B. 1984. Regional geology of the central part of the Central Mineral Belt, Labrador. *In* Memoir - Government of Newfoundland and Labrador, Department of Mines and Energy, Mineral Development Division, **3**: 185.
- Ryan, B. 1990a. Preliminary geological map of the Nain Plutonic Suite and surrounding rocks (Nain-Nutak, NST 14SW). Newfoundland Department of Mines and Energy, 90-44.
- Ryan, B. 1990b. Does the Labrador-Quebec border area of the Rae (Churchill) Province preserve vestiges of an Archean history? *Geoscience Canada*, **17**: 225-229.
- Ryan, B. 1991. Makhavinekh Lake pluton, Labrador, Canada: geological setting, subdivisions, mode of emplacement and comparison with Finnish rapakivi granites. *Precambrian Research*, **51**: 193-225.
- Ryan, B. 1995. Anorthosite-granite (AMCG) suites. *In* The Geology and Mineral Deposits of Labrador: A guide for the Exploration Geologist (Compiled by R.J. Wardle and D.H.C. Wilton). Newfoundland Department of Natural Resources – Center for Earth Resources Research Report, pp. 53-67.

- Ryan, B. 1997. The Mesoproterozoic Nain Plutonic Suite in eastern Canada, and the setting of the Voisey's Bay Ni-Cu-Co sulfide deposit. *Geoscience Canada*, **24**: 173-181.
- Ryan, A.B. and Lee, D. 1985. Geological Map of the Reid Brook Area, Labrador North District (NTS 14D/8). Government of Newfoundland and Labrador, Department of Natural Resources, Geological Survey Branch, Map 89-18.
- Ryan, B. and Emslie, R.F. 1994. Pre-Elsonian mafic magmatism in the Nain igneous complex, Labrador: the Bridges layered intrusion-comment. *Precambrian Research*, **68**: 179-181.
- Ryan, B. and Morse, S.A. 1985. Nain Plutonic Suite. *In* *Lexicon of Canadian Stratigraphy, Volume VI. Editors G.L. Williams, L.R. Fyfe, R.J. Wardle, S.P. Colman-Sadd, R.C. Boehner and J.A. Watt. Canadian Society of Petroleum Geologists*, pp. 266-267.
- Ryan, B., Krogh, T.E., Heaman, L., Scharer, U., Philippe, S. and Oliver, G. 1991. On recent geochronological studies in the Nain Province, Churchill Province, and the Nain Plutonic Suite. *In* *Current Research, Newfoundland Department of Mines and Energy, Geological Survey Branch, Current Research, Report 91-1*, pp. 257-261.
- Ryan, B., Hynes, A. and Ermanovics, I. 1997. Geology of the Nain Plutonic Suite and its country-rock envelope, Alliger Lake area (NST 14E/1), Labrador. *In* *Current Research, Newfoundland Department of Mines and Energy, Geological Survey Branch, Current Research, Report 97-1*, pp. 29-47.
- Ryan, B., Phillips, E., Shwetz, J. and Machado, G. 1998. A tale of more than ten plutons. [Geology of the region between Okak Bay and Staghorn Lake, Labrador (part of NTS Maps 14E/2,7,8)]. *In* *Current Research, Newfoundland Department of Mines and Energy, Geological Survey Branch, Current Research, Report 98-1*, pp. 143-171.
- Ryan, B., Wardle, R.J., Gower, C.F., and Nunn, G.A.C. 1995. Nickel-copper-sulphide mineralization in Labrador: the Voisey's Bay discovery and its exploration implications. *In* *Current Research, Geological Survey, Department of Natural Resources, Government of Newfoundland and Labrador, Report 95-1*, pp. 177-204.
- Scoates, J.S. and Mitchell, J.A.N. 2000. The evolution of troctolitic and high al basaltic magmas in Proterozoic anorthosite plutonic suites and implications for the Voisey's Bay Massive Ni-Cu sulfide Deposit. *Economic Geology*, **95**: 677-701.
- Scott, D.J. 1995a. U-Pb geochronology of the Nain craton on the eastern margin of the Torngat Orogen, Labrador. *Canadian Journal of Earth Sciences*, **32**: 1859-1869.
- Scott, D.J. 1995b. U-Pb geochronology of a Paleoproterozoic continental magmatic arc on the western margin of the Archean Nain craton, northern Labrador, Canada. *Canadian Journal of Earth Sciences*, **32**: 1870-1882.
- Scott, D.J. 1998. An overview of the U-Pb geochronology of the Paleoproterozoic Torngat Orogen, northeastern Canada. *Precambrian Research*, **91**: 91-107.

- Scott, D.J. and Campbell, L.M. 1993. Evolution of the Paleoproterozoic Torngat Orogen, Labrador, Canada: Recent advances using U-Pb geochronology and Nd isotope systematics. In Geological Society of America. Programs with Abstracts, **35**: A-237.
- Scott, D.J. and Gauthier, G. 1996. Comparison of TIMS (U-Pb) and laser ablation microprobe ICP-MS (Pb) techniques for age determination of detrital zircons from Paleoproterozoic metasedimentary rocks from northeastern Laurentia, Canada, with tectonic implications. *Chemical Geology*, **131**: 127-142.
- Scott, D.J. and Machado, N. 1994. U-Pb geochronology of northern Torngat Orogen: implications for the evolution of NE Laurentia. *In*: Precambrian crustal evolution in the North Atlantic regions. *Terra Nova*: **6-2**: 17.
- Scott, D.J. and Machado, N. 1995. U-Pb geochronology of the northern Torngat Orogen, Labrador, Canada: a record of Paleoproterozoic magmatism and deformation. *Precambrian Research*, **70**: 169-190.
- Schiøtte, L., Compston, W. and Bridgwater, D. 1989a. U-Th-Pb ages of single zircons in Archean supracrustals from Nain Province, Labrador, Canada. *Canadian Journal of Earth Sciences*, **26**: 2636-2644.
- Schiøtte, L., Compston, W. and Bridgwater, D. 1989b. Ion probe U-Th-Pb zircon dating in polymetamorphic orthogneisses from northern Labrador, Canada. *Canadian Journal of Earth Sciences*, **26**: 1533-1556.
- Schiøtte, L., Noble, S. and Bridgwater, D. 1990. Petrological and whole rock isotopic characteristics of tectonically juxtaposed Archean gneisses in the Okak area of the Nain Province, Labrador: relevance for terrane models. *Precambrian Research*, **63**: 239-323.
- Shaw, D.M. 1968. A review of K-Rb fractionation trends by covariance analysis. *Geochimica et Cosmochimica Acta*, **32**:573-601.
- Smyth, W.R. and Knight, I. 1978. Correlation of Archean supracrustal sequence, Nain Province, Northern Labrador. *In* Report of Activities for 1977, Newfoundland Department of Mines and Energy, Report 76-1, pp. 59-64.
- Stacey, J.S. and Kramers, J.D. 1975. Approximation of terrestrial lead isotope evolution by a two-stage model. *Earth and Planetary Science Letters*, **26**: 207-221.
- Stern, R.J. and Dowoud, A.S. 1991. Late Precambrian (740 Ma) charnokite, enderbite and granite from Jebel Moya, Sudan: a link between Mozambique Belt and the Arabian-Nubian Shield? *Journal of Geology*, **99**: 649-660.
- Stern, R.A., Percival, J.A. and Mortensen, J.K. 1994. Geochemical evolution of the Minto block: a 2.7 Ga continental magmatic arc built on the Superior proto-craton. *Precambrian Research*, **65**: 115-153.
- Sun S.-S. 1980. Lead isotopic study of young volcanic rocks from mid-oceanic ridges, ocean island and island arcs. 1980. *Philosophical Transactions of the Royal Society of London, Series A: Mathematical and Physical Sciences*, **297**: 409-445.

- Sun S.-S. and McDonough, W.F. 1989. Chemical and isotopic systematics of oceanic basalts: implications for mantle composition and process. Geological Society [London], Special Publication, 42: 313-345.
- Taylor, F.C. 1971. A revision of Precambrian structural provinces in northeastern Quebec and northern Labrador. Canadian Journal of Earth Sciences, 8: 579-584.
- Taylor, F.C. 1979. Reconnaissance geology of a part of the Precambrian Shield in northeastern Quebec, northern Labrador and Northwestern Territories. Geological Survey of Canada, Memoir 393, 313 pp.
- Taylor, S.R. and McLennan, S.M. 1985. The Continental Crust: its Composition and Evolution. Blackwell Scientific Publications, 312 pp.
- Theriault, R.J. and Ermanovics, I. 1997. Sm-Nd isotopic and geochemical characterisation of the Paleoproterozoic Torngat orogen, Labrador, Canada. Precambrian Research, 81: 15-35.
- Theriault, R.J., Hamilton, M.A. and Ermanovics, I. 1994. Nd isotopic and geochemical investigations in the Torngat Orogen, North River-Nutak Area, Eastern Canadian Shield Onshore-Offshore Transect (ECSOOT) Transect Meeting, LITHOPROBE Report 45, pp. 83-89.
- Touret, J.L.R. 1996. LILE-depletion in granulites: Myth or reality? In Petrology and Geochemistry of magmatic suites of rocks in the continental and oceanic crusts. A volume dedicated to Professor Jean Michot. Edited by D. Demaitfe, pp. 53-72.
- van Kranendonk, M.J. 1990. Structural history and geotectonic evolution of the eastern Torngat Orogen in the North River map area, Labrador. In: Current research: Part C, Canadian Shield. Geological Survey of Canada, Paper, pp. 81-96.
- van Kranendonk, M.J. 1996. Tectonic evolution of the Paleoproterozoic Torngat Orogen: evidence from pressure-temperature-time-deformation paths in the North River map area, Labrador. Tectonics, 15: 843-869.
- van Kranendonk, M.J. and Ermanovics, I. 1990. Structural evolution of the Hudsonian Torngat Orogen in the North River map area, Labrador: evidence for east-west transpressive collision of Nain and Rae continental block. Geoscience Canada, 17: 238-288
- van Kranendonk, M.J. and Scott, D.J. 1992. Preliminary report on the geology and structural evolution of the Komaktorvik Zone of the Early Proterozoic Torngat Orogen, Eclipse Harbour area, northern Labrador. In Current Research, Part C, Geological Survey of Canada, Paper 92-1C, pp. 59-68.
- van Kranendonk, M.J. and Wardle, R.J. 1996. Burwell domain of the Paleoproterozoic Torngat Orogen, northeastern Canada: titled cross-section of a magmatic arc caught between a rock and a hard place. In Precambrian Crustal Evolution in the North Atlantic Region. Edited by T.S. Brewer. Geological Society of London Special Publication, 112: 91-115.
- van Kranendonk, M.J. and Wardle, R.J. 1997. Crustal-scale flexural slip folding during late tectonic amplification of an orogenic boundary perturbation in the Paleoproterozoic Torngat orogen, northeastern Canada. Canadian Journal of Earth Sciences, 34: 1545-1565.

- van Kranendonk, M.J., Wardle, R.J., Mengel, F.C., Campbell, L.M. and Reid, L. 1994. New results and summary of the Archean and Paleoproterozoic geology of the Burwell domain, northern Torngat Orogen, Labrador, Quebec and Northwest Territories. *In* Current Research, Geological Survey of Canada, Paper 1994-C, pp. 321-332.
- van Kranendonk, M.J., Wardle, R.J., Mengel, F.C., Ryan, B. and Rivers, T. 1992. Lithotectonic divisions of the northern part of the Torngat Orogen, Labrador, Quebec and N.W.T. Eastern Canadian Shield Onshore-Offshore Transect (ECSOOT) Transect Meeting, LITHOPROBE Report 32, pp. 21-31.
- Wardle, R.J. 1983. Nain-Churchill province cross-section, Nachvak Fiord, Northern Labrador. *In* Current Research, Government of Newfoundland and Labrador, Department of Mines and Energy, Mineral Development Division Newfoundland, Report 83-1, pp. 68-69.
- Wardle, R.J. 1984. Nain-Churchill province cross-section, Riviere Baudancourt-Nachvak Lake. *In* Current Research, Government of Newfoundland and Labrador, Department of Mines and Energy, Mineral Development Division Newfoundland, Report 84-11, pp. 1-11.
- Wardle, R.J. 1995. Introduction. *In* The Geology and Mineral Deposits of Labrador: A guide for the Exploration Geologist (Compiled by R.J. Wardle and D.H.C. Wilton). Newfoundland Department of Natural Resources – Center for Earth Resources Research Report, pp. 2-14.
- Wardle, R.J. and Wilton, D.H.C. 1995. The Nain Province. *In* The Geology and Mineral Deposits of Labrador: A guide for the Exploration Geologist (Compiled by R.J. Wardle and D.H.C. Wilton). Newfoundland Department of Natural Resources – Center for Earth Resources Research Report, pp. 14-24.
- Wardle, R.J., Bridgwater, D., Mengel, F., Campbell, L., van Kranendonk, M.J., Hauman, A., Churchill, R. and Reid, L. 1994. Mapping in the Torngat Orogen, northernmost Labrador: Report 3, the Nain Craton (including a note on ultramafic dyke occurrences in northernmost Labrador). *In* Current Research, Government of Newfoundland and Labrador, Department of Mines and Energy, Mineral Development Division Newfoundland, Report 94-1, pp. 399-407.
- Wardle, R.J., Gower, C.F., Ryan, B., Nunn, G.A., James, D.T. and Kerr, A. 1997. Geological Map of Labrador: 1:1 million scale. Government of Newfoundland and Labrador, Department of Mines and Energy, Geological Survey, Map 97-07.
- Wardle, R.J., Ryan, B., Nunn, G.A.G. and Mengel, F.C. 1990. The eastern Churchill Province, Torngat and New Quebec orogens: An overview. *Geoscience Canada*, 17: 217-222.
- Wardle, R.J., Swinden, S. and James, D.T. 1995. The Southeastern Churchill Province. *In* The Geology and Mineral Deposits of Labrador: A guide for the Exploration Geologist (Compiled by R.J. Wardle and D.H.C. Wilton). Newfoundland Department of Natural Resources – Center for Earth Resources Research Report, pp. 26-42.
- Wardle, R.J., van Kranendonk, M.J., Mengel, F. and Scott, D. 1992. Geological mapping in the Torngat Orogen, northernmost Labrador: preliminary results. *In* Current Research, Government of

- Newfoundland and Labrador. Department of Mines and Energy. Geological Survey Branch. Report 92-1: pp. 413-429.
- Wheeler, E.P. 1942. Anorthosite and associated rocks about Nain, Labrador. *Journal of Geology*, **50**: 611-642.
- Wheeler, E.P. 1960. Anorthosite-adamellite complex of Nain, Labrador. *Geological Society of America Bulletin*, **71**: 1755-1762.
- Wiebe, R.A. 1980. Commingling of contrasted magmas in the plutonic environment: examples from the Nain anorthosite complex. *Journal of Geology*, **88**: 197-209.
- Wiebe, R.A. 1985. Proterozoic basalt dikes in the Nain anorthosite complex, Labrador. *Canadian Journal of Earth Sciences*, **22**: 1149-1157.
- Wiebe, R.A. 1990. Dioritic rocks in the Nain Complex, Labrador. *Scheizerische Mineralogische und Petrographische Mitteilungen*, **70**: 199-208.
- Wooden, J.L., Czamanske, G.K., Fedorenko, V.A., Arndt, N.T., Chauvel, C., Bouse, R.M., King, B.-S.W., Knight, R.J. and Siems, D.F. 1993. Isotopic and trace-element constraints on mantle and crustal contributions to Siberian continental flood basalts, Noril'sk area, Siberia. *Geochemica et Cosmochemica Acta*, **57**: 3677-3704.

Appendix A

Analytical Methods

A.1 MAJOR AND TRACE ELEMENT ANALYSES

The following is a description of the analytical techniques used to determine the major and trace element whole rock geochemical data presented throughout this thesis.

The sample preparation begins with the selection of large (5-12 kg) representative rock samples that have any weathered surfaces removed. The samples are crushed in a clean jaw crusher, and to minimize cross-contamination small amounts of sample were crushed and discarded before final crushing. A tungsten-carbide puck mill was used to powder the randomly selected rock chips to a size of <200 mesh. Between each sample the puck mill was extensively cleaned, and in order to avoid cross-contamination of samples, a small amount of the rock chips was pulverised and discarded prior to final powdering. The sample was then stored in a clean plastic vial. All aspects of the sample preparation were carried out at Memorial University of Newfoundland, Department of Earth Sciences.

A.1.1. X-ray Fluorescence (XRF)

Major oxides and selected trace elements were analysed as pressed powder pellets at Memorial University of Newfoundland, Department of Earth Sciences, X-Ray Fluorescence (XRF) Lab and were performed using the Fisons/ARL 8420+ sequential wavelength-dispersive X-Ray spectrometer. The pellets were made from 5.00 g of fresh rock powder and 0.70 g BRP-5933 Bakelite phenolic resin that had been placed in a glass

jar and homogenized for ten minutes on a roller mixer. The resulting mixture was placed in a Herzog pellet press (29 μm diameter) for 5 seconds at a pressure of 20 tons. The samples were then baked in an oven for 15 minutes at 200 °C and labelled on the side in contact with the oven tray. Further details on the sample preparation are outlined in Longerich (1995).

The data are collected by an automated computer system attached to the XRF. Along with the pressed pellets, four quality control reference materials (AVG-1, DNC-1, JG-2, BCR-1), and five internal standards were analysed (Longerich, 1995). The reference materials used include 1) PACS-1, National Research Council of Canada reference material; 2) BHVO-1, DST-1, United States Geological Survey (USGS) reference standards (basalt, dunite); SY-2 and SY-3, syenite from the Canadian Certified Reference Materials Project (CCRMP). Published data on these standards can be found in Potts et al. (1992), Jenner et al. (1990) and Longerich et al. (1990).

Detailed analytical procedures including calibration and matrix corrections, precision and accuracy, have been described by Longerich (1995). The limits of detection vary depending on the element group. The major element analysis is only semi-quantitative, but still provides a good approximation of the major oxide compositions. Limits of detection for major oxides range from 120 ppm for Na_2O and MgO to less than 20 ppm for MnO , K_2O and CaO , detection limits for trace elements are (in brackets as ppm): Sc(6), V(6), Cr(7), Ni(5), Cu(4), Zn(3), Ga(3), Rb(0.7), Sr(1.2), Y(0.7), Zr(1.2), Nb(0.7), Ba(23) and Pb(4) (values after Longerich, 1995). The five standards are run to determine precision and accuracy of analysis. For the major oxides a precision and

accuracy of <1% for concentrations above 1% and <3% for concentrations below 1% was determined. Trace element analysis had a precision and accuracy of below 1% for most elements, except for Zn (4%). Table A.1 presents the precision and accuracy for standard DNC-1 (diabase) from the period analytical data was collected for this thesis.

A.1.2 Inductively Coupled Plasma Mass Spectrometry (ICP-MS)

The majority of the samples analysed for trace elements and the REE were prepared by the HF-HNO₃ method. The masses measured were ⁷Li, ⁸⁵Rb, ⁸⁶Sr, ⁸⁹Y, ⁹⁰Zr, ⁹³Nb, ⁹⁵Mo, ¹³³Cs, ¹³⁷Ba, ¹³⁹La, ¹⁴⁰Ce, ¹⁴¹Pr, ¹⁴⁵Nd, ¹⁴⁷Sm, ¹⁵¹Eu, ¹⁵⁷Gd, ¹⁵⁹Tb, ¹⁶⁰Gd, ¹⁶³Dy, ¹⁶⁵Ho, ¹⁶⁷Er, ¹⁶⁹Tm, ¹⁷³Yb, ¹⁷⁵Lu, ¹⁷⁷Hf, ¹⁸¹Ta, ²⁰³Tl, ²⁰⁶Pb, ²⁰⁷Pb, ²⁰⁸Pb, ²⁰⁹Bi, ²³²Th, ²³⁸U and ²⁵⁴(UO). This sample preparation procedure is summarized after Jenner et al. (1990) and involves the digestion of a 0.1 g powdered sample aliquot by HF and NO₃ in screw-top Teflon bombs. The sample is rehydrated with HF-HNO₃, evaporated to dryness, rehydrated with 2-3 ml of 8N HNO₃, and then transferred to a 125 ml bottle and diluted to 90 g with water.

The sample is then analysed using a modified SCIEX ELAN model 250 ICP-MS, the modifications have been described in Longerich et al. (1986), Longerich (1989a, b, c and 1993) and Jackson et al. (1990). Data acquisition is completed, using software supplied by SCIEX. The concentration calculations are done offline using a commercial spreadsheet program.

The analysis package used (exploration) can run up to 27 samples, including reference materials, reagent blanks, and duplicates. Data are acquired in runs of 9 cycles of 12 solutions: 2 standards, 1 flush, 1 calibration blank (0.2 N HNO₃), first sample, first

sample (spiked), flush. second sample, second sample (spiked), flush. third sample. third sample (spiked), flush. The spike is used as an internal standard and is added to the second set of samples offline at 1:1 and is a solution containing Li, Sr, Zr, Cs, Ba, La, Pr, Nd, Sm, Er, Tm, Bi, and U. Two external standards are used to calibrate most elements, except for Nb, Ta, and Mo which are calibrated using Zr or Hf as surrogates, the external standards are: Standard A (Li, Rb, Sr, Y, Zr, Cs, Ba, La, Ce, Pr, Tb, Dy, Ho, Er, Tm, Yb, Tl, Pb, Bi, Th, and U) and Standard B (Rb, Cs, Ce, Nd, Sm, Eu, Gd, Lu and U). The data are acquired at each mass for 10 seconds using a dwell time of 0.05 seconds.

All samples and standards are background corrected using the mean of all calibration blanks in the run. Corrections are applied for oxide interference as well as isobaric overlap using correspondent factors normalized to the UO/U in the sample relative to the UO/U ratio in the standard. The average detection limits in this study for the HF-nitric method are as follows: 0.6 to 0.2 ppm for Ba*, Sr*, Rb* and Li; 0.09 ppm for Cs and Tl; 0.07 ppm for Pb; 0.06 ppm for Zr*; 0.03 ppm for Nd, Sm, Eu, and Gd; 0.02 ppm for Mo, La, Ce, Dy, Er and U; 0.01 ppm for Pb, Tm, Lu, Hf and Bi; below 0.00 ppm for Y*, Nb*, Tb, Ho, Yb, Ta and Th (* these elements were measured, but the XRF values were presented in the data as these elements can suffer solution instability and potential memory problems (Jenner et al., 1990)).

With the HF-HNO₃ method, the more resistant phases, particularly zircon that traps REE, may not completely dissolve. In order to measure if there were dissolution problems, duplicate samples were analysed using the sodium peroxide (Na₂O₂) sinter method of Longerich et al (1990). The trace elements analysed are much fewer and are: ⁸⁹Y, ⁹⁰Zr, ⁹³Nb, ¹³⁷Ba, ¹³⁹La, ¹⁴⁰Ce, ¹⁴¹Pr, ¹⁴⁵Nd, ¹⁴⁷Sm, ¹⁵¹Eu, ¹⁵⁷Gd, ¹⁵⁹Tb, ¹⁶³Dy, ¹⁶⁵Ho.

^{167}Er , ^{169}Tm , ^{173}Yb , ^{175}Lu , ^{177}Hf , ^{181}Ta and ^{232}Th . In this method, sample preparation varies in that 0.2 g of powdered sample and 0.8 g of Na_2O_2 are mixed in a Ni crucible and sintered in a muffle furnace at 480 °C for 1.5 hours. After cooling for 20 minutes, 10 ml of distilled water is slowly added a few drops at a time. The sample is then transferred to a centrifuge tube, additional distilled H_2O is added to a volume of 30 ml, and then centrifuged for 10 minutes. The water is decanted from the tube, distilled H_2O is added and the centrifuge and decant steps are repeated two more times. The sinter cake is then placed into a 125 ml bottle and dissolved in 2.5 ml of 8N HNO_3 , 1 ml of 2% oxalic acid and diluted to 90 g with water.

Although both of these sample preparation methods result in a sample analysis on the same ICP-MS, the Na_2O_2 sinter method varies in that each run consists of 56 samples, including standards, blanks and duplicates. Data are acquired in cycles of 12 samples: 7 unknowns, 4 standards and 1 calibration blank. The samples are spiked with an internal solution standard of Rb, Cs, Tl, and U at a 1 part of spike to 2 part sample for a total flow rate of 1 g/min. Total counting time per mass is 10 seconds using a dwell time of 0.5 seconds.

The calibration blanks in the run were used to make background corrections. Corrections are applied for oxide interference using the OU/U ratio in the standards. Matrix corrections were completed using the mass interpolated ratio of the intensity of the spike in the samples and the standards. The calibration was done using the 4 external standards for most elements, except Nb and Ta, which were calibrated using Zr and Hf surrogates.

The analytical detection limits for sinter method in this study are at the sub-ppm level: 0.07 ppm for Ba*, 0.03 ppm for Gd, Tb and Zr*; 0.01 ppm for Dy and Nd; below 0.00 ppm for Y*, Nb, La, Ce, Pr, Tb, Ho, Tm, Lu, Hf*, Ta and Th (* these elements were measured but the XRF values were presented in the data for the same reasons stated previously). The precision and accuracy of a standard (MRG-1) from the period of January 2000 to October 2000 when data were collected for this thesis are presented in table A.2.

Although, this method is a more aggressive digestion, the HF-nitric method was preferred in this study because it allowed for the analysis of a much larger number of trace elements. The samples that were duplicated by both methods show similar rare earth element patterns (Figure A.1) and thus dissolution was not a problem with the HF-nitric method. In addition, the linear fit between the XRF and the ICP-MS analysis for Y (Figure A.2a) displays a good agreement between the techniques, and thus further diminishes concerns about inadequate dissolution. There is scatter between the ICP-MS and XRF values for the high field strength elements, particularly Zn and Nb (Figure A.2c and A.2d). This may be due to solution instability and potential memory problems with these elements (Jenner et al., 1990). For this reason, the XRF results for Zr and Nb were utilised. Another concern with trace element analysis is the potential contamination of the sample during powdering with the tungsten-carbide mill, this can result in contamination by Ta and Nb. This was not a factor in this study as the samples were as markedly depleted in these elements.

A.2. RADIOGENIC ISOTOPES

A.2.1 Sm-Nd and Rb-Sr Isotope

All aspects of the rubidium-strontium and samarian-niodimium isotopic analysis were carried at the Atlantic Universities Radiogenic Isotope Facilities (AURIF) at Memorial University of Newfoundland. Sample preparation and analytical techniques were as follows. Powdered samples that were prepared as above are accurately weighed to within a fifth decimal place and dissolved with 1 ml each of HNO₃ and HF. All reagents were doubly distilled in Teflon containers. The samples are then left to rest and reflux for a period of 2 to 7 days; any samples with residual white fluoride precipitate must be redissolved prior to column chemistry. The samples are then split and accurately weighed into isotopic concentration and isotopic dilution fractions. The isotopic dilution fractions are spiked with an accurately weighed Oak Ridge National Labs (ORLN) ¹⁵⁰Nd-¹⁴⁷Sm mixed spike, that is based on the whole rock Nd concentrations measured by ICP-MS analysis. The Rb-Sm spikes and spike weights are based on Sr whole rock concentrations. After spiking, both fractions of the sample are loaded into EICHROM TRU-Spec resin and initial Rb-Sr and REE group separation is done. Rb-Sr separates are collected using 2B 3N HNO₃ and REE are collected using 2B H₂O that was doubly distilled in a Teflon bottle. These fractions are then allowed to evaporate to dryness. The Rb-Sr samples are loaded into the EICHROM Sr-Spec resin: this retains Sr and removes other trace elements. After loading, 2B 3NO₃ is used to collect the Rb and 2B H₂O is used to collect the Sr. The Rb-Sr fractions are ready to be loaded for measurements into the thermal-ionization mass-spectrometry (TI-MS).

The Sm-Nd isotopic concentrations and dilution fractions are then pipetted in Teflon columns using 2X 0.15N HCl to separate these elements from the rest of the REE. The LREE are stripped off using 2X 0.15N HCl. The Nd is removed from both isotopic and dilution fraction using 2X 0.17N HCl this is followed by removal of the Sm from the isotope dilution fraction using 2X 0.50N HCl. Two drops of phosphoric acid are then added to each of the three collected samples. each of the samples is then evaporated to a single drop and is ready to be loaded on the thermal-ionization mass-spectrometry (TIMS).

The Rb fractions are loaded into the VG MM30B thermal-ionization mass spectrometer that utilises either a Daly or Faraday detector to measured the $^{87}\text{Rb}/^{85}\text{Rb}$ ratio. The drops of the Sr fractions are loaded into the Finnigan MAT 262V thermal-ionization mass spectrometer using outgassed Re double filaments. The isotope dilution Sr fraction is analysed with a static Faraday multicollector routine which measures $^{84}\text{Sr}/^{86}\text{Sr}$ and $^{87}\text{Sr}/^{86}\text{Sr}$ ratios with each analysis containing 5 blocks of 20 scans each, resulting in 100 scans with on line drift and mass fractionation correction and statistical analysis. A static Faraday multicollector routine was used to measure $^{87}\text{Sr}/^{86}\text{Sr}$ ratio of the isotopic composition fraction. The $^{87}\text{Sr}/^{86}\text{Sr}$ ratios are measured off the mass spectrometer and are reported with a 95% confidence level. Data reduction software is used to compute the $^{87}\text{Rb}/^{86}\text{Sr}$ ratio based on the measured spike $^{87}\text{Rb}/^{85}\text{Rb}$ and $^{84}\text{Sr}/^{86}\text{Sr}$ ratios. The 2σ errors are absolute and are calculated by quadratically adding the 2σ errors of the measured isotopic $^{87}\text{Rb}/^{85}\text{Rb}$ and $^{84}\text{Sr}/^{86}\text{Sr}$ ratios.

The Sm-Nd fractions were loaded separately on outgassed Re double filaments for the Finnigan MAT 262V thermal ionization mass spectrometer (TI-MS). The isotopic composition fractions were measured using the Faraday multicollector routine which collects 5 blocks of 20 scans for a total of 100 scans, with on line drift and mass fractionation correction and statistical analysis. The $^{143}\text{Nd}/^{144}\text{Nd}$ errors are reported to 2σ (95%) confidence intervals and were directly measured from the mass spectrometer. The $^{147}\text{Sm}/^{144}\text{Nd}$ errors are reported as absolute 2σ (of the mean) and are quadratically added using the 2σ errors of the measured $^{147}\text{Sm}/^{149}\text{Sm}$ and $^{150}\text{Nd}/^{144}\text{Nd}$ isotopic ratios. The ϵ_{Nd} values are calculated using the $^{143}\text{Nd}/^{144}\text{Nd}$ (CHUR) of 0.512638 and $^{147}\text{Sm}/^{144}\text{Nd}$ (CHUR) of 0.1967.

A.2.2 Pb-Pb Isotope

The lead isotope analyses were carried out at Université de Québec à Montréal, Québec. Powdered whole rock samples were digested using a mixture of HF and concentrated HNO_3 and then evaporated to dryness. The resultant salts were re-hydrated using a 0.8N HBr media. The Pb was separated from solution using a two-step anion exchange chromatography procedure after (Mahnes et al., 1980).

The isotopic concentrations were measured on an IsoProbe MC-ICP mass spectrometer. The $^{206}\text{Pb}/^{204}\text{Pb}$ and $^{207}\text{Pb}/^{204}\text{Pb}$ isotopic ratios were measured using one block of 50 scans of 10-second integration each. A thallium spike was added to measure for instrumental mass bias by simultaneously analysing the $^{205}\text{Tl}/^{203}\text{Tl}$ ratio in order to

later correct for this bias. The Pb isotopic ratios are reported at the 95 % (2σ) level of confidence.

A.3 U-Pb ZIRCON TIMS ANALYSIS

All aspects of this technique were carried out at the Department of Earth Sciences, Memorial University of Newfoundland. For each sample, zircons were selected for analysis based on morphology and clarity. The morphologically similar zircons were grouped together into fractions in order to increase the precision of analysis. The zircons were abraded following the technique of Krogh (1982), in an attempt to remove outer edges that may have suffered alteration and lead-loss. The abraded zircon fractions were washed in distilled HNO_3 , doubly distilled H_2O and finally in distilled acetone. Following this, the samples were weighed on a microbalance and loaded into Teflon Krogh-type dissolution bombs. Each sample was spiked with a mixed $^{205}\text{Pb}/^{235}\text{U}$ tracer, in addition to ~25 drops of distilled HF and 1 drop of HNO_3 . Samples were spiked according to their weight, expected age and U concentration. The bombs were then sealed and placed into an oven at 210°C for 5 days. Once the sample had dissolved, ion chemistry was done according to the procedure set out by Krogh (1973), the columns and reagent volumes were decreased to one tenth the amounts used in 1973. The purified U and Pb samples were collected into a single drop of ultrapure H_3PO_4 in a clean beaker.

Lead and uranium were bound in a silica gel with dilute H_3PO_4 and loaded together onto a degassed single Re filaments. The isotopic analysis was conducted on a thermal ionization mass-spectrometry (TI-MS) using a Finnigan MAT 262 mass

spectrometer equipped with an ion-counting secondary electron multiplier (SEM). Large Pb samples were measured using the static mode and ^{204}Pb measured in ion counting mode on the scanning electron multiplier (SEM). Smaller Pb samples were measured in peak jumping mode on the ion counter, with the measurement times weighted by the amounts of each mass present. The Faraday cups used in the multicollector are calibrated through out the run with NBS 981, and the ion counter is calibrated against a Faraday cup by measuring a known ratio. Double static Faraday collection was used to measure U. Measurements were taken in a series of sets in the temperature range of 1400-1550 °C for Pb and 1550-1640 °C for U, the best sets are combined to produce a mean value for each ratio. A correction, determined by repeated analysis of the NBS standard (0.1%/amu), is applied to the measured ratios to account for U and Pb fractionation. The ratios are then corrected for laboratory procedure blanks (2-10 pg, Pb: 2 pg, U), in addition to common lead above the laboratory blank predicted for the age of the sample by Stacey and Kramers' (1975) two-stage model. The ages are calculated using the decay constants of Jeffrey et al. (1971).

Isotopic ratio and age uncertainties are calculated with an unpublished Royal Ontario Museum program and are reported at absolute 2 sigma (σ). The sources of uncertainties included at 2σ are as follows: isotopic ratio measurements by mass spectrometry, assigned 80% uncertainty on the fractions of Pb and U, assigned 50% uncertainty on the volume of Pb and U blanks, and a 4% uncertainty on the isotopic composition of the Pb used to subtract from the common Pb above the laboratory blank. The uncertainties are quadratically added to determine the absolute 2σ errors that are

reported. The program by Davies (1982) is used to calculate discordia lines using the individual data points having 2σ errors and is reported at the 95% confidence interval.

A.4 U-Pb LASER ABLATION MICROPROBE-INDUCTIVELY COUPLED PLASMA-MASS SPECTROMETRY (LAM-ICP-MS)

All aspects of the U-Pb zircon analysis by LAM-ICP-MS were done at the Department of Earth Sciences, Memorial University of Newfoundland. This technique is still in its developmental stage. The zircons analysed by this method were from the same samples separated for U-Pb TIMS analysis, underwent the same sample preparation up till the TIMS samples were abraded as the LAM-ICP-MS samples were not.

The zircons were selected for analysis based on clarity and varied morphology. The chosen grains were mounted in an epoxy resin and left to set. Once dry, the grain mounts were polished until the zircons cores were exposed. The grains were then imaged by back-scattered-electron (BSE) microscopy, in order to identify potential cores and rims within individual grains.

The analyses were done on a VG Plasma Quad S+ instrument coupled to an in-house built 266 nm NdYAG laser 0.1-0.5 mJ/Pulse (Jackson et al., 1992; Longerich et al., 1995). The laser is 10-15 μm in diameter is defocused by 200 μm and migrates down the optical tube of a petrographic microscope to the sample cell. Site selection and ablation procedures were observed using a TV camera and monitor. The ablated zircon material was flushed from the sample cell with a helium gas carrier then combined with an argon solution before entering the ICP-MS. In addition, a Th-U-Bi-Np tracer solution is

simultaneously aspirated with the sample to the plasma. This was done to make real-time correction for instrument mass bias. The zircons were ablated by stage rastering in lines (20x10–40x10 μm), which results in ablation of <0.0005 mg of the sample.

Analysis was performed in peak-jumping mode, using 1 point per mass peak with a 60 second gas blank. There is a 180 second signal; the time is limited by the rastering technique. The typical acquisition of element menu was masses: ^{202}Hg , ^{203}Tl , ^{205}Tl , ^{206}Pb , ^{207}Pb , ^{209}Bi , ^{235}U , ^{238}U , ^{237}Np and oxide masses of 249, 253 and 254. Any U-Pb fractionation due to volatility differences during laser ablation was corrected by using the back-calculated intercept of the time resolved signal. The procedural runs included 4 standards and 5 unknowns (STD 1-1-2-2, UNK 1-2-3-4-5, STD 1-1-2-2).

The two-zircon external standards (3200 kamo and 91500) were analysed twice after every 5 unknown analysis and used were corrected for mass bias. The standards had average precision levels of 2 sigma errors of 2.4% for the $^{207}\text{Pb}/^{235}\text{U}$ ages, and average of 3.1% for the $^{206}\text{Pb}/^{238}\text{U}$ and 3.2% for $^{207}\text{Pb}/^{206}\text{Pb}$ ages. Data were reduced using the software U-Pb zircon software of Jan Kosler. Most of the U-Pb LAM-ICP-MS data were within error of the previous TIMS data.

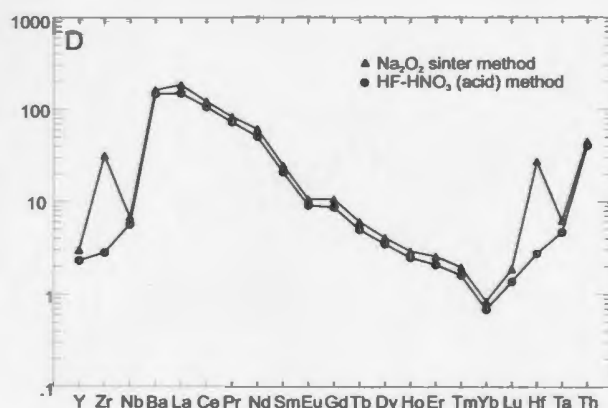
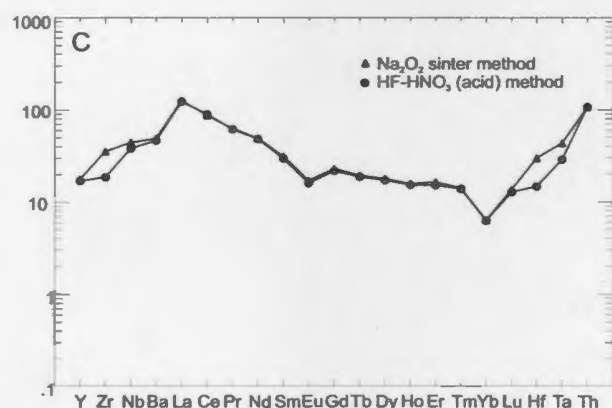
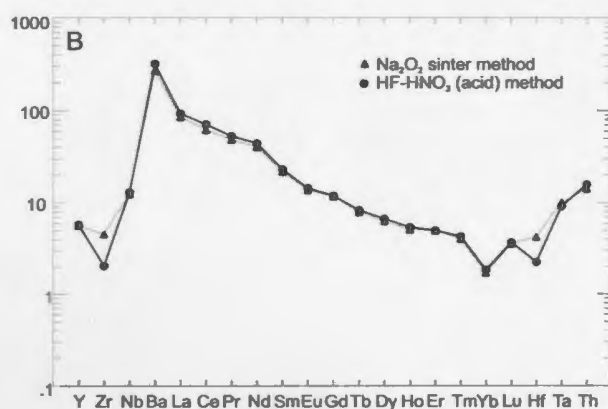
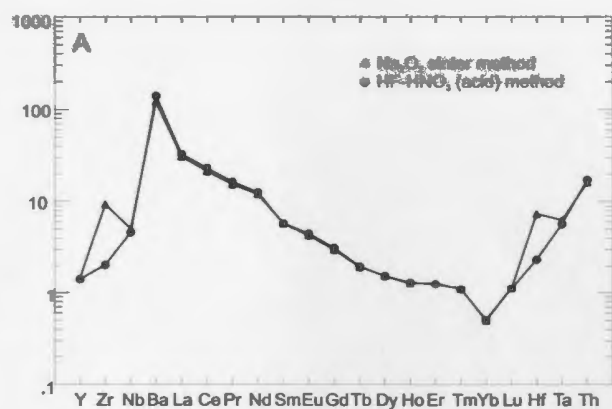


Figure A.1. Primitive mantle normalized extended trace element spider diagrams of Paleoproterozoic metaplutonic suite samples prepared by HF-nitric or Na_2O_2 sinter method for ICP-MS trace element analysis. A) Meta-tonalitic sample DDH-496-517, B) Meta-quartz diorite sample DDH-496-530, C) Meta-tonalitic sample VB-99-82, and D) Archean quartzo-feldspathic gneiss sample VB-99-101.

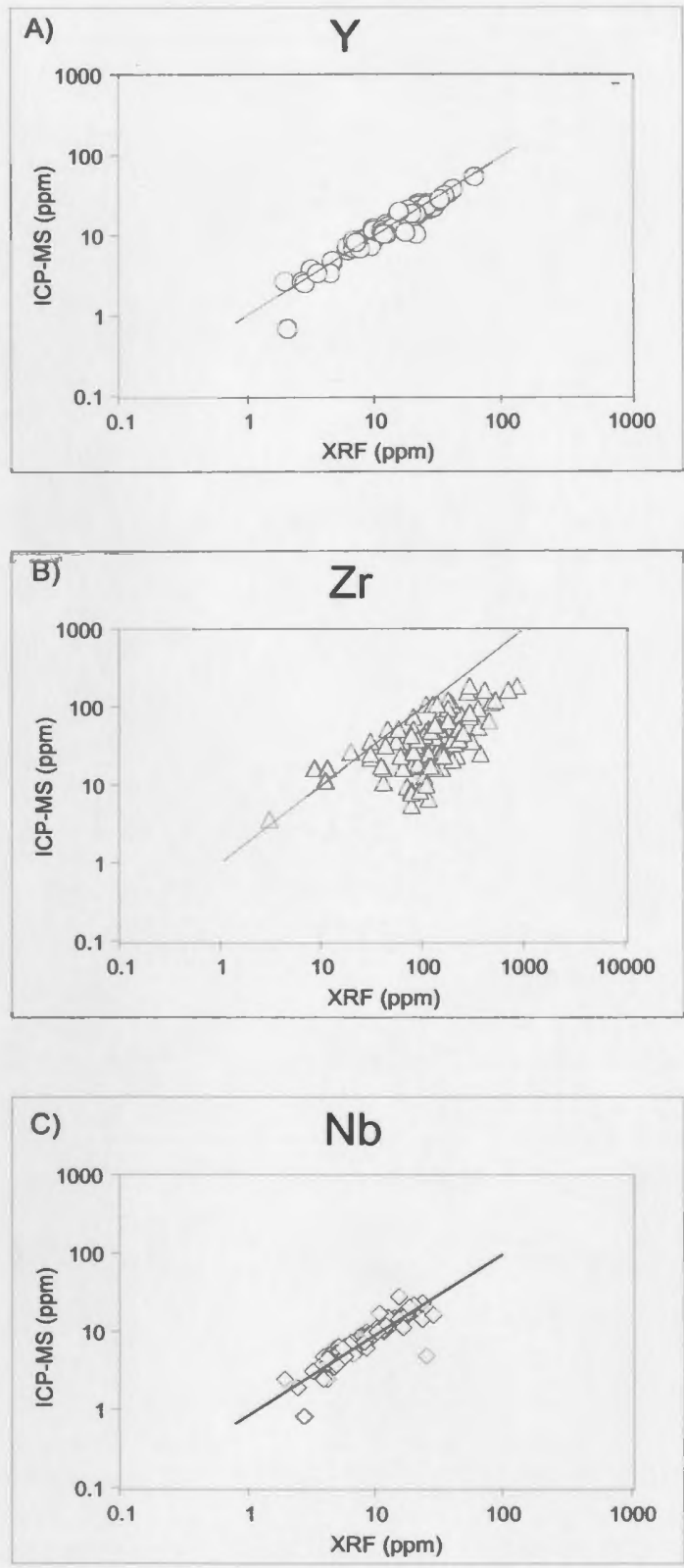


Figure A.2. Comparison of certain element concentrations analysed by ICP-MS (HF-nitric method) versus XRF pressed pellet analysis. A) Y, B) Zr, and C) Nb.

Table A.1. - Precision and accuracy for XRF analysis of standard DNC-1. Data represent seven analyses from November 1999 to December 2000.

Element ^a	Minimum	Maximum	Std. Deviation	Mean (n=7)	Quoted MUN Values ^{a,b}	RSD (%) ^c	RD (%) ^d
SiO ₂	41.41	44.73	3.23	43.01	43.56	0.08	-1.26
TiO ₂	0.42	0.47	0.05	0.44	0.45	0.12	-2.40
Al ₂ O ₃	17.16	19.66	1.52	18.30	17.67	0.08	3.59
Fe ₂ O _{3 Total}	9.42	10.17	0.66	9.74	10.12	0.07	-3.72
MnO	0.14	0.15	0.01	0.14	0.15	0.07	-4.56
MgO	9.57	10.43	0.84	9.91	9.9	0.08	0.07
CaO	10.30	11.61	1.08	10.84	11.02	0.10	-1.61
Na ₂ O	1.91	2.08	0.15	2.00	1.94	0.08	2.84
K ₂ O	0.24	0.28	0.03	0.26	0.26	0.11	-1.54
P ₂ O ₅	0.09	0.10	0.01	0.10	0.89	0.10	-89.06
S	944	1195	81	1139	1032	7.13	10.38
Cl	790	981	80	847	871	9.50	-2.77
Sc	16.3	39.3	8.6	24.9	31.0	34.59	-19.58
V	125.9	151.6	16.8	139.8	148.0	12.03	-5.51
Cr	280.3	304.7	25.7	290.0	307.0	8.87	-5.54
Ni	235.8	242.3	2.6	239.5	252.0	1.07	-4.95
Cu	80.4	86.8	2.6	83.6	87.0	3.09	-3.87
Zn	44.1	53.7	3.0	49.2	60.0	6.03	-18.02
Ga	13.3	17.8	1.6	15.0	14.0	10.74	7.24
As	<LD	<LD	-	<LD	<LD (13) ^e	-	-
Rb	2.4	4.6	0.7	3.6	3.4	20.19	7.24
Sr	142	144	1	144	142	0.41	0.95
Y	15.1	16.4	0.6	15.8	15.9	3.76	-0.49
Zr	34.7	39.8	2.1	36.7	36.0	5.62	1.93
Nb	0.5	3.1	0.8	1.7	1.9	46.64	-8.81
Ba	61	139	24	107	115	22.18	-6.69
Ce	<LD	<LD	-	<LD	<LD (39) ^e	-	-
Pb	2.0	13.0	4.4	7.4	7.3	59.37	1.55
Th	<LD	3.7	-	<LD	<LD (2.8) ^e	-	-
U	<LD	<LD	-	<LD	<LD (3.4) ^e	-	-

^aMajor element oxides reported as wt. % and trace elements as ppm.

^bData represent extended durations means of Longerich (1995).

^cRSD is the relative standard deviation (standard deviation/mean).

^dRD is the relative difference to the standard value [(mean-quoted value)/quoted values].

^eValues in the standard are below the limit of detection (LD) values quoted in parantheses.

Table A.2. - Precision and accuracy for analysis of a standard (MRG-1) by ICP-MS. Data represent eight analyses from January 2000 to October 2000. Good precision and accuracy is defined as 3-7%, while excellent is 0-3% (Jenner et al., 1990)

Element ^a	Minimum	Maximum	Std. Deviation	Mean (n=8)	Quoted MUN Values ^a	RSD (%) ^b	RD (%) ^c
Li	3.0	4.3	0.39	3.7	3.7	0.11	-1.57
Rb	6.1	7.6	0.47	6.8	7.7	0.07	-10.56
Sr	231.0	289.3	18.65	261.2	274.0	0.07	-4.68
Y	9.9	13.0	0.96	11.2	11.6	0.09	-3.49
Zr	82.1	98.6	5.30	90.4	93.7	0.06	-3.57
Nb	19.3	26.4	2.29	22.7	22.3	0.10	1.80
Mo	1.2	8.5	2.50	2.7	1.3	0.92	115.23
Cs	0.5	0.6	0.05	0.6	0.6	0.09	-5.83
Ba	39.9	50.6	3.27	45.3	47.5	0.07	-4.64
La	7.8	9.9	0.65	8.7	9.1	0.08	-4.21
Ce	23.7	30.9	2.41	25.7	26.2	0.09	-1.87
Pr	3.3	4.2	0.28	3.7	3.8	0.08	-3.09
Nd	15.5	20.1	1.36	17.6	18.3	0.08	-4.05
Sm	4.0	4.9	0.30	4.3	4.5	0.07	-3.95
Eu	1.2	1.5	0.09	1.4	1.5	0.07	-5.94
Gd	3.4	4.3	0.29	3.9	4.1	0.07	-4.40
Tb	0.5	0.6	0.03	0.5	0.6	0.06	-3.24
Dy	2.7	3.2	0.18	2.9	3.0	0.06	-4.34
Ho	0.4	0.5	0.03	0.5	0.5	0.07	-5.68
Er	1.1	1.3	0.08	1.2	1.2	0.07	-3.34
Tm	0.1	0.2	0.03	0.2	0.2	0.18	6.86
Yb	0.7	0.9	0.05	0.8	0.8	0.06	-3.08
Lu	0.1	0.1	0.02	0.1	0.1	0.16	-13.03
Hf	3.1	4.1	0.33	3.5	3.8	0.09	-6.76
Ta	0.7	1.1	0.12	0.8	0.8	0.15	-3.62
Tl	0.0	0.1	0.03	0.1	0.1	0.51	20.10
Pb	4.2	10.9	2.22	5.5	5.2	0.40	6.03
Bi	0.1	0.3	0.07	0.2	0.1	0.42	22.44
Th	0.6	0.9	0.09	0.8	0.8	0.12	-3.76
U	0.2	0.4	0.05	0.3	0.3	0.21	2.94

^aTrace elements values are reported as ppm.

^bRSD is the relative standard deviation (standard deviation/mean).

^cRD is the relative difference to the standard value [(mean-quoted value)/quoted values].

Appendix B. Sample details and locations.

Sample	Easting	Northing	Sample Description ^a	Location ^b	T.S. ^c	Chem ^{c†}	Chron ^{c‡}
VB-99-001	554896.14	6243349.30	Troctolite	Disco Hill			
VB-99-002	555098.08	6243661.99	Meta-tonalite	Disco Hill			
VB-99-003	554967.80	6243271.13	Mafic dyke	Disco Hill			
VB-99-004	554668.13	6243420.96	Gossan (vb cpy)	Disco Hill			
VB-99-005	557586.54	6243232.05	Meta-dionite	GPS Hill			
VB-99-006	559122.29	6253928.53	B. qtz-felds ogn	Mathews Point			
VB-99-007	560232.97	6252518.19	Troc (olive-gab?)	Mushuau Int			
VB-99-008	560132.00	6252299.95	Troctolite	Mushuau Int			
VB-99-009	557992.06	6243192.97	Meta-Anorthosite	GPS Hill			
VB-99-010	558167.94	6243219.02	Qtz porphyry Granite	F.E.D.	*		
VB-99-011	557586.54	6243232.05	Cpx Meta-Hornblende Gabbro	F.E.D.	*		
VB-99-012	559213.00	6243545.00	Olivine Weibstente	F.E.D.	*		
VB-99-013	559301.00	6243425.00	Bt-Hbl-Opx Meta-gabbroic dyke	F.E.D.	*		
VB-99-014	559301.00	6243425.00	Meta-anorthosite	F.E.D.	*		
VB-99-015	559367.61	6243742.72	Quartzite	F.E.D.	*		
VB-99-016	559704.00	6243582.00	Bt Granite	F.E.D.	*		
VB-99-017	559497.11	6243653.22	Qtz-Di Meta-sediments	F.E.D.	*		
VB-99-018	559435.22	6243653.98	Bt-Crd-Qtz Meta-sediments	F.E.D.	*		
VB-99-019	559399.05	6243615.35	Opx-Crd-Qtz Meta-sediments	F.E.D.	*		
VB-99-033	559325.00	6253950.00	Quartzo-feldspathic Banded Hbl Orthogneiss	Mathews Pt	*		
VB-99-034	557894.00	6256236.00	Quartzo-feldspathic Banded Hbl-Opx Orthogn	Burnt Is	*		
VB-99-035	557894.00	6256236.00	Quartzo-feldspathic Banded Hbl-Opx Orthogn	Burnt Is	*		
VB-99-036	554986.00	6231546.00	Crd-Grt Meta-pelite	Makhavinekh Mtn	*	*	
VB-99-046	556959.00	6242422.00	Troctolite	E.D.	*	*	
VB-99-047	559000.00	6242574.00	Bt Qtz porphyry granite	E.D.	*		
VB-99-048	559000.00	6242574.00	Fine grained granite	E.D.	*		
VB-99-049	559550.00	6246778.00	Melatroctolite	Mushuau Int	*		
VB-99-050	559582.00	6246821.00	Cpx-bearing Leucotroctolite	Mushuau Int	*		
VB-99-051	560587.00	6246718.00	Bt-Tr-Qtz Meta-Sediments	Mushuau Int	*		
VB-99-052	563200.00	6247647.00	Opx-bearing Leucotroctolite	Mushuau Int	*		
VB-99-053	563432.00	6247842.00	Dark Anorthosite	Mushuau Int	*		
VB-99-054	558922.00	6242133.00	Cpx Meta-tonalite	East E.D.	*		
VB-99-055	560048.00	6242378.00	Meta-tonalite	East E.D.	*		
VB-99-056	560048.00	6242378.00	Amphibolite	East E.D.	*		
VB-99-057	560328.00	6242333.00	Amphibolite	East E.D.	*		
VB-99-058	560586.00	6242247.00	Hbl Olivine Gabbro	East E.D.	*		
VB-99-058b	560038.00	6242573.00	Qtz monzonite	East E.D.	*		
VB-99-059	560493.00	6242839.00	Opx-bearing Cpx Troctolite	East E.D.	*		
VB-99-060	559863.00	6242926.00	Cpx-bearing Meta-anorthosite	East E.D.	*		
VB-99-061	561778.00	6242366.00	Hbl Qtz porphyry Granite	East E.D.	*		
VB-99-061b	561207.00	6242283.00	gneiss xenolith in granite	East E.D.	*		
VB-99-062	561778.00	6242366.00	amphibolite xenolith in qtz-monzonite	East E.D.	*		
VB-99-063	561787.00	6242146.00	Qtz-monzonite	East E.D.	*		
VB-99-064	562627.00	6241902.00	Hbl Qtz porphyry Granite	East E.D.	*		
VB-99-065	554121.00	6255617.00	Quartzo-feldspathic banded orthogneiss	Little IIs	*	*	
VB-99-066	554121.00	6255617.00	Alt'd Quartzo-feldspathic Banded Tr-Act ortho	Little IIs	*	*	
VB-99-067	554121.00	6255617.00	Opx-Bt-Grt-Qtz-Crd Meta-pelite	Little IIs	*		
VB-99-068	554121.00	6255617.00	Meta-sediments (diopside/quartz)	Little IIs	*		
VB-99-069	554121.00	6255617.00	Meta-sediments (diopside/quartz)	Little IIs	*		
VB-99-070	554121.00	6255617.00	Opx-Bt-Grt-Qtz-Crd Meta-pelite	Little IIs	*		
VB-99-071	554121.00	6255617.00	Meta-pelite	Little IIs	*		
VB-99-072	554121.00	6255617.00	Meta-pelite	Little IIs	*		
VB-99-073	558048.00	6242449.00	Olivine Gabbro	East E.D.	*		
VB-99-074	561382.00	6243003.00	Cpx-bearing Troctolite	East E.D.	*		
VB-99-075	556998.01	6243539.36	Bt-Opx-Hbl-Cpx Meta-tonalite	Detail on GPS	*		
VB-99-076	556992.93	6243562.56	Opx-Cpx-Bt Meta-tonalite	Detail on GPS	*	*	
VB-99-077	556990.29	6243571.84	Opx-Cpx-Hbl Meta-quartz dionite	Detail on GPS	*	*	
VB-99-078	556990.73	6243579.35	Atc-Bt Meta-hornblende gabbro	Detail on GPS	*	*	
VB-99-079	557006.19	6243588.18	Opx-Bt-Hbl-Cpx Meta-tonalite	Detail on GPS	*	*	
VB-99-080	557003.54	6243577.58	Hbl-Bt-Opx Meta-gabbro	Detail on GPS	*	*	
VB-99-081	557003.76	6243563.88	Alt'd Act-Tr Meta-gabbro	Detail on GPS	*	*	

^abt, biotite; cpx, clinopyroxene; opx, orthopyroxene; act, actinolite; tr, tremolite; hbl, hornblende; alt'd, altered; crd, cordierite; gnt, garnet; qtz, quartz; l, olivine; di, diopside

^bFED, far eastern deeps; ED, eastern deeps; Mtn, mountain; int, intrusion; Pt, point; K-bay, Kangekluak Bay

^cTS, thin section; Chem, XRF and ICP-MS; Chron, U-Pb zircon

[†]Indicate yes to field, s indicates a sample was taken but analyses was not done

Appendix B. (continued).

Sample	Easting	Northing	Sample Description ^a	Location	T.S.	Chem	Chron
VB-99-082	557000.89	6243544.01	Bt-Opx-Cpx Meta-tonalite	Detail on GPS	•	•	
VB-99-083	557007.51	6243550.18	Cpx Meta-hornblende gabbro	Detail on GPS	•		
VB-99-084	557002.66	6243548.63	Cpx Meta-hornblende gabbro	Detail on GPS	•		
VB-99-085	557016.13	6243553.94	Cpx Meta-hornblende gabbro	Detail on GPS	•	•	
VB-99-086	557026.96	6243568.08	Alt'd Bt-Cpx-Hbl-Act Meta-gabbro	Detail on GPS	•		
VB-99-087	557034.25	6243574.70	Pegmatite vein	Detail on GPS	•		
VB-99-088	557022.54	6243606.07	Bt-Cpx Meta-hornblende gabbro	Detail on GPS	•		
VB-99-089	557018.56	6243570.73	Opx-Bt Meta-dionte	Detail on GPS	•		
VB-99-090	557019.88	6243588.84	Opx-Bt Meta-gabbro	Detail on GPS	•		
VB-99-091	556998.68	6243552.39	Bt Meta-hornblende gabbro	Detail on GPS	•	•	
VB-99-092	557512.24	6243361.55	Cpx-Opx-Bt Meta-dionte	East of GPS	•	•	
VB-99-093	557452.16	6243343.88	Cpx-Opx-Bt Meta-tonalite	East of GPS	•		
VB-99-094	558384.47	6248685.52	Melatroctolite	Mushuau Int	•		
VB-99-095	558379.44	6248471.48	Troctolite	Mushuau Int	•		
VB-99-096	559323.73	6248788.76	Qtz-rich Amphibolite Dyke	Mushuau Int	•		
VB-99-097	558421.00	6248167.00	Leucotroctolite	Mushuau Int	•		
VB-99-098	559008.00	6248009.00	Quartzite	Mushuau Int	•		
VB-99-099	559119.00	6247828.00	Amphibolite	Mushuau Int	•		
VB-99-100	559598.00	6248345.00	Amphibolite	Mushuau Int	•		
VB-99-101	557826.00	6256124.00	Bt-Quartzo-feldspathic Orthogneiss	Burnt Is	•	•	s
VB-99-102	557888.00	6256152.00	Quartzo-feldspathic Orthogneiss	Burnt Is	•		
VB-99-103	557830.00	6256230.00	Pegmatite vein	Burnt Is	•	•	
VB-99-104	553995.00	6255408.00	Pegmatite vein	Little Is	•	•	
VB-99-105	554141.00	6255479.00	Pegmatite vein	Little Is	•	•	
VB-99-106	557675.00	6243404.00	Cpx-Bt-Opx Meta-Hornblende Gabbro	GPS Hill	•	•	•
VB-99-107	557688.00	6243482.00	Meta-tonalite	GPS Hill	•		
VB-99-108	557504.00	6243436.00	Bt-Cpx-Opx Meta-tonalite	GPS Hill	•	•	•
VB-99-109	558709.00	6253662.00	Amphibolite	Mathews Pt	•	•	
VB-99-110	558709.00	6253662.00	Plag phenocryst gabbroic dyke	Mathews Pt	•		s
VB-99-111	558626.90	6253578.00	Pegmatite vein	Mathews Pt	•	•	s
VB-99-112	558505.00	6253491.00	Quartzo-feldspathic Orthogneiss	Mathews Pt	•	•	s
VB-99-113	558900.00	6253800.00	Bt-Amphibolite	Mathews Pt	•		
VB-99-114	558900.00	6253800.00	Amphibolite	Mathews Pt	•	•	
VB-99-115	558603.00	6253564.00	Quartzo-feldspathic Orthogneiss	Mathews Pt	•	•	s
VB-99-116	558724.00	6253666.00	Pegmatite vein	Mathews Pt	•		s
VB-99-117	558724.00	6253666.00	Pegmatite vein (older)	Mathews Pt	•		s
VB-99-118	558724.00	6253666.00	Pegmatite vein (older)	Mathews Pt	•		s
VB-99-119	558671.00	6253555.00	Qtz-feldspathic Banded Bt-Hbl Orthogneiss	Mathews Pt	•	•	s
VB-99-120	558582.60	6253545.00	Pegmatite vein (older)	Mathews Pt	•		s
VB-99-121	558582.60	6253545.00	Pegmatite vein (older)	Mathews Pt	•		s
VB-99-122	558463.00	6253455.00	Pegmatite vein (younger)	Mathews Pt	•		s
VB-99-123	558470.00	6253444.00	Pegmatite vein (younger)	Mathews Pt	•		s
VB-99-124	558470.00	6253444.00	Pegmatite vein (younger)	Mathews Pt	•		s
VB-99-125	558470.00	6253444.00	Pegmatite vein (younger)	Mathews Pt	•		s
DDH-99-496	559780.00	6243135.00		GPS Hill			
DDH-99-497	554945.00	6242479.00		Disco Hill			
AR-00-001	554745.00	6243332.00	alt'd Gabbro (poss. Troctolite)	Disco Hill	•		
AR-00-002	554740.00	6243331.00	alt'd Meta-hornblende gabbro	Disco Hill	•	•	
AR-00-003	554736.00	6243327.00	Plagioclase phenocrysts gabbroic dyke	Disco Hill	•	•	
AR-00-004	554642.00	6243270.00	Cpx-Bt-Opx Meta-tonalite	Disco Hill	•	•	
AR-00-005	554138.00	6243418.00	Gnt-Cordierite Metapelite	Disco Hill	•	•	
AR-00-006	560648.00	6245060.00	Melatroctolite	S.L. Mushuau	•		
AR-00-007	560733.00	6244737.00	Cpx-bearing Leucotroctolite	S.L. Mushuau	•		
AR-00-008	555933.00	6247603.00	Cpx-Bt-Hbl Meta-quartz dionte	Halfway Hill	•	•	s
AR-00-009	555669.00	6247608.00	Cpx-Bt Meta-quartz dionte	Halfway Hill	•	•	
AR-00-010	556951.00	6246816.00	Bt Granite	Halfway Hill	•	s	
AR-00-011	556670.00	6246878.00	Gnt Amphibolite	Cheeks	•	•	
AR-00-012	556793.00	6246957.00	Quartzite	Cheeks	•	•	
AR-00-013	556277.00	6247218.00	Quartzite	Cheeks	•	•	
AR-00-014	555910.00	6248471.00	Granite	Halfway Hill	•	s	
AR-00-015	555770.00	6248426.00	Amphibolite	Halfway Hill	•	•	
AR-00-016	555770.00	6248427.00	Amphibolite	Halfway Hill	•	•	
AR-00-017	555381.00	6248619.00	Bt-Cpx Meta-tonalite	Halfway Hill	•	•	
AR-00-018	561917.00	6244786.00	Opx-bearing Leucotroctolite	S.L. Mushuau	•	s	
AR-00-019	561352.00	6244483.00	Leucogabbro	S.L. Mushuau	•	s	
AR-00-020	561358	6244524	Melatroctolite	S.L. Mushuau	•	s	
AR-00-021a	561371	6244469	Alt'd Act/Tr Gabbro	S.L. Mushuau	•	s	

Appendix B. (continued).

Sample	Eastng	Northing	Sample Description ^a	Location	T.S.	Chem
AR-00-021b	561371	6244469	Alr'd Act/Tr Tonalite	S.L. Mushuau	•	s
AR-00-022	562640	6244572	Sil-Crd-Qtz Metapelite	S.L. Mushuau	•	•
AR-00-023	562852	6244114	Amphibolite	S.L. Mushuau	•	•
AR-00-024	565037.00	6244518.00	Hbl Meta-gabbro	S.L. Mushuau	•	•
AR-00-025	560471.00	6245739.00	Leucotroctolite	N of S.L. Mushuau	•	s
AR-00-026	561196.00	6245821.00	Amphibolite	N of S.L. Mushuau	•	•
AR-00-027	561415.00	6245853.00	Bt-Sil-Qtz Meta-sediments	N of S.L. Mushuau	•	•
AR-00-028	561655.00	6245734.00	Alr'd Act/Tr Meta-sediments	N of S.L. Mushuau	•	•
AR-00-029	563869.00	6245487.00	Bt Granite	W of K-Bay	•	s
AR-00-030	558054.00	6248360.00	Quartzite	C.L. Mushuau	•	•
AR-00-031	557815.00	6248355.00	Tonalite	C.L. Mushuau	•	•
AR-00-032	557739.00	6248230.00	Hbl-Bt Meta-tonalite	C.L. Mushuau	•	•
AR-00-033	558365.00	6248466.00	Cpx-bearing Troctolite	C.L. Mushuau	•	s
AR-00-034	558849.00	6248328.00	Melatroctolite	C.L. Mushuau	•	s
AR-00-035	558896.00	6248312.00	Cpx-bearing Troctolite	C.L. Mushuau	•	•
AR-00-036	560579.00	6248110.00	Qtz-Feldspathic Banded Bt-Hbl Orthogneiss	C.L. Mushuau	•	•
AR-00-037	561801.00	6248215.00	Opx-bearing Quartzo-Feldspathic Orthogneiss	C.L. Mushuau	•	•
AR-00-038	560550.00	6249809.00	Opx-bearing Quartzo-Feldspathic Orthogneiss	N of Sarah	•	•
AR-00-039	561250.00	6250996.00	Alr'd Gabbro (px's gone)	N of Sarah	•	s
AR-00-040	560581.00	6250610.00	Leuco-Olivine Nonte	Sarah Gnd	•	s
AR-00-041	560293.00	6250832.00	Cpx-bearing Olivine Nonte	Sarah Gnd	•	•
AR-00-042	559707.00	6250170.00	Alr'd Gabbro (px's gone)	Sarah Gnd	•	s
AR-00-043	559494.00	6250240.00	Alr'd Melatroctolite	Sarah Gnd	•	•
AR-00-044	559090.00	6251240.00	Amphibolite	Chnsta	•	•
AR-00-045	559164.00	6251502.00	Quartzo-Feldspathic Orthogneiss	Chnsta	•	•
AR-00-046	560129.00	6251102.00	Cpx-bearing Olivine Nonte	E of Chnsta	•	s
AR-00-047	560282.00	6251120.00	Alr'd Nonte (px's gone)	E of Chnsta	•	s
AR-00-048	563136.00	6250060.00	Foliated gabbro	Ashini Gnd	•	s
AR-00-049	562300.00	6243350.00	Amphibolite	N of Otter Pond	•	•
AR-00-050	554260.00	6246528.00	Bt-Cpx Meta-quartz diorite	E of Cheeks	•	•
AR-00-051	560354.00	6246827.00	Quartzite	E of CL Mush	•	•
AR-00-052	556054.00	6253636.00	Sil-Bt-Crd-Grt Meta-pelite	Old Joe	•	•
AR-00-053	555763.00	6253387.00	Bt-Opx-Cpx Meta-tonalite	Old Joe	•	•
AR-00-054	557019.00	6243442.00	Opx- Hbl-Cpx-Bt Meta-tonalite	GPS Hill	•	•
AR-00-055	562552.00	6250487.00	Hbl foliated Gabbro	E of Chnsta	•	•
AR-00-056	561940.00	6252064.00	Gabbro nonte	E of Stephen	•	•
AR-00-057	557261.00	6242445.00	Bt-Opx Meta-Gabbro	DDH-00-543	•	•
AR-00-058	557815.00	6242434.00	Bt-Opx Meta-Gabbro	DDH-00-530	•	•
AR-00-059	557815.00	6242434.00	Bt-Opx-Hbl Meta-Gabbro	DDH-00-530	•	•
AR-00-060	557815.00	6242434.00	Opx-Bt Meta-Gabbro	DDH-00-530	•	•
AR-00-061	557815.00	6242434.00	Opx-bearing Quartzo-Feldspathic Orthogneiss	DDH-00-530	•	•
AR-00-062	557815.00	6242434.00	Opx-bearing Quartzo-Feldspathic Orthogneiss	DDH-00-530	•	•
AR-00-063	557815.00	6242434.00	Alr'd Opx-bearing Quartzo-Feldspathic Orthog	DDH-00-530	•	•
AR-00-064	557815.00	6242434.00	Opx-bearing Quartzo-Feldspathic Orthogneiss	DDH-00-530	•	•
AR-00-065	557815.00	6242434.00	Bt-Opx Meta-Gabbro	DDH-00-530	•	•
AR-00-066	557815.00	6242434.00	Bt-Opx Meta-Gabbro	DDH-00-530	•	•
AR-00-067	557815.00	6242434.00	Bt-Opx Meta-Gabbro	DDH-00-530	•	•
AR-00-068	557815.00	6242434.00	Bt-Opx-Hbl Meta-Gabbro	DDH-00-530	•	•

NOTE TO USERS

Oversize maps and charts are microfilmed in sections in the following manner:

LEFT TO RIGHT, TOP TO BOTTOM, WITH SMALL OVERLAPS

This reproduction is the best copy available.

UMI

